CATALYTIC PERFORMANCE ENHANCEMENT OF NICKEL DOPED CALCIUM OXIDE FOR BIODIESEL PRODUCTION

PHANG KAI SHENG

A project report submitted in partial fulfilment of the requirements for the award of Bachelor of Engineering (Honours) Chemical Engineering

**Lee Kong Chian Faculty of Engineering and Science
Universiti Tunku Abdul Rahman**

April 2020

DECLARATION

I hereby declare that this project report is based on my original work except for citations and quotations which have been duly acknowledged. I also declare that it has not been previously and concurrently submitted for any other degree or award at UTAR or other institutions.

Signature : _____

Name   : Phang Kai Sheng

ID No.   : 15UEB03554

Date   : 15th May 2020

APPROVAL FOR SUBMISSION

I certify that this project report entitled **"CATALYTIC PERFORMANCE ENHANCEMENT OF NICKEL DOPED CALCIUM OXIDE FOR BIODIESEL PRODUCTION"** was prepared by **PHANG KAI SHENG** has met the required standard for submission in partial fulfilment of the requirements for the award of Bachelor of Engineering (Honours) Chemical Engineering at Universiti Tunku Abdul Rahman.

Approved by,

Signature	:	
Supervisor	:	Dr. Sim Jia Huey
Date	:	15th May 2020

ACKNOWLEDGEMENT

ABSTRACT

The demand of energy is growing continuously with the increase in population around the world annually. The development of clean and renewable energy sources has become important owing to rapid surge in crude oil price, diminishing fossil fuel reserves and increasing environmental pollution due to fuel burning from petroleum-fueled engines. In this context, biodiesel is emerged as a renewable and eco-friendly alternative to the conventional diesel fuel as it is non-toxic and biodegradable. However, in the current state of energy crisis urgency, the biodiesel has yet to replace the fossil-based diesel fuel effectively as the primary energy source ascribed to the high cost which is contributed significantly from the synthesis of catalyst used in biodiesel production. In this regard, waste eggshells are chosen as the raw materials to derive a cost-effective and environmental-friendly catalyst in reducing the overall biodiesel production cost. The catalytic activity of waste eggshells-derived CaO catalyst is improved by synthesising it in nanocrystalline form, while the metal dopants are impregnated to CaO catalyst in order to further enhance its catalytic performance as the rate of transesterification catalysed by neat CaO is still inadequate for practical application. In this research, the active doped CaO nanocatalyst is synthesised by the calcination of waste eggshells at 900 ℃ under air flow before being wet impregnated with nickel dopants at the amount varying from 1 wt% to 5 wt%, followed by re-calcination at the temperature varying from 600 ℃ to 900 ℃. The physicochemical properties of synthesised catalysts are analysed using X-ray diffraction (XRD), scanning electron microscopy (SEM), energy dispersive X-ray (EDX) spectroscopy, temperature-programmed desorption of carbon dioxide (CO_2-TPD) and thermogravimetric analysis (TGA). The analysis results reveal that the doping process is capable of enhancing the properties of CaO catalyst such as particle size, surface area and basicity. From XRD analysis, the crystallite size of CaO catalyst is reduced from 59.62 nm to a minimum of 41.25 nm after the impregnation of Ni dopant. SEM analysis reveals that the doping process transforms the morphology of catalyst from uniform (coral) shape into irregular shape along with the increment in surface porosity and reduction in particle size, signifying an increased surface area. Based on CO_2-TPD analysis, the

impregnation of Ni dopant is able to enhance the basicity of CaO catalyst, where it shows an increment from 1599.53 $\mu mol\ CO_2/g$ to a maximum of 2957.16 $\mu mol\ CO_2/g$ with CO_2 desorption temperature which is greater than 600 ℃, evincing the formation of strong CO_2 adsorption sites on catalyst surface. The optimum calcination temperature for synthesising the doped CaO catalyst after wet impregnation is determined from TGA, where it is analogous to the temperature required for complete decomposition of carbonates into oxides. The catalytic performance of synthesised catalysts is investigated via transesterification reaction catalysed by 5 wt% of Ni doped CaO with respect to oil, where it is carried out at 60 ℃ for 3 hours with methanol-to-oil molar ratio of 10:1 and is compared against CaO derived from natural calcium carbonate sources. The biodiesel yield obtained from transesterification catalysed by both undoped and doped CaO are determined using gas chromatography (GC). Upon the impregnation of Ni dopant, CaO catalyst shows an improvement in the catalytic performance towards transesterification reaction. Nevertheless, the biodiesel yield is reduced with a further increase in Ni loading above 2 wt% and calcination temperature above 700 ℃. Under optimum conditions, a maximum biodiesel yield of 94.19 % is achieved after three hours of reaction by CaO catalyst which is doped with 1 wt% Ni and recalcined at 600 ℃.

TABLE OF CONTENTS

CHAPTER

LIST OF TABLES

LIST OF FIGURES

LIST OF SYMBOLS / ABBREVIATIONS

Al	Aluminium
Al^{3+}	Aluminium ion
$AlCl_3$	Aluminium chloride
Al_2O_3	Aluminium oxide
$AlPO_4$	Aluminium phosphate
Ar	Argon
Ba	Barium
$BaCl_2$	Barium chloride
BaO	Barium oxide
C	Carbon
$C_6H_8O_7$	Citric acid
$C_6H_8O_7 \cdot H_2O$	Citric acid monohydrate
Ca	Calcium
Ca^{2+}	Calcium ion
CaO	Calcium oxide
$CaCl_2$	Calcium chloride
$CaCO_3$	Calcium carbonate
$Ca_2Fe_2O_5$	Dicalcium diiron pentaoxide
$Ca(NO_3)_2$	Calcium nitrate
$Ca(NO_3)_2 \cdot 4H_2O$	Calcium nitrate tetrahydrate
$Ca(OH)_2$	Calcium hydroxide
$CaZn(OH)_4$	Calcium zincate
Ce	Cerium
CeO_2	Cerium oxide
$C_2HF_3O_2$	Trifluoroacetic acid
CH_3KO	Potassium methoxide
CH_3NaO	Sodium methoxide
$C_2H_4(OH)_2$	Ethylene glycol
CH_3SO_3H	Methanesulphonic acid
CO_2	Carbon dioxide
Fe	Iron

Fe^{3+}	Iron (III) ion
$Fe(HSO_4)_3$	Iron (III) hydrogen sulphate
Fe_3O_4	Iron (II,III) oxide
$FeSO_4 \cdot 7H_2O$	Iron (II) sulphate heptahydrate
$Fe_2(SO_4)_3 \cdot 7H_2O$	Iron (III) sulphate heptahydrate
HCl	Hydrochloric acid
$HClSO_3$	Chlorosulphonic acid
He	Helium
HF	Hydrofluoric acid
HNO_3	Nitric acid
H_2O	Water
H_3PO_4	Phosphoric acid
H_2SO_4	Sulphuric acid
K	Potassium
K^+	Potassium ion
$KCaF_3$	Potassium calcium fluoride
K_2CO_3	Potassium carbonate
KF	Potassium fluoride
$KMgF_3$	Potassium magnesium fluoride
KNO_3	Potassium nitrate
KOH	Potassium hydroxide
K_3PO_4	Tripotassium phosphate
La^{3+}	Lanthanum ion
LaO	Lanthanum oxide
Li	Lithium
Li^+	Lithium ion
Li_2CO_3	Lithium carbonate
$LiNO_3$	Lithium nitrate
Mg	Magnesium
Mg^{2+}	Magnesium ion
$MgCl_2$	Magnesium chloride
MgO	Magnesium oxide
Mo	Molybdenum

MoO_3	Molybdenum trioxide
N_2	Nitrogen
Na	Sodium
Na^+	Sodium ion
Na_2CO_3	Sodium carbonate
$NaNO_3$	Sodium nitrate
NaOH	Sodium hydroxide
Na_2ZrO_3	Sodium zirconate
Nb	Niobium
NH_3	Ammonia
$(NH_4)_6Mo_7O_{24} \cdot 4H_2O$	Ammonium heptamolybdat-tetrahydrate
Ni	Nickel
Ni^{2+}	Nickel ion
$Ni(NO_3)_2$	Nickel (II) nitrate
$Ni(NO_3)_2 \cdot 6H_2O$	Nickel (II) nitrate hexahydrate
NiO	Nickel (II) oxide
O	Oxygen
Si	Silicon
SiO_2	Silicon dioxide
$SO_4{}^{2-}$	Sulphate ion
SO_3H	Sulphonic acid
Sr	Strontium
$Sr_3Al_2O_6$	Strontium aluminate
SrO	Strontium oxide
TiO	Titanium (II) oxide
TiO_2	Titanium dioxide
WO_3	Tungsten trioxide
Zn	Zinc
Zn^{2+}	Zinc ion
$Zn(CH_3COO)_2$	Zinc acetate
$ZnCl_2$	Zinc chloride
ZnO	Zinc oxide
Zr	Zirconium

Zr^{4+}	Zirconium ion
ZrO_2	Zirconia
$ZrOCl_2 \cdot 8H_2O$	Zirconyl chloride octahydrate
ZrO_4H_4	Zirconium hydroxide
BET	Brunauer-Emmett-Teller
BSA	Benzenesulphonic acid
BTAH	Benzyltrimethylammonium hydroxide
DTA	Differential thermal analysis
EDX	Energy dispersive X-ray
FAME	Fatty acid methyl ester
FFA	Free fatty acid
GC	Gas chromatography
HPA	Heteropoly acid
LPG	Liquefied petroleum gas
PTSA	p-Toluenesulphonic acid
SEM	Scanning electron microscopy
TCD	Thermal conductivity detector
TEA	Triethylamine
TEOS	Tetraethyl orthosilicate
TGA	Thermogravimetric analysis
TMAH	Tetramethylammonium hydroxide
TMG	Tetramethylguanidine
TPD	Temperature-programmed desorption
TSA	Tungstosilicic acid
XRD	X-ray diffraction

LIST OF APPENDICES

CHAPTER 1

INTRODUCTION

1.1 Background and Overview of Study

The challenge of energy supply has always aroused around the globe in view of the rapid increase in crude oil price, limited crude oil originated from fossil fuel resources as well as environmental issues. As of 2018, it was estimated that the world consumption had achieved up to 12,480 million tonnes of oil equivalent where about 87 % of this energy was originated from fossil sources (Hossein, et al., 2018). The large energy demand in the developed countries, most prominently in transportation sector has subsequently caused the increase of pollution upon the utilisation of fossil fuels, indicating the need to search for renewable energy sources which possess minimal environmental impacts. It directs the scientists and researchers to develop alternative sources as a substitute for oil-based fuels, where the potential fuel is expected to be acquired easily, environmentally benign and practically assessible based on technical and economic point-of-view (Meher, Vidga and Naik, 2006).

Although a number of renewable energy sources such as solar, hydropower and biomass have been discovered, fossil fuels are still deemed to account for a larger portion of energy consumption across the globe. By referring to Figure 1.1, 86 % of the world energy source was represented by oil, natural gas and coal in 2018, where approximately 5.7 % increase in coal consumption had been encountered in the same year (Hossein, et al., 2018). It was reported that coal has surpassed the average growth rate, experiencing the most rapid growth among non-renewable energy sources. Based on Figure 1.2, the primary energy consumption across the globe is forecasted to augment to almost 20,000 million tonnes equivalent by 2050, where it is projected that about 19 % of the world primary energy consumption is contributed by the oil including biofuels in 2050 (Mota, Pinto and Lima, 2017). It is expected that oil, coal and natural gas derived from fossil fuel resources are finite with the aforementioned consumption rate, and eventually the resources based on fossil fuels will be depleted in the near future.
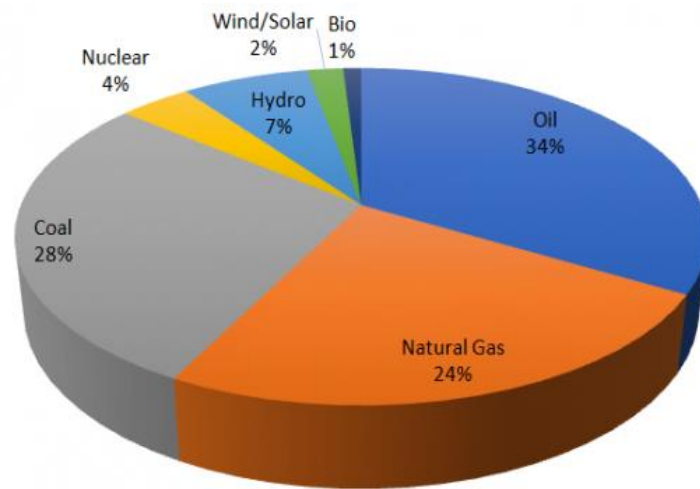
Figure 1.1: Global Energy Consumption in 2018 (Hossein, et al., 2018).
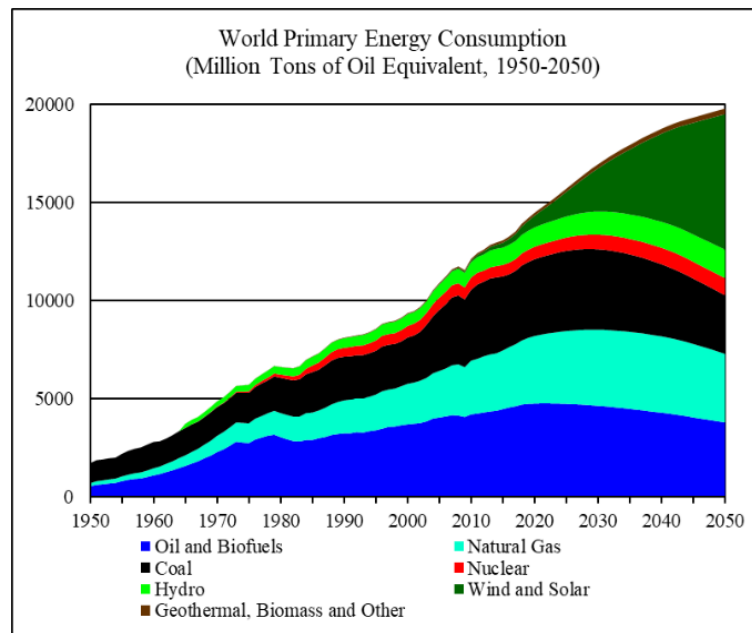
Figure 1.2: Preceding and Forecasted World Primary Energy Consumption from 1950 to 2050 (Mota, Pinto and Lima, 2017).

Since there is a significant increase of energy demand in Malaysia on account of the continuous economic development and growth, the emergence of renewable energy sources has gained a lot of attentions as the substitute for fossil fuels. Particularly, biodiesel has received a lot of attention recently as one of the favourable candidates to replace fossil fuels as it is environmental-friendly in nature. According to López, et al. (2009), the biodiesel possesses with almost similar properties as petroleum-derived diesel.
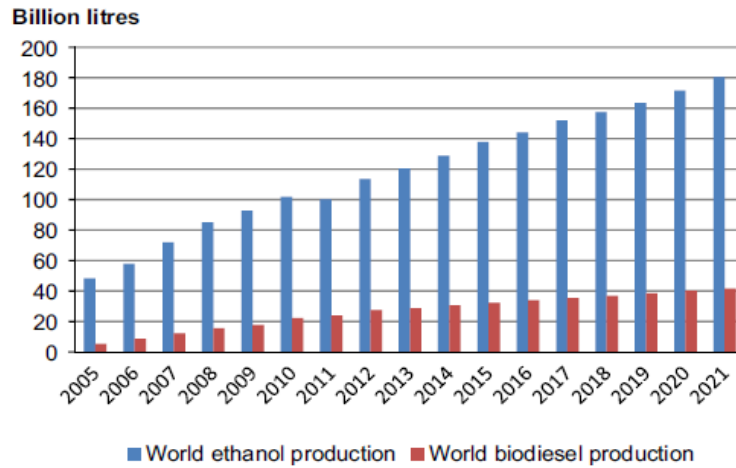
Figure 1.3: World Annual Biodiesel and Bioethanol Production between 2005 and 2021 (Xue, Grift and Hansen, 2011).

According to the statistics in Figure 1.3, the biodiesel is produced at a large scale in recent years, and it is expected to increase up to 42 billion litres by 2021 (Xue, Grift and Hansen, 2011).

In Malaysia, palm oil is the main raw material or feedstock used for biodiesel production as Malaysia is one of the largest producers of palm oil around the globe. Thus, it is strongly expected that the long-term development of biodiesel production will not only fulfil the energy demand for the country, but also allow the country to dominate the biodiesel production industry.

1.1.1 Challenges on Energy Sustainability

The current and forecasted final energy demand in member economies of Asia-Pacific Economic Cooperation (APEC) was reported by Lee (2019), as illustrated in Figure 1.4.
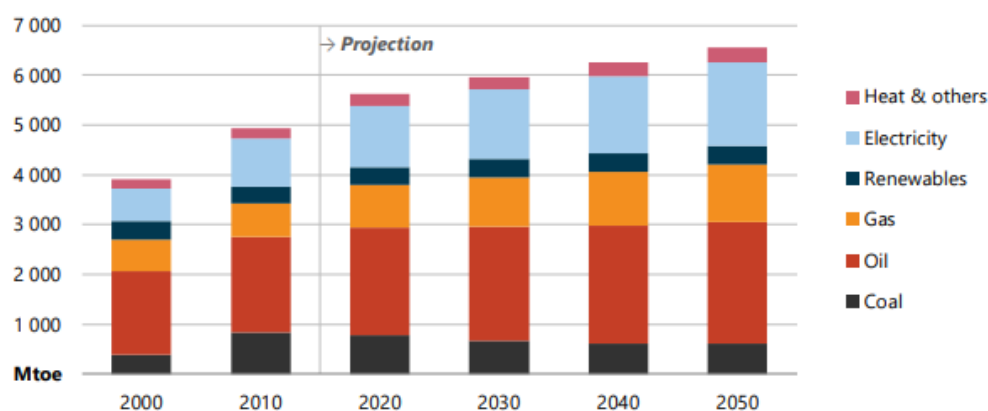
Figure 1.4: Current and Projected Final Energy Demand in Economies of APEC (Lee, 2019).

By referring to Figure 1.4, it is predicted that the total energy demand will achieve about 6,560 million tons of oil equivalent in 2050, which is approximately 21 % increase from 5,400 million tonnes of oil equivalent in 2016. Fossil fuels remain as the dominant energy source in the economies of APEC, where the demand for fossil fuels is forecasted to increase by 14 % to 4,200 million tonnes of oil equivalent in 2050. However, the energy demand for renewables is relatively lower than fossil fuels, where it is expected to show an overall growth from 330 million tonnes of oil equivalent in 2016 to 376 million tonnes of oil equivalent in 2050, which is largely driven by the transition from conventional fuels to biofuels in transport (Lee, 2019).

According to Omer (2018), Malaysia mainly relies on the energy sources such as diesel, motor petrol, liquefied petroleum gas, natural gas, coal and coke, with less dependency on fuel oil and biodiesel. The final energy demand based on different sources in Malaysia between 2010 and 2017 is summarised and illustrated in Table 1.1 and Figure 1.5 respectively.

Table 1.1: Final Energy Demand Based on Source in Malaysia from 2010 to 2017 (Omer, 2018).

Year	Final Energy Demand by Fuel Type (kilotons of oil equivalent)							
	Diesel	Fuel Oil	Motor Petrol	LPG	Natural Gas	Coal and Coke	Biodiesel	Total
2010	8,388	478	9,560	2,920	6,254	1,826	-	29,426
2011	8,712	414	8,155	2,892	8,515	1,759	24	30,471
2012	9,410	768	10,843	2,892	10,206	1,744	115	35,978
2013	9,568	329	12,656	2,946	10,076	1,539	188	37,302
2014	10,161	246	12,705	2,632	9,641	1,709	300	37,394
2015	9,377	498	12,804	2,261	9,566	1,778	389	36,673
2016	9,254	513	13,411	3,497	12,304	1,785	389	41,153
2017	9,747	579	13,437	3,514	16,838	1,804	379	46,298
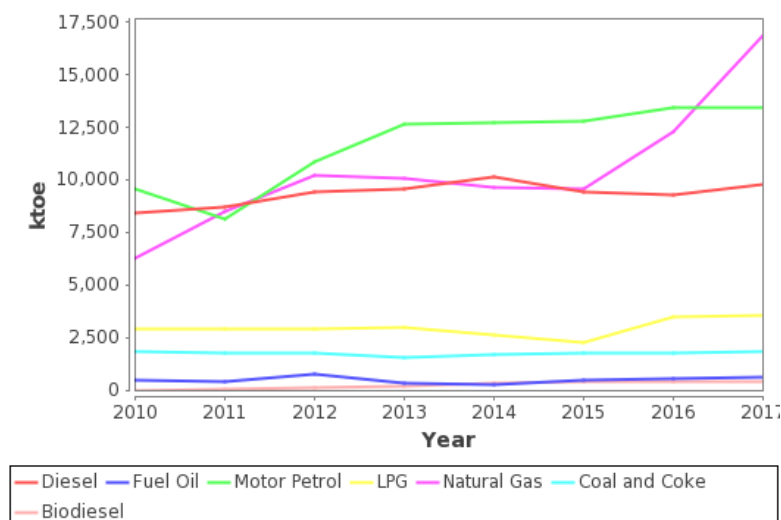
Figure 1.5: Final Energy Demand Based on Source in Malaysia from 2010 to 2017 (Omer, 2018).

The total energy demand in the country was increased from year to year where 46,298 thousand tonnes of oil equivalent was recorded in 2017. According to the statistics done by Omer (2018), the final energy demand of 2017 experienced a 12.5 % increase when compared with that of 2016. The energy demand in 2017 was contributed largely by natural gas (36.4 %), followed by motor petrol (29 %) and diesel (21.1 %). Since the derivatives of fossil fuels, namely crude oil and natural gas comprise a large percentage of energy demand, it is necessary for the country to reduce the overall dependence on fossil fuels and shift the demand to other alternative energy sources due to the fact the non-renewable energy sources are most likely to suffer from depletion in the near future. In spite of the forecast that the exhaustible fossil fuels will be dominating the energy sources, they are not able to cater for energy demand in long-term. Thus, the renewable and sustainable energies such as biofuel, wind, solar, water and wave can be developed as the potential fuel alternatives.

There is a positive relation between economy and energy demand in which they are growing in parallel, leading to the change in energy consumption (Hossein, et al., 2018). By referring to Dodić, et al. (2010), the energy consumption is speculated to achieve 83.5 million tons of oil equivalent with a growth rate of 5.4 % per annum up to 2020, where most of the energy are used in industrial, manufacturing and transportation sectors, as summarised and illustrated in Table 1.2 and Figure 1.6 respectively.

Table 1.2: Final Energy Demand Based on Sectors in Malaysia from 2010 to 2017 (Omer, 2018).

Year	Final Energy Demand by Sectors (kilotons of oil equivalent)					
	Industrial	**Transport**	**Agriculture**	**Non-Energy**	**Residential and Commercial**	**Total**
2010	12,928	16,828	1,074	3,696	6,951	41,477
2011	12,100	17,070	916	6,377	6,993	43,456
2012	13,919	19,757	1,053	7,497	7,065	49,291
2013	13,496	22,357	1,051	7,277	7,403	51,584
2014	13,162	24,327	1,045	6,217	7,458	52,209
2015	13,989	23,435	895	5,928	7,559	51,806
2016	16,019	24,004	415	8,729	8,049	57,216
2017	17,463	23,522	1,033	12,517	8,313	62,848
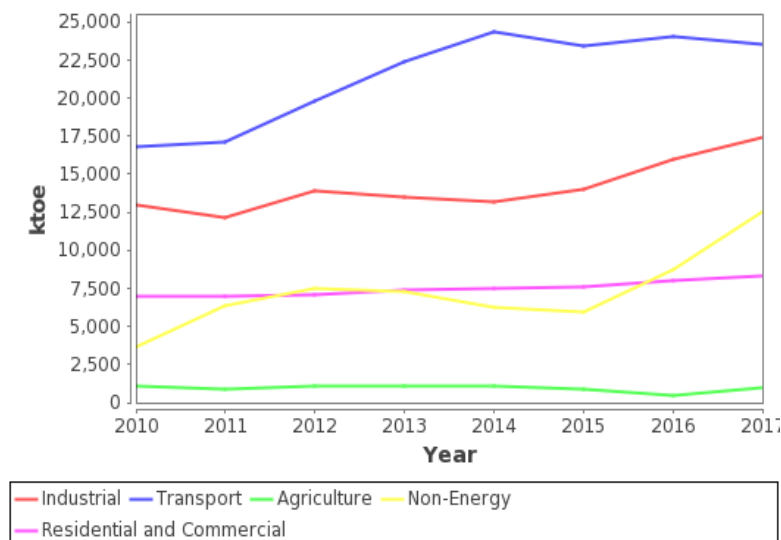
Figure 1.6: Final Energy Demand Based on Sectors in Malaysia from 2010 to 2017 (Omer, 2018).

Based on Table 1.2 and Figure 1.6, the maximum energy demand of 62,848 thousand tonnes of oil equivalent was achieved in 2017, where the main portion is contributed by transportation sector (37.4 %), followed by industries (27.8 %) and non-energy sector (19.9 %) (Omer, 2018). Although the industrial sector has recently exceeded other sectors, transportation still consumes a large portion of energy in Malaysia, where it plays a significant role to induce economy as well as globalisation. It is forecasted that the final energy consumption of Malaysia will possess an annual growth at the rate of 4.8 % up to 2030. Besides, the speculations have been made by Azman, et al. (2011) where each sector constitutes different increment in energy consumption for the coming 25 years, including transportation by 5.3 %, industry by 4.8 % as well as other sectors such as residential, commercial and agricultural sectors by 5.3 %, 4.8 % and 4.2 % per year respectively.

The transportation sector significantly constitutes adverse environmental impacts while consuming the finite non-renewable energy sources, especially the crude oil-based fuels, where it is suggested by Baumert, Herzog and Jonathan (2005) that about 13.5 % of global warming issues are emerged from transportation sector. Hence, there is a need to look for new energy sources, more precisely renewable energy sources that are more environment-friendly.

According to Hossein, et al. (2018), Malaysia as a developing country, is expected to experience an abrupt growth of energy demand at the rate of 3.3 % between 2005 and 2012, before possessing a slight increment to 3.4 % afterward until 2030. It is obvious that Malaysia requires more energy sources in order to meet the demand for energy source in the rapid growing economy in spite of the fact that Malaysia owns the second largest oil reservoir in Asia Pacific with total oil reserve of 5.6 billion barrel. Based on the production volume in 2005, the oil reserve in Malaysia is expected to be reliable for 15 years, whereas the country can only rely on its gas reserve for 29 years (Hossein, et al., 2018). Therefore, it is deduced that Malaysia will be depending on the oil imports starting from 2020 onwards if there is insufficient oil supply. Thus, Malaysia National Energy Policy 1979 aims for an environmentally benign energy supply with high efficiency, safety and reliability in the future, besides highlighting the need to introduce a clean and sufficient energy (Sulaiman, et al., 2011). Hence, the renewable energy sources should be investigated thoroughly as an alternative energy supply in order to cope with the accelerated economic development in Malaysia.

1.1.2   Renewable Energies in Global Countries and Malaysia

According to Demirbas (2009), petrodiesel fuels are finite reserves found in certain regions around the world, where these sources are projected to encounter the risk of attaining their peak production. Since the resources of fossil fuel are diminished progressively, the scarcity of known petroleum reserves tends to direct the society towards the exploration of renewable energy sources. Renewable energy is acquired from a natural process, where it does not utilise the scarce resources such as fossil fuels. Solar energy, wind energy, hydropower, biomass and geothermal energy are deemed as the commonly employed renewable energy sources around the world. The global consumption of renewable energy in 2023 is forecasted by Oh, Pang and Chua (2018) based on the current world consumption of renewable energy in 2017, as shown in Figure 1.7 and Table 1.3.

Figure 1.7: Current and Projected Global Renewable Energy Consumption in 2017 and 2023 (Oh, Pang and Chua, 2018).

Table 1.3: Current and Projected Global Renewable Energy Consumption in 2017 and 2023 (Oh, Pang and Chua, 2018).

Year	Renewable Energy Consumption (million tons of oil equivalent)				
	Biofuel	Hydropower	Wind	Solar	Geothermal
2017	460.1 (50.1 %)	283.5 (30.9 %)	84.7 (9.2 %)	68.3 (7.4 %)	21.7 (2.4 %)
2018-2023 (Expected Growth)	75.9	31.4	58.4	76.4	8.1
2023 (Forecasted)	536 (45.9 %)	314.9 (26.9 %)	143.1 (12.2 %)	144.7 (12.4 %)	29.8 (2.6 %)

As a matter of fact, biofuel is overlooked at all times as the promising renewable energy source. It is used as a renewable fuel for transportation as well as for heat delivery in industry. Biofuel accounted for half of all renewable energy consumed in 2017, where it provided three times the contribution of wind and solar energy combined. With the exception of solar energy, biofuel is expected to constitute the largest growth in renewable energy consumption over the period of 2018 to 2023, where it will account for about 30 % of the growth in total renewable energy consumption. By referring to Oh, Pang and Chua (2018), biofuel will remain as the predominant source of renewable energy in 2023 in spite of the decline in total energy consumption by 4.2 % on account of the accelerated expansion of both solar and wind energy in the electricity sector.

Besides natural gas, crude oil, coal and hydropower that are mainly employed as energy sources in Malaysia, the government has been investigating and searching for other possible sources of renewable energy. According to

Sulaiman, et al. (2011), the renewable energy only represents about 2 % of world energy utilisation in spite of the rapid growth in energy consumption. Malaysia is well endowed with immense sources of renewable energy including solar, mini hydropower, wind and biomass. Although the country has attained visible results by employing such renewable energy sources, yet more efforts are required in order to optimise the usage of renewable energy in Malaysia. Table 1.4 summarises the potentials of renewable energy in generating power in Malaysia. In fact, the biomass is currently being studied as an alternative fuel (Oh, Pang and Chua, 2018).

Table 1.4: Renewable Energy Potential in Malaysia (Oh, Pang and Chua, 2018).

Renewable Energy	Potential (MW)
Hydropower	22,000
Mini-hydro	500
Biomass	1,300
Municipal Solid Waste	400
Solar Photovoltaic	6,500

Malaysia has been actively implementing a broad range of policies with the purpose to stimulate the development in renewable energy field. The Five-Fuel Policy was introduced under the Eighth Malaysia Plan over a period between 2001 and 2005 where the renewable energies were incorporated in the list of fuel mix for power generation alongside natural gas, coal, oil and hydropower (Komor and Bazilian, 2005). The optimisation of fuel mix and exploration of renewable energy sources as alternative fuels will be given priority to mitigate the dependency of country on fossil fuels for electricity generation.

1.1.3   Biodiesel as Alternative for Renewable Fuel

It is stated by Demirbas, Balat and Balat (2009) that biomass energy constitutes about 10 to 15 % of the energy consumption around the world, causing it to emerge as one of the important energy sources in most of the Asian countries. Numerous countries in Asia including Malaysia have targeted to use biomass-derived fuels as an alternative renewable fuel (Mahlia, et al., 2001). Among various sources of renewable energy, biodiesel fuels are significantly attracting a lot of attentions around the globe as the blending components or direct substitute for diesel fuel in vehicle engines (Demirbas, 2008). It is a renewable fuel synthesised from biological sources such as vegetable oils or animal fats, targeting to replace petroleum diesel or petrodiesel fuel, where a variety of oil feedstocks such as palm oil, soybean oil and rapeseed oil are currently employed for biodiesel production. It is stated by Leung, Wu and Leung (2010) that the demand towards biodiesel is projected to attenuate the dependency of the country on conventional fossil fuels as the latter diesel fuel has greatly contributed to global warming with the emission of greenhouse gases such as carbon dioxide, and hazardous compounds such as sulphur, particulate matter and nitrogen oxide.

Biodiesel is applicable in any mixture with petroleum-based fuel as an additive due to the fact that it possesses nearly similar characteristics with petrodiesel, which is accompanied by an additional advantage where it only creates low exhaust emissions upon burning as a fuel. Eventually, it can be mixed with normal petroleum-based diesel at any ratio, where it can retain the performance of engine without any deterioration. (Ahmad, et al., 2011). Besides, biodiesel is also considered as an environmentally benign and sustainable fuel as it can be used as a 100 % fuel in any diesel engine without further modification (Banković–Ilić, et al., 2014). As a matter of fact, biodiesel is the first and only alternative fuel for commercial diesel that possesses a complete evaluation of emission results. By referring to Demirbas (2009), biodiesel fuel possesses several outstanding benefits over petrodiesel fuel as it is renewable, biodegradable, non-toxic and essentially free of sulphur and aromatics. According to Banković–Ilić, Stamenković and Veljković (2012), the biodiesel can be derived from oils and fats disposed as waste which are originated from

restaurants, households as well as food industry, and hence reducing the production cost and resolving waste disposal issues.

In general, an alternative fuel to petrodiesel must be technically feasible, economically competitive, environmentally sustainable and highly available. Currently, biodiesel is able to fulfil all the criteria for the alternative diesel fuel as it provides other advantages over other renewable and clean engine fuel alternatives, such as reducing greenhouse gas emissions as well as improving regional development and social structure, especially for developing countries (Demirbas and Demirbas, 2007). In other words, the use of biodiesel is expected to seek a balance between agriculture, economic development and environment (Demirbas, 2007). It is proved by Demirbas (2008) that biodiesel is a superior lubricant where it performs about 66 % better than conventional petrodiesel, which is mainly due to the absence of sulphur content. Hence, biodiesel methyl esters are capable in improving the lubrication properties of diesel fuel blend, and thus reducing the long-term engine wear in diesel engines, leading to a better durability of engine.

Table 1.5: Top 10 Countries in Terms of Absolute Biodiesel Production in 2018 (Johnston and Holloway, 2018).

Country	Volume (million litres)	Production Cost ($/L)
Malaysia	14,540	0.53
Indonesia	7,595	0.49
Argentina	5,255	0.62
United States	3,212	0.70
Brazil	2,567	0.62
Netherlands	2,496	0.75
Germany	2,024	0.79
Philippines	1,234	0.53
Belgium	1,213	0.78
Spain	1,073	1.71

The 10 worldwide leading producers of biodiesel are listed in Table 1.5. It is known that the biodiesel production in Malaysia is beyond other countries as the oil palm is abundantly available which primarily drives for its

development in the biodiesel industry. In fact, it is required to possess a consistent inflow of feedstock at a reasonable price in order to retain its competitive advantages over petroleum-derived diesel. However, Malaysia is not dependent on the import of raw materials from other countries for further development in view of the high availability of oil feedstocks. Besides, the independence in raw materials supply allows the biodiesel producers in Malaysia to possess a more effective control on cost and quality (Abdullah, et al., 2009). Thus, it is adequate to affirm that the substantial oil palm resources are able to cater for biodiesel production in industrial scale to replace fossil fuels.

Currently, the capacity of biodiesel is estimated to be 15 billion litres in Malaysia (Wei, May and Board, 2018). According to Sumathi, Chai and Mohamed (2018), it was recorded that more than 20 biodiesel plants were operating in Malaysia, constituting an annual production capacity of 14.54 billion litres of biodiesel in late 2018. Meanwhile, the efficiency of energy acquired from oil palm is 50 % or corresponds to eight million tons of oil equivalent, which is projected to save around RM7.5 billion of crude oil annually (Hossein, et al., 2018).

1.2   Importance of Study

By referring to Demirbas (2009), the fossil fuel resources available at the present time are forecasted to be exhausted before 2050 due to the fact that the consumption is five times faster than the production from natural resources. Hence, biodiesel is used as an alternative diesel fuel derived from renewable sources with high quality in order to fulfil the energy demand in the country which is previously catered by fossil diesel oil. With the advancement of biodiesel industry in Malaysia, the production capacity of biodiesel becomes inevitably extensive. In this study, a high-performance catalyst is aimed to be developed and synthesised in order to accelerate the transesterification rate for the production of biodiesel, besides enhancing the solubility of alcohol in oil. After verifying the catalyst through in-depth literature reviews, researches and laboratory works, it can serve as a potential guide for industrial use on account of its superior catalytic activity. In industrial perspectives, it is indispensable to develop a catalyst which is able to produce high biodiesel yield to cope with the high-demand biodiesel production.

Particularly, the nano CaO catalyst is synthesised from waste eggshells as the carrier, where it is a universal catalyst that can cater for a broad range of oil feedstocks. According to Banković–Ilić, et al. (2017), CaO catalyst itself is cheap, easily available, non-corrosive, environment-friendly and easy to handle, besides possessing an ability to be regenerated and reused. It is well informed by other researchers regarding the performance of neat CaO catalyst, where it possesses certain limitation such as low basic strength. Thus, the Ni dopant is incorporated into CaO nanocatalyst as an additive by means of wet impregnation to increase the active sites of catalyst in order to improve the overall catalytic performance. Besides, the NiO dopant is incorporated into CaO nanocatalyst by means of sol-gel method, where it is used to screen with Ni doped CaO nanocatalyst synthesised via wet impregnation in order to identify the more effective dopant. In other words, two possible catalyst synthesis techniques, namely wet impregnation and sol-gel method producing Ni/CaO nanocatalyst and NiO/CaO nanocatalyst respectively are investigated based on their catalytic performance. In this context, the parameters such as amount of dopant loading on CaO nanocatalyst and calcination temperature which are expected to affect the catalytic activity are studied and optimised for achieving maximum biodiesel yield.

1.3   Problem Statement

The biodiesel is viable to replace the petroleum-based diesel in the future to reduce the dependency of scarce fossil fuels, besides ensuring a greener environment. However, the production cost of biodiesel is 1.5 to 3 times higher than that of fossil-derived diesel on account of the high demand for edible oil (Demirbas, 2007). The cost for producing biodiesel must be more competitive and economical than that of fossil fuels in order to use it as substitute. In fact, the catalyst synthesis for biodiesel production is significant as it generally contributes up to 75 % of the overall production cost of biodiesel (Gui, Lee and Bhatia, 2008). Hence, there is a need to develop a cost-effective catalyst by synthesising from biomass such as waste eggshells.

Heterogeneous or solid base catalysts are the ultimate choice for biodiesel production as they are neither dissolved nor consumed in the reaction medium, allowing an easy separation from the product (Takagaki, et al., 2006).

According to Singh, et al. (2014), heterogeneous base catalysts are recovered easily to be reutilised in the reaction, and thus reducing the catalyst consumption. Moreover, they are generally non-corrosive, besides constituting a longer catalyst life (Konwar, Boro and Deka, 2014). In the context of economics, the high production cost of biodiesel is mainly owing to the expensive catalyst. Among various heterogeneous base catalysts in the market, the metal oxide such as calcium oxide is commonly employed to produce biodiesel owing to its low cost, superior activity and easy availability (Gotch, Reeder and McCormick, 2009). Hence, the cost of catalyst synthesis can be subsequently reduced by synthesising the catalyst from calcium oxide derived from natural resources.

It is known that the reagent-grade CaO poses an extremely high price as it requires various chemicals to establish multiple preparation steps (Smith, et al., 2013). Hence, a more environmentally friendly catalyst has been extensively investigated through a substantial number of studies in order to replace the conventional heterogeneous base catalyst. In this study, the CaO catalyst is synthesised from waste eggshells in order to produce the biodiesel which is more sustainable, environmentally benign and cost-effective. Generally, the $CaCO_3$ enriched eggshells will be calcined at high temperature before converting to CaO as CaO is proven as the base catalyst with high activity in producing biodiesel. In fact, CaO catalyst can be derived from $CaCO_3$ in limestone, but it is non-renewable and possesses a synthesis route that is burdensome in terms of length and cost (Correia, et al., 2014). Hence, it makes the organic wastes such as waste eggshells to become more outstanding due to their non-toxicity, low cost, safe handling and storing procedure, abundant availability and most importantly they are originated from renewable sources (Smith, et al., 2013). Besides, the use of renewable materials will contribute to less environmental problems and significantly reduce the cost associated with their disposal as it is biodegradable. According to Buasri, et al. (2013), waste eggshells are mainly composed of 96 to 98 % of $CaCO_3$, making them a better option of renewable source to synthesise the CaO-derived catalyst.

Although the heterogeneous CaO catalyst is regenerable, the presence of three-phase system comprising of solid catalyst, alcohol and oil tends to cause mass transfer problem. According to Zabeti, Daud and Aroua (2009), these three components are highly immiscible with each other, limiting the diffusion

efficiency, and thus lowering the rate of reaction. Besides, the solid CaO catalyst is microporous and possesses a relatively low number of active sites (Lam, Lee and Mohamed, 2010). In fact, a large specific surface area in terms of hydrophobicity and external active sites as well as large pore diameter should be the criteria to select a feasible catalyst (Macario and Giordano, 2013).

In this context, the biodiesel production can be further improved by developing a nano-sized CaO catalyst where it is targeted to enhance the catalytic activity by augmenting the specific surface area in nano form. It is inferred by Galchar, J.B. (2017) that the large ratio of surface area to volume characterised by the nanocrystalline CaO catalyst can augment the active basic sites which are responsible for the catalytic activity. In addition, it also constitutes a large pore size, enhancing the performance of CaO catalyst. Thus, the nano CaO catalyst can in turn increase the conversion rate of oil feedstock as well as the production yield of biodiesel by significantly reducing the reaction time.

Besides, the catalyst must be sustainable for continuous production of biodiesel. Hence, the Ni dopant is incorporated to the nano CaO catalyst by means of wet impregnation to occupy the vacant lattice sites within the active catalyst by altering the catalyst properties with the purpose to improve the overall performance of nano CaO catalyst. It is expected that by incorporating the dopant such as transition metal to the nano CaO catalyst, the reaction will take lesser time, which in turn increases the reaction rate for a more economical production with a higher biodiesel yield. Thus, it can be presumed that the waste-derived CaO nanocatalyst with Ni dopant is able to achieve the outstanding performance in terms of reaction rate for an upgraded production of biodiesel as a whole, besides reducing the production cost. In addition, the NiO doped CaO nanocatalyst which is expected to constitute good catalyst performance, is synthesised by means of sol-gel method for preliminary study, where the efficiency of both dopant types are evaluated to select the catalyst that constitutes a higher catalytic performance in terms of biodiesel yield before conducting parameter studies and optimisation.

1.4   Aims and Objectives

The aim of this research is to investigate the performance of Ni doped CaO nanocatalyst after the treatment of wet impregnation-calcination as well as NiO doped CaO nanocatalyst after the treatment of sol-gel-calcination in catalysing transesterification reaction for biodiesel production. The general outline of project objectives is listed as follows:

(i)   To screen for the suitable dopant of CaO catalyst between Ni doped CaO synthesised via wet impregnation and NiO doped CaO synthesised via sol-gel method for catalysing transesterification reaction.

(ii)   To conduct the characterisation studies on the physical and chemical properties of doped CaO catalyst synthesised at different dopant dosage and calcination temperature.

(iii)   To study the effect of dopant loading and calcination temperature on the catalytic performance of doped CaO catalyst in transesterification reaction.

(iv)   To optimise the dopant loading and calcination temperature for achieving maximum biodiesel yield in transesterification reaction catalysed by doped CaO catalyst.

1.5   Scope and Limitation of Study

The scope of this research is outlined based on the objectives, where it mainly focuses on the approach of synthesising doped CaO catalyst. The feasibility of catalyst is indispensable due to its capability to expedite the biodiesel production in long-term. Hence, it is essential to study the appropriateness of catalyst to be employed in biodiesel production. Besides, a wide variety of methods including wet impregnation and sol-gel for catalyst synthesis are also reviewed alongside different natures of catalyst in industrial application.

The activity of Ni doped CaO catalyst prepared via wet impregnation and NiO doped CaO catalyst prepared via sol-gel method are investigated for preliminary study. The performance of doped CaO catalyst is analysed and evaluated based on the biodiesel yield produced from transesterification reaction in order to identify the more effective dopant. The ultimate CaO catalyst which possesses superior performance in respect of biodiesel yield will

be selected before conducting the characterisation and parameter studies. The physicochemical properties of the synthesised catalyst such as phase identity, surface morphology, elemental composition, thermal stability and basicity are determined through catalyst characterisation using various analytical instruments such as x-ray diffractometer, scanning electron microscope, energy dispersive x-ray spectrometer, thermogravimetric analyser and temperature-programmed desorption analyser. The parameters such as dopant loading and calcination temperature are examined to determine the effectiveness of catalyst in terms of biodiesel yield.

However, there are several limitations needed to be considered for further improvement in the near future. The study is predominantly focused on the catalyst synthesis process alongside the optimisation of parameters affecting the catalytic performance. Meanwhile, other operating parameters affecting the rate of transesterification in biodiesel production such as catalyst loading, alcohol-to-oil molar ratio, reaction temperature and reaction time are only studied in literature review instead of being investigated in experimental works. There are limited number of slots available for several characterisation instrument, including TGA. Besides, the specific surface area analysis is not able to be carried out due to the unavailability of BET instrument.

1.6   Contribution of Study

In this research, the most feasible catalyst for biodiesel production will be figured out as it plays a key role in enhancing the rate of transesterification. The findings on the improvement of biodiesel production with the utilisation of catalyst is crucial to the energy system of local country as well as worldwide countries as the biodiesel is the potential renewable energy source to replace fossil fuels which are getting scarce and expected to be depleted in the near future. Besides expediting the rate of biodiesel production, the catalyst is also important in minimising the wastes generated during the production of biodiesel in order to conserve the environment by continuously maintaining the atmospheric stability.

1.7   Outline of Report

This report is divided into five major chapters, where it is started off with the background of research which explains the purpose of this study. Chapter 1 details the significance of employing biodiesel as the energy source, the current challenges faced in the biodiesel production and the solution to overcome it.

Chapter 2 is the literature review on the potential feedstocks and catalysts that are commonly used in biodiesel production. Besides, the widely employed technologies for catalyst synthesis are discussed and reviewed, followed by the evaluation on the parameters that affect the performance of catalyst in biodiesel production as well as the characterisation in determining the physicochemical properties of catalyst. Eventually, the type of catalyst and the dopant to be used in enhancing the rate of biodiesel production as well as minimising the production cost are selected for catalyst synthesis and further analysis.

Chapter 3 shows the methodology of study starting with the catalyst preparation either from waste eggshells or commercial chemicals, followed by the doping process before carrying out the transesterification to produce biodiesel. Other than that, the characterisation to be conducted are elucidated in order to study the physical and chemical properties of synthesised doped catalyst.

Chapter 4 presents the results obtained from both the characterisation and experiment as well as the discussion on the analysis results. The two selected dopants for CaO catalyst, namely Ni for wet impregnation and NiO for sol-gel method are first screened in terms of biodiesel yield before proceeding with subsequent analysis. The effect of impregnation of metal dopant into catalyst as well as several parameters which include dopant loading and calcination temperature on physicochemical properties of doped catalyst and catalytic performance in transesterification reaction with respect to biodiesel yield are discussed in detail. The optimum parameters of catalyst synthesis are outlined at last in order to determine the most efficient catalyst for biodiesel production.

Chapter 5 is the conclusion and recommendation for further improvement in future study, which are mainly due to the imperfection of methodology found while conducting the research.

CHAPTER 2

LITERATURE REVIEW

2.1   Potential Feedstocks for Biodiesel Production

There are numerous raw materials that can be utilised to produce biodiesel. According to Kumar and Sharma (2016), there are currently more than 350 oil feedstocks available globally for biodiesel production. Several prominent examples are vegetable oils, animal fats, algae oils as well as microbial oils. The purity and composition of biodiesel are varied according to their respective raw material sources as claimed by Mahdavi, Abedini and Darabi (2015). Hence, the selection of feedstock is indispensable as it not only affects the composition and purity, but also determines the cost of raw material incurred as well as the final yield of biodiesel produced. Dennis, Leung and Leung (2010) inferred that the cost of raw materials makes up about 60 to 80 % of the total cost of biodiesel production. Therefore, it is crucial to select a suitable feedstock in producing high quality biodiesel as the type of feedstock chosen is one of the chief factors in determining the properties of biodiesel produced.

The available feedstocks are categorised according to the source type, which are typically comprised of vegetable oils (edible and non-edible oils) and waste cooking oils (Demirbas, 2009). The selection of raw materials in producing biodiesel is also dependent upon the country. For instance, soybean oil is widely utilised as one of the main sources to produce biodiesel in United States, whereas the biodiesel production in Europe and other tropical countries is mainly contributed by palm oil and rapeseed oil (Singh and Singh, 2010). By analysing and evaluating the physical properties, chemical composition, oil content as well as its suitability of raw material, the selection of feedstock can be accomplished in order to achieve promising biodiesel yield.

The raw materials are termed as renewable oils as they can be extracted from widely available crop seeds based on agro-climatic conditions in various regions. For instance, soybean oil is derived mostly in United States, canola oil in Canada, and rapeseed oil in northern Europe. For tropical countries like Malaysia, edible oils such as palm oil, coconut oil and sunflower oil are commonly extracted from their respective sources for biodiesel production. The

extraction of animal fats such as bovine fat, fish oil, pig fat, duck and beef tallow as well as lard are also considered as renewable oils which are developed in Ireland (Karmakar, Karmakar and Mukherjee, 2010).

Table 2.1: Sources of Oil and Fats for Biodiesel Production (Ambar, Srivastava and Sillanpää, 2018).

1st Generation	2nd Generation		3rd Generation
Edible Oils	Non-edible Oils	Waste Oils or Animal Fats	Microalgal Oils
Sunflower oil	Jatropha oil	Mutton fat	Algae oil
Soybean oil	Stillingia oil	Broiler chicken waste	Microalgae oil
Rapeseed oil	Karanja oil	Pork lard	Bacteria
Peanut oil	Neem oil	Waste cooking oil	Fungi
Olive oil	Castor oil	Pine and kapok oil	Microbial oil
Canola oil	Sylbum marianum oil	Waste fish oil	
Palm oil	Rubber seed oil		
Coconut oil	Cottonseed oil		
Mustard oil	Tobacco seed oil		
Linseed oil	Mahua oil		
Almond kernel oil	Jojoba oil		
Walnut kernel oil	Salmon oil		
Sesame oil			
Rice bran oil			
Barley oil			
Corn oil			

Table 2.1 summarises the various raw material sources including edible oils, non-edible oils, waste oils or animal fats and microalgal oils for biodiesel production. In the research done by Kumar and Sharma (2016), biodiesel production from palm oil is infeasible in India as more than 68 % of edible oils are imported from Malaysia and Indonesia to meet the food requirement. Hence, the non-edible oils as the 2nd generation feedstocks have become the alternatives to replace edible oils for biodiesel production. However, these oils suffer from low yields and space constraints as there is a need of large land area for their

production. Nowadays, the 3rd generation microalgal oil feedstocks are developed due to their rapid oil production which is nearly 30 times more than vegetable oils in short period of time with small land requirement.

Edible oils such as soybean oil, sunflower oil, rapeseed oil and palm oil are employed as main feedstocks for biodiesel production all over the world. Karmakar, Karmakar and Mukherjee (2010) stated that non-edible oils including jatropha oil, neem oil and pongamia oil have been proven to be potential feedstocks as substitutes in developing countries where edible oils are not abundantly available. By referring to the research conducted by Borugadda and Goud (2012), rapeseed oil has been the ultimate choice in the older days and is still leading in the biodiesel production with over 80 % of utilisation as raw material source due to its high suitability. Over 10 % of the biodiesel production utilises sunflower oil as feedstock, which is followed by soybean oil. Recently, several biodiesel feedstocks are emerged as potential alternatives, which include mustard oil, castor oil, peanut oil, coconut oil, cottonseed oil, corn oil, neem oil, mahua oil, rice bran oil, sesame oil, karanja oil, tobacco oil, passion seed oil, algae oil, grape oil, babassu oil, waste vegetable oil, hemp and coffee ground (Karmakar, Karmakar and Mukherjee, 2010).

2.1.1 Edible Oils

There are more than 95 % of biodiesel production that utilise edible oils as feedstocks due to the fact that they are produced at large quantities in many regions worldwide. Besides, the properties of biodiesel produced from these oils are more promising to become the substitute for diesel fuel (Borugadda and Goud, 2012). However, the utilisation of edible oils in producing biodiesel is greatly affected by food use. In other words, the practice of supplying the currently available renewable oil from industrialised agriculture for biodiesel production can strike a conflict between the crop production for energy use, as opposed to food (Karmakar, Karmakar and Mukherjee, 2010). The imbalance has been drawn a lot of attentions and concerns from the society as the competition of biodiesel production with the food market is known to unfavourably affect the biodiesel price in a long run (Gashaw and Lakachew, 2014). Atabani, et al. (2013) stated that the use of edible vegetable oils as the feedstocks for biodiesel production might cause starvation especially in the

developing countries due to overutilisation of arable lands for food crops. The ecological imbalances are created as the deforestation is required for plantation purposes, which subsequently endangers the wildlife in the forests. Table 2.2 shows the edible oils as potential feedstocks and the oil content as well as oil yield for each feedstock.

Table 2.2: Edible Oils as Feedstocks for Biodiesel Production (Karmakar, Karmakar and Mukherjee, 2010).

Feedstock	Oil Content (%)	Oil Yield (L/ha)
Sunflower Oil	25-35	952
Soybean Oil	15-20	446
Rapeseed Oil	38-46	1190
Peanut Oil	45-55	1059
Olive Oil	45-70	1212
Canola Oil	40-45	-
Palm Oil	30-60	5950
Coconut Oil	63-65	2689
Linseed Oil	40-44	-
Palm Kernel Oil	44-65	-
Corn Oil	48	172
Rice Bran Oil	15-23	828
Sesame Oil	50	696

2.1.2 Non-edible Oils

The use of edible oils for biodiesel production is not feasible due to the fact that there is a large difference in supply and demand of these oils as the source of food. Since the biodiesel produced from edible oil feedstocks will be expensive as a result of higher demand as food source, the utilisation of edible vegetable oils in producing biodiesel is diverted to non-edible oils such as castor oil, jatropha oil and neem oil. One of the most significant advantage is that the costs incurred for non-edible feedstocks are lower than that for edible oils, besides avoiding the competition with food market (Aransiola, et al., 2014). Furthermore, the biodiesel produced by non-edible oils does not contain sulphur

or aromatic compounds, leading to the reduction of carbon monoxides, particular matters and hydrocarbons emission upon combustion (Shu, et al., 2010).

Non-edible vegetable oils are not suitable for food in view of the presence of certain toxic components (Ahmad, et al., 2011). The biodiesel production from non-edible oils can overcome the problems related to edible oils in terms of food versus fuel, environmental and economic issues. Besides, the cultivation cost for non-edible oil crops is lower than that of edible oil crops because a reasonably high biodiesel yield still can be sustained without intensive care (Dennis, Leung and Leung, 2010). According to Ahmad, et al. (2011), the non-edible feedstocks are considered as sustainable and alternative fuels in order to produce biodiesel as the non-edible biodiesel development can help to alleviate the poverty in rural areas as well as providing energy security in general and particularly to rural areas by upgrading the rural non-farm sectors.

However, most of the non-edible oils involve the procedure comprising of multiple steps or alternative approaches in producing biodiesel as they contain a higher content of FFAs, leading to the increased production cost. The methyl ester yield of biodiesel may be reduced below the standards under certain circumstances. Table 2.3 shows the non-edible oils as potential feedstocks and the oil content as well as oil yield for each feedstock.

Table 2.3: Non-edible Oils as Feedstocks for Biodiesel Production (Karmakar, Karmakar and Mukherjee, 2010).

Feedstock	Oil Content (%)	Oil Yield (L/ha)
Jatropha Oil	30-40	1892
Stillingia Oil	44.15	-
Karanja Oil	27-39	-
Neem Oil	20-30	-
Castor Oil	45-50	1413
Rubber Seed Oil	53.74-68.35	-
Cottonseed Oil	18-25	325
Mahua Oil	35-42	-

Tobacco Seed Oil	30-43	-
Jojoba Oil	45-50	1818

2.1.3 Waste Oils and Animal Fats

Waste oils are derived from edible oils, non-edible oils, petroleum oils or even synthetic oils once they become unsuitable for its original purpose after several usage or handling procedures (Borugadda and Goud, 2012). The properties of waste oils are undesirable due to the presence of impurities. However, the waste oils can be made full use in biodiesel production. For instance, even though the used frying oil is not appropriate to be consumed, but it is one of the feasible feedstocks for biodiesel production.

The waste lipids are produced in enormous amount from food processing industries, restaurants, fast food shops, roadside stalls and residential areas. According to Dennis, Leung and Leung (2010), the environmental problems are literally arisen in most of the countries around the world and become more severe nowadays mainly due to the disposal of waste cooking oils and fats. In fact, the waste oils can be managed properly by utilising them as the feedstocks for biodiesel fuel instead of disposing them. The used cooking oils available from restaurants and households are gaining a lot of attention from researchers as they are cheaper to be used as potential alternatives for biodiesel production. In other words, the usage of waste oils significantly reduces the cost incurred for biodiesel production on account of the higher raw material costs contributed by crude and refined vegetable oils. Furthermore, the use of waste cooking oil as a feedstock for biodiesel production does not directly conflict with food accessibility (Dennis, Leung and Leung, 2010).

Animal fats are another raw material source for biodiesel production. For example, the food processing and service facilities based on animal meats produce a large amount of waste animal fats after collecting and processing animal carcasses (Janaun and Ellis, 2010). Hence, it is viable to produce biodiesel by utilising animal fats as raw materials with less cost incurred. Common animal fats including pork lard, mutton or beef tallow as well as the residues from fish oil as a result of the production of omega-3 fatty acids are the waste products from meat industries, leather industries as well as fish processing (Paul, Patel and Prem, 2014). Among those animal fats, chicken fat, tallow and

lard have been successfully processed as potential feedstocks for biodiesel production in industrial scale.

Generally, waste fats from animal containing low saturated fatty acids possess outstanding stability towards oxidation, high calorific value as well as short hold-up in ignition (Adewale, Dumont and Ngadi, 2015). Although animal waste feedstocks have significant food security, environmental and economical advantages in comparison with edible oils, the complicated production techniques are required by the waste fats from animal containing high saturated fatty acids as well as FFAs. Thus, a relatively higher temperature is required for the biodiesel production from waste animal fats as compared to the conversion processes of used cooking oils (Ngo, et al., 2008).

2.1.4 Microalgal Oils

Apart from edible and non-edible oils, the current researchers are more focusing towards sustainable and renewable oils since the life span posed by raw materials is an important parameter and needs to be assessed for a better quality of biodiesel besides oil percentage and oil yield (Demirbas, 2009). Hannon, et al. (2010) stated that microalgae have become one of the alternative precursors for biodiesel production recently as it is more environmental-friendly and considered as a potential inexhaustible source of biodiesel. By referring to Paul, Patel and Prem (2014), microalgae are getting a lot of attentions from the society following the price surging of non-renewable petrodiesel fuel as well as serious global warming and greenhouse effect due to the combustion of fossil fuels. As compared with edible oils, microalgae are very economical because it produces a higher oil yield compared to other oil crops. Besides, microalgae are easier to grow as they do not require farmland or fresh water for cultivation (Mata, Martins and Caetano, 2010). Scott, Davey and Dennis (2010) claim that microalgae are biodegradable and relatively harmless if they are unintentionally spilled to the environment.

Many microalgae yield a considerably high oil productivity which greatly exceeds the biodiesel yield from the best producing oil crops. By referring to the research done by Ahmad, et al. (2011), microalgae such as Schizochytrium with high oil content up to 77 % is potential to yield biodiesel that is up to 25 times higher than the yield produced by traditional biodiesel

crops, such as palm oil. Hence, microalgae have been recognised as a potential source for biodiesel production which is previously dominated by palm oil as it is able to produce a more promising biodiesel yield. In another research conducted by Hossain, et al. (2008), microalgae can produce up to 250 times of the oil yield per acre as soybean oils. Yusuf (2007) reported that microalgae is emerged to be the only source of renewable oils that is capable to fulfil the global demand for transport fuels. Microalgae feedstocks are receiving great attention as energy sources because they possess rapid growth potential coupled with reasonably high carbohydrate, lipid and nutrient contents (Singh and Gu, 2010).

However, microalgal oils constitute certain drawbacks as biodiesel feedstocks because there is a need to incur a high investment in converting algae to biofuels. Besides, other challenges such as extraction of oil, processing of fuel and management of residues are also arisen as the concern among the researchers in the development of algal oil to produce biodiesel (Ambar, Srivastava and Sillanpää, 2018).

2.1.5 Comparison on Advantages and Disadvantages of Biodiesel Feedstocks

Table 2.4: Advantages and Disadvantages of Potential Feedstocks for Biodiesel Production (Ambar, Srivastava and Sillanpää, 2018).

Biodiesel Feedstock		Advantages	Disadvantages
1st Generation	Edible Oils	➢ Properties are suitable to be used as diesel fuel substitute	➢ Increases demand for food as well as fuel ➢ Creates serious ecological imbalances
2nd Generation	Non-edible Oils	➢ Eliminates food imbalance ➢ Reduces production cost of biodiesel ➢ Less requirement of land for cultivation ➢ Eco-friendly in nature	➢ Highly viscous in nature ➢ Production is not up to commercial demand ➢ More alcohols are required for transesterification
	Waste Oils and Animal Fats	➢ Low processing cost ➢ Food accessibility remains unaffected	➢ Contains undesirable impurities such as water and FFAs

3rd Generation	**Microalgal Oils**	➢ High growth rate and productivity ➢ Higher percentage of oil content ➢ Less effect on food chain balance ➢ Lower competition towards agricultural land ➢ Reduces greenhouse effect	➢ Sunlight is required for growth ➢ Suffers from difficulties in oil extraction ➢ Production on commercial scale is still under development ➢ Large capital and production costs

2.2   **Catalytic Processes in Biodiesel Production**
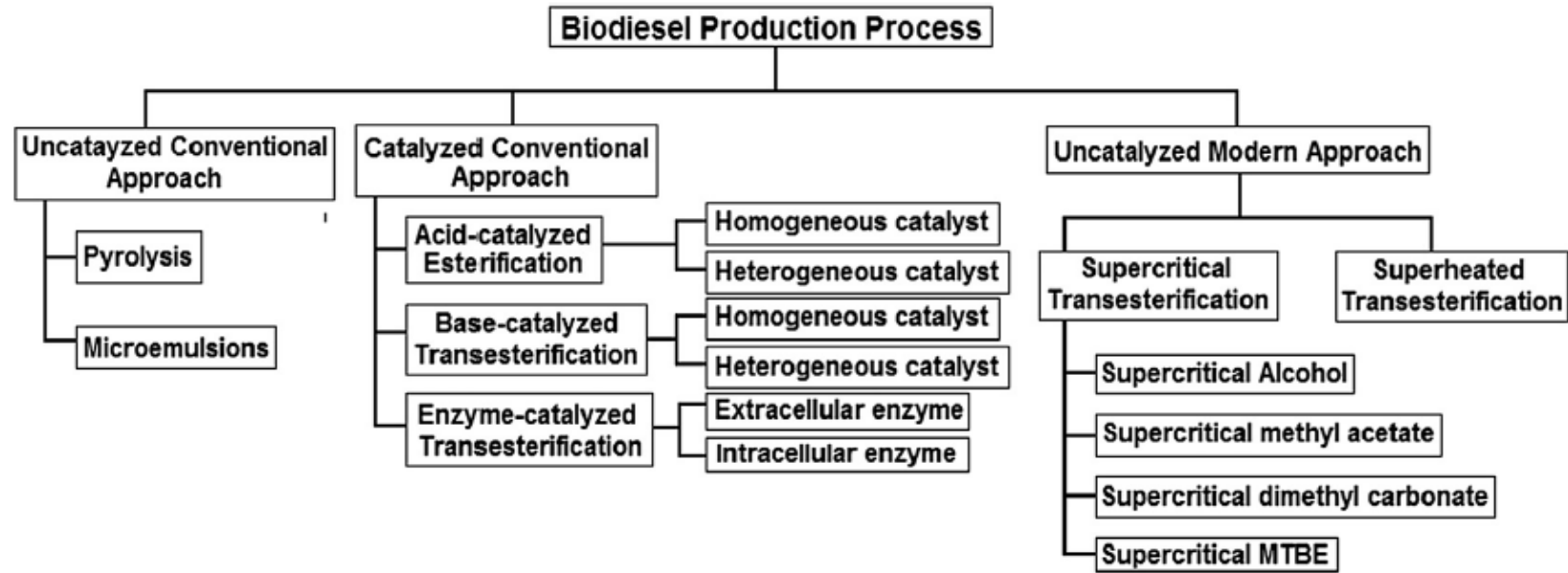
Figure 2.1: Overview of Various Approaches in Biodiesel Production (Karmakar and Halder, 2019).

Transesterification is recognised as one of the most commercially viable methods for biodiesel production, which typically involves the reaction between triglyceride and alcohol to form ester (biodiesel) and glycerol. In general, transesterification can be carried out either with or without catalyst. Non-catalytic transesterification is typically slow and requires high temperature and pressure. Kusdiana and Saka (2004) have studied the transesterification process using rapeseed oil and supercritical methanol in the absence of catalyst and discovered that the amount of water in the reaction does not bring any impact to the oil conversion. Conversely, the formation of methyl ester is increased in the presence of certain amount of water if the esterification of FFAs occurs simultaneously in single stage. Although the absence of base or acid catalyst makes the separation of products to become easier, high temperature of 250 to 400 °C and pressure of 35 to 60 MPa with high molar ratio of oil to methanol are required for the supercritical process (Tan, Lee and Mohamed, 2010). In fact, supercritical process does not require any catalyst to initiate the reaction. It possesses certain advantages as compared to transesterification using catalysts, in which the final product of biodiesel is not required to be purified. Since the presence of water does not affect the reaction under supercritical condition, this method is applicable for the feedstock with high water content (Saka and Kusdiana, 2001).

Nowadays, the catalyst is widely employed in biodiesel production as it is able to increase the reaction rate and enhance the solubility of alcohol in oil. Generally, the transesterification process can be catalysed by homogeneous and heterogeneous catalysts, where both the catalysts are further categorised into acid and base catalysts.

2.2.1 Homogeneous Catalysts

Homogeneous catalysts are considered as the most preferable catalysts for biodiesel production as they are simple to use and require less reaction time. Homogeneous catalysts possess similar physical phase with reactants, therefore they are usually miscible with the reactants. Homogeneous catalysts possess certain advantages, in which they are cheap and give a better biodiesel yield by only requiring mild operating conditions to carry out the transesterification reaction (Meher, Sagar and Naik, 2006).

However, the homogeneous catalysts tend to be consumed after involving several times of biodiesel washing and purification especially in large-scale biodiesel production, besides generating a substantial volume of wastewater (Semwal, et al., 2011). The saponification which involves the formation of soap as by-product is commonly taken place through the reaction of the FFAs with the presence of homogeneous catalysts if the FFA content of biodiesel feedstock is more than 2 %, resulting in low conversion of biodiesel (Sharma and Singh, 2009). Other drawbacks of utilising homogeneous catalysts include low effectiveness in separating the catalyst from the product after the reaction as well as corrosion of reactor, leading to high capital and maintenance costs (Marchetti and Errazu, 2008). Since the homogeneous catalysts tend to be consumed during the reaction, they cannot be reused or regenerated (Vicente, Martínez and Aracil, 2007). Hence, the limitation posed by homogeneous catalysts have been looked into and investigated by the researchers in order to develop new technologies for a better catalytic performance.

2.2.1.1 Base Catalysts

The base-catalysed transesterification process is conventionally used in biodiesel production as it is relatively fast which produces high biodiesel yield over a comparatively short period of time. According to Kamel, et al. (2018), homogeneous base catalysts possess catalysis rate which is more than 4000 times higher than that of homogeneous acid catalysts. Homogeneous base catalysts including sodium hydroxide, potassium hydroxide, sodium methoxide and potassium methoxide have been used extensively in industrial scale as they are cheap, abundantly available and possess superior activity (Mangesh, et al., 2006). Besides, they are economical and competent in terms of the ability to catalyse the reaction under atmospheric pressure at low temperature, resulting in enhanced conversion to biodiesel in shorter time (Edgar, et al., 2005). By referring to Yong, et al. (2006), the only limitation of homogeneous base catalysts is that it can only be used for refined vegetable oil with FFA content which is less than 0.5 wt% or acid value which is less than 1 mg KOH/g oil.

According to Helwani, et al. (2009), the FFA level of biodiesel feedstocks should not exceed 3 wt% when the homogeneous base catalyst is employed, beyond which the reaction will not take place. The alkali-catalysed

transesterification cannot be taken place with such high FFA content if the acid-catalysed transesterification does not perform as a pre-treatment step, mainly due to soap formation emerged from the reaction of FFAs and base catalyst. Furthermore, the water content in the biodiesel feedstocks is critical. From the literature done by Hideki, Akihiko and Hideo (2001), the feedstocks used in base-catalysed transesterification have to be anhydrous as the presence of water will lead to hydrolysis of oils to FFAs. Since the homogeneous base catalyst is limited by FFA and water content of the feedstock, both the aforementioned components are preferable to be lower than 0.5 wt% and 0.05 wt% respectively in order to impede any saponification during the reaction. The saponification process is undesirable as it not only reduces the yield of alkyl esters but also makes the separation of biodiesel and glycerol to become more difficult, causing a large volume of wastewater to be generated and thus incurring an additional operational cost (Atadashi, et al., 2013).

Besides, the purification of biodiesel which is also known as water washing will become ineffective due to the formation of emulsions in the reaction product (Borugadda and Goud, 2012). Thus, the transesterification is first carried out using acid catalysts to reduce the FFA content before employing base-catalysed transesterification to alleviate the processing difficulties (Chongkhong, Tongurai and Chetpattananondh, 2009). Ramadhas, Jayaraj and Muraleedharan (2005) evinced that the conversion of biodiesel can be increased up to 98 % by adopting two-step transesterification technique for biodiesel production. In fact, the pure vegetable oil is the only biodiesel feedstock that is suitable to be used in base-catalysed transesterification without extensive pre-treatment (Meher, Naik and Das, 2014).

In addition, the base-catalysed reaction is reported to be extremely sensitive to the purity of feedstock. By referring to Dias, Alvim-Ferraz and Almeida (2008), the sample produced from virgin oil constitutes a higher purity than waste frying oil, which is up to 99.4 wt% by utilising 0.8 wt% of catalyst. In short, it can be deduced that the performance of the homogeneous base catalysts is contingent on the impurities content in biodiesel feedstocks. The reaction mechanism of homogeneous base-catalysed transesterification is illustrated in Figure 2.2.
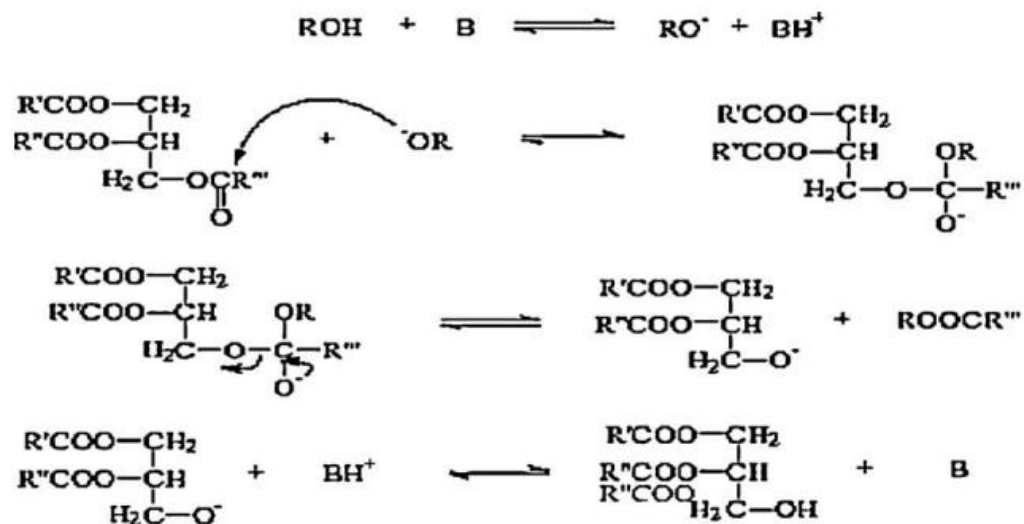
Figure 2.2: Schematic Representation of Homogeneous Base-Catalysed Transesterification Process (Singh and Singh, 2010).

Table 2.5 shows the homogeneous base catalysts used for biodiesel production from various feedstocks under different operating conditions and their respective biodiesel yield.

Table 2.5: Homogeneous Base-Catalysed Transesterification.

No.	Feedstock	Catalyst	Operating Parameters				Biodiesel Yield (%)	Reference
			Catalyst Loading (wt %)	Alcohol to Oil Molar Ratio	Reaction Temperature (°C)	Reaction Time (min)		
1	Soybean Oil	NaOH	1	6:1	60	60	90	Keera, Sabagh and Taman (2011)
	Cottonseed Oil						97	
2	Sunflower Oil	NaOH	0.6	6:1	60	60	97	Dias, Alvim-Ferraz and Almeida (2008)
		CH_3NaO						
		KOH	1				95	
3	Waste Frying Oil	NaOH	0.5	7.5:1	50	30	96	Uzun, et al. (2012)
4	Duck Tallow	KOH	1	6:1	65	180	97.1	Chung, Kim and Lee (2009)
		NaOH					81.3	
		CH_3NaO					83.6	
5	Heckel Fish Oil	KOH	0.5	6:1	32	60	96	Fadhil and Ali (2013)
6	Soybean Oil	KOH	1	4.5:1	45	120	96	Li, et al. (2012)

7	Cottonseed Oil	KOH	1	5:1	25	60	91.5	Fernandes, et al. (2012)
8	Waste Cooking Oil	CH_3NaO	0.75	6:1	Microwave heating @ 750 W	3	97.9	Chen, et al. (2012)
					65	90	96.6	
9	Soybean Oil	KOH	1	6:1	Ultrasonic @ 20 kHz, 750 W	6	98	Brito, et al. (2012)
			0.5	12:1	60	60	95	
10	Cottonseed Oil	TMAH / BTAH	2	6:1	65	120 / 90	98	Karavalakis, et al. (2010)
11	Cottonseed Oil	TMG	3	12:1	65	90	98.6	Karavalakis, Anastopoulos and Stournas (2011)
12	Cottonseed Oil	TEA / TEA-KOH	6	9:1	190	180	55.3 / 94.1	Yao, et al. (2010)

2.2.1.2   Acid Catalysts

The saponification arisen from the reaction of FFAs with homogeneous base catalyst is unfavourable as it produces less biodiesel. Hence, the separation and purification are further required due to the formation of soap, which make the transesterification process to become complicated (Avhad and Marchetti, 2015). Hence, the acid catalyst is usually deemed as an alternative to replace the homogeneous base catalyst as it is able to catalyse not only the esterification of FFAs, but also the esterification and transesterification of triglyceride simultaneously as a pre-treatment step for feedstocks with high FFAs and water content without forming the soap as by-product (Borugadda and Goud, 2012).

Generally, the acid-catalysed transesterification employs sulphuric acid, hydrochloric acid, boron trifluoride, phosphoric acid and organic sulphonic acids in order to convert FFAs or soaps to esters for biodiesel production. Unlike homogeneous base catalysts, the homogeneous acid catalysts are insensitive to the presence of FFAs and water content in biodiesel feedstock (Mangesh, et al., 2006). Hence, they are mostly applicable for low-grade feedstock. For instance, the biodiesel can be directly produced from oil feedstocks with low cost and quality, such as used cooking oils and greases, which commonly contain more than 3 wt% of FFA levels. In other words, the performance of homogeneous acid catalysts is not strongly affected by the presence of FFA content in the feedstock. Thus, the homogeneous acid catalysts are developed with the purpose to overcome the limitation posed by homogeneous base catalysts due to the fact that the base-catalysed transesterification is not able to cope with the oil or fat feedstock with high concentration of FFAs (Borugadda and Goud, 2012). According to Zhang, et al. (2003), the acid-catalysed process is proven to be more economically beneficial than base-catalysed process as the latter process requires an additional step to convert FFAs to methyl esters for biodiesel production.

In general, the acid-catalysed transesterification features a high alcohol-to-oil molar ratio, low-to-moderate operating conditions such as temperature and pressure, high acid catalyst concentration and low reaction rate (Yong, et al., 2006). Freedman, Pryde and Mounts (1984) reported that 99 % of oil conversion can only be achieved by employing methanol-to-oil molar ratio of 30:1 and 1 mol% of sulphuric acid catalyst after 69 hours of reaction. It indicates

that the reaction conditions that are more critical, for instance prolonged time for reaction and high molar ratio of alcohol-to-oil are required by the acid-catalysed transesterification. Freedman, Pryde and Mounts (1984) continued with their preliminary study where the soybean oil transesterification with various types of alcohols including butanol, ethanol and methanol is investigated in the presence of 1 % concentrated sulphuric acid, each employing 6:1, 20:1 and 30:1 of alcohol-to-oil molar ratio at reaction time of 3, 18 and 50 hours, respectively. However, the high conversion of oil to methyl ester can only be attained by using molar ratio of 30:1 after a long period of reaction time, in which both the reactions that employ the molar ratio of 6:1 and 20:1 have resulted in undesirable conversions for biodiesel production.

Although the homogeneous acid catalysts do not encounter the problem regarding FFAs in the feedstock, their usage in biodiesel production is neglected because they pose a comparatively lower catalysis rate than the homogeneous base catalysts (Sharma, et al., 2018). Besides, the biodiesel production process will be adversely affected if the water content in the reaction mixture exceeds a certain threshold value (Avhad and Marchetti, 2015). In addition, it is corrosive due to its highly acidic properties. Thus, it is not widely utilised as the prioritised catalytic technology in commercial applications. The reaction mechanism of homogeneous acid-catalysed transesterification is illustrated in Figure 2.3.
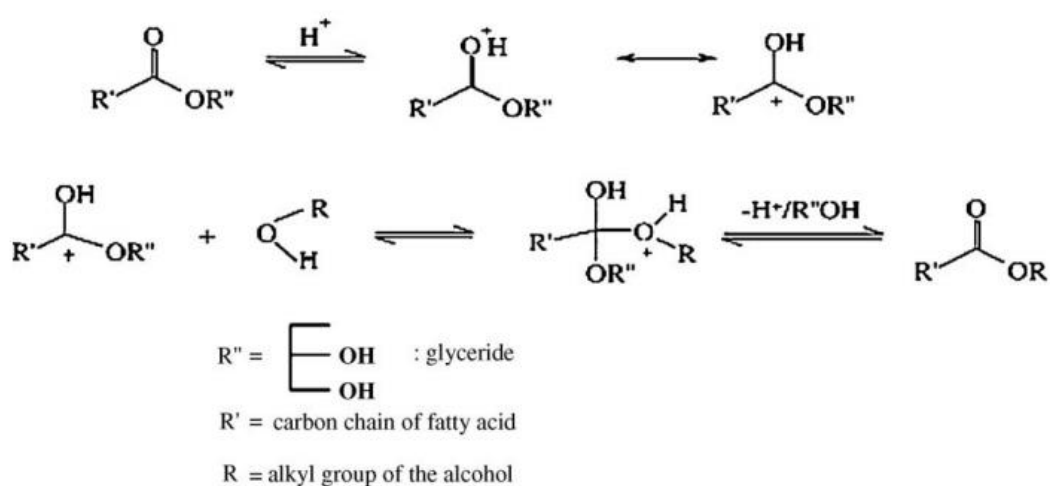
Figure 2.3: Schematic Representation of Homogeneous Base-Catalysed Transesterification Process (Singh and Singh, 2010).

Various homogeneous acid catalysts employed in producing biodiesel, followed by the operating parameters and conversion or yield after transesterification are summarised in Table 2.6.

Table 2.6: Homogeneous Acid-Catalysed Transesterification.

No.	Feedstock	Catalyst	Operating Parameters				Biodiesel Yield, Y/Conversion, C (%)	Reference
			Catalyst Loading (wt %)	Alcohol to Oil Molar Ratio	Reaction Temperature (°C)	Reaction Time (min)		
1	Oleic Acid in Sunflower Oil and Soybean Oil	H_2SO_4	2.5	6:1	60	60	96.6 (C)	Farag, El-Maghraby and Taha (2011)
		HCl				120	87.9 (C)	
		$AlCl_3$					87.98 (C)	
2	Palm Oil Fatty Acid	H_2SO_4	0.1	3:1[a]	130	60	92 (C)	Aranda, et al. (2007)
		CH_3SO_3H					91 (C)	
		H_3PO_4					50 (C)	
3	Oleic Acid in Sunflower Oil	H_2SO_4	2.261	6.126:1	55	240	96 (C)	Marchetti and Errazu (2008)
4	Acid Oil (One-Step)	H_2SO_4	-	3:1	80	360	85.58 (Y)	Park, et al. (2010)
	Acid Oil (Two-Step)						88.96 (Y)	
5	Oleic Acid	H_2SO_4	5	Ethanol 3:1[a]	Ultrasonic @ 40 kHz, 700W	120	93 (C)	Hanh, et al. (2009)
				1-Propanol		60	92 (C)	
				1-Butanol		300	87 (C)	

				2-Propanol			78 (C)	
				2-Butanol			42 (C)	
6	**Soybean Oil**	$C_2HF_3O_2$	2 M[b]	20:1	80	360	98.4 (Y)	Miao, Li and Yao (2009)
7	**Canola Oil**	$AlCl_3$	5	24:1	110	1080	98 (C)	Soriano, Venditti and Argyropoulos (2009)
8	**Corn Oil**	**PTSA**	4	10:1	80	120	97.1 (Y)	Guan, et al. (2009)
		BSA			60	480	82 (Y)	
		H_2SO_4					65 (Y)	

[a] Alcohol-to-acid ratio

[b] Catalyst concentration

2.2.2 Heterogeneous Catalysts

Although the homogeneous catalysts are extensively employed in producing biodiesel as they possess comparatively high catalytic activity and low costs, there is a trade-off in which the residual catalyst has to be discarded from the reaction mixture, besides disposing a large amount of wastewater generated from the biodiesel washing and purification (Semwal, et al., 2011). According to Avhad and Marchetti (2015), all these post-reaction treatment steps have consequently increased the overall processing expenses and may indirectly affect the biodiesel price. Besides, the homogeneous catalysts possess a low reusability as they tend to be consumed during the reaction and are not able to be regenerated for continuous usage (Vicente, Martínez and Aracil, 2007).

In biodiesel production, heterogeneous catalysts mostly remain in a separate phase with the reactants, where the heterogeneous catalyst usually lies in solid phase, whereas methanol and oil feedstock are in liquid phase. Heterogeneous catalysts are also known as contact catalysts because they function by adsorbing the reactants over their surfaces (Sharma, et al., 2018). According to Nurfitri, et al. (2013), heterogeneous catalysts are generally derived from waste resources. Besides, they can also be derived from renewable biomass or natural resources such as mollusc shells, egg shells, ashes and rocks (Chakraborty, Bepari and Banerjee, 2011). By referring to Granados, et al. (2007), metal oxides such as calcium oxide, magnesium oxide, zirconium oxide have been evinced to be the most significant and widely used heterogeneous catalysts for biodiesel production. Besides metal oxides, metal hydroxides, metal complexes and other supported catalysts are also considered as the promising heterogeneous catalysts that possess superior catalytic performance (Wang and Yang, 2007).

The heterogeneous catalysts are more ecologically sustainable than homogeneous catalysts as it is regenerable and can be reutilised (Sharma and Singh, 2009). In other words, they are not consumed or dissolved in the reaction mixture and can be easily separated from final product. Hence, the products formed do not contain any catalyst impurities, which can subsequently simplify the cleaning and purification process of biodiesel, resulting in less energy and water consumption which in turn reduces the cost of separation (Borugadda and Goud, 2012). Dossin, et al. (2006) stated that heterogeneous catalysts are more

environmentally benign as neither acid or water treatment is required in the separation step. Unlike homogeneous catalysts, heterogeneous catalysts are able to tolerate high fatty acid and water content (Baskar and Aiswarya, 2016). Hence, the heterogeneous catalysts are applicable in the transesterification of both animal fats and vegetable oils containing high FFAs percentage, such as frying oils generated from food processing industries as well as restaurants. For heterogeneous catalysts, there is a less tendency towards the undesired saponification when compared to homogeneous catalysts, and thus becoming a better alternative for homogeneous catalysts as it is less corrosive in nature.

However, the activity of heterogeneous catalysts is substantially dependent upon their stability towards high temperature, structural morphology, active sites and porosity, which in turn raises up a lot of concerns among researchers (Avhad and Marchetti, 2015). For instance, the activity of heterogeneous catalysts is subject to the formation of three phases with oil and alcohol, leading to mass transfer limitations that can possibly decrease the reaction rate (Mbaraka and Shanks, 2006). Yet, the diffusion limitations can be resolved with the help of co-solvent such as n-hexane, tetrahydrofuran, dimethyl sulphoxide and ethanol, which improves the miscibility of oil and alcohol, thus accelerating the reaction rate (Furuta, Matsuhashi and Arata, 2006). Furthermore, structural promoters or catalyst supports can also be the potential options to overcome the mass transfer problems associated with heterogeneous catalysts. Borges and Diaz (2012) reported that both structural promoters and catalyst supports are able to provide more specific surface area and pore for active species in order to react with large triglyceride molecules. Sharma, et al. (2018) reported that a higher reaction temperature and reactant amount are able to resolve the limitation posed by heterogeneous catalysts as they generally possess a lower reaction rate.

It is observed that the overall catalytic activity of heterogeneous catalysts can be enhanced by performing elemental doping step as it alters the lattice parameters of catalysts (Sharma, et al., 2018). Since the reaction is catalysed by heterogeneous catalysts through adsorption, it is necessary to acquire a large surface area in order to initiate the transesterification reaction. Tangy, et al. (2017) suggested that nanocomposite materials have been proven as the best candidate for heterogeneous catalysts. In another research study

conducted by Baskar, Selvakumari and Aiswarya (2018), nanoporous materials possess excellent surface properties required for a better biodiesel yield, for instance large surface area and nano-scaled pore size with uniform distribution of pores. Thus, the heterogeneous catalyst concentration can be adjusted via designing an effective nanocomposite with improved surface properties, including high surface-to-volume ratio and even dispersion of nano-pores (Gurunathan and Ravi, 2015).

2.2.2.1 Base Catalysts

The heterogeneous base-catalysed process is expected to produce the biodiesel in an effective way with less impact towards environment and lower cost incurred as the heterogeneous base catalysts are possible to simplify the purification and production process under modest conditions. Besides, they can be regenerated easily and is less corrosive in nature, leading to a safer, cheaper and more environmentally friendly as well as more ecological sustainable process. By referring to Baskar and Aiswarya (2016), the base catalysts are only required in lesser amount in order to proceed the transesterification process. However, heterogeneous base catalysts pose a limitation in which they can only be used for the oil feedstock containing FFAs which are less than or equal to 1 % (Borugadda and Goud, 2012).

Hence, the researchers have been actively investigating a number of alkali as well as metal oxide with alkaline earth as the base element to be used as heterogeneous base catalysts, expecting their high potential in transesterification reaction. Among various base catalysts, calcium oxide, magnesium oxide, strontium oxide, oxides with mixed metal, oxides supported by alkali or alkaline earth metal, zeolites, anionic resins as well as hydrotalcites are commonly employed for biodiesel production, in which calcium oxide is relatively favourable to be used in most of the research works (Granados, et al., 2007). It is extensively researched heterogeneous base catalyst due to the fact that it possesses high basicity and low methanol solubility. Besides, it is cost-effective and can be handled easily as it is synthesised from low-cost sources such as limestone containing calcium carbonate and slaked lime containing calcium hydroxide, thus only prone to low cost (Avhad and Marchetti, 2015).

Zabeti, Daud and Aroua (2009) reported that calcium oxide which is prepared by the calcination of pulverized limestone such as calcium carbonate at 900 °C for less than two hours is employed to produce biodiesel from soybean oil. It is observed that the reaction has yielded about 93 % of fatty acid methyl esters by employing the methanol-to-oil ratio of 12:1 under reflux condition. The soybean oil is then substituted with waste cooking oil containing 2.6 % of FFAs for identical reaction conditions, in which the biodiesel yield is reduced to 66 % due to the formation of soluble substance such as calcium diglyceroxide during the transesterification process. Thus, the ion-exchange resin process is carried out as an additional purification step in order to remove the soluble substance from biodiesel (Borugadda and Goud, 2012). The reaction mechanism of heterogeneous base-catalysed transesterification is illustrated in Figure 2.4.
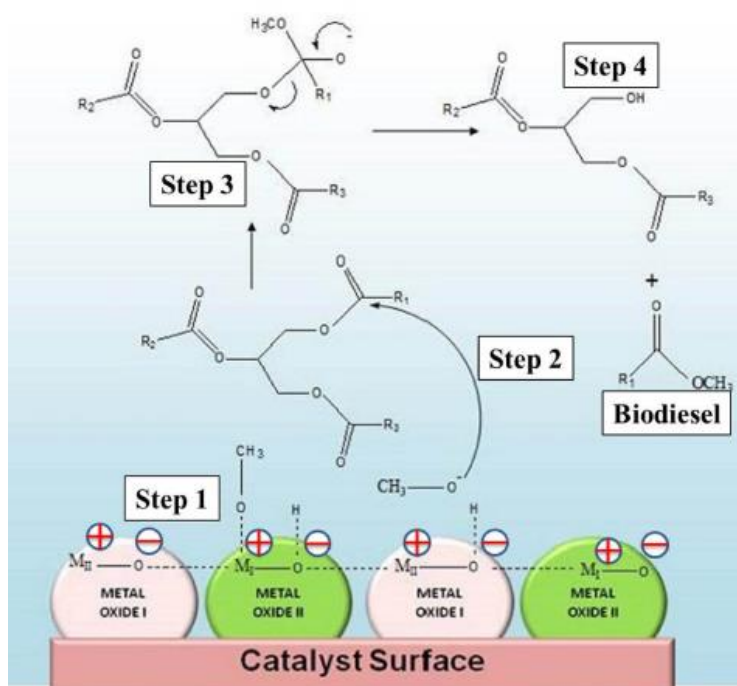
Figure 2.4: Schematic Representation of Heterogeneous Base-Catalysed Transesterification Process (Lee, et al., 2016).

The effects of different heterogeneous base catalysts as well as their respective reaction variables such as catalyst amount, alcohol-to-oil molar ratio, reaction temperature and time on the performance of heterogeneous base-catalysed transesterification are summarised in Table 2.7.

Table 2.7: Heterogeneous Base-Catalysed Transesterification.

No.	Feedstock	Catalyst	Operating Parameters				Biodiesel Yield, Y/Conversion, C (%)	Reference
			Catalyst Loading (wt %)	Alcohol to Oil Molar Ratio	Reaction Temperature (°C)	Reaction Time (min)		
1	**Rapeseed Oil**	**CaO**	1 gm[a]	26 wt%[b]	60	180	90 (Y)	Kawashima, Matsubara and Honda (2009)
2	**Palm Oil**	**CaO (Capiz Shell)**	3	8:1	60	360	92.83 (Y)	Suryaputra, et al. (2013)
3	**Sunflower Oil**	**CaO (Egg Shell)**	3	9:1	60	180	94.73 (C)	Correia, et al. (2014)
		CaO (Crab Shell)		6:1		240	82.87 (C)	
4	**Soybean Oil**	**CaO (Mussel Shell)**	12	24:1	60	480	94.1 (Y)	Rezaei, Mohadesi and Moradi (2013)
5	**Canola Oil**	**MgO**	3	20:3	190	120	82.8 (Y)	Jeon, et al. (2013)
		Templated-MgO					98.2 (Y)	
6	**Olive Oil**	**SrO**	5	6:1	65	15	82 (C)	Chen, et al. (2012)

7	Fried Oil	CaO	5	6:1	65	180	92 (Y)	Viola, et al. (2012)
		SrO					86 (Y)	
		K_3PO_4					78 (Y)	
8	Karanja Oil / Jatropha Oil	Li/CaO	5	6:1	65	60 / 120	99 (C)	Kaur and Ali (2011)
9	Soybean Oil	Ca/Al_2O_3	1	32:1	120	360	94.7 (Y)	Tonetto and Marchetti (2010)
		Na/Al_2O_3					97.1 (Y)	
		K/Al_2O_3					98.9 (Y)	
		K/Al_2O_3-Monolith	0.5				59.1 (Y)	
10	Sunflower Oil	$CaZn(OH)_4$	3	20:1	78	180	95 (Y)	Rubio-Caballero, et al. (2013)
11	Soybean Oil	Na_2ZrO_3	3	3:1	65	180	98.3 (C)	Santiago-Torres, Romero-Ibarra and Pfeiffer (2014)
12	Soybean Oil	$Sr_3Al_2O_6$	1.3	25:1	60	61	95.7 (Y)	Rashtizadeh, Farzanesh and Talebpour (2014)
13	Soybean Oil	Ce-Hydrotalcite	5	9:1	67	240	90 (Y)	Dias, et al. (2012)

			a			b		
14	Soybean Oil	Mg/Al/Fe Hydrotalcite	3	21:1	65	240	81 (C)	Wang, et al. (2012)
15	Yellow Horn Seed Oil	Amberlite IRA 900	3	8:1	60	90	96 (C)	Li, et al. (2012)

[a] Catalyst amount

[b] Oil amount

CaO catalysts have received a lot of scientific and industrial attentions as the calcium species are abundantly available from natural resources. Kawashima, Matsubara and Honda (2009) reported that when the CaO catalyst is being activated with methanol, it constitutes a higher catalytic activity when compared to non-activated CaO catalyst in the transesterification of rapeseed oil with methanol. The rate of transesterification is inferred to be dependent on the amount of methanol, in which the more the methanol used to activate the catalyst, the higher the transesterification reaction rate. It was identified by Kawashima, Matsubara and Honda (2009) that the CaO catalyst reacts with the glycerol produced in transesterification, causing the CaO-glycerin complex to be formed. The formation of CaO-glycerin complex is desirable as it is able to expedite the rate of transesterification. There are a few resources originated from the nature and waste that are being studied extensively before deriving the active calcium-based catalysts with low cost. The calcium-based species obtained from natural resources will be converted to CaO catalyst via thermal treatment such as calcination, where it is considered as the most employed technique for biodiesel production. Suryaputra, et al. (2013) reported that the CaO catalyst produced after the calcination of waste capiz shells at 900 ℃ for two hours is used to catalyse the transesterification of palm oil with methanol, in which about 92.83 % of biodiesel yield is acquired at 60 ℃ after six hours of reaction by employing methanol-to-oil molar ratio of 8:1, with the aid of 3 wt% of CaO.

Correia, et al. (2014) studied the transesterification of sunflower oil with methanol using crab shells or egg shells as the sources to synthesise CaO catalyst. The egg shell-derived CaO was reported to exhibit a higher activity owing to its higher basicity, where 94.73 % of oil conversion is achieved at 60 ℃ over a reaction period of three hours by employing 3 wt% of CaO. It was suggested by Rezaei, Mohadesi and Moradi (2013) that the mussel shell-derived CaO is extracted from reaction mixture using methanol during transesterification. Besides, the CaO catalyst is tested for its recyclability for five reaction cycles, where it is deduced that the recalcination tends to adversely affect the chemical composition of catalyst, which reduces the catalytic sites and subsequently lowers the production yield of biodiesel. It can be proven by Rezaei, Mohadesi and Moradi (2013) in which the biodiesel yield is dropped

abruptly from 94.1 % in the first reaction cycle to 37.13 % after five reaction cycles by employing recalcined CaO catalyst.

2.2.2.2 Acid Catalysts

The heterogeneous acid catalysts have a strong potential to replace heterogeneous base catalysts mainly because they can be employed for both esterification and transesterification process simultaneously (Kathlene, et al., 2008). By referring to Borugadda and Goud (2012), heterogeneous acid catalysts are generally insensitive to water and FFA content in the oil, besides featuring low product contamination. According to Jitputti, et al. (2006), it is not necessary to perform the biodiesel washing and purification process if heterogeneous acid catalysts are employed as it is easier for the catalyst to be separated from the reaction medium. The heterogeneous acid catalysts can also be beneficial when compared to homogeneous acid catalysts in producing biodiesel as the former catalysts are easy to be regenerated and can be recycled for continuous use, resulting in low cost incurred (Mangesh, et al., 2006). Typically, there is no significant issue regarding the corrosion even with the presence of acid catalysts (Suarez, et al., 2007).

However, the research on direct use of heterogeneous acid catalysts for biodiesel production has not been widely explored as it possesses certain limitations such as slow reaction and possible side reactions which are generally undesirable (Borugadda and Goud, 2012). Besides, the acid catalyst is necessary to be thermally stable as severe reaction conditions are required for complete conversion of oil to biodiesel (Avhad and Marchetti, 2015). In fact, Mangesh, et al. (2006) suggested that the ideal heterogeneous acid-catalysed reaction should feature an interconnected system of large pores, high number of accessible active sites, moderate-to-high acid strength as well as hydrophobic surface in order to mitigate the issues related to diffusion.

Although the acid catalysts are not receiving much attention in comparison with base catalysts as supported by low reaction rate, the use of various heterogeneous acid catalysts is still being comprehensively studied in producing biodiesel. According to Avhad and Marchetti (2015), there are abundant heterogeneous acid catalysts utilised to produce biodiesel that are based on the modified inorganic mixed oxides, for instance sulphated and

tungstated zirconia or zeolites, silica, heteropoly acids, superacid catalysts and cation-exchange resins. Satoshi, Hiromi and Arata-Kazushi (2004) studied the methanolysis of soybean oil by employing heterogeneous superacid catalysts such as tungstated zirconia-alumina, sulphated zirconia-alumina and sulphated tin oxide, in which all the reactions are conducted under similar reaction conditions of atmospheric pressure at 200 to 300 ℃. It was reported that the alumina tungstated with zirconia is the most superior heterogeneous acid catalyst in producing biodiesel from soybean oil, with the oil conversion of over 90 %. The reaction mechanism of heterogeneous acid-catalysed transesterification is illustrated in Figure 2.5, where AS indicates the acid site on catalyst, R_1 indicates the alkyl group of fatty acid and R_2 indicates the alkyl group of triglyceride.
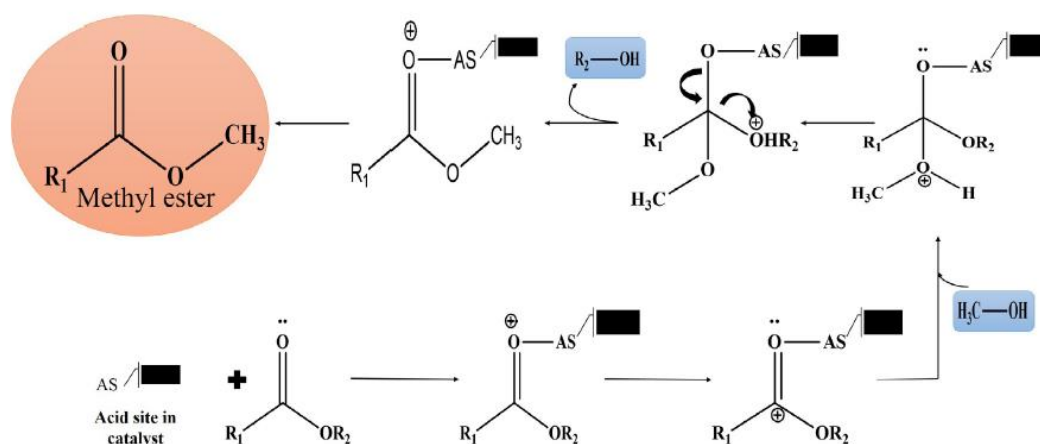
Figure 2.5: Schematic Representation of Heterogeneous Acid-Catalysed Transesterification Process (Sharma, et al, 2018).

The heterogeneous acid catalysts used for biodiesel production from various feedstocks under different reaction conditions and their respective catalytic performance in terms of yield or conversion are summarised in Table 2.8.

Table 2.8: Heterogeneous Acid-Catalysed Transesterification.

No.	Feedstock	Catalyst	Operating Parameters				Biodiesel Yield, Y/Conversion, C (%)	Reference
			Catalyst Loading (wt %)	Alcohol to Oil Molar Ratio	Reaction Temperature ($°C$)	Reaction Time (min)		
1	Crude Palm Oil	Propyl-SO_3H-SBA-15	6	20:1	140	120	72 (Y)	Melero, et al. (2010)
		Arene-SO_3H-SBA-15					78 (Y)	
		Arene-SO_3H-SBA-15 (Capped)					90 (Y)	
		Amberlyst-36					32 (Y)	
		SiO_2-Tosic Acid					65 (Y)	
2	Sunflower Oil	Nb-MCM-41	7.5	12:1	200	240	95 (Y)	García-Sancho, et al. (2011)
3	Oleic Acid	Sulphated Zirconia	0.5 gm[a]	40:1[b]	60	720	90 (Y)	Patel, Brahmkhatri and Singh (2013)
4	Oleic Acid	Chlorosulphonic Zirconia	3	8:1[b]	100	720	100 (Y)	Zhang, Wong and Yung (2014)
5	Sunflower Oil	15 % WO_3/Zr-MCM-41	1.5 gm[a]	12:1	200	150	82 (Y)	Jiménez-López, et al. (2011)

6	Soybean Oil	30 % $WO_3/AlPO_4$	5	30:1	180	300	72.5 (Y)	Xie and Yang (2012)
7	Oleic Acid	11.4 % WO_3/USY Zeolite	10	6:1[b]	200	120	74 (Y)	Costa, et al. (2012)
8	Soybean Oil	Ce/HUSY Zeolite	0.001 mol[a]	30:1	200	1440	99.8 (C)	Borges, et al. (2013)
9	Oleic Acid	Sulphated LaO/HZSM-5	10	5:1[b]	100	420	100 (C)	Vieira, et al. (2013)
		Sulphated LaO					96 (C)	
		HZSM-5		20:1[b]			80 (C)	
10	Waste Oil	$Fe(HSO_4)_3$	1	15:1	205	240	94.5 (Y)	Alhassan, et al. (2013)
11	Oleic Acid	30 % TSA/Zeolite Hβ	100 mg[a]	20:1[b]	60	600	86 (C)	Narkhede and Patel (2013)
	Soybean Oil		200 mg[a]	4:1	65	480	95 (C)	
12	Acid Oil	$SO_4{}^{2-}/ZrO_2$-TiO_2/La^{3+}	5	15:1	200	120	96.24 (Y)	Li, et al. (2010)
13	Polanga Oil	Sulphonated Carbon	7.5	30:1	180	300	99 (C)	Dawodu, et al. (2014)

14	**Palmitic Acid**	**Sulphonated Carbon Nanohorn**	3	33:1[b]	64	300	93 (Y)	Poonjarernsilp, Sano and Tamon (2014)
15	**Oleic Acid**	**CH-A Cation Exchange Resins**	20 gm[a]	9:1[b]	82	480	93 (C)	Jiang, et al. (2013)

[a] Catalyst amount

[b] Alcohol-to-acid ratio

2.2.3   Comparison on Advantages and Disadvantages of Biodiesel Catalysts

Table 2.9: Advantages and Disadvantages of Homogeneous and Heterogeneous Catalysts for Biodiesel Production.

Type of Catalyst	Examples	Advantages	Disadvantages	Reference
		Homogeneous		
Base	NaOH, KOH, CH_3NaO, CH_3KO	- High catalytic activity - High yield in short reaction time - Reaction is 4000 times faster than acid catalyst - Less corrosive - Low cost - Favourable kinetics - Relatively moderate operational conditions and thus less energy required	- Less tolerant towards FFA content in feedstock, generally <1 wt% - Highly sensitive to water - Formation of soap as by-product and thus reducing biodiesel yield - Formation of emulsion - High water and energy consumption - High generation of wastewater from purification, leading to high purification cost - Catalyst is non-recyclable	Leung, Wu and Leung (2010), Konwar, Boro and Deka (2014), Tariq, Ali and Khalid (2012), Helwani, et al. (2009), Demirbas, A. (2006), Predojević, Z.J. (2008), Sharma, Singh and Upadhyay (2008)

| Acid | H_2SO_4, HCl, HF, H_3PO_4, PTSA | • Insensitive to FFA and water content in oil
• Catalyst can be used for simultaneous esterification and transesterification reactions
• Avoid soap formation
• High biodiesel yield | • Low reaction rate with long reaction time
• Equipment corrosion
• Higher reaction temperature and pressure
• High alcohol-to-oil molar ratio requirement
• Low catalytic activity
• Difficult to be recycled
• More waste as a result of neutralization
• High purification cost
• Energy-intensive
• Difficult to be separated from product | Leung, Wu and Leung (2010),
Konwar, Boro and Deka (2014),
Tariq, Ali and Khalid (2012),
Helwani, et al. (2009),
Thiam and Bhatia (2008),
Demirbas, A. (2006),
Casanave, Duplan and Freund (2007) |

		Heterogeneous		
Base	CaO, SrO, MgO, mixed oxide and hydrotalcite	- Non-corrosive - Environmentally friendly - Catalyst can be recycled - Less problems related to disposal - Easier separation from product - Relatively higher reaction rate than acid catalyst - Higher selectivity - Longer catalyst life - Mild reaction condition requirement and thus consuming less energy	- Slower reaction in comparison with homogeneous catalyst - Less tolerant towards FFA content in feedstock, generally <1 wt% - Require anhydrous condition - Soap formation and thus reducing biodiesel yield - Poisoning when exposed to ambient air - Substantial wastewater generation from purification - Leaching of active catalyst sites - Mass transfer constraint due to formation of three phases - High-cost and complicated synthesis route - More cost incurred for catalyst synthesis	Leung, Wu and Leung (2010), Konwar, Boro and Deka (2014), Tariq, Ali and Khalid (2012), Helwani, et al. (2009)

| Acid | ZnO, TiO, ZrO, sulphonated carbon-based catalyst, zeolites, sulphonic modified mesostructured silica, ion-exchange resin and HPA | • Insensitive to water and FFAs in feedstock

• Catalyst can be used to catalyse both esterification and transesterification simultaneously

• Catalyst is regenerable and eco-friendly

• Easy separation from product

• Non-corrosive to reactor and reactor parts | • Low reaction rate with prolonged reaction time

• Higher reaction temperature and pressure

• High alcohol-to-oil molar ratio requirement

• Weak catalytic activity

• Low acidic site

• Low microporosity

• Leaching of active catalyst sites and thus causing product contamination

• Diffusion limitations due to formation of three phases

• High-cost and complicated synthesis route

• More cost incurred for catalyst synthesis

• More energy requirement | Leung, Wu and Leung (2010),
Konwar, Boro and Deka (2014),
Tariq, Ali and Khalid (2012),
Helwani, et al. (2009) |

2.3   Nanocatalytic Technologies in Biodiesel Production

The cost-effective nanomaterials with advanced functions, including nanoparticles, nanofibers, nanocomposites, nanoclays, nanowires, carbon nanotubes and other nanoporous materials have been actively investigated by the scientists for a wide variety of applications over the last few decades (Banković–Ilić, et al., 2017). According to Bensebaa (2013), the quasi-spherical or spherical nanoparticles possess less than 100 nm of diameter, where they are proven to enhance a wide range of catalytic processes. In fact, it is considered as one of the oldest applications of nanotechnology.

According to Bensebaa (2013), the use of nanocatalysts is vital due to their high recoverability, durability, selectivity as well as activity. Thus, it is essential to understand the correlation between composition, structure of catalyst surface and relevant properties in the application of nanocatalysts. Generally, nanocatalysts are characterised by the spatial organisation of active sites where the geometrical and electronic structures of catalyst can affect the catalytic processes (Banković–Ilić, et al., 2017).

Nanocatalysts are expected to achieve certain important characteristics such as immensely high activity, 100 % selectivity, long lifetime and low energy consumption, where it can be to be accomplished by regulating the size, shape, surface composition, electronic structure, spatial distribution as well as the chemical and thermal stability of nanocomponent in a precise way (Kung and Kung, 2007). By referring to Philippot and Serp (2013), the application of nanocatalysts in chemical industries is advantageous as it can improve the economy and energy efficiency, reduce global warming as well as optimise the utilisation of feedstock. In addition, it is deemed as a safer catalyst which produces minimum chemical wastes.

According to Baskar and Aiswarya (2016), nanocatalysts are considered as a potential candidate in biodiesel industries due to various favourable catalytic properties including extremely high activity, stability, reusability and surface reactivity as well as large surface area and pore size in comparison with the catalysts with macroscopic structure. Particularly, the bottleneck problems related to transesterification reaction for biodiesel production using other non-nanocatalysts can be resolved by the large specific surface area of the nanocatalyst where it can enhance the interaction between reactant and catalyst.

Besides constituting high selectivity on account of nano-dimensional pores on the surface, the nanoparticles tend to mitigate the limitations posed by diffusion (Baskar and Aiswarya, 2015). When the catalyst size is decreased, the active surface, which is the most crucial property of catalysts will increase. Hence, with the nanocatalysts comprising of smaller particles, the surface-to-volume ratio is augmented where there is less amount of catalyst required for reaction, and thus enhancing the reaction efficiency (Banković–Ilić, et al., 2017).

Sodium titanate nanotubes were investigated by Hernandez-Hipolito, et al. (2014) where the specific surface area of catalyst was $200 \ m^2/g$ with a pore volume of $0.61 \ cm^3/g$, which resulted in about 98 % of biodiesel yield by using methanol-to-oil molar ratio of 20:1 and 1 % of nanocatalyst loading. Another study was reported by Shahraki, Entezari and Goharshadi (2015) in which the KF/γ-Al_2O_3 was employed as solid base nanocatalyst for biodiesel production where the reaction was carried out in the sonication mode by applying sound energy to agitate the nanoparticles at 45 W, resulting in 95 % of biodiesel yield. According to Wen, et al. (2010), heterogeneous catalysis is the most widespread approach for nanocatalyst technology as the heterogeneous catalyst is typically comprised of a highly porous support material which is dispersed with a number of nanoparticles, possessing up to $250 \ m^2/g$ of surface area. Among various nano-sized heterogeneous catalysts that are investigated in producing biodiesel, Ca-based compounds are deduced as one of the most promising catalysts to be synthesised in nano form to produce biodiesel from various feedstocks. According to Kesić, et al. (2016), they only require mild operating conditions during reaction in order to produce biodiesel with high yield.

2.3.1   Nano CaO as Promising Heterogeneous Catalyst

Among various types of alkali earth metal oxides, CaO is most widely employed to produce biodiesel from a variety of oil feedstocks as it is easily available in nature, where it can be derived from natural calcium resources from wastes that are rich in calcium carbonate which serves as the main precursor of CaO, such as eggshell, clamshell, mollusk shell and bone (Gardy, et al., 2017). Hence, it can facilitate in reducing the cost of catalyst synthesis as well as eliminating the wastes in industrial and domestic areas. By referring to Chen, et al. (2014), the CaO derived from eggshell exhibits the highest catalytic performance owing to

a relatively higher surface area and pore volume as compared to other waste shell-derived CaO, which eventually contributes to a higher FAME yield. According to Hoora, et al. (2018), CaO constitutes low cost, long life time and minor toxicity, making it a more cost-effective and environmentally benign catalyst as compared to other heterogeneous catalysts. Besides, it possesses low solubility in methanol, easy separation from reaction mixture, high activity under mild reaction conditions, which eventually lead to high methyl ester yield. In general, CaO appears as white colour with spherical shape, besides possessing high porosity and narrow distribution of particle size (Sidra, et al. (2016).

In spite of the effectiveness of heterogeneous base catalyst in the catalysis of transesterification, Harsha-Hebbar, Math and Yatish (2018) reported that nano-sized CaO catalyst is found to possess a conversion rate which is around 30 times higher than meso CaO catalyst due to higher catalytic activity. Besides, it poses a relatively large pore size as well as surface area-to-volume ratio, where it increases the availability of active sites, leading to a higher catalytic activity with more catalytic reactions carried out simultaneously. The reduced particle size due to an increase in specific surface area tends to reduce the internal diffusion limitation as the paths for reactant molecules to access the active sites are shortened, which in turn augment the number of active sites present. From the research done by Banković–Ilić, et al. (2017), the rate of transesterification catalysed by CaO nanocatalyst is about 30 times higher than powdered CaO catalyst within 30 minutes of reaction. Furthermore, the nano CaO catalyst is employed to save the production cost as there are less amount of catalyst required for the reaction as well as constituting easy separation and better recovery, recyclability and reusability (Nor Azyan, Sarina and Parveen, 2018). Thus, it is recommended to employ CaO nanocatalyst in boosting the biodiesel production industries by minimising the by-products and wastes generated from the reaction as well as rendering a better energy efficiency.

2.3.2   Synthesis Methods for Nano CaO Catalysts

The nano-sized CaO does not require much effort for preparation in comparison with other heterogeneous catalysts. In general, the nano CaO catalysts is synthesised in two major stages, where the nanoparticles are prepared prior to

the activation. The catalyst synthesis is started off by employing a variety of methods such as thermal decomposition, impregnation (wet impregnation, incipient wetness impregnation), sol-gel, co-precipitation and mixing, whereby the nanoparticles produced are subsequently calcined in attaining the activity of catalyst (Banković–Ilić, et al., 2017). The nano CaO catalysts can be employed to produce biodiesel from various raw materials including the oil feedstock and alcohol once the specific surface area is augmented.

Generally, the CaO-based nanoparticles are activated by means of calcination at elevated temperatures via two different routes, which are:

(i)   Calcination of CaO precursor subsequent to washing and air drying, or afterwards using hydration (Yoosuk, et al., 2010).

(ii)   Calcination of neat, doped or loaded CaO catalyst after a variety of synthesis methods, for instance wet impregnation, chemical precipitation, incipient wetness impregnation or mixing (Hu, et al., 2012).

Table 2.10 summarises various CaO-based nanocatalysts with their corresponding synthesis method and characterisation.

Table 2.10: Preparation and Characterisation of Nano CaO Catalysts.

No.	Catalyst (Precursor)	Catalyst Preparation		Catalyst Characterisation					Reusability	Reference
		Synthesis	Calcination (°C, h)	Morphology	Diameter (nm)	Diameter (nm)/Volume of Pore (cm^3/g)	Surface Area (m^2/g)	Basicity (mmol HCl/g)/Basic Strength (H_)[a]		
Thermal Decomposition										
1	CaO (Calcite)	①Mixing $CaCl_2$ with Na_2CO_3 at room temperature for 30 seconds ②Centrifugation of $CaCO_3$ precipitate ③Washing with pure water and acetone for 3 times ④Drying	1000, 2	Large and irregular crystals[b]	-	15-100 / 0.0249	5.3	-	-	Bai, et al. (2009)
2	CaO, 97.2 (Calcite)	①Thermal decomposition of fresh calcite ($CaCO_3$) ②Hydration at 60 °C for six hours ③Filtration ④Heating overnight at 120 °C	600, 3	Very rough and highly textured particles[b]	42.2[c]	- / 0.25	25	1532.4[d] / 12.2 < H_ < 15	5 (slightly lowered activity after the second repetition)	Yoosuk, et al. (2010)

			Impregnation							
3	**LiC/CaO**	①Wet impregnation of Li_2CO_3 from aqueous solution ②Stirring for two hours ③Evaporation to dry ④Heating at 120 ℃ for 24 hours	-	Hexagonal and oval shaped clusters[e] of smaller particles[b,c]	4000[e], 50[f] (70[c])	-	-	15 < H_ < 18.4	-	Kumar and Ali (2010)
4	Li^+/CaO	①Wet impregnation of $LiNO_3$ from aqueous solution ②Stirring for two hours ③Evaporation to dry ④Heating at 120 ℃ for 24 hours			2000[e], 50-70[f] (40[c])	95.02 / 0.004	1.7			Kaur and Ali (2011)
5	**Ni/CaO**	①Wet impregnation of $Ni(NO_3)_2 \cdot 6H_2O$ from aqueous solution ②Stirring for three hours ③Drying	650, 12	Agglomerates of hexagonal, cubic and oval shaped particles[b,f]	10[f]	-	14.7	9.9 / 15 < H_ < 18.4	7 (recovering by filtration, washing with hexane and drying at 100 ℃) with gradual activity loss	Kumar, Abida and Ali (2016)

6	**Ba/CaO**	①Dropwise addition of $BaCl_2$ solution onto CaO ②Stirring for 10 hours ③Filtration under vacuum pressure ④Drying at 120 ℃ for 16 hours	900	Spherical and non-uniform size particles[b]	-	-	4.86	0.2375 / 15 < H_ < 18.4	4 (recovering by filtration, washing with methanol and drying at 120 ℃) with slight activity loss	Boro, et al. (2014)
7	**K/CaO**	①Wet impregnation of KOH from aqueous solution ②Stirring for three hours ③Heating at 180 ℃ for 24 hours	-	Hexagonal and irregular shaped clusters[e] of hexagonal shaped particles[f]	2000-5000[e], 50[f] (40[c])		5.84	11.1 < H_ < 15	3 (recovering by filtration, washing with hexane and drying) with partial activity loss	Kumar and Ali (2012)
8	**KF/CaO**	①Impregnation of KF from aqueous solution for one hour ②Backing at 105 ℃ for four to six hours	600, 3	Evenly distributed granules and abundant large pores	30-100[b,c,f]	97 / -	109	0.94 / 15 < H_ < 18.4	16 (final biodiesel yield: 91 %)	Wen, et al. (2010), Hu, et al. (2012)
9	K_2CO_3/CaO	Incipient wetness impregnation: ①Dropwise addition of K_2CO_3 solution onto CaO	500, 3	Rounded particles[b]	50-100	-	12.85	0.96 / 9.8 < H_ < 15	5 (recovering by catalyst separation, washing with methanol and	Degirmen-basi, et al. (2015)

No.	Catalyst	Preparation	Calcination	Morphology	Particle size				Reusability	Reference
		②Drying at 120 ℃ for 16 hours								n-hexane, drying)
10	Zn/CaO	①Impregnation of $Zn(CH_3COO)_2$ from aqueous solution ②Stirring for three hours ③Air drying	550, 12	Hexagonal, cubic and irregular-shaped clusters[b] of smaller particles[f]	2000-5000[b], 13[f] (23[c])		10.95	$15 < H\_ < 18.4$	5 (recovering by filtration, washing with hexane and calcination)	Kumar and Ali (2013)
11	Zr/CaO	①Wet impregnation of $ZrOCl_2 \cdot 8H_2O$ from aqueous solution ②Stirring for four hours ③Evaporation to dry ④Heating at 120 ℃ for 24 hours	700	Irregular shaped clusters[e] of further smaller quasi-spherical particles (monoclinic crystallite)[c,f]	500-2000[b], 30[f] (28.5[c])	-	1.86	20.21 / $11.1 < H\_ < 15$	4 (recovering by filtration, washing with hexane and calcination); FAME yield: > 99 % (second run), 80 % (third run) and 40 % (fourth run)	Kaur and Ali (2014)
12	(Mo/Zr)/CaO	①Wet impregnation of $(NH_4)_6Mo_7O_{24} \cdot 4H_2O$ and ZrO_4H_4 from aqueous solution ②Stirring for four hours	650, 4	Moderately crystalline shaped particles[b]	-		6.5	20.94	2 (recovering by simple centrifugation, washing twice with acetone followed by hexane and drying at 110 ℃) with	Nasar Mansir, et al. (2018)

		③Drying at 120 ℃ for 24 hours							partial activity loss	
Co-precipitation, Mixing and Impregnation										
13	**CaO/Fe_3O_4**	Magnetic core preparation by co-precipitation: ①Dropwise addition of NH_3 in solution of $FeSO_4 \cdot 7H_2O$ and $Fe_2(SO_4)_3 \cdot 7H_2O$ ②Stirring ③Aging for one hour ④Water washing ⑤Adding magnetic core in $CaCl_2$ solution ⑥Titration by NaOH or Na_2CO_3 under stirring ⑦Aging at 65 ℃ for 18 hours ⑧Precipitation in magnetic field ⑨Washing	800, 8	Cuboid particles[b]	49.76[c]	-	3.72	-	4 (no decrease in activity); FAME yield: > 90 % (fifth run), 70 % (tenth run)	Liu, et al. (2010)

		⑩Vacuum drying at 80 ℃ for 12 hours							
14	**KF/(CaO/Fe_3O_4)**	Magnetic core preparation by co-precipitation: ①Dropwise addition of $NH_3 \cdot H_2O$ in solution of $FeSO_4 \cdot 7H_2O$ and $Fe_2(SO_4)_3 \cdot 7H_2O$ ②Stirring for 30 minutes ③Aging for one hour ④Water washing ⑤Drying at 60 ℃ for 24 hours ⑥Precipitate pulverization ⑦Mixing Fe_3O_4 with CaO ⑧Impregnation of KF from aqueous solution ⑨Drying at 105 ℃ for 24 hours	600, 3	Particles with a unique porous structure[f]	50[f]	42	20.8	-	14 (recovering by catalyst separation from permanent magnet, washing with anhydrous methanol, drying); 10 % decrease in activity	Hu, et al. (2011)

15	**KF/(CaO/NiO)**	Support preparation: ①Suspension of NiO in water and adding $Ca(NO_3)$ ②Stirring of slurry for five hours ③Drying at 120 ℃ for 24 hours ④Calcination to mixed oxide CaO/NiO at 500 ℃ ⑤Wet impregnation of KF from aqueous solution CaO/NiO ⑥Stirring for four hours ⑦Drying at 120 ℃ for 24 hours	700	Clusters[b] with rhombus shaped particles[f]	1800[b], 150[f] (41.7[c])	-	0.9	6.11 / 15 < H_ < 18.4	4 (recovering by filtration, washing with hexane and drying at 20 ℃; no decrease in activity); 50 % conversion after fifth run	Kaur and Ali (2014)
16	**KF/(CaO/MgO)**	Support separation via co-precipitation: ①Dropwise addition of solution of $CaCl_2$ and $MgCl_2$ in solution of Na_2CO_3 and NaOH	600, 3	Grains mesoporous structure[f]	100-300[f], 35[c]	34	113.8	-	6 (FAME yield: 90 %)	Wang, et al. (2009)

		②Aging at 60 ℃ for six hours ③Filtration ④Water washing ⑤Drying ⑥Calcination at 800 ℃ for four hours ⑦Isochoric impregnation by KF								
		Sol-gel								
17	**CaO/SiO_2**	①Dissolving $Ca(NO_3)_2 \cdot 4H_2O$ and TEOS in deionised water alongside HCl ②Vigorous stirring at 65 ℃ for two hours ③Addition of NH_3 to mixture ④Heating at 75 ℃ for five hours ⑤Drying at 110 ℃ for 20 hours	650, 3	-	-	-	-	-	-	Mohadesi, Hojabri and Moradi (2014)

18	**CaO**	①Dissolving $Ca(NO_3)_2 \cdot 4H_2O$ in water ②Addition of $C_2H_4(OH)_2$ to mixture ③Dropwise addition of NaOH to purified water ④Mixing for two hours ⑤Water washing for four times ⑥Elimination of NaOH and pH adjustment to 10 ⑦Heating at 80 ℃ for 20 hours ⑧Drying for one hour	800, 1	Spherical particles[b]	61[b]	-	-	-	-	Tahvildari, et al. (2015)
19	**NiO/CaO**	①Mixing $Ca(NO_3)_2 \cdot 4H_2O$, $Ni(NO_3)_2 \cdot 6H_2O$ and $C_6H_8O_7 \cdot H_2O$ with distilled water ②Vigorous stirring at 90 ℃ for two hours	700, 4	Fine particles with spherical shape	-	-	-	-	-	Vitiyaa Selva Kumar, et al. (2019)

	③Drying at 100 ℃ for three hours

^a Hammett indicator   ^d μmol CO_2/g

^b Scanning electron microscopy (SEM)   ^e Field emission scanning electron microscopy (FESEM)

^c X-ray diffraction (XRD)   ^f Transmission electron microscopy (TEM)

2.3.2.1 Thermal Decomposition

Thermal decomposition involves the pre-treatment of calcite as the fresh raw material at an elevated temperature, where it is decomposed to augment the number of active sites at the catalyst surface (Banković–Ilić, et al., 2017). In general, the availability of basic sites on catalyst surface determines the efficiency of catalysis process. For instance, it is unfavourable where water and carbon dioxide are chemisorbed onto the basic sites of CaO catalyst when the catalyst is in contact with the air, as it reduces the active sites for catalytic reaction, and thus suppressing the catalytic activity of CaO (Banković–Ilić, et al., 2017). The calcination conditions, predominantly temperature tend to affect the nature of basic sites on catalyst surface. The desorption of molecules is greatly affected by the increase of calcination temperature, causing the obstruction of active sites as well as the rearrangement of catalyst atoms on the surface (Hattori, 1995).

The $CaCO_3$ acquired from mineral calcite was employed by Bai, et al. (2009) and Yoosuk, et al. (2010) as the precursor of nano CaO catalyst in view of its environmental-friendly behaviour with low toxicity and cost, besides constituting high basicity. An elementary route with low cost was developed by Bai, et al. (2009) to derive the CaO catalyst constituting a new morphology with superior activity. By mixing $CaCl_2$ with Na_2CO_3, the spherical $CaCO_3$ precursor was produced before undergoing thermal decomposition, where the large and irregular nano-sized CaO crystals were formed after the calcination of nano-sized $CaCO_3$ particles at 1000 ℃.

It was reported by Yoosuk, et al. (2010) that the CaO in either neat or modified form such as loaded CaO and doped CaO synthesised after the calcination of calcite is feasible to be employed as a heterogeneous catalyst in producing biodiesel. However, there are certain drawbacks posed by the modified CaO where it is less effective than homogeneous catalyst on account of its low basicity and surface activity. Hence, the activity of nano-sized catalyst can be improved in terms of specific surface area and basicity through the integration of natural calcite thermal decomposition with a two-step procedure comprising of hydration and dehydration. By referring to Yoosuk, et al. (2010), this integrated technique is able to generate the nano CaO catalyst with numerous basic sites, besides exhibiting superior textural properties, which is

more suitable to be employed as a heterogeneous catalyst in biodiesel production. Generally, the catalyst was prepared in which the carbonate material was thermally decomposed into CaO before further undergoing hydration for the formation of basic sites, where the calcite that is calcined after both thermal decomposition and hydration possesses a higher catalytic activity than the natural calcite which is solely treated by thermal decomposition.

2.3.2.2 Impregnation

The impregnation method can be used to synthesise supported and mixed catalysts, whereby a definite volume of solution containing the precursor of active phase is contacted with the solid, where the latter can be the support or another active solid phase, which is followed by the subsequent drying process to remove the solvent (Perego and Villa, 1997). In general, there are two methods of contacting the solid with solution, which are wet impregnation and incipient wetness impregnation depending on the volume of solution added. According to Deraz (2018), the solution is added in excess in wet impregnation, where the solid is separated which is followed by the removal of excess solvent by drying after a certain period. On the other hand, the volume of solution with appropriate concentration is added in either equal or slightly less than the pore volume of support or another active solid phase in incipient wetness impregnation. It is then dried and calcined at elevated temperature once the catalyst is impregnated onto the support or another active solid phase.

The active catalyst precursor is usually incorporated via impregnation to acquire CaO catalysts with dopant. According to Banković–Ilić, et al. (2017), the impregnation of alkali metal ions onto the CaO nanoparticles is able to improve the basic strength of CaO catalysts. Typically, after the CaO carrier is suspended in water, it is added with the desired precursor in aqueous solution. The calcination is then performed within the temperature range of 500 ℃ and 900 ℃ to activate the precursor. It was reported by Wen, et al. (2010) that although the calcination temperature is required to be sufficiently high in order to promote the interaction of carrier with active precursor for the generation of active sites, overheating may trigger surface sintering due to agglomeration of particles, causing the specific surface area to reduce and eventually deteriorating the activity of catalyst. A little amount of moisture present in the feedstock is

tolerable in doped CaO catalyst as it tends to increase the conversion rate as well as FAME yield. However, the strong Lewis base will be converted back to weak Brønsted base with the presence of a high amount of water in the feedstock, followed by saponification.

According to Banković–Ilić, et al. (2017), there are several variables affecting the activity of CaO catalyst with dopant, which include the type of impregnated metal ion, availability of basic sites on catalyst surface as well as the interaction of metal ions with CaO catalyst. The ions of alkali metal for instance Li^+, Na^+ and K^+ are commonly used as the precursor for impregnation by varying the ion concentration. It was reported by Kumar and Ali (2010) that the specific surface area of alkali metal ion impregnated CaO nanocatalyst is higher in comparison with neat CaO catalyst where the lithium-impregnated CaO exhibits the highest specific surface area. Besides, it was inferred by Banković–Ilić, et al. (2017) that the increase of ion size tends to reduce the basic strength constituted by CaO impregnated with alkali metal ion, and thus suppressing the activity in producing biodiesel.

By referring to the studies done by various researchers, the CaO impregnated with 1.5 % Li^+ ions shows a high activity (Kumar and Ali, 2010), along with 1.75 % Li^+ ions impregnated CaO catalyst (Kaur and Ali, 2011), where the amount of dopant is added in relative to the amount of carrier. As for K^+ ions impregnated CaO catalyst, the most promising amount of dopant is 3.5 %, which is added in relative to the carrier amount (Kumar and Ali, 2012), and also about 3 % which is added corresponding to the oil amount (Degirmenbasi, et al., 2015). However, Kumar and Ali (2013) stated that the nano CaO doped with alkali metal possesses low stability as the active species might be leached into the reaction mixture. Thus, the use of transition metal ions such as manganese, iron, cobalt, copper, nickel, zinc and cadmium were investigated to activate the CaO catalyst, where the Zn^{2+} ions impregnated CaO catalyst was revealed to be the best catalyst among the synthesised catalysts under optimised reaction conditions in view of its highest basic strength (Kumar and Ali, 2013). Unlike neat CaO, the nano Zn/CaO catalyst is more resistant towards moisture even after the exposure to atmosphere. Besides, Kumar and Ali (2013) discovered that the catalytic activity of Zn/CaO can be improved by augmenting the concentration of Zn^{2+} up to 1.5 %, where the activity of catalyst

is not significantly affected by a subsequent increase in the ion concentration. On the other hand, Kaur and Ali (2014) reported that the Zr/CaO nanocatalyst evinces a better catalytic activity upon doping with about 15 % of Zr^{2+} ions.

In addition, the mixed oxides were also investigated by Hu, et al. (2011) and Kaur and Ali (2014) through the preparation of CaO/Fe_3O_4 and CaO/NiO respectively prior to the impregnation of KF in order to enhance the activity posed by CaO. The activity constituted by mixed oxides comprising of a combination of metals is normally higher when compared to the corresponding pure oxides due to the fact that either dopant itself or oxygen atom can be their active centers (Kaur and Ali, 2014). According to Kaur and Ali (2014) and Hu, et al. (2011), CaO/NiO and CaO/Fe_3O_4 catalysts exhibit the best activity with 20 wt% and 25 wt% of K^+ions impregnated respectively. It was reported that any further increase in the amount of K^+ions will not increase the catalyst basicity as KF has covered all the active centers present on the surface of catalyst, and thus increasing the time required to drive the triglyceride conversion to completion. On the other hand, it was suggested by Wen, et al. (2010), Hu, et al. (2011) and Kaur and Ali (2014) that the increase in KF concentration for impregnation causes $KCaF_3$ to be formed as new phase, and hence affecting the stability and activity.

2.3.2.3 Mixing

The physical mixing method is usually used to obtain the catalyst comprising of a mixture of metal oxides where an active component with substantial amount is applied to the oxide, where the active component plays a role as the carrier (Banković–Ilić, et al., 2017). According to Kawashima, Matsubara and Honda (2008), the specific surface area resulted from the mixing of metal oxides is smaller, which in turn cause a reduction in the number of basic sites on the catalyst. The CaO/NiO catalyst was synthesised as a carrier via mixing method by Kaur and Ali (2014) before performing KF impregnation with the purpose to acquire the desired mixed oxide nanocatalyst, where it is expected to drive the waste cottonseed oil conversion to completion through the transesterification with methanol.

2.3.2.4 Co-precipitation

The co-precipitation method can be employed to synthesise either single component catalysts or supported and mixed catalysts. The precursors of active component, which are usually in their salt forms are first dissolved in water or suitable medium before mixing with alkali solutions, leading to the formation of homogeneous solution (Perego and Villa, 1997). The solution is then subjected to either pH adjustment or evaporation to precipitate out the salts, where the salts may be hydrolysed into hydroxide forms during the hydrothermal process. The filtration and drying step are carried out in which the solid mass is collected before drying gradually to about the boiling point of medium. Since the dry mass acquired is in a loose state with irregular shape, it is first ground into powder form. After incorporating the binder to bind the powders together, the calcination process is carried out to convert the salt or hydroxide form of the active components to oxides by reacting with air at appropriate temperature (Deraz, 2018).

The co-precipitation method is generally applied to prepare the catalysts which possess superior basicity. Wang, et al. (2009) investigated the synthesis of CaO/MgO mixed oxide catalyst as the complex carrier with binary components before establishing KF impregnation under isochoric condition with the aim to produce the nano-sized catalyst with mesoporous structure and large specific surface area. It was reported that the mesoporous catalyst possesses easier separation from the product in comparison with the nano-sized catalyst. Besides, the performance of a nanomagnetic catalyst was studied by Liu, et al. (2010) where CaO is loaded onto Fe_3O_4 by employing aqueous solutions of Na_2CO_3 or NaOH as a precipitation reagent. By calcining the precursors, $Ca_2Fe_2O_5$ emerged as a cuboid crystalloid with high activity was observed under SEM, where a portion of the neat CaO was attached onto the surface. The $Ca^{2+}:Fe_3O_4$ proportion of 7:1 was reported to show the most promising biodiesel yield as at the proportion exceeding 10:1, it is suggested that an increased pure CaO is available on the surface of particle, and thus impeding the contact of reagents with catalyst. On the other hand, it was noticed that there are less active crystalloids formed at a lower proportion of 5:1.

2.3.2.5 Sol-Gel Method

The sol-gel method is the preparation of catalyst from solution through a transformation from liquid precursors to a sol, which is also known as colloidal suspension, and finally to a network structure called a gel. According to Ambat, Srivastava and Sillanpää (2018), it is used to synthesise the catalyst where it involves hydrolysis reactions, predominantly for the production of colloidal particles. The nanoparticles precipitation is attained using a precursor with appropriate amount. The sol-gel method is suitable for synthesising catalysts with high specific surface area and controlled sizes of both particle and pore, leading to the enhancement of catalytic properties (Aguilar, et al., 2001).

It was reported by Danks, Hall and Schnepp (2016) that the citric acid is used as the chelating agent during the catalyst synthesis, which is also known citrate sol-gel method. It is commonly employed for the synthesis of metal oxide powders, where the aqueous metal salts, for example nitrates are mixed with citric acid before being heated to form a viscous solution or gel. Optionally, the bases such as ammonia or ethylene diamine can be added to the resulting solution to modify the pH and enhance the binding capability of cations to the citrate. The conversion of gel to metal oxide is then attained by pyrolysis in air, with the desired temperature depending on the specific system. In fact, the method has been extensively employed to synthesise binary, ternary and quaternary metal oxides in both crystalline and amorphous forms. By referring to Vitiyaa Selva Kumar, et al. (2019), the sol-gel synthesis route enables the formation of NiO which disperses uniformly on the surface of CaO, where the finely dispersed NiO is capable of separating the CaO particles from aggregation, and thus can effectively reduce the sintering effect at elevated temperature.

Mohadesi, Hojabri and Moradi (2014) had found out that the CaO catalyst supported by SiO_2 which is synthesised via sol-gel approach, as well as their respective catalyst precursors including $Ca(NO_3)_2 \cdot 4H_2O$ and TEOS possess an impact on the catalytic activity, where the catalyst loading of 60 % is required to acquire a maximum values of biodiesel purity and yield. Besides, it was reported by Mohadesi, Hojabri and Moradi (2014) that CaO/SiO_2 catalyst produces the highest biodiesel purity and yield when compared to MgO/SiO_2 and BaO/SiO_2, which are 97.3 % and 82.1 % respectively.

In another research study done by Tahvildari, et al. (2015), the nano CaO and MgO catalysts were successfully developed using sol-gel method and employed to produce biodiesel. The nano CaO catalyst that is synthesised using sol-gel method constitutes a better efficacy, reaction duration, repeatability, methanol amount, catalyst weight percentage and biodiesel yield as compared to nano MgO catalyst synthesised using sol-gel self-combustion with urea fuel. It was reported that nano MgO catalyst is not capable to catalyse the transesterification by itself on account of its weaker basic affinity. However, when it is employed together with nano CaO catalyst, the basicity is augmented due to its surface structure, and thus allowing it to become the proper base for the catalyst with the aim to increase the contact surface of CaO and subsequently improve the biodiesel yield after transesterification reaction.

2.3.3 Doped Nano CaO as Promising CaO-based Catalyst

Besides enlarging the surface area by reducing the particle size of catalyst, the catalytic activity of neat CaO can also be improved by increasing the number of basic sites in order to expedite the transesterification reaction, where it is achieved by doping CaO that serves as both a catalyst and carrier with alkaline compound as an active ingredient. According to Marinković, et al. (2016), various alkali and organic compounds are used as doping materials such as alkali oxides, alkaline earth metals and transition metals in order to enhance the catalytic performance of CaO. A systematic survey of studies using the doped CaO nanocatalysts by various researchers are summarised in Table 2.11, where certain doped catalysts are tolerant towards high amount of FFA and moisture, while some other doped catalysts possess high reusability, which leads to a more cost-effective biodiesel production.

Table 2.11: Review of Doped CaO Catalysts Used in Biodiesel Production.

Feedstock	Catalyst	Optimal Reaction Conditions				Biodiesel Yield (Conversion) (%)/Reaction Time (hr)	Advantages of Catalyst	Reference
		Stirring Speed (rpm)	Methanol to Oil Molar Ratio (mol/mol)	Catalyst Loading (wt% with respect to oil)	Reaction Temperature (°C)			
Rapeseed Oil	$LiNO_3$/CaO, $NaNO_3$/CaO, KNO_3/CaO	600	6:1	5	60	(100)/3	Complete conversion of non-edible oil	MacLeod, et al. (2008)
Waste Cottonseed Oil	LiC/CaO	-	12:1	5	65	(100)/0.75	Complete conversion of non-edible oil having a high amount of moisture and FFAs	Kumar and Ali (2010)
Karanja Oil	Li^+/CaO	-	12:1	5	65	(99)/1	Complete conversion of non-edible oil	Kaur and Ali (2011)
Waste Cottonseed Oil	K/CaO	-	12:1	7.5	65	> 99/1.25	①High tolerance to FFA and moisture contents ②Reusable	Kumar and Ali (2012)

Chinese Tallow Seed Oil	**KF/CaO**	-	12:1	4	65	96/2	①Reusable ②Good anti-acidic ability ③Superior activity and stability ④Higher activity and greater tolerance to FFA poisoning as compared to pure CaO	Wen, et al. (2010)
Rapeseed Oil	**KF/CaO**	-	-	-	81.5	93.7/-	①Wet washing of biodiesel is not required, therefore no environmental pollution ②Continuous process with automatic glycerol separation and cyclic utilisation of methanol	Hu, et al. (2012)

							③Long lifetime and good stability, thus reducing production cost	
Canola Oil	K_2CO_3/**CaO**	600	9:1	3	65	97.67/8	①High activity ②Reusable	Degirmenbasi, et al. (2015)
Waste Cottonseed Oil	**Zn/CaO**	500	9:1	5	65	99/0.75	①Reusable ②Complete conversion of waste and non-edible oils with high FFA content ③High tolerance to FFA and moisture contents ④Short reaction time	Kumar and Ali (2013)
Jatropha Oil	**Zr/CaO**	500	15:1	5	65	99/1.83	①Reusable ②High tolerance to FFA and moisture contents	Kaur and Ali (2014)

Karanja Oil	**Li/CaO, Na/CaO, K/CaO**	600	12:1	2	65	90.3/8	①High activity ②Reusable	Meher, et al. (2006)
Food Grade Sunflower Oil	**Li/CaO**	1000	14:1	0.2	60	90/1.5	①High activity ②Reusable	Alonso, et al. (2009)

Numerous researchers have employed wet impregnation method in order to synthesise the doped CaO catalyst in nano form to be used for transesterification of feedstocks containing FFAs. The catalytic performance of neat CaO is improved by the impregnation of metal dopants, where it was affirmed by Marinković, et al. (2016) that the doping of alkali metal ions to CaO can form strong basic sites on catalyst surface, which eventually leads to a high basic strength and thus enhancing the catalytic activity in transesterification reaction. It was reported by Kumar and Ali (2010) that LiC/CaO shows a superior catalytic performance in the transesterification reaction of vegetable oil as the complete conversion is achieved only in 45 minutes at 65 ℃ as well as within 6 hours at 35 ℃. Hence, LiC/CaO is inferred as a potential nanocatalyst in converting the cheap feedstocks containing high FFA and moisture contents to biodiesel, which in turn reduces the production cost. Besides, Kaur and Ali (2011) found that the Li impregnated CaO catalyst possesses a higher specific surface area as compared to neat CaO. According to Kumar and Ali (2012), the CaO doped with K^+ ions was proved to be effective in the transesterification of various feedstocks such as jatropha, karanja, castor, Chinese tallow seed, rapeseed, cotton and soybean oils. Another doped catalyst, K_2CO_3/CaO renders the advantages of easy impregnation, low cost and inert to environment (Degirmenbasi, et al., 2015). It is also highlighted that Zn/CaO and Zr/CaO are able to facilitate the complete conversion of waste oil and non-edible oil respectively in transesterification reaction at 65 ℃.

A distinct correlation between basic strength and activity was found by MacLeod, et al. (2008), where the alkali metal doped CaO catalysts including $LiNO_3$/CaO, $NaNO_3$/CaO, KNO_3/CaO have attained a conversion higher than 99 % within 3 hours in methanolysis of rapeseed oil. By referring to Kumar and Ali (2012) and Kumar and Ali (2013), K and Zn doped CaO are feasible to be used in transesterification of various waste and non-edible oils with a high FFA content without any pre-treatment as both the doped CaO catalysts are highly tolerate to variations of FFA and moisture contents. In addition, it was claimed by Wen, et al. (2010) that the KF impregnated CaO is highly efficient in biodiesel production from feedstocks with a high FFA value, where the methyl ester yield achieved is higher than 96 % within two and a half hours of transesterification of Chinese tallow seed oil containing 40 to 70 % FFAs under

mild reaction condition. Hence, it signifies that the doped CaO catalyst is able to withstand saponification and renders a better resistance to acid, making it a more useful catalyst as the soap formation is not favourable in biodiesel production which might cause a decline in biodiesel yield. It was further reported that KF/CaO remains active and stable through 16 successive cycles, whereby the FAME yield in the last cycle is above 91 %.

2.3.4   Parameters Affecting Performance of Nano CaO Catalysts

Calcination is the most commonly employed method to prepare the biomass-derived CaO catalyst where it involves the thermal treatment in the absence or limited supply of air or oxygen to decompose or break down the compound into a smaller constituent. It is typically performed at the temperature ranging from 300 to 1000 ℃, conditional upon the type of feedstock used. For instance, $CaCO_3$ in the organic compound such as waste shell is broken down into CaO upon combustion at high temperature and emits CO_2 gas at the same time. Figure 2.6 shows the conventional procedure to synthesise the waste shell-derived CaO catalyst.
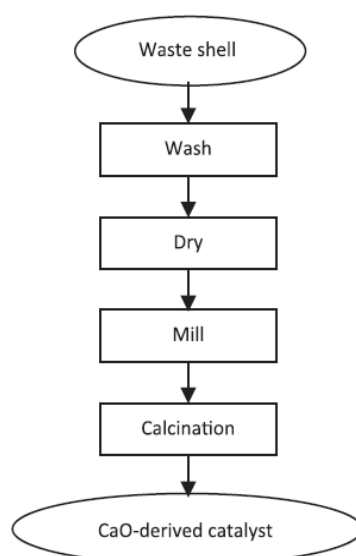
Figure 2.6: General Procedure for Preparation of CaO-derived Catalyst (Sharifah, et al., 2017).

Besides, the doping of some catalytically active species into a CaO carrier is performed during the preparation of CaO-based catalyst in order to improve its basic strength by increasing the number of basic sites, leading to a higher catalytic activity in doped CaO as compared to neat CaO. By referring to Banković–Ilić, et al. (2017), the oxides of alkali and transition metals are the loaded materials that are most commonly used as dopants in impregnation method. The doping process is started off with the calcination of catalyst precursor which corresponds to the metal targeted, where they are the porous substances that are thermally non-stable at high temperatures, followed by wet impregnation before converting the catalyst into active form by re-calcination, as shown in Figure 2.7.

Similar with undoped CaO catalyst, the selection of calcination temperature for doped CaO catalyst depends on the type of feedstock used for biodiesel production. In wet impregnation, the highly basic metal salt as active metal precursor is typically amalgamated with the CaO in organic or aqueous solution before undergoing calcination to synthesise the doped catalyst, where the metal salt tends to diffuse into the porous structure of catalyst during impregnation. The impregnated calcined sample is then subjected to thermal activation to remove the moisture and other volatile matters as well as to deposit the metal salt on the surface of catalyst (Sharifah, et al., 2017).
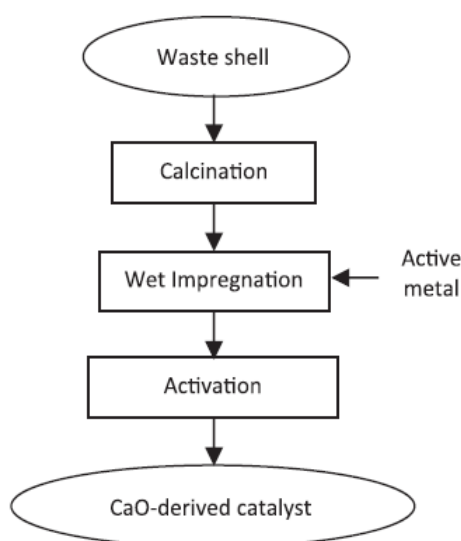
Figure 2.7: General Procedure for Preparation of CaO-derived Catalyst with Active Metal as Dopant (Sharifah, et al., 2017).

There are a number of catalytic variables that are needed to be optimised for nano CaO-based catalyst with the aim to acquire a promising biodiesel yield, which include

(i)   Dopant type.

(ii)   Dopant concentration.

(iii)   Calcination temperature.

(iv)   Calcination duration.

2.3.4.1   Types of Dopant

The use of various alkali metal ions including Li^+, Na^+ and K^+ for the nano CaO-based catalyst was investigated by Kumar and Ali (2010) for the waste cottonseed oil transesterification. It was known that the basic strength and activity tend to be reduced with the increase of alkali metal ion size, where the Li/CaO nanocatalyst was found to possess the highest activity owing to the formation of strong basic sites on catalyst surface and high specific surface area. Besides, the doping of K^+ ions on CaO produces a catalyst which is effective in catalysing transesterification using various feedstocks including soybean, jatropha, karanja, rapeseed, Chinese tallow seed, castor and cotton oils. However, the activation of alkali metal ion doped CaO some drawbacks as such catalyst shows a poor stability due to the fact that the active species tend to be leached in reaction medium. Hence, the use of transition metal ions is served as the potential alternative to activate the CaO nanocatalysts.

The activity of transition metal ion doped CaO nanocatalysts was evaluated by Kumar and Ali (2013) where different ions of transition metal such as manganese, iron, cobalt, nickel, copper, zinc and cadmium are incorporated to CaO through doping, in which 1.5 wt% of transition metal ion is doped in each case. Figure 2.8 illustrates the effect of various transition metal ions towards biodiesel yield by employing 5 wt% of catalyst loading with respect to oil, methanol-to-oil molar ratio of 9:1, reaction temperature of 65 °C and reaction duration of 45 minutes, with the calcination temperature of 550 °C and calcination duration of 12 hours employed during catalyst synthesis.
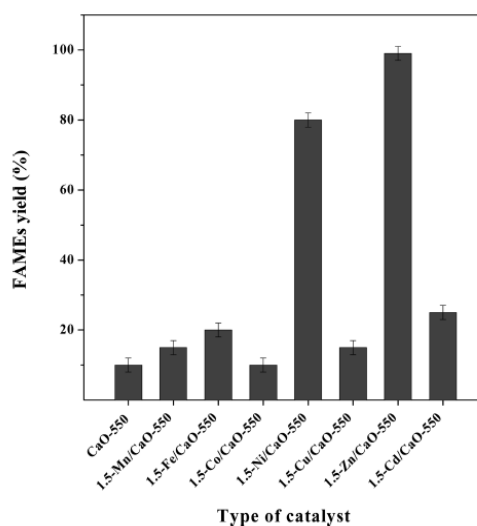
Figure 2.8: Effect of Type of Transition Metal Ions on Biodiesel Yield (Kumar and Ali, 2013).

By investigating the effect of various transition metal ions on the catalytic activity of CaO, Zn/CaO was reported to possess the highest activity towards transesterification of waste cottonseed oil under optimised reaction conditions among the doped catalysts, with an increase of FAME yield in the following order: Co/CaO < neat CaO < Cu/CaO < Mn/CaO < Fe/CaO (all with yields less than 20 %) < Cd/CaO < Ni/CaO (80 % yield) < Zn/CaO (98 % yield). It is known that the activity of heterogeneous base catalyst in transesterification reaction is a function of the basic strength, where Zn/CaO was observed to have the maximum basicity among various other transition metal doped CaO catalysts, resulting in a higher catalytic activity (Kumar and Ali, 2013). The higher activity of nanocrystalline Zn/CaO catalyst is attributed to the formation of stronger basic sites after the doping of Zn. Besides, the Zn-doped CaO nanocatalyst is proven to be more resistant towards moisture without undergoing deterioration, unlike pure CaO where it may lose activity even after being exposed to the moisture in atmosphere.

2.3.4.2 Amount of Dopant Loading

The optimum impregnated ion content for different nano CaO-based catalysts to acquire complete conversion is summarised in Table 2.12.

Table 2.12: Optimum Concentration of Impregnated Ion for Various Nano CaO Catalysts.

Feedstock	Nanocatalyst	Ion Concentration (wt%)	Reference
Waste Cottonseed Oil	LiC/CaO	1.5	Kumar and Ali (2010)
Karanja Oil	Li^+/CaO	1.75	Kaur and Ali (2011)
Waste Cottonseed Oil	Ni/CaO	0.5	Kumar, Abida and Ali (2016)
Waste Cooking Oil	Ba/CaO	1	Boro, et al. (2014)
Waste Cottonseed Oil	K/CaO	3.5	Kumar and Ali (2012)
Chinese Tallow Seed Oil	KF/CaO	25	Wen, et al. (2010), Hu, et al. (2012).
Waste Cottonseed Oil	Zn/CaO	1.5	Kumar and Ali (2013)
Jatropha Oil	Zr/CaO	15	Kaur and Ali (2014)
Waste Cooking Palm Oil	(Mo/Zr)/CaO	10	Nasar Mansir, et al. (2018)
Canola Oil	K_2CO_3/CaO	3	Degirmenbasi, et al. (2015)
Waste Cottonseed Oil	KF/(CaO/NiO)	20	Kaur and Ali (2014)
Rapeseed Oil	KF/(CaO/MgO)	25	Wang, et al. (2009)
Stilingia Oil	KF/(CaO/Fe_3O_4)	25	Hu, et al. (2011)

A series of catalysts was synthesised with various metal ion concentration prior to the transesterification under different operating conditions with the aim to identify the optimum amount of metal ion required to be impregnated onto the CaO surface. The optimum Ni^{2+} content to attain the minimum time for complete transesterification was reported to be 0.5 wt% by Kumar, Abida and Ali (2016), whereas the optimum concentration of Li^+ ion was found to be 1.5 wt% by Kumar and Ali (2010), or 1.75 wt% by Kaur and Ali (2011). Meanwhile, the optimum K^+ concentration falls within a broad range, where it is contingent upon the nanocatalyst and feedstock type used. For instance, 25 wt% with KF/(CaO/MgO) and rapeseed oil, 20 wt% with KF/(CaO/NiO) and waste cottonseed oil as well as 25 wt% with KF/CaO and Chinese tallow seed oil were proposed by Wang, et al. (2009), Kaur and Ali (2014) and Wen, et al. (2010), Hu, et al. (2012) respectively.

It was found by Kumar and Ali (2012) that basic strength of potassium impregnated CaO might be affected by the K^+ concentration, where the amount of impregnated potassium is varied from 1.5 to 5.5 wt% in determining the optimum K^+ concentration that exhibit the most superior activity. It was reported that the reaction time needed to drive the transesterification towards completion is reduced from 2.5 to 1.25 hours when the mass fraction of potassium in CaO increases from 1.5 to 3.5 wt%. In fact, the pure nano CaO catalyst produces the biodiesel with less than 10 % even after 10 hours of transesterification reaction, suggesting that the K^+ doping is required in enhancing the activity of potassium impregnated CaO. A subsequent increase in K^+ concentration above 3.5 wt% will neither increase the basic strength nor catalytic activity, concluding that 3.5 wt% K^+ concentration is the optimum dopant loading for attaining the maximum catalytic activity.

In another study done by Kumar and Ali (2013), the nano CaO catalyst was doped with different concentration of Zn^{2+} in determining the optimum dopant concentration to improve the activity. Figure 2.9 illustrates the impact of Zn^{2+} concentration towards the biodiesel yield by employing 5 wt% of catalyst loading with respect to oil, methanol-to-oil molar ratio of 9:1, reaction temperature of 65 ℃ and reaction duration of 45 minutes, with the calcination

temperature of 550 ℃ and calcination duration of 12 hours employed during catalyst synthesis.
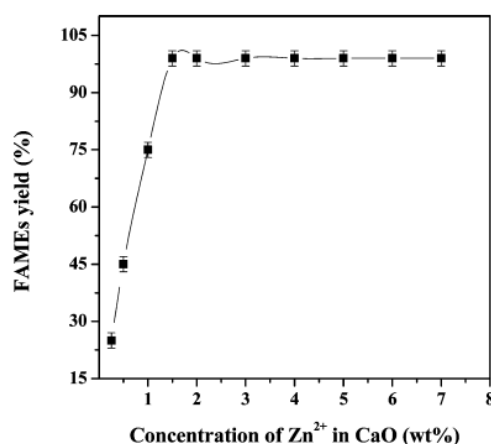
Figure 2.9: Effect of Zn^{2+} Concentration on Biodiesel Yield Using Zn/CaO Catalyst (Kumar and Ali, 2013).

By referring to Figure 2.9, the basic strength of Zn/CaO catalyst is affected by the increase in the Zn^{2+} concentration, which can in turn influence the catalytic activity. Kumar and Ali (2013) suggested that the activity of Zn/CaO catalyst is improved only with the increase of Zn^{2+} concentration up to 1.5 wt%, where neither basic strength nor activity of Zn/CaO has been affected by a subsequent increase in Zn^{2+} concentration, with no significant change in biodiesel yield. Table 2.13 summarises the basic strength of Zn/CaO nanocatalyst by varying the concentration Zn^{2+} as dopant.

Table 2.13: Effect of Zn^{2+} Concentration on Various Parameters of Zn/CaO Catalyst (Kumar and Ali, 2013).

Catalyst Type	Basicity (pK_{BH+})
CaO	$9.8 < pK_{BH+} < 10.1$
0.25-Zn/CaO-550	$10.1 < pK_{BH+} < 11.1$
0.5-Zn/CaO-550	$11.1 < pK_{BH+} < 15.0$
1-Zn/CaO-550	$11.1 < pK_{BH+} < 15.0$
1.5-Zn/CaO-550	$15.0 < pK_{BH+} < 18.4$
2-Zn/CaO-550	$15.0 < pK_{BH+} < 18.4$

3-Zn/CaO-550	$15.0 < pK_{BH+} < 18.4$
4-Zn/CaO-550	$15.0 < pK_{BH+} < 18.4$
5-Zn/CaO-550	$15.0 < pK_{BH+} < 18.4$
6-Zn/CaO-550	$15.0 < pK_{BH+} < 18.4$
7-Zn/CaO-550	$15.0 < pK_{BH+} < 18.4$

Note: 1.5-Zn/CaO-550; 1.5 = dopant concentration (wt%), 550 = calcination temperature (℃)

According to Banković–Ilić, et al. (2017), the basicity and activity of nano CaO-based catalyst remain constant when the metal ion is doped at a higher amount than the optimal one. Besides, the reaction time required for complete oil conversion is reduced to a minimum value where it does not encounter any further change. It was reported by Kaur and Ali (2014) that the highest basic strength is attained by employing 15 wt% of zirconium when Zr^{4+} ion is doped to the CaO nanocatalyst.

2.3.4.3 Calcination Temperature

The calcination temperature is a crucial parameter that needs to be considered in forming CaO-based catalyst and developing its surface morphology as it determines the structural and catalytic properties of catalyst. According to Sharifah, et al. (2017), the total specific surface area of CaO-based catalyst is indicated by the particle size developed on the surface of catalyst as the waste shells are generally non-porous. Thus, the activity of CaO-based catalyst is said to be immensely contingent upon the temperature employed for calcination as it is able to generate the catalytic sites which are actively present on the catalyst surface. By referring to Banković–Ilić, et al. (2017), the calcination is required to be carried out at sufficiently high temperature for definite time span as it is able to eliminate the adsorbed CO_2 molecules and moisture from the surface of catalyst, and consequently restoring catalytic activity.

A series of different calcination temperatures was investigated by Smith, et al. (2013) on bovine bone waste where it was observed that the yield of FAME is not prominently changed when the sample is treated under the calcination temperature ranging from 350 ℃ to 550 ℃. Thus, it is inferred that the

temperature employed for calcination does not provide sufficient energy to convert $CaCO_3$ in the bovine bone into CaO. It was affirmed by Smith, et al. (2013) in their further study that CaO in the calcined bone sample is present once the temperature is increased by 300 ℃ from 650 ℃ for calcination, where the catalyst calcined at the temperature of 750 ℃ results in the highest FAME yield for biodiesel production. In addition, the additional void is created on the surface of catalyst due to CaO formation, and thus augmenting the pore diameter and total pore volume of synthesised catalyst simultaneously, where both serve as the prerequisites to establish a higher catalytic activity. However, a substantial activity reduction was reported by Smith, et al. (2013) with the further increment in the calcination temperature surpassing 950 ℃ on account of low pore volume accompanied by the presence of micropores, which in turn reducing the number of accessible active sites on the catalyst surface.

Besides, the effect of calcination temperature on the surface morphology of calcined CaO sample was studied by Boro, Deka and Thakur (2012), where the catalyst surface is observed to possess uneven and clustered arrangement under the calcination temperature of 600 ℃. It is inferred that the additional pores are present on the surface of catalyst since the total pore volume does not show any significant change. On the other hand, CaO catalyst particles are comprised of different shapes and sizes when the sample is calcined at a higher temperature ranging from 700 to 900 ℃, where the higher degree of calcination causes the specific surface area to increase in view of the growth of CaO crystals in the calcined sample. Besides surface area, the porous structure is developed on catalyst surface as the pore volume in the waste shell is increased after calcination.

There are a number of attempts in optimising the calcination temperature of various CaO-based nanocatalysts, where the optimum temperature for calcination of different CaO-based nanocatalysts are summarised in Table 2.14.

Table 2.14: Optimum Calcination Temperature for Various Nano CaO Catalysts.

Catalyst	Calcination Temperature (°C)	Biodiesel Yield, Y/Conversion, C (%)	Reference
CaO (Calcit)	1000	98.72 (Y)	Bai, et al. (2009)
CaO, 97.2 (Calcit)	600	95.7 (Y)	Yoosuk, et al. (2010)
Ni/CaO	650	99 (Y)	Kumar, Abida and Ali (2016)
KF/CaO	600	96 (Y)	Wen, et al. (2010), Hu, et al. (2012)
K_2CO_3/CaO	500	97.67 (Y)	Degirmenbasi, et al. (2015)
Zn/CaO	550	99 (Y)	Kumar and Ali (2013)
Zr/CaO	700	99 (Y)	Kaur and Ali (2014)
CaO/Fe_3O_4	800	99 (C)	Liu, et al. (2010)
KF/(CaO/NiO)	700	99 (Y)	Kaur and Ali (2014)
KF/(CaO/Fe_3O_4)	600	95 (Y)	Hu, et al. (2011)
KF/(CaO/MgO)	600	95 (Y)	Wang, et al. (2009)

There are a variety of doped CaO nanocatalysts used to study the impact of calcination temperature towards the biodiesel yield. According to Kumar, Abida and Ali (2016), by employing Ni doped CaO nanocatalyst, the amount of biodiesel produced increases when the calcination temperature is increased, which is followed by the decrease in biodiesel yield after the optimal calcination temperature. It is inferred that the active centers of catalyst are well developed when the optimum calcination temperature is applied, which in turn enhance the catalyst efficiency. However, the reduction in the number of active sites on catalyst surface occurs at the temperature exceeding the optimal one as the

prolonged calcination will probably lead to surface sintering, which causes the specific surface area of catalyst to reduce. Besides, Kaur and Ali (2014) reported the similar experimental result by employing the CaO/NiO composite nanocatalyst loaded with KF where the biodiesel yield is increased along with calcination temperature as the high specific surface area of catalyst crystals are gradually developed with outstanding stability. Upon reaching the maximum allowable biodiesel yield, a small fraction of the catalytically active component is probably to be lost under higher calcination temperatures, and thus reducing the biodiesel yield due to severe catalyst agglomeration.

In another study done by Kumar and Ali (2013), the Zn doped CaO nanocatalyst was calcined at the temperature ranging from 150 ℃ to 950 ℃ in determining the optimum temperature for calcination to enhance the activity, where the FAME yield was reported to increase to 99 % from 38 % when the calcination temperature is raised from 150 ℃ to 550 ℃. It was revealed by Kumar and Ali (2013) that $Ca(OH)_2$ is the dominant phase at the temperature below 550 ℃, while CaO starts to predominate in Zn/CaO catalyst at 550 ℃ or above. Since CaO is more basic than the corresponding derivative, $Ca(OH)_2$, the former component shows a better catalytic activity towards transesterification reaction. Moreover, the surface area of Zn doped CaO catalyst is higher at the calcination temperature of 550 ℃, which in turn increase the concentration of CaO at the catalyst surface. Figure 2.10 illustrates the effect of calcination temperature on the biodiesel yield by employing 5 wt% of catalyst loading with respect to oil, methanol-to-oil molar ratio of 9:1, reaction temperature of 65 ℃ and reaction duration of 45 minutes, with the calcination duration of 12 hours employed during catalyst synthesis.
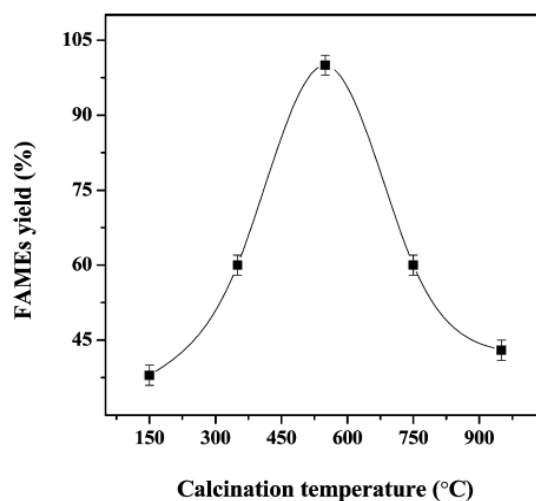
Figure 2.10: Effect of Calcination Temperature on Biodiesel Yield Using Zn/CaO Catalyst (Kumar and Ali, 2013).

By referring to Figure 2.10, the FAME yield was reported to reduce significantly with a subsequent rise in the temperature above 550 ℃ for calcination as the specific surface area and basic strength possessed by the catalyst are reduced owing to the sintering effect of Zn/CaO particles, leading to lower catalytic activity. Table 2.15 summarises the basic strength, surface area and average crystallite size of Zn/CaO nanocatalyst for various calcination temperatures.

Table 2.15: Effect of Calcination Temperature on Various Parameters of Zn/CaO Catalyst (Kumar and Ali, 2013).

Catalyst Type	Basicity (pK_{BH+})	BET Surface Area (m^2/g)	Average Crystallite Size (nm)[a]
CaO	$9.8 < pK_{BH+} < 10.1$	3.96 ± 0.01	104
1.5-Zn/CaO-150	$11.1 < pK_{BH+} < 15.0$	4.49 ± 0.01	27
1.5-Zn/CaO-350	$11.1 < pK_{BH+} < 15.0$	5.08 ± 0.02	27
1.5-Zn/CaO-550	$15.0 < pK_{BH+} < 18.4$	10.95 ± 0.01	23
1.5-Zn/CaO-750	$15.0 < pK_{BH+} < 18.4$	9.17 ± 0.04	30
1.5-Zn/CaO-950	$11.1 < pK_{BH+} < 15.0$	2.52 ± 0.01	75

Note: 1.5-Zn/CaO-550; 1.5 = dopant concentration (wt%), 550 = calcination temperature (℃)

[a] On a (200) reflection plane by Debye-Scherrer method

2.3.4.4 Calcination Duration

The holding time for calcination is crucial in developing the CaO-based catalyst due to the fact that it plays a significant role to generate the active sites as well as enhance the catalytic and structural performance of catalyst. According to Sharifah, et al. (2017), the short holding time is deemed to constitute certain drawbacks due to the fact that the CaO is possibly to be underdeveloped, leading to inferior activity. Hence, a sufficiently long calcination duration is necessary to completely convert $CaCO_3$ to CaO, which to be used as a carrier before incorporating the dopant to further enhance the activity of CaO catalyst. However, sintering is expected to be taken place through prolonged calcination, resulting in the coalescence and agglomeration of particles. Thus, the following shrinkage of catalyst grains tends to reduce the total effective surface area, and thus significantly suppressing the catalytic activity (Roschat, et al., 2012).

Similar with calcination temperature, the calcination duration is optimised in order to restore and further improve the activity of CaO-based catalyst. The optimum calcination duration of different CaO-based nanocatalysts are tabulated in Table 2.16 by referring to a number of findings done by researchers.

Table 2.16: Optimum Calcination Duration for Various Nano CaO Catalysts.

Catalyst	Calcination Duration (hrs)	Biodiesel Yield, Y/Conversion, C (%)	Reference
CaO (Calcit)	2	98.72 (Y)	Bai, et al. (2009)
CaO, 97.2 (Calcit)	3	95.7 (Y)	Yoosuk, et al. (2010)
KF/CaO	3	96 (Y)	Wen, et al. (2010), Hu, et al. (2012)
K_2CO_3/CaO	3	97.67 (Y)	Degirmenbasi, et al. (2015)
CaO/Fe_3O_4	8	99 (C)	Liu, et al. (2010)
KF/(CaO/Fe_3O_4)	3	95 (Y)	Hu, et al. (2011)
KF/(CaO/MgO)	3	95 (Y)	Wang, et al. (2009)

By referring to Table 2.16, it can be deduced that the nano CaO-based catalysts are mostly calcined over a period of two to three hours. Degirmenbasi, et al. (2015) reported that the biodiesel yield increases alongside the calcination duration by employing K_2CO_3-doped CaO nanocatalyst, where upon achieving a maximum yield value it encounters a gradual drop due to prolonged calcination. In another study done by Liu, et al. (2010), a relatively greater holding time for calcination was attempted where the CaO/Fe_3O_4 mixed oxide nanocatalyst is calcined for eight hours. Although there is a possibility for the catalyst system to encounter sintering effect in view of extended calcination period, it was proved by Liu, et al. (2010) that the calcination duration attempted is deemed ample to synthesise the catalyst with good performance which possesses a high number of active sites for catalytic reaction. However, some of the active components of CaO/Fe_3O_4 mixed oxide nanocatalyst are subject to certain extent of destruction under prolonged calcination, leading to the reduction in active sites and subsequently lowering the specific surface area of catalyst. According to Banković–Ilić, et al. (2017), the catalyst agglomeration caused by the calcination for extended period of time tends to reduce the total biodiesel yield.

2.4   Production of Biodiesel

Transesterification is the most conventional approach for biodiesel production, where it is a chemical reaction between triglyceride molecules present in animal fats or vegetable oils and alcohol with or without the presence of catalyst to produce fatty acid alkyl esters and glycerol. It consists of a sequence of three consecutive reversible reactions, which is illustrated in Figure 2.11 using methanol as the example of alcohol.
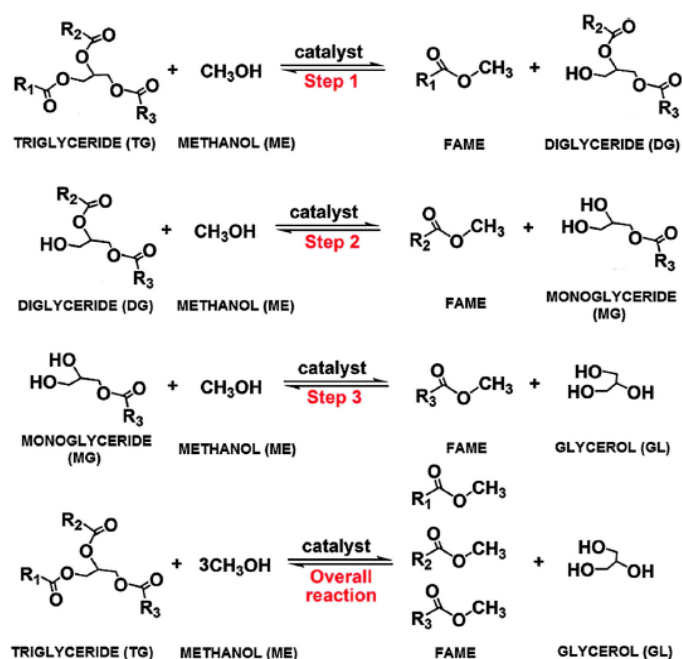
Figure 2.11: Transesterification Reaction Steps of Triglycerides with Methanol (Borges and Díaz, 2012).

It is known that an ester is produced in each step and thus three ester molecules are produced from one triglyceride molecule, where the formation of methyl esters from monoglycerides is known to be the step that determines the rate of transesterification reaction as monoglycerides are the most stable intermediate compounds (Ma and Hanna, 1999). The transesterification reaction generally requires a homogeneous or heterogeneous catalyst to split the oil molecules and alcohol in order to combine with the separated esters, where its elemental function is to improve the rate of transesterification reaction and enhance the biodiesel yield. Transesterification is more preferred over other methods such as pyrolysis or catalytic cracking and microemulsion as it is able to lower the viscosity of triglycerides, besides producing glycerol as the by-product which possesses a commercial value. Among all the existing alternatives for biodiesel production, transesterification seems to be the best choice as the physical properties of FAMEs produced are very close to those of diesel fuel (Demirbas, 2009). Moreover, it is a relatively simple process.

The transesterification reaction proceeds by reacting the oil feedstock with primary or secondary monohydric aliphatic alcohols containing 1 to 8 carbon atoms. Among various alcohols such as methanol, ethanol, propanol,

butanol and amyl alcohol, methanol and ethanol are the most frequently used alcohols in the transesterification reaction. According to Demirbas (2005), ethanol is preferred over methanol as it is generally renewable and biologically less objectionable in the environment due to the fact that it can be derived from agricultural products. Still, methanol is more preferred as it is cheaper and possesses wide industrial availability, besides possessing certain physical and chemical advantages as it is the polar and shortest chain alcohol. Since every step of transesterification process is reversible in nature, excess alcohol is added alongside the catalyst in order to accelerate the forward reaction, shifting the equilibrium to the right and thereby increasing the rate of biodiesel formation. By referring to Issariyakul and Dalai (2014), the purity of biodiesel is examined by various analytical instrument such as gas chromatography, liquid chromatography, nuclear magnetic resonance spectroscopy, infra-red spectroscopy or thin layer chromatography, besides comparing different fuel properties of biodiesel such as density, viscosity, flash point and calorific value with petroleum diesel.

2.4.1　Parameters Affecting Biodiesel Yield

There are several process parameters that affect the biodiesel yield, which are listed as follows:

(i)　Catalyst loading.

(ii)　Alcohol-to-oil molar ratio.

(iii)　Reaction temperature.

(iv)　Reaction time.

Since the stated parameters play a key role in biodiesel production, it is necessary to optimise the reaction conditions following the synthesis of nano CaO-based catalyst in order to attain the promising amount of biodiesel.

2.4.1.1　Catalyst Loading

The amount of catalyst needed in producing biodiesel constitutes significant environmental and economical impact. By referring to Kouzu, et al. (2010), the nano CaO catalyst that possesses strong basic strength is able to expedite the transesterification of oil feedstock even at small catalyst concentration. In

general, the biodiesel yield is augmented by increasing the catalyst amount as it can predominantly increase the number of active sites available on catalyst surface for transesterification, besides accelerating the reaction to forward direction (Zhao, Qiu and Stagg-Williams, 2013). However, there is an optimum amount of the catalyst, depending on the feedstock used and reaction conditions applied. Table 2.17 summarises the optimum amount of catalyst loading with respect to oil for transesterification of different nano CaO-based catalysts by referring to several findings done by researchers.

Table 2.17: Optimum Catalyst Amount for Transesterification of Various Nano CaO Catalysts.

| Catalyst | Catalyst Loading Attempted (wt%) | Optimal Reaction Conditions | | Reference |
		Catalyst Loading (wt%)	Biodiesel Yield, Y/Conversion, C (%)	
CaO (Calcit)	3	-	98.72 (Y)	Bai, et al. (2009)
CaO, 97.2 (Calcit)	7	-	95.7 (Y)	Yoosuk, et al. (2010)
LiC/CaO	1-8	5	100 (C)	Kumar and Ali (2010)
Li^+/CaO	1-10	5	99 (C)	Kaur and Ali (2011)
Ni/CaO	2-7	5	99 (Y)	Kumar, Abida and Ali (2016)
Ba/CaO	0.1-1.4	1	98 (C)	Boro, et al. (2014)
K/CaO	2.5-12.5	7.5	99 (Y)	Kumar and Ali (2012)
KF/CaO	1-5	4	96 (Y)	Wen, et al. (2010), Hu, et al. (2012)
K_2CO_3/CaO	1-7	3	97.67 (Y)	Degirmenbasi, et al. (2015)

Zn/CaO	1-10	5	99 (Y)	Kumar and Ali (2013)
Zr/CaO	1-6	5	99 (Y)	Kaur and Ali (2014)
(Mo/Zr)/CaO	1-5	3	90.1 (Y)	Nasar Mansir, et al. (2018)
CaO/Fe_3O_4	2	-	99 (C)	Liu, et al. (2010)
KF/(CaO/NiO)	1-6	5	99 (Y)	Kaur and Ali (2014)
KF/(CaO/Fe_3O_4)	1	-	95 (Y)	Hu, et al. (2011)
KF/(CaO/MgO)	3	-	95 (Y)	Wang, et al. (2009)

By referring to Zhao, Qiu and Stagg-Williams (2013), the biodiesel yield does not increase notably when the catalyst concentration applied is higher than the optimal one mainly owing to the formation of three-phase reaction mixture with higher viscosity alongside the mass transfer resistance, where the emulsion formed suppresses the efficiency of biodiesel recovery. Moreover, there is a possibility to initiate the saponification reaction with the amount catalyst loading which exceeds the optimum value.

In spite of the fact that the rate of transesterification reaction is typically increased by employing a higher concentration of catalyst, a minimum amount of catalyst is always preferable in order to ensure a more economically viable and greener production of biodiesel. The transesterification by employing Jatropha oil was investigated by Kaur and Ali (2014) to determine the optimum amount of catalyst loading where the Zr concentration impregnated on CaO nanocatalyst is altered from 1 to 6 wt% in regard to oil. Figure 2.12 illustrates the effect of catalyst concentration on the FAME conversion by employing methanol-to-oil molar ratio of 15:1, reaction temperature of 65 ℃ and reaction time of 105 minutes.
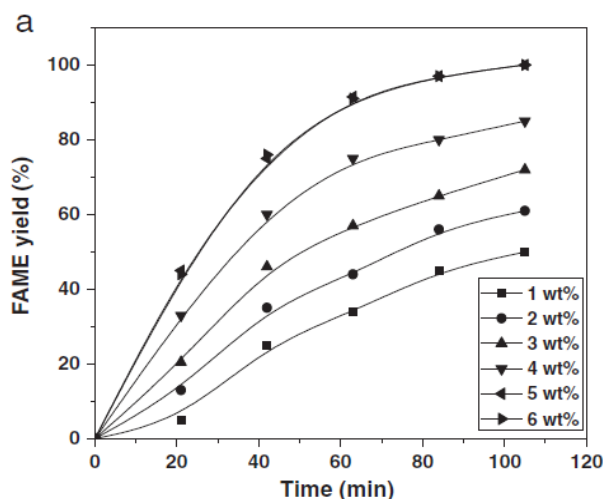
Figure 2.12: Effect of Catalyst Concentration on FAME Yield Using Zr/CaO Catalyst (Kaur and Ali, 2014).

It was reported by Kaur and Ali (2014) that the FAME yield is prominently increased by augmenting the catalyst amount by 4 wt% from 1 wt%, where a 5 wt% catalyst concentration requires 105 min for the complete Jatropha oil conversion into corresponding FAME, which is attributed to the sufficient number of active catalytic sites available for the reaction. On the other hand, the macropore structures of catalyst provide sufficient external surface which acts as the active site for rapid mass transfer in transesterification. Based on Figure 2.12, the reaction time and FAME yield are not significantly reduced by a subsequent increase in catalyst concentration above 5 wt% due to the fact that the reaction mixture with higher catalyst loading becomes more viscous which may resist the diffusion in the methanol-oil-catalyst system. Moreover, the catalyst with dosage that is beyond the optimum level might adsorb more products, which consequently reduce the biodiesel yield.

In another study done by Kumar and Ali (2013), a series of waste cottonseed oil methanolysis was carried out with 1 to 10 wt% Zn doped CaO nanocatalyst by employing methanol-to-oil molar ratio of 9:1, reaction temperature of 65 ℃ and reaction time of 45 minutes, where the biodiesel yield was reported to be enhanced when the catalyst concentration is augmented by 4 wt% from 1 wt%. It was reported that the methanolysis by utilising 5 wt% of catalyst requires the minimum time, which is 45 minutes for the complete conversion of waste cottonseed oil into corresponding FAMEs. Similarly with

Jatropha oil methanolysis using Zr doped CaO nanocatalyst done by Kaur and Ali (2014), the FAME yield is not significantly affected at a higher catalyst loading exceeding 5 wt% due to the fact that the formation of viscous reaction mixture can possibly cause poor mass transfer in the three-phase system.

2.4.1.2 Alcohol-to-Oil Molar Ratio

Alcohol-to-oil molar ratio is also a crucial parameter that can bring impact towards the biodiesel production, where a lower molar ratio may affect the conversion ability of triglycerides into FAMEs, whereas a higher molar ratio tends to reduce the FAME yield. Although the stoichiometric alcohol-to-oil molar ratio of 3:1 is considered as the theoretical minimal molar ratio to ensure complete conversion of oil, the transesterification reaction is normally carried out with an excess of alcohol, for example methanol.

Methanol consisting of polar hydroxyl group causes the emulsification of glycerol as well as the formation of biodiesel during transesterification reaction, where the backward reaction such as recombination of glycerol and FAMEs is possible to be taken place which can decrease the biodiesel yield. Since the transesterification reaction is reversible in nature, a large amount of alcohol is needed to keep the reaction in forward direction (Nautiyal, Subramanian and Dastidar, 2014). According to Kaur and Ali (2014), a high methanol-to-oil molar ratio is required especially for heterogeneous catalysis not only to drive the equilibrium towards forward direction for acquiring the highest yield of biodiesel, but also to desorb the product molecules away from the surface of catalyst for active sites regeneration.

Even though there is nearly no restriction for molar ratio of alcohol-to-oil, it is simply ineffective if this ratio is increased beyond a certain extent. By referring to Degirmenbasi, et al. (2015), the transesterification rate increases when the alcohol-to-oil molar ratio is increased until achieving an extent above which the time span taken by the reaction possesses insignificant reduction, where this limit is also known as the optimum alcohol-to-oil molar ratio. Table 2.18 summarises the optimum alcohol-to-oil molar ratio for transesterification of different nano CaO-based catalysts by referring to several findings done by researchers.

Table 2.18: Optimum Alcohol-to-Oil Molar Ratio for Transesterification of Various Nano CaO Catalysts.

Catalyst	Alcohol-to-Oil Molar Ratio Attempted (mol/mol)	Optimal Reaction Conditions		Reference
		Alcohol-to-Oil Molar Ratio (mol/mol)	Biodiesel Yield, Y/Conversion, C (%)	
CaO (Calcit)	9:1	-	98.72 (Y)	Bai, et al. (2009)
CaO, 97.2 (Calcit)	15:1	-	95.7 (Y)	Yoosuk, et al. (2010)
LiC/CaO	3:1-18:1	12:1	100 (C)	Kumar and Ali (2010)
Li^+/CaO	3:1-15:1	12:1	99 (C)	Kaur and Ali (2011)
Ba/CaO	3:1-15:1	6:1	98 (C)	Boro, et al. (2014)
K/CaO	6:1-21:1	12:1	99 (Y)	Kumar and Ali (2012)
KF/CaO	6:1-18:1	12:1	96 (Y)	Wen, et al. (2010), Hu, et al. (2012)
K_2CO_3/CaO	6:1-18:1	9:1	97.67 (Y)	Degirmenbasi, et al. (2015)
Zn/CaO	3:1-18:1	9:1	99 (Y)	Kumar and Ali (2013)
Zr/CaO	3:1-18:1	15:1	99 (Y)	Kaur and Ali (2014)
(Mo/Zr)/CaO	5:1-25:1	15:1	90.1 (Y)	Nasar Mansir, et al. (2018)
CaO/Fe_3O_4	15:1	-	99 (C)	Liu, et al. (2010)
KF/(CaO/NiO)	3:1-18:1	15:1	99 (Y)	Kaur and Ali (2014)
KF/(CaO/Fe_3O_4)	12:1	-	95 (Y)	Hu, et al. (2011)
KF/(CaO/MgO)	12:1	-	95 (Y)	Wang, et al. (2009)

It was inferred by Zhao, Qiu and Stagg-Williams (2013) that the decrease of oil conversion to FAMEs encountered after augmenting the molar ratio which exceeds the optimum one is mostly caused by the difficulty in phase separation. Besides, Kaur and Ali (2014) deduced that the molar ratio of methanol-to-oil which is larger than 15 causes the calcination and separation of glycerol from biodiesel to become more problematic in the Jatropha oil transesterification using Zr doped CaO, concluding that the molar ratio should be set within the range of 12 and 15. Meanwhile, the molar ratio of alcohol-to-oil beyond 30 is even undesirable as it may make the glycerine product to become more soluble in the reaction mixture if the high pressure autoclave or elevated temperature is not applied to the reaction (Xie and Wang, 2013). In addition, the use of extremely excess alcohol may cause the biodiesel production cost to increase, besides contributing to inherent toxicity which is harmful to mankind.

Kaur and Ali (2014) investigated the Zr/CaO catalysed transesterification reaction of Jatropha oil with methanol-to-oil molar ratio ranging from 3:1 to 18:1 in order to identify the optimum molar ratio. Figure 2.13 illustrates the effect of methanol-to-oil molar ratio on the FAME conversion by employing reaction temperature of 65 ℃, reaction time of 105 minutes and catalyst loading of 5 wt % with respect to oil.
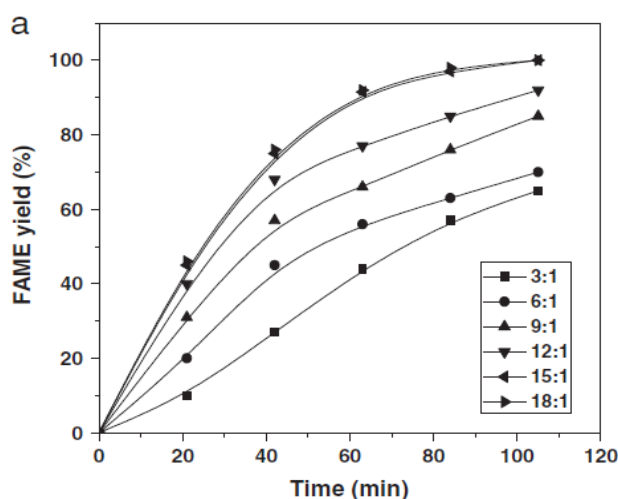
Figure 2.13: Effect of Methanol-to-Oil Molar Ratio on FAME Yield Using Zr/CaO Catalyst (Kaur and Ali, 2014).

It was reported that the rate of transesterification reaction increases in terms of biodiesel yield where it increases from 60 % to 99 % by increasing the methanol-to-oil molar ratio up to 15:1. It is inferred that an increase in methanol-to-oil molar ratio stoichiometrically facilitate the conversion of triglycerides to monoglycerides, indicating a high catalytic activity for the reaction in liquid phase as there are adequate active sites provided by the catalyst. By referring to Figure 2.13, a subsequent increase in the molar ratio does not significantly reduce the time taken for reaction as well as the FAME yield. It is suggested that the excess molar ratio tends to increase the solubility of glycerol in FAME, subsequently leading to the reduction in FAME yield. According to Amani, et al. (2014), the decrease in biodiesel yield might be owing to the dilution effect of catalyst, which in turn causing the methanol to become insoluble in oil.

2.4.1.3 Reaction Temperature

Reaction temperature is one of the significant parameters affecting the mass transfer process, which in turn determine the overall transesterification rate. Reddy, Oshel and Verkade (2006) investigated the transesterification reaction of soybean oil under room temperature, where approximately 24 hours of reaction time are required for complete conversion by employing the CaO nanocatalyst. Although the reaction performed at room temperature is proven to be successful, the transesterification rate shows a significant increase when the reaction temperature is increased based on reaction kinetics (Wen, et al., 2010). In the case of methanol as the raw material alongside oil feedstock with the utilisation of appropriate CaO-based nanocatalyst, most of the researchers have inferred that the boiling point of methanol at atmospheric pressure, which is about 65 ℃ is the optimum temperature for the methanolysis of oil in biodiesel production. Table 2.19 summarises the optimum temperature for transesterification of different nano CaO-based catalysts by referring to several findings done by researchers.

Table 2.19: Optimum Reaction Temperature for Transesterification of Various Nano CaO Catalysts.

| Catalyst | Reaction Temperature Attempted (°C) | Optimal Reaction Conditions | | Reference |
		Reaction Temperature (°C)	Biodiesel Yield, Y/Conversion, C (%)	
CaO	25	-	99 (C)	Reddy, Oshel and Verkade (2006)
CaO (Calcit)	65	-	98.72 (Y)	Bai, et al. (2009)
CaO, 97.2 (Calcit)	60	-	95.7 (Y)	Yoosuk, et al. (2010)
LiC/CaO	35-85	65	100 (C)	Kumar and Ali (2010)
Li^+/CaO	35-75	65	99 (C)	Kaur and Ali (2011)
Ni/CaO	35-150	110	99 (Y)	Kumar, Abida and Ali (2016)
Ba/CaO	50-75	65	98 (C)	Boro, et al. (2014)
K/CaO	35-75	65	99 (Y)	Kumar and Ali (2012)
KF/CaO	50-70	65	96 (Y)	Wen, et al. (2010), Hu, et al. (2012)
K_2CO_3/CaO	25-75	65	97.67 (Y)	Degirmenbasi, et al. (2015)
Zn/CaO	35-75	65	99 (Y)	Kumar and Ali (2013)
Zr/CaO	35-85	65	99 (Y)	Kaur and Ali (2014)
(Mo/Zr)/CaO	60-100	80	90.1 (Y)	Nasar Mansir, et al. (2018)
CaO/Fe_3O_4	70	-	99 (C)	Liu, et al. (2010)

KF/(CaO/NiO)	35-75	65	99 (Y)	Kaur and Ali (2014)
KF/(CaO/Fe_3O_4)	65	-	95 (Y)	Hu, et al. (2011)
KF/(CaO/MgO)	70	-	95 (Y)	Wang, et al. (2009)

As a matter of fact, the biodiesel yield is relatively lower when the reaction is conducted at low temperature ranging from 50 ℃ to 55 ℃, which is mainly attributed to the mass transfer and solubility limitations. The increase in temperature is able to accelerate the reaction, resulting in more biodiesel yield as the reactants may gain sufficient kinetic energy, which will expedite the mass transfer rate among the oil-methanol-catalyst phases (Boro, et al., 2014). According to Mohammed Takase, et al. (2014), a higher reaction temperature may cause the viscosity of oil feedstock to reduce, and thus ensuring a better mixing of oil with alcohol during transesterification and faster separation of glycerol from biodiesel. However, any further increase above the optimum point will cause the yield of biodiesel to dip on account of evaporative alcohol losses (Abbah, et al., 2017). In addition, the side reaction such as hydrolysis of FAMEs to corresponding acid and alcohol occur more rapidly at higher temperature in contrast to transesterification, and hence reducing the biodiesel yield. Hence, the temperature is usually set below the boiling temperature of alcohol during the transesterification. However, there is still a possibility to carry out the reaction by employing higher temperature under high pressure or reflux conditions, which were investigated by Abbah, et al. (2017) and Jiang, et al. (2010) respectively.

By referring to Zhao, Qiu and Stagg-Williams (2013), the further increase in temperature which exceeds the optimum temperature will neither augment the oil conversion for biodiesel production nor reduce the reaction time. It was inferred by Wen, et al. (2010) that the methanol begins to evaporate once the reaction achieves the temperature above its boiling point, where the contact time of methanol with oil is lowered, which in turn reduces the biodiesel yield. Although the CaO-based nanocatalyst possesses high effectiveness at 65 ℃, the oil conversion can be driven towards completion at lower temperature, for

instance 35 ℃ but an extended reaction time is required, which was proposed by Kaur and Ali (2011) and Kumar and Ali (2013).

Kaur and Ali (2014) investigated the optimum activity of Zr impregnated CaO nanocatalyst by performing in the temperature ranging from 35 to 85 ℃. Figure 2.14 illustrates the effect of reaction temperature on the FAME conversion by employing methanol-to-oil molar ratio of 15:1, reaction time of 105 minutes and catalyst loading of 5 wt % with respect to oil.
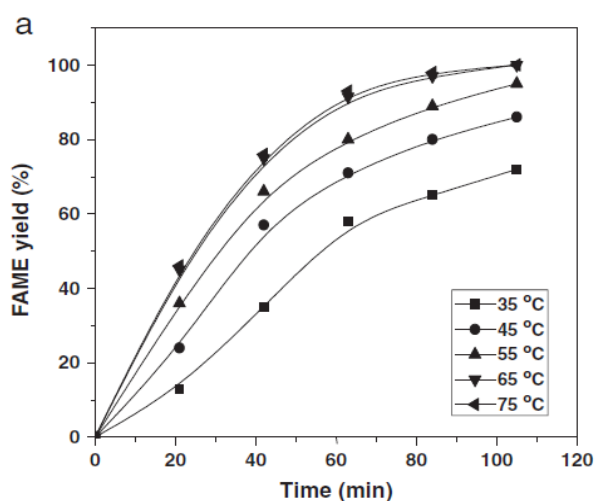
Figure 2.14: Effect of Reaction Temperature on FAME Yield Using Zr/CaO Catalyst (Kaur and Ali, 2014).

In spite of the fact that the transesterification involving Jatropha oil is able to be completed at 35 ℃, the reaction temperature of 65 ℃ is more preferable as the time needed to drive the transesterification towards completion reduces from 5 to 1.75 hours with the increase of temperature by 30 ℃ from 35 ℃, alongside the regular increase of FAME yield. By referring to Figure 2.14, the reaction time as well as FAME yield are not significantly reduced by a subsequent increase in temperature for reaction. It is deduced that the saponification of triglyceride may take place at a higher reaction temperature above 65 ℃, triggering the formation of large bubbles, which subsequently inhibit the reaction in inter-phase comprising of methanol, oil and solid catalyst (Amani, et al., 2014).

2.4.1.4 Reaction Time

It is noted that once the three aforementioned parameters are optimised, the time required will become minimal in order to achieve the complete transesterification reaction. The complete conversion to biodiesel is attributed to the sufficient reaction time acquired to cross the energy barrier by the reactant to transform triglyceride and alcohol into methyl esters. Table 2.20 summarises the optimum reaction time for transesterification of different nano CaO-based catalysts by employing the optimised reaction conditions which are inclusive of reaction temperature, catalyst loading and molar ratio of alcohol-to-oil.

Table 2.20: Optimum Reaction Time for Transesterification of Various Nano CaO Catalysts.

Catalyst	Reaction Time (hrs)	Biodiesel Yield, Y/Conversion, C (%)	Reference
CaO (Calcit)	3	98.72 (Y)	Bai, et al. (2009)
CaO, 97.2 (Calcit)	0.75	95.7 (Y)	Yoosuk, et al. (2010)
LiC/CaO	0.75	100 (C)	Kumar and Ali (2010)
Li^+/CaO	1	99 (C)	Kaur and Ali (2011)
Ba/CaO	3	98 (C)	Boro, et al. (2014)
K/CaO	1.25	99 (Y)	Kumar and Ali (2012)
KF/CaO	2	96 (Y)	Wen, et al. (2010), Hu, et al. (2012)
K_2CO_3/CaO	8	97.67 (Y)	Degirmenbasi, et al. (2015)
Zn/CaO	0.75	99 (Y)	Kumar and Ali (2013)
Zr/CaO	1.75	99 (Y)	Kaur and Ali (2014)

(Mo/Zr)/CaO	3	90.1 (Y)	Nasar Mansir, et al. (2018)
CaO/Fe_3O_4	4	99 (C)	Liu, et al. (2010)
KF/(CaO/NiO)	4	99 (Y)	Kaur and Ali (2014)
KF/(CaO/Fe_3O_4)	3	95 (Y)	Hu, et al. (2011)
KF/(CaO/MgO)	3	95 (Y)	Wang, et al. (2009)

As a matter of fact, the oil conversion is relatively low at a shorter reaction duration, for instance 1 hour, which is attributed to the heterogeneous mass transfer system of catalyst. Generally, the heterogeneous catalysis system comprising of solid surface is impenetrable to the reactants that surround it when the fluid containing the reactants (methanol and oil) and products (FAME and glycerol) flows past the catalytically active surface (Amani, et al., 2014). In order for the reaction to take place, the reactant molecules must be transported to the catalyst surface and the product molecules must be transported away from the surface as well. Hence, a complete conversion to biodiesel at the catalyst surface will never be achieved in an insufficient reaction duration due to the limited transportation rate.

Nasar Mansir, et al. (2018) investigated the (Mo/Zr)/CaO catalysed transesterification reaction of waste cooking palm oil in order to determine the optimum reaction duration. Figure 2.15 illustrates the effect of reaction time on the FAME yield by employing reaction temperature of 80 ℃, methanol-to-oil molar ratio of 15:1 and catalyst loading of 3 wt % with respect to oil.
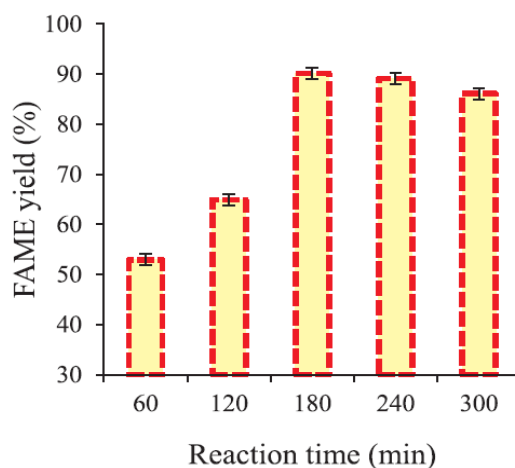
Figure 2.15: Effect of Reaction Time on FAME Yield Using (Mo/Zr)/CaO Catalyst (Nasar Mansir, et al., 2018).

It was reported that the FAME yield is increased when the reaction is prolonged up to 3 hours. However, a gradual decrease in biodiesel yield is observed with the subsequent increase of reaction duration to 4 hours and 5 hours, which is most probably due to the formation of soap in the product as a result of esters hydrolysis. In addition, the white emulsion and gel will cause the biodiesel to become more viscous, which subsequently make the downstream processing of FAME to become more difficult.

Among the aforementioned variables which have been optimised for biodiesel production, reaction temperature possesses the most straightforward synergistic interaction with duration of the reaction. It is notable that an increase in the temperature of transesterification will cause a rise in the rate of transesterification, and thereby the transesterification reaction should theoretically require a shorter period of time before achieving complete oil conversion to FAMEs. By referring to Freedman, Pryde and Mounts (1984), the biodiesel yield seems to be contingent upon the reaction temperature during the initial phase of reaction, such the first 30 minutes. Besides, the transesterification of safflower oil at different reaction temperatures by employing CaO catalyst was investigated by Rashid and Anwar (2008), where it possesses a similar progression of transesterification up to 80 % during the first 10 minutes of reaction, regardless of the temperature of reaction mixture. However, the rate of conversion to FAMEs varies for each temperature after a total reaction time of two hours, where the highest biodiesel yield is acquired at

60 ℃. Thus, it is further proven that the duration and temperature of transesterification reaction have a synergistic effect on the biodiesel yield.

2.5 Characterisation Studies of Nano CaO Catalysts

2.5.1 X-ray Diffraction (XRD) Analysis

X-ray diffraction (XRD) is an analytical technique used to characterise the crystallographic structure of nano CaO catalyst and determine the relative abundance of crystalline compounds, besides providing information on unknown crystalline substances present in nano CaO catalyst. It is used to identify the crystalline phases present in the nano CaO catalyst by means of lattice structural parameters and obtain the crystallite size which can be calculated using Debye-Scherrer equation shown in Equation 2.1.

$$L = \frac{K\lambda}{\beta cos\theta} \tag{2.1}$$

where

L = mean size of crystalline domains

K = Scherrer shape factor

λ = X-ray wavelength

β = line broadening at half the maximum intensity; full width at half maximum (FWHM)

θ = angle of maximum diffraction peak; Bragg angle

It is known that the Scherrer shape factor equals to 0.89 for spherical crystals with cubic symmetry. According to Kumar and Ali (2013), Cu K-α radiation with wavelength of 1.54 Å is usually used in XRD analysis as it is monochromatic and possesses a higher intensity than K-β radiation, producing a more efficient diffraction pattern of crystalline solid materials. The CaO nanocatalyst is required to be finely ground and homogenised before performing XRD analysis. Table 2.21 summarises the crystallite size obtained by Debye-Scherrer equation using powder XRD data for different nano CaO-based catalysts which are treated by various approaches including thermal decomposition, hydration-dehydration, wet impregnation and sol-gel method.

Table 2.21: Crystallite Size of Treated Nano CaO-based Catalysts.

Catalyst	Synthesis Method	Crystallite Size (nm)	Reference
CaO (Snail Shell)	Thermal Decomposition	40	Krishnamurthy, Sridhara and Ananda-Kumar (2019)
CaO, 97.2 (Calcit)	Hydration-Dehydration	42.2	Yoosuk, et al. (2010)
1.75-Li^+/CaO	Wet Impregnation	40	Kaur and Ali (2011)
1.5-LiC/CaO		70	Kumar and Ali (2010)
3.5-K/CaO		39	Kumar and Ali (2012)
1.5-Zn/CaO-550		23	Kumar and Ali (2013)
15-Zr/CaO-700		13.87 (tetragonal) / 28.53 (monoclinic)	Kaur and Ali (2014)
1-Zn/CaO		34.2	Borah, et al. (2019)
20-KF/(CaO/NiO)-700		41.7	Kaur and Ali (2014)
CaO	Sol-Gel	61	Tahvildari, et al. (2015)
NiO/CaO		-	Vitiyaa Selva Kumar, et al. (2019)

Note: 1 Å = 0.1 nm

1.5-Zn/CaO-550; 1.5 = dopant concentration (wt%), 550 = calcination temperature (℃)

Kaur and Ali (2011) performed the powder XRD studies of neat CaO and CaO impregnated with 1-3 wt% Li^+ to compare the XRD patterns as illustrated in Figure 2.16, where the intense peaks are located nearly the same on the XRD graph for all the Li^+ impregnated CaO catalyst studied. The intense peaks at 2θ of 37.33°, 53.94° and 32.25° show the presence of CaO, while peaks at 2θ of 34.16°, 18.18° and 47.15° show the presence of $Ca(OH)_2$.
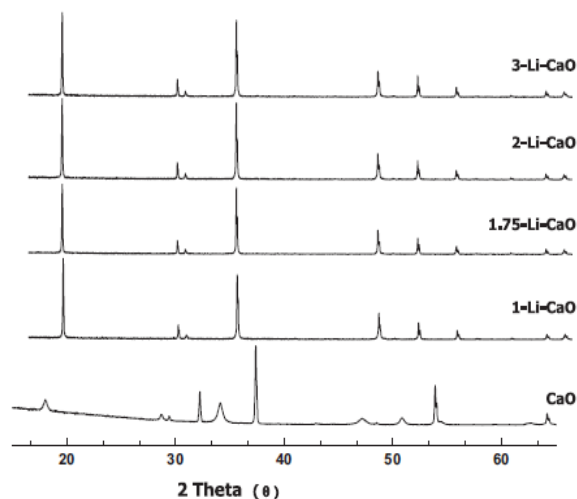
Figure 2.16: Comparison of Powder XRD Patterns of Neat CaO and 1-3 wt% Li^+/CaO (Kaur and Ali, 2011).

The structure and crystallite size of neat CaO as well as K/CaO with K^+ concentration ranging from 1.5 to 5.5 wt% were investigated by Kumar and Ali (2012) through XRD studies, as shown in Figure 2.17 where * = CaO, ◆ = $Ca(OH)_2$ and □ = $CaCO_3$.
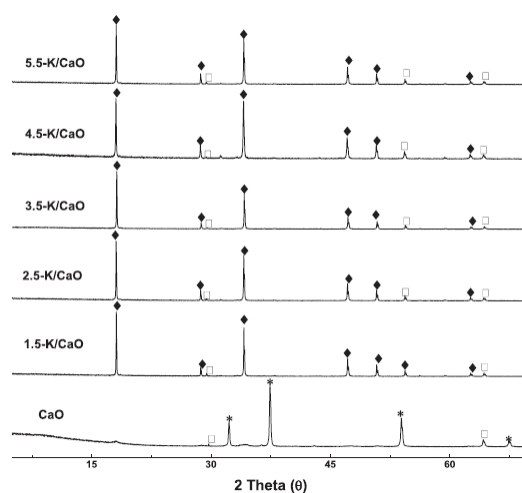
Figure 2.17: Comparison of Powder XRD Patterns of Neat CaO and 1.5-5.5 wt% K/CaO (Kumar and Ali, 2012).

The neat CaO exhibits peaks at 2θ of 32.24°, 37.46° and 53.95°, indicating the formation of cubic CaO. The presence of $CaCO_3$ in minor amount as calcite in neat CaO is revealed by the low intensity peaks at 2θ of 29.4° and 64.4°. The $Ca(OH)_2$ in hexagonal form is formed upon the impregnation of K^+ as dopant, which is depicted by the appearance of major peaks at 2θ of 18.04°, 34.08° and 47.16° for K/CaO. It was reported by Kumar and Ali (2012) that the structure of CaO is not affected by the change of K^+ concentration as exhibited by similar diffraction patterns depicted for K/CaO with K^+ concentration ranging from 1.5 to 5.5 wt%. The absence of characteristic peaks of dopant source, KOH located at 2θ of 27.4°, 32.1°, 32.5° and 33.7° in diffraction peaks proves a high extent of K^+ dispersion on the surface of potassium impregnated CaO. Besides, the crystallite size of potassium impregnated CaO is identified from XRD line width of active plane (011) using Debye-Scherrer approach where it is reduced by 60 nm from 104 nm with the impregnation of 1.5 wt% K^+. However, the crystallite size is not significantly affected by a subsequent increase of K^+ loading, which is ranging from 39 to 45 nm.

Kumar, Abida and Ali (2016) investigated the effect of Ni concentration ranging from 0.5 to 6 wt% on the structure of Ni/CaO at constant calcination temperature of 650 ℃ through powder XRD studies, as shown in Figure 2.18 where * = CaO and • = NiO.
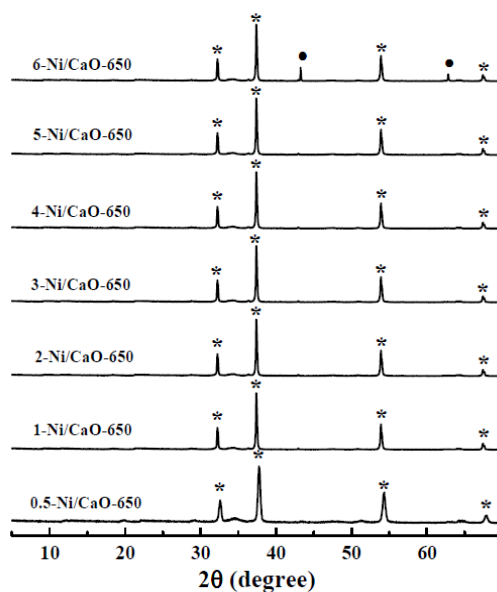
Figure 2.18: Comparison of Powder XRD Patterns of 0.5-6 wt% Ni/CaO Calcined at 650 ℃ (Kumar, Abida and Ali, 2016).

It was reported that there is no peak corresponding to NiO in powder XRD profiles as long as the nickel loading in Ni/CaO remains to be equal or less than 5 wt%. It is inferred that Ni^{2+} particles pose a high degree of dispersion in CaO. According to Kumar, Abida and Ali (2016), low intensity peaks at 2θ of 43.2°, 62.7° are emerged upon increasing the Ni concentration up to 6 wt%, denoting the presence of NiO in cubic phase. It is deduced that a maximum amount of 5 wt% can be doped without altering the regular CaO structure.

Besides, Kumar, Abida and Ali (2016) performed the powder XRD studies to determine the catalyst structure of CaO impregnated with 0.5 wt% Ni by employing the temperature ranging from 150 to 950 ℃ for calcination. Figure 2.19 illustrates the XRD patterns of neat CaO and Ni/CaO to investigate the effect of calcination temperature on the structure of Ni/CaO by maintaining the nickel concentration at 0.5 wt%, where * = CaO, ◆ = $Ca(OH)_2$ and □ = $CaCO_3$.
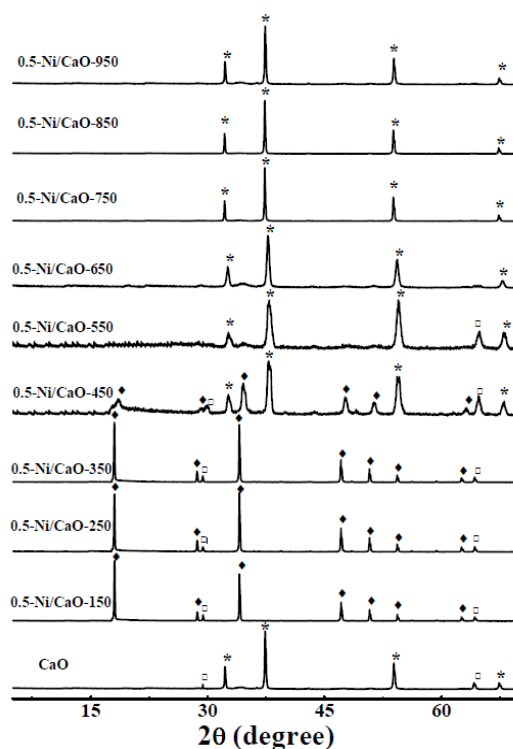
Figure 2.19: Comparison of Powder XRD Patterns of Neat CaO and 0.5 wt% Ni/CaO Calcined at Temperature Ranging from 150 to 950 ℃ (Kumar, Abida and Ali, 2016).

By referring to Figure 19, it is noticed that $Ca(OH)_2$ is the major phase with the calcination temperature up to 350 ℃, where it is attributed to the reaction of CaO with water which is employed as reaction medium during doping process. There are also a few $CaCO_3$ phases observed in low intensity, which is most probably owing to the reaction of CaO with atmospheric CO_2, as proved from the XRD profiles of Ni/CaO calcined up to 550 ℃. The XRD peaks indicating the formation of CaO phase are observed at 450 ℃ as $Ca(OH)_2$ is inferred to undergo partial thermal decomposition. According to Kumar, Abida and Ali (2016), both $Ca(OH)_2$ and $CaCO_3$ are completely decomposed at the calcination temperature above 550 ℃, which is denoted by the emergence of a single CaO phase. The calcination process transforms the Brønsted basic sites ($-OH$) into Lewis basic sites (-O-), where the latter are found to be more active during transesterification.

In another study done by Kumar and Ali (2013), the XRD patterns exhibited by neat CaO and CaO doped with Zn^{2+} with its concentration ranging

from 0.25 to 7 wt% at calcination temperature of 550 ℃ were compared, as illustrated in Figure 2.20 where * = CaO and ● = ZnO.
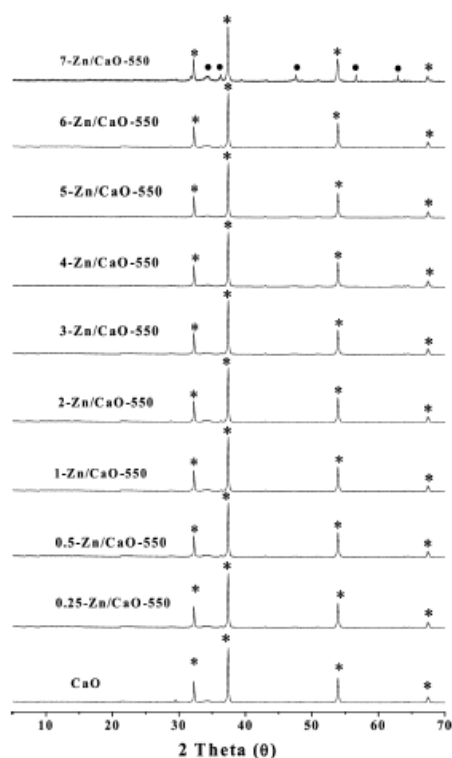
Figure 2.20: Comparison of Powder XRD Patterns of Neat CaO and 0.25-7 wt% Zn/CaO Calcined at 550 ℃ (Kumar and Ali, 2013).

The XRD graph of pure CaO shows the characteristic peaks of cubic CaO, whereas the XRD graph of Zn/CaO exhibits the typical diffraction patterns of CaO in cubic phase. There is no definite peak corresponding to the ZnO phase noticed below 6 wt% of Zn^{2+} concentration, in which Zn/CaO in a single cubic phase is said to be formed where Zn^{2+} has substituted the sites occupied by Ca^{2+}. It was reported by Kumar and Ali (2013) that a further increase in the Zn^{2+} concentration to or above 7 wt% causes the ZnO in a hexagonal phase to be formed, which is supported by the low-intensity peaks at 2θ of 34.3°, 36.3°, 47.8°, 56.5° and 62.6°. Thus, it can be said that a 6 wt% of Zn^{2+} in CaO is possible to form a saturated solid solution, where Zn/CaO and CaO·ZnO are formed as two distinct phases due to a further increase in the Zn^{2+} concentration.

Besides, Kumar and Ali (2013) compared the XRD patterns of CaO doped with 1.5 wt% Zn which is calcined at temperature ranging from 150 to 950 ℃ to investigate the impact of calcination temperature towards the structure of Zn/CaO, which are depicted in Figure 2.21 where * = CaO and ◆ = $Ca(OH)_2$.
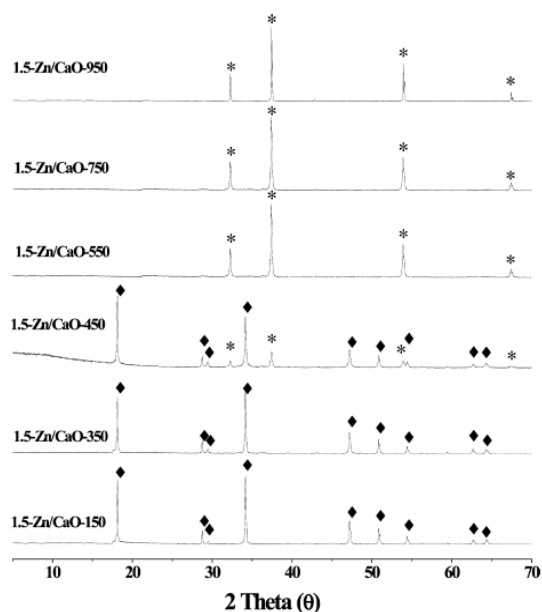
Figure 2.21: Comparison of Powder XRD Patterns of 1.5 wt% Zn/CaO Calcined at Temperature Ranging from 150 to 950 ℃ (Kumar and Ali, 2013).

The XRD patterns of Zn/CaO calcined up to 350 ℃ reveal the emergence of major phase, hexagonal $Ca(OH)_2$ and minor phase, CaO. There is a phase change initiated at 450 ℃ due to the decomposition of $Ca(OH)_2$ into CaO, which is proven by the diffraction patterns emerged for both the phases. According to Kumar and Ali (2013), a further increase in the calcination temperature exceeding 550 ℃ leads to the formation of pure CaO in cubic phase, where similar XRD patterns are observed for Zn/CaO calcined up to 950 ℃, indicating that an increase in the calcination temperature from 550 to 950 ℃ has not initiate any chemical or structural change in Zn/CaO. Besides, the crystallite size of Zn/CaO is determined by employing Debye-Scherrer method where the crystallite size of 1.5 wt% Zn^{2+} impregnated CaO is increased from 23 to 75 nm following the increase of temperature for calcination by 400 ℃ to 950 ℃ due to sintering effect posed towards Zn/CaO particles.

Kaur and Ali (2014) performed the powder XRD studies to determine the catalyst structure and crystallite size of CaO impregnated with 15 wt% Zr by employing the temperature ranging from 300 to 900 ℃ for calcination. Figure 2.22 illustrates the XRD patterns of Zr/CaO to investigate the effect of calcination temperature on the structure of Zr/CaO by maintaining the zirconium concentration at 15 wt%, where * = monoclinic ZrO_2, ● = tetragonal ZrO_2, ○ = perovskite $CaZrO_3$, ◆ = cubic CaO and Δ = $Ca(OH)_2$.
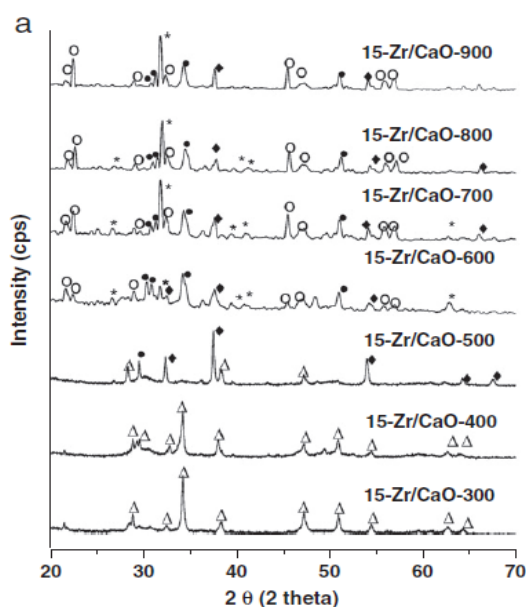
Figure 2.22: Comparison of Powder XRD Patterns of 15 wt% Zr/CaO Calcined between Temperature of 300 and 900 ℃ (Kaur and Ali, 2014).

Based on Figure 2.22, the ZrO_2 phase remains absent up to the calcination temperature of 400 ℃ owing to the formation of homogeneous solid solution of $ZrO_2/Ca(OH)_2$. The $Ca(OH)_2$ is thermally decomposed into CaO in cubic phase at 500 ℃ before achieving completion at 600 ℃, where there is no diffraction patterns posed by $Ca(OH)_2$. The phases of tetragonal ZrO_2, monoclinic ZrO_2 and perovskite $CaZrO_3$ are also produced when the temperature exceeds 600 ℃ for calcination. Kaur and Ali (2014) studied the dependency of crystallite size possessed by monoclinic and tetragonal ZrO_2 phases on the temperature applied for calcination using Debye-Scherrer method. It is known that only tetragonal ZrO_2 phase exists with a crystallite size of

nearly 36 nm at the calcination temperature of 500 ℃ without the presence of monoclinic phase. Upon reaching the calcination temperature of 600 ℃, the crystallite size of 27 nm is resulted from monoclinic ZrO_2 besides tetragonal phase, where the formation of monoclinic ZrO_2 causes the crystallite size of tetragonal phase to be reduced until 16 nm. It was inferred that the monoclinic ZrO_2 is formed from the current tetragonal phase. It was reported that a subsequent increase in temperature for calcination above 700 ℃ has neither encouraged the new ZrO_2 phase to be formed nor remarkably altered the crystallite size.

In addition, the effect of Zr concentration ranging from 5 to 20 wt% on the structure of Zr/CaO at constant temperature of 700 ℃ for calcination was investigated by Kaur and Ali (2014) through powder XRD studies, as shown in Figure 2.23.
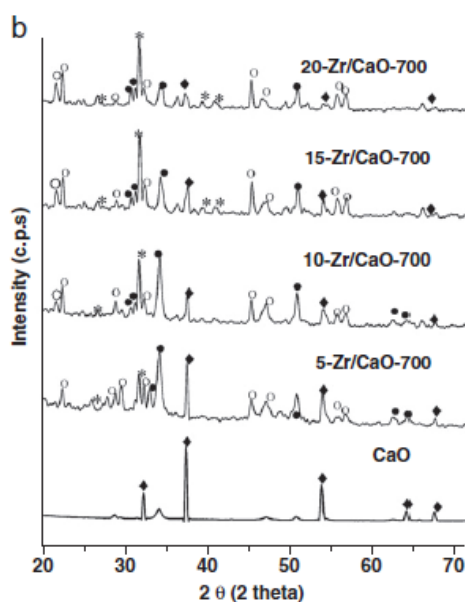
Figure 2.23: Comparison of Powder XRD Patterns of Neat CaO and 5-20 wt% Zr/CaO Calcined at 700 ℃ (Kaur and Ali, 2014).

It was reported that there is no emergence of new phase in Zr impregnated CaO through the variation of Zr concentration. Nevertheless, the ratio of tetragonal phase to monoclinic phase was reported to reduce as a result of an increase in Zr concentration, where it is inferred that the monoclinic ZrO_2 is predominantly formed with the increase of Zr concentration impregnated on Zr/CaO when the temperature of 700 ℃ is employed for calcination.

Recently, Borah, et al. (2019) performed the powder XRD studies to determine the crystallite size and catalyst structure of CaO nanocatalyst doped with Zn at the calcination temperature of 900 ℃, where the XRD patterns of undoped CaO and Zn doped CaO with Zn^{2+} concentration varying from 0.5 to 2 wt% are illustrated in Figure 2.24.
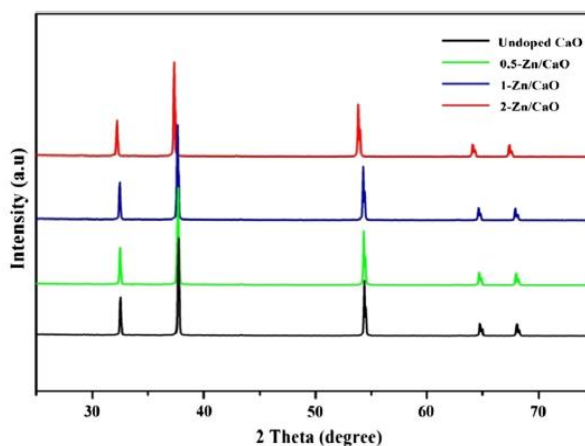
Figure 2.24: Comparison of Powder XRD Patterns of Neat CaO and 0.5-2 wt% Zn/CaO (Borah, et al., 2019).

It is known that the formation of sharp peak in XRD graph indicates the formation of highly crystalline materials. The diffraction peaks that appear at 2θ of 32.43°, 37.14°, 53.65°, 64.49° and 67.24° can be indexed to the crystal planes of (1 1 1), (2 0 0), (2 2 0), (3 1 1) and (2 2 2) respectively, indicating the diffraction of CaO in cubic form. According to Borah, et al. (2019), there is no extra peaks in regard to any impurity or ZnO observed from the XRD pattern. However, the most prominent peak at (2 0 0) plane is shifted towards a lower 2θ value when the Zn loading increases from 0.5 to 2 wt%, where it is more significant in the case of 2-Zn/CaO. It was reported by Borah, et al. (2019) that the average crystallite size of the most intense peak at (2 0 0) plane is calculated where the average crystallite size of undoped CaO nanoparticles is 39.1 nm and it is noticed to be decreased with the increase of Zn concentration. It was inferred that the reduction in crystallite size is predominantly due to the disruption of CaO carrier lattice by foreign Zn^{2+} impurities.

The XRD patterns for calcium-based catalyst are illustrated in Figure 2.25 based on the powder XRD studies conducted by Vitiyaa Selva Kumar, et al. (2019).
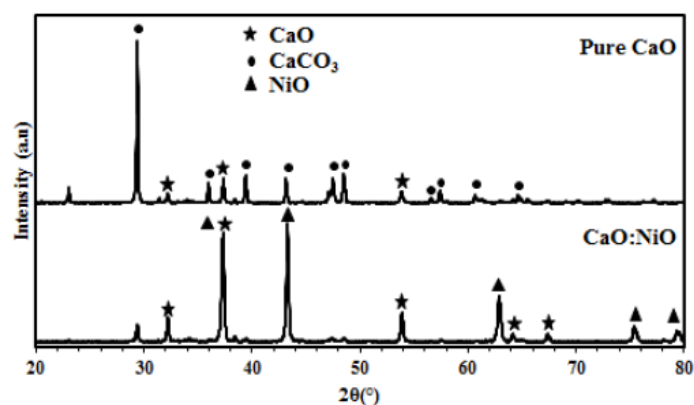
Figure 2.25: XRD patterns of Pure CaO and NiO/CaO (Vitiyaa Selva Kumar, et al., 2019).

It is noticed that both calcium-based catalysts exhibit distinct and well-crystallised phase, where it is observed that CaO and NiO are the primary compounds for NiO/CaO catalyst synthesised from $Ca(NO_3)_2 \cdot 4H_2O$ and $Ni(NO_3)_2 \cdot 6H_2O$ precursors. CaO poses the main characteristic peaks at 2θ of 32.3°, 37.2°, 53.6°, 64.3° and 67.3°, which correspond to the crystal plane of (1 1 1), (2 0 0), (2 0 2), (3 1 1) and (2 2 2) respectively, whereas the NiO peaks can be observed at 2θ of 37.6°, 43.2°, 62.7°, 75.2° and 79.5°. By referring to Figure 2.22, the pure CaO consists of CaO and $CaCO_3$ on account of the reaction between CaO powder and CO_2 during the cooling and storage step after calcination, leading to the formation of $CaCO_3$. It is apparent that the precursors employed during the synthesis process have completely decomposed which result in the formation of metal oxide through calcination.

2.5.2 Brunauer-Emmett-Teller (BET) Analysis

Brunauer-Emmett-Teller (BET) analysis precisely evaluates on specific surface area of nano CaO catalyst by nitrogen multilayer adsorption as a function of relative pressure using a fully automated analyser. The volume of gas adsorbed to the surface of particles is measured at the boiling point of nitrogen (-196 ℃),

where the amount of adsorbed gas is correlated to the total surface area of nano CaO catalyst. It covers external surface area and pore area analysis to determine the specific surface area of nano CaO catalyst. Besides, it is also employed to determine the specific pore volume using gas adsorption and desorption techniques, where it further characterises the pore size distribution in nano CaO catalyst, which is denoted as surface porosity (Lapham and Lapham, 2019).

The generalized BET equation for gas adsorption is described as follows:

$$\frac{1}{v\left[\left(\frac{p}{p_0}\right)-1\right]} = \frac{c-1}{v_m c}\left(\frac{p}{p_0}\right) + \frac{1}{v_m c} \tag{2.2}$$

where

v = volume of adsorbed gas

v_m = volume of adsorbed gas to form a monolayer

p = equilibrium gas pressure of adsorbed gas

p_0 = saturation pressure of adsorbed gas

c = BET constant; heat of adsorption

The total surface area can be calculated from Equation 2.3.

$$S_{total} = \frac{v_m NA}{V} \tag{2.3}$$

where

N = Avogradro's number, typically equivalent to 6.022×10^{23}

A = cross-sectional area of adsorbed gas, typically equivalent to 16.2 Å^2 for nitrogen

V = molar volume of adsorbed gas at Standard Temperature and Pressure (STP), typically equivalent to 22,400 mL/mol

The specific surface area is computed based on the total surface area, as shown in Equation 2.4.

$$S_{BET} = \frac{S_{total}}{m} \tag{2.4}$$

where

m = mass of nanomaterials or adsorbent

The total pore volume of nano CaO catalyst is derived from the amount of vapor adsorbed at a relative temperature close to unity by assuming that the pores are filled with liquid adsorbate (Lapham and Lapham, 2019), which is depicted in Equation 2.5.

$$V_{total} = \frac{p_a v V_m}{RT}$$ (2.5)

where

p_a = ambient pressure

v = volume of adsorbed gas

V_m = molar volume of liquid adsorbate

R = universal gas constant

T = ambient temperature

It is noted that the total pore volume is indicated by the volume of liquid nitrogen in the pore. The average pore size is estimated from the pore volume by assuming cylindrical pore geometry using Equation 2.6 (Lapham and Lapham, 2019).

$$r_p = \frac{2V_{total}}{A}$$ (2.6)

where

r_p = average pore radius

A = cross-sectional area of adsorbed gas, typically equivalent to 16.2 Å^2 for nitrogen

Table 2.22 summarises the specific surface area, pore volume and pore size distribution obtained through BET analysis for different nano CaO-based catalysts which are treated by various approaches including thermal decomposition, hydration-dehydration and wet impregnation.

Table 2.22: BET Findings for Treated Nano CaO-based Catalysts.

Catalyst	Synthesis Method	Specific Surface Area (m^2/g)	Pore Volume (cc/g)	Pore Size (Å)	Reference
CaO (Snail Shell)	Thermal Decomposition	9.37	0.0538	11.45	Krishnamurthy, Sridhara and Ananda-Kumar (2019)
CaO, 97.2 (Calcit)	Hydration-Dehydration	25	0.25	-	Yoosuk, et al. (2010)
1.75-Li^+/CaO		1.7	0.004	95.02	Kaur and Ali (2011)
1.5-LiC/CaO		6.5	-	-	Kumar and Ali (2010)
0.5-Ni/CaO-650		14.7	-	-	Kumar, Abida and Ali (2016)
1-Ba/CaO		4.86	-	-	Boro, et al. (2014)
3.5-K/CaO		5.84	-	-	Kumar and Ali (2012)
KF/CaO	Wet Impregnation	109	-	970	Wen, et al. (2010), Hu, et al. (2012)
1.5-Zn/CaO-550		10.95	-	-	Kumar and Ali (2013)
15-Zr/CaO-700		1.86	-	-	Kaur and Ali (2014)
10-(Mo/Zr)/CaO		6.5	-	-	Nasar Mansir, et al. (2018)
20-KF/(CaO/NiO)-700		0.9	-	-	Kaur and Ali (2014)

Note: 1 Å = 0.1 nm

1.5-Zn/CaO-550; 1.5 = dopant concentration (wt%), 550 = calcination temperature (℃)

The surface area of pure CaO and Ni/CaO obtained through BET are tabulated in Table 2.23 for comparison.

Table 2.23: Effect of Calcination Temperature on Surface Area of Ni/CaO Catalyst (Kumar, Abida and Ali, 2016).

Catalyst	BET Surface Area (m^2/g)
CaO	3.9
0.5-Ni/CaO-150	3.8
0.5-Ni/CaO-250	3.8
0.5-Ni/CaO-350	4.8
0.5-Ni/CaO-450	12.9
0.5-Ni/CaO-650	14.7
0.5-Ni/CaO-850	11.7
0.5-Ni/CaO-950	3.9

It was reported by Kumar, Abida and Ali (2016) that the thermal decomposition of $Ca(OH)_2$ which is taken place simultaneously with the removal of water molecule from the catalyst cause the surface area to increase from 4.8 to 14.7 m^2/g with the increase of calcination temperature from 350 to 650 ℃. It is inferred that the exclusion of water molecules leaves voids in catalyst particles, which in turn augments the surface area of catalyst. However, the surface area of catalyst is reduced with a subsequent increase in the calcination temperature from 750 to 950 ℃, which is mainly due to the sintering of smaller particles to be agglomerated into relatively larger particles.

According to Kaur and Ali (2011), the surface area and pore volume of 1.75 wt% Li^+ impregnated CaO were found to be less than neat CaO due to the plugging of pore on CaO catalyst upon lithium impregnation. In contrast, by referring to Kumar and Ali (2010), the specific surface area of CaO impregnated with 1.5 wt% Li is relatively higher when compared to pure CaO in spite of the fact that both CaO catalysts are doped with similar alkali metal ion. In another study done by Kumar and Ali (2012), the surface area of pure CaO was found to increase to 5.84 m^2/g from 3.96 m^2/g when it was impregnated with 3.5 wt% K^+, where it is inferred to be caused by the defects formation in regular CaO

structure after being impregnated with K^+, causing disorder in atomic arrangement and subsequently generating more active sites as well as enhancing the catalytic activity due to higher surface area. Furthermore, it was reported by Kumar and Ali (2013) that the 1.5 wt% Zn^{2+} impregnated CaO possesses a reduced surface area from 10.95 to 2.52 m^2/g due to a subsequent increase in the calcination temperature from 550 to 950 ℃ in view of the sintering of Zn/CaO particles. By referring to Kaur and Ali (2014), the CaO/NiO possesses a progressively reduced specific surface area with the increase of KF concentration mainly because of the pore plugging of the support after KF impregnation, indicating its non-porous nature.

In addition, it was reported by Nasar Mansir, et al. (2018) that the surface area of Mo/Zr impregnated CaO was found to increase by 0.5 m^2/g from 6 m^2/g with the increase of Mo/Zr loading by 5 wt% from 5 wt%. Still, the Mo/Zr loading up to 25 wt% causes the pores to be filled in catalyst, where the reduction of surface area is deduced to be the main reason. Eventually, the surface area achieves its minimum value at 4.8 m^2/g as the Mo/Zr loading is increased up to 20 wt %. It was inferred by Nasar Mansir, et al. (2018) that a high Mo/Zr loading causes Mo/Zr to be impregnated onto CaO, where it forms a homogeneous solid solution, causing the reduction in specific surface area. Hence, there are fewer active sites accessible for transesterification in view of the low surface area of catalyst.

2.5.3 Scanning Electron Microscopy-Energy Dispersive X-ray (SEM-EDX) Spectroscopy Analysis

Scanning electron microscopy (SEM) is an analytical tool used to analyse the surface topography concerning the surface features of nano CaO catalyst, morphology with regards to the shape, size and arrangement of the particles making up the nano CaO catalyst and crystallography regarding the atomic arrangement in nano CaO catalyst. Meanwhile, energy dispersive X-ray (EDX) spectroscopy is used in conjunction with SEM to determine the elements present and acquire the elemental composition on the surface of nano CaO catalyst, allowing for a more quantitative result than that provided solely by SEM analysis.

SEM is generally similar to its optical counterpart except that the electron beams are used rather than light beams to generate a variety of signals at the surface of nano CaO catalyst, besides providing images with magnification up to 50,000x to project the surface features, where it allows the submicron-scale features to be seen, which is well beyond the range of optical microscope. The EDX detector separates the characteristic X-rays of different elements into an energy spectrum, where the software of EDX system is used to analyse the energy spectrum in order to determine the abundance of specific elements present in nano CaO catalyst. It is known that energy peaks correspond to the various elements in the catalyst system. Table 2.24 summarises the surface topography and morphology analysed through SEM as well as the chemical composition of element determined through EDX for different nano CaO-based catalysts which are treated by various approaches including thermal decomposition, hydration-dehydration, wet impregnation and sol-gel method. It is inferred that the doping of active component to nano CaO will alter the morphology and surface feature of catalyst, where there is a pronounced reduction in the particle size observed in doped CaO catalyst, denoting that the dopant tends to restrain the growth of catalyst particles.

Table 2.24: SEM and EDX Findings for Treated Nano CaO-based Catalysts.

| Catalyst | Synthesis Method | SEM | | | EDX | Reference |
| | | Surface Topography | Morphology | | Elemental Composition | |
		Surface Feature	Particle Shape	Average Particle Size (μm)		
CaO (Snail Shell)	Thermal Decomposition	Multi-pore structure with three crystallographic surfaces	Amorphous structures with spherical in shape with significant particles agglomeration	-	Weight %: Ca (48.94 %) O (51.06 %) Atomic %: Ca (27.67 %) O (72.33 %)	Krishnamurthy, Sridhara and Ananda-Kumar (2019)
CaO, 97.2 (Calcit)	Hydration-Dehydration	Highly textured and very rough surface	-	-	-	Yoosuk, et al. (2010)
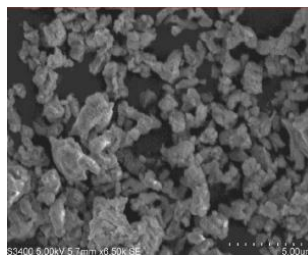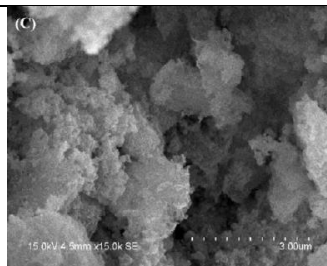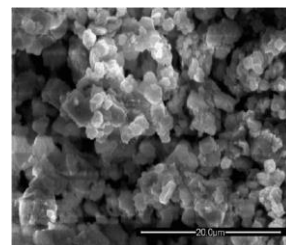
1.75-Li^+/CaO		-	Hexagonal and oval-shaped particles	~2	-	Kaur and Ali (2011)
1.5-LiC/CaO	Wet Impregnation	-	Hexagonal and oval-shaped particles	~4	-	Kumar and Ali (2010)
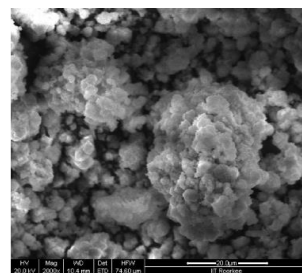
0.5-Ni/CaO-650	-	Agglomerates of hexagonal, cubic and oval shaped particles	-	-	Kumar, Abida and Ali (2016)
3.5-K/CaO	-	Hexagonal and irregular shaped cluster of particles	2-5	-	Kumar and Ali (2012)
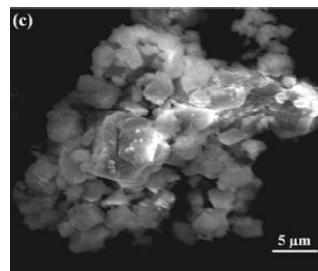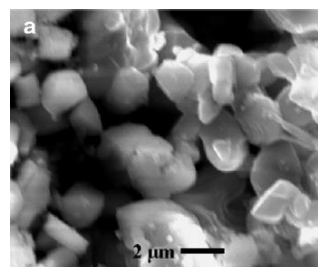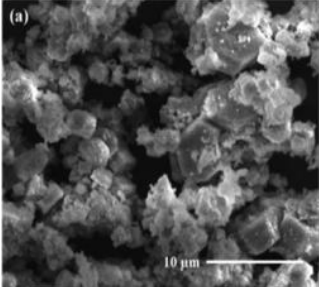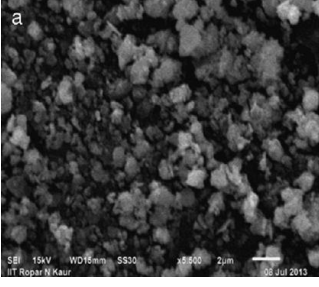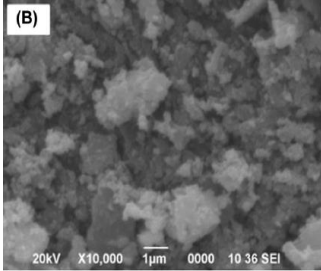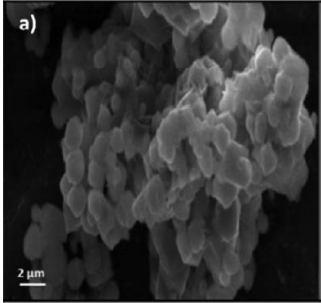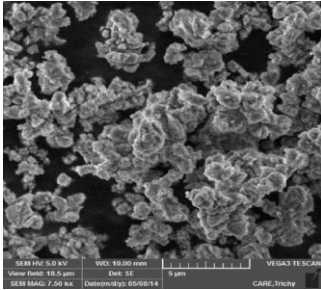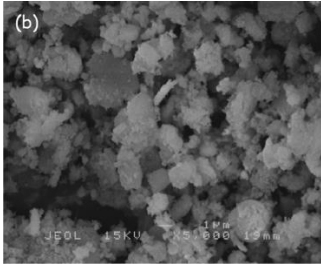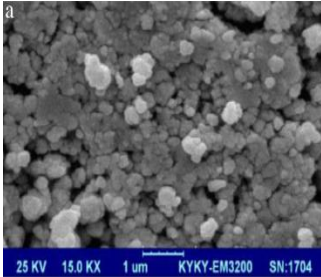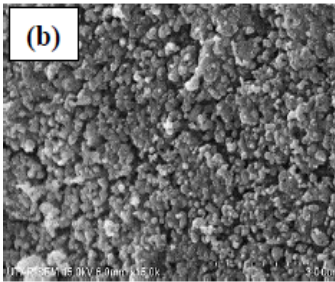
1.5-Zn/CaO-550	-	Cubic, hexagonal and irregular-shaped particles	2-5	1.4 wt% Zn^{2+}	Kumar and Ali (2013)
15-Zr/CaO-700	-	Irregular shaped particles	0.5-2	~17 wt% Zr	Kaur and Ali (2014)

1-Zn/CaO	-	Spherical shaped-particles with non-uniform size	-	-	Borah, et al. (2019)
20-KF/(CaO/NiO)-700	-	Clusters of particles due to agglomeration	1.8	-	Kaur and Ali (2014)

KBr/CaO	-	Particles with spherical structure that are agglomerated into lumps	-	-	Mahesh, et al. (2015)
10-(Mo/Zr)/CaO	-	Moderately crystalline-shaped particles due to increase in Mo/Zr loading	-	Weight %: C (8.82 %) O (41.71 %) Ca (39.35 %) Mo (3.16 %) Zr (6.97 %)	Nasar Mansir, et al. (2018)

CaO		-	Spherical-shaped particles 	-	-	Tahvildari, et al. (2015)
NiO/CaO	Sol-Gel	-	Fine particles with almost spherical structure 	<3	Ca (31 wt%) Ni (41 wt%) O (28 wt%)	Vitiyaa Selva Kumar, et al. (2019)

Note: 1.5-Zn/CaO-550; 1.5 = dopant concentration (wt%), 550 = calcination temperature (℃)

2.5.4 Temperature-Programmed Desorption (TPD) of CO_2 Analysis

Temperature-programmed desorption (TPD) is a technique to study the reactivity by characterising the active sites present in the nano CaO catalyst. In other words, it is implemented to acquire the adsorption and desorption behaviour and provide an estimate on the distribution of adsorption sites on the surface of nano CaO catalyst. Since the nano CaO catalyst is considered as heterogeneous base catalyst, CO_2 is used as the probe molecule to detect the number of basic sites present, which in turn determining the basic strength of nano CaO catalyst. The catalyst with a greater basic strength is more favourable as the higher the basicity, the higher the activity of catalyst, which subsequently enhancing the biodiesel yield through transesterification reaction. By referring to Azizul Hakim, et al. (2015), CaO catalyst possesses a high CO_2 adsorption capacity and low energy consumption for regeneration, and thus exhibiting high performance in TPD analysis.

An analysis oven that acts as the reactor is filled with nano CaO catalyst where the catalyst sample is degassed at 100 ℃ for one hour in flowing helium or argon gas to remove water vapor before raising the temperature steadily from room temperature to 1000 ℃ at a ramp rate of 10 ℃/min in order to remove the strongly bound species and activate the sample. After cooling to 120 ℃ in a stream of flowing inert gas, the catalyst sample is then saturated with CO_2. The desorption is performed by ramping the catalyst sample at 10 ℃/min to 1000 ℃, where the thermal conductivity detector (TCD), or preferably a mass spectrometer measures the concentration of desorbed species and quantifies the density of basic sites at certain temperature which corresponds to the temperature where the reaction takes place. The total area under the curve indicates the total amount of desorbed CO_2 molecules, where it determines the total basic sites quantified by total CO_2 molecules adsorbed on the surface of nano CaO catalyst (Filho and Murzin, 2018). Table 2.25 summarises several pre-treatment procedures that can be accomplished prior to TPD analysis.

Table 2.25: Typical Pre-Treatment Procedures of Temperature-Programmed Analysis (Mikhaylov, et al., 2018).

Pre-Treatment	Species Flow	Purpose
Surface Cleaning	Inert gases (N_2/He/Ar)	• Removes adsorbed pollutants from the catalyst, for example water • Removes hydrogen chemisorbed on active sites
Oxidation	Oxygen gas	• Removes oxidable pollutants, for example carbon residuals • Oxidises deposited metals
Reduction	Hydrogen gas	• Removes oxygen and carbonaceous species bounded to metal surface
Saturation	Targeted reactive gas	• Introduces oxygen gas to fully replenish the vacancy of active sites • Chemisorbs oxygen gas for analysis or experiment

As mentioned previously, the CO_2-TPD analysis is performed to investigate the number of basic sites and basicity constituted by nano CaO catalyst. Table 2.26 summarises the TPD findings for different nano CaO-based catalysts which are treated by various approaches including hydration-dehydration and wet impregnation.

Table 2.26: TPD Findings for Treated Nano CaO-based Catalysts.

Catalyst	Synthesis Method	Basic Strength[a] (pK_{BH+})	Basicity ($\mu mol\ CO_2/g$)	Basic Site Density ($\mu mol\ CO_2/m^2$)	Reference
CaO	Hydration-Dehydration	$15 < pK_{BH+} < 18.4$	874.7	-	Roschat, et al. (2018)
CaO, 97.2 (Calcit)		$12.2 < pK_{BH+} < 15$	1532.4	61.3	Yoosuk, et al. (2010)
1.75-Li^+/CaO		$15 < pK_{BH+} < 18.4$	-	-	Kaur and Ali (2011)
1.5-LiC/CaO		$15 < pK_{BH+} < 18.4$	-	-	Kumar and Ali (2010)
0.5-Ni/CaO-650		$15 < pK_{BH+} < 18.4$	9.9[b]	-	Kumar, Abida and Ali (2016)
1-Ba/CaO		$15 < pK_{BH+} < 18.4$	-	-	Boro, et al. (2014)
3.5-K/CaO	Wet Impregnation	$11.1 < pK_{BH+} < 15$	-	-	Kumar and Ali (2012)
1.5-Zn/CaO-550		$15 < pK_{BH+} < 18.4$	-	-	Kumar and Ali (2013)
15-Zr/CaO-700		$11.1 < pK_{BH+} < 15$	20.21[b]	-	Kaur and Ali (2014)
10-(Mo/Zr)/CaO		-	20.94[b]	-	Nasar Mansir, et al. (2018)
20-KF/(CaO/NiO)-700		$15 < pK_{BH+} < 18.4$	6.11[b]	-	Kaur and Ali (2014)

Note: [a] determined using Hammett indicators

[b] mmol HCl/g

1.5-Zn/CaO-550; 1.5 = dopant concentration (wt%), 550 = calcination temperature (℃)

It is noted that the basic strength of most of the doped CaO nanocatalysts are determined using Hammett indicator test instead of CO_2-TPD analysis, and therefore the findings on the basicity of nano CaO catalysts synthesised via hydration-dehydration method are included as reference. It is known that the specific surface area correlates with the basic site present on the catalyst, where the basic strength is stronger due to a higher basic site at larger surface area, providing more accessible active sites for catalytic reaction and thus improving the activity of CaO catalyst.

By referring to Yoosuk, et al. (2010), the natural calcite possesses an extremely small surface area and negligible basicity, where an attempt was made to increase the solid surface area by hydration followed by the use of thermal decomposition technique. It was reported that the calcite containing 97.2 % CaO exhibits a greater and stronger basic strength than commercial CaO which is determined through Hammett indicator experiment. Besides, Yoosuk, et al. (2010) also measured the basicity of calcite by employing the CO_2-TPD technique, whereby the TPD results agree well with the order of basic strength obtained by Hammett indicator experiment, which further reveals that the basic sites of treated CaO are stronger than that of commercial CaO. It is evident that the calcined calcite constitutes a high number of total basic sites when compared to commercial CaO, where it possesses a relatively higher concentration of strong basic sites after hydration and subsequent thermal dehydration. Furthermore, it was further reported that the active sites produced by the calcination of the hydrated sample at 600 ℃ have a higher basicity than those generated from the calcination of fresh calcite at 800 ℃.

According to Kaur and Ali (2011), the Li^+ impregnated CaO is expected to constitute a higher activity towards transesterification reaction when compared to neat CaO in view of a significantly higher basic strength. It was inferred by Kumar and Ali (2010) that the highest basic strength possessed by 1.5 wt% Li impregnated CaO is mainly on account of the formation of strong basic sites on CaO surface, resulting in the highest activity towards transesterification of vegetable oil. In another study done by Kumar and Ali (2012), the basic strength of pure CaO used as support was reported to fall between 9.8 and 10.1, where it can be enhanced up to the range of 11.1 to 15.1 by doping 3.5 wt% of K^+ onto CaO. However, the basic strength of catalyst was

reported to remain unaltered with a subsequent increase in K^+ concentration exceeding 3.5 wt%. In other words, the basic strength cannot be enhanced to any further extent by simply increasing the K^+ concentration above the optimum value. Besides, Kumar and Ali (2013) reported that the basic strength of Zn/CaO will no longer be increased with a subsequent increase in Zn^+ concentration up to 7 wt%, whereby the improvement of basic strength is mainly dependent on the formation of base sites on CaO surface upon the doping of Zn before being calcined at the temperature higher than 550 ℃.

The basicity of Ba doped catalysts with different Ba loadings are tabulated in Table 2.27.

Table 2.27: Effect of Dopant Amount on Basicity of Ba/CaO (Boro, et al., 2014).

Catalyst	Basicity (mmol/g)
CaO	0.1
0.5-Ba/CaO	0.16845
1-Ba/CaO	0.2375
1.5-Ba/CaO	0.1925

It was found by Boro, et al. (2014) that the basicity of doped catalysts is increased up to 1 wt% of Ba loading beyond which it is decreased for 1.5 wt% Ba doped CaO. It is inferred that the increase in the basicity of 0.5 wt% and 1 wt% Ba impregnated CaO might be owing to the presence of active species which are comprised of BaO and CaO. On the other hand, the CaO species are reduced in 1.5 wt% impregnated CaO as the Ba dopants are predominantly associated as the major species. Thus, it can be concluded that the doped catalysts are highly basic in nature as compared to the parent catalyst, but constitute a reduced basicity at higher dopant loading.

By referring to Kaur and Ali (2014), an increase in Zr concentration by 10 wt% from 5 wt% before increasing the temperature by 400 ℃ from 300 ℃ for calcination has caused the Lewis base sites to augment. It was reported that the strong Lewis base sites are created in Zr/CaO at high calcination temperature above 600 ℃ owing to the thermal decomposition of hydroxides into corresponding oxides, where the maximum basicity of 20.21 mmol HCl/g was

observed in 15 wt% Zr impregnated CaO calcined at 700 ℃, resulting in stronger basic sites. In another study done by Kaur and Ali (2014), the impregnation of 5 to 25 wt% KF was accomplished in order to further enhance the basic strength of CaO/NiO mixed oxide catalyst. It was reported that a successive increase in KF concentration in CaO/NiO tends to increase the basic strength and total basic sites, where a maximum basicity of 6.11 mmol HCl/g was acquired upon 20 wt% of KF impregnation.

In another study done by Nasar Mansir, et al. (2018), CO_2-TPD analysis was used to measure the density distribution of basic sites possessed by Mo/Zr impregnated CaO, where the TPD profile detailing the CO_2 desorbed from Mo/Zr impregnated CaO is illustrated in Figure 2.26.
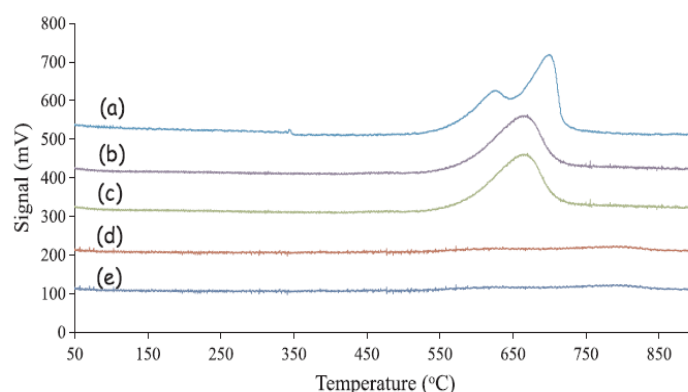
Figure 2.26: CO_2-TPD Profile of (a) 5-(Mo/Zr)/CaO, (b) 10-(Mo/Zr)/CaO, (c) 15-(Mo/Zr)/CaO, (d) 20-(Mo/Zr)/CaO and (e) 25-(Mo/Zr)/CaO (Nasar Mansir, et al., 2018).

The TPD profiles indicate major CO_2 desorption peaks at different temperatures, whereby the degree of basic strength is designated by the respective CO_2 desorbed peak. It is known that a strong basic strength is supported by the peak at high temperature, whereas a weak basic strength is denoted by the peak at low temperature. It was reported by Viriya-empikul, et al., (2012) that the peaks at below 360 ℃ indicate that CO_2 is desorbed from weak basic site, whereas the CO_2 desorption from modest basic site occurs at the temperature ranging from 360 to 700 ℃. On the other hand, CO_2 is desorbed from strong basic site when the temperature exceeds 700 ℃, which is supported by the peaks at elevated temperature. Based on Figure 2.26, there are two maximum CO_2 desorptions at

633 and 697 ℃ for 5-(Mo/Zr)/CaO with a basicity of about 38 mmol/g, indicating the presence of modest basic sites. Similarly, the moderate basic strength is also possessed by 10-(Mo/Zr)/CaO and 15-(Mo/Zr)/CaO as the desorption peaks are observed at 668 and 678 ℃, with the basicity of 20.94 and 15.5 mmol/g respectively. The appearance of desorption peaks at the maximum temperature up to 700 ℃ is most probably because CO_2 tends to interact with modest basic sites of MoO_3-ZrO-CaO. On the other hand, 20 and 25 wt% Mo/Zr impregnated CaO is observed to desorb a very low amount of adsorbed CO_2, where it is inferred that an increased Mo/Zr loading on CaO surface impedes the CO_2 to be adsorbed onto active sites. The overloaded Mo/Zr tends to remain in bulk quantities on the composite where CaO is difficult to interact with MoO_3 and ZrO, which in turn reduce the basicity, where it is about 4.49 mmol/g for 25-(Mo/Zr)/CaO.

2.5.5   Thermogravimetric Analysis (TGA)

Thermogravimetric analysis (TGA) is a technique to monitor the mass change of nano CaO catalyst as a function of increasing temperature (with constant heating rate) or time (with constant temperature or constant mass loss), where it is subjected to a controlled temperature program in a controlled atmosphere. The purge gas, either inert or reactive gas is channelled into the furnace and flows over the catalyst sample in order to control the sample environment. The TGA instrument can quantify the change in the mass of nano CaO catalyst on account of various thermal events such as desorption, adsorption, sublimation, vaporization, oxidation, reduction, decomposition, desolvation and dehydration when the catalyst sample is subjected to a program of temperature change. TGA is usually performed by gradually raising the temperature of catalyst sample in the furnace, while its weight is measured using the analytical balance outside the furnace. In fact, a mass loss is observed is the thermal event involves the loss of volatile component from catalyst sample.

Most TGA experiments utilise an inert purge gas such as argon and nitrogen so that the catalyst sample only reacts to temperature during decomposition, where it is also known as pyrolysis when the sample is heated in an inert atmosphere. As for the reactive purge gas, oxygen is usually used whereby it is a common technique to identify the amount of carbon content in

the catalyst sample. The TGA instrument should be run within the temperature range of 25 °C and 900 °C on routine basis, where it can be sustained up to 1000 °C. According to Roschat, et al. (2018), the maximum heating rate up to 100 °C/min is allowable, while the weight of catalyst sample can range from 1 to 150 mg, preferably more than 10 mg. It is noted that the TGA findings of nano CaO catalysts are incorporated in this context due to unavailability of the characterisation results for doped CaO nanocatalysts.

In the study done by Roschat, et al. (2018), the resulted material obtained from commercial CaO after refluxing with water in hydration process was analysed using TGA, where the TGA thermogram is illustrated in Figure 2.27.
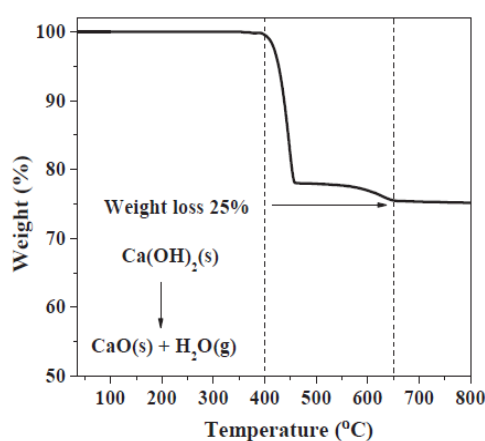
Figure 2.27: TGA Thermogram of Hydrated CaO (Roschat, et al., 2018).

Based on Figure 2.27, a major degradation peak with a total weight loss of about 24.5 wt% is observed at the temperature ranging from 400 to 450 °C, as proved by the decomposition of $Ca(OH)_2$ to CaO and H_2O. Besides, the weight possesses a slight loss of approximately 0.5 wt% from 450 to 650 °C, which indicates that CO_2 is removed during the decomposition of $CaCO_3$ to CaO. Hence, it was suggested that the calcination temperature of 650 °C is selected as the feasible condition to synthesise the nano CaO catalyst via hydration-dehydration process.

In another study done by Krishnamurthy, Sridhara and Ananda-Kumar (2019), TGA was employed alongside differential thermal analysis (DTA) to determine the thermal stability of CaO nanocatalyst as a function of increasing time (with constant temperature) or increasing temperature (with constant

heating rate), where the TGA/DTA curves for nano CaO catalyst are shown in Figure 2.28.
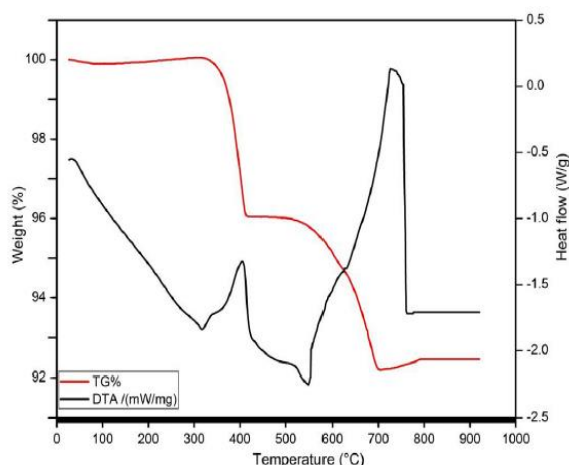
Figure 2.28: TGA/DTA Graph for Synthesised Nano CaO Catalyst (Krishnamurthy, Sridhara and Ananda-Kumar, 2019).

Based on Figure 2.28, the TGA measurement shows that the weight losses of catalyst are initially observed in the temperature ranging from 380 to 420 ℃, indicating the decomposition of $Ca(OH)_2$. It was reported by Krishnamurthy, Sridhara and Ananda-Kumar (2019) that the first endothermic peak (also known as valley) in TGA curve obtained from dehydration reaction results to possess a lower performance in terms of efficiency in the transesterification reaction when compared to its counterpart oxide. Meanwhile from DTA graph, there is a second weight loss occurs at the temperature range of 550 ℃ and 740 ℃, where it is inferred that all $CaCO_3$ are decomposed into CaO and CO_2. Thus, it is suggested that the calcination temperature of 500 ℃ is sufficient for complete dehydration of $Ca(OH)_2$ to form CaO based on the result of both thermal analysis, in spite of the postulation that the process requires a greater temperature.

CHAPTER 3

METHODOLOGY AND WORK PLAN

3.1   Introduction

The project flow chart of this research is illustrated in Section 3.4, where it is started off with the literature review on synthesising neat and doped CaO nanocatalyst for transesterification reaction to produce biodiesel. Ni and NiO are chosen as the dopants to synthesise the doped CaO nanocatalyst via wet impregnation method and sol-gel method respectively upon completion of literature review. The catalyst preparation for both synthesis methods will be included in the following sections.

Based on the characterisation studies reviewed in Section 2.5, a few characterisation tests are conducted to study the physical and chemical properties of doped CaO nanocatalyst by employing several analytical instruments after selecting the more effective dopant. XRD is used to identify the crystalline substances present and determine the crystallite size of catalyst. It is then followed by SEM which is used to analyse the surface topography and morphology of catalyst, while EDX is employed in conjunction with SEM to determine the elemental composition of catalyst. Besides, TPD of CO_2 is used to study the basicity of catalyst, whereas TGA is also carried out to examine the mass change of catalyst upon decomposition with increasing temperature. Meanwhile, BET analysis will not be performed due to equipment constraint.

The transesterification reaction is catalysed by the doped CaO nanocatalyst to produce biodiesel, whereby the catalytic performance of catalyst is determined based on the biodiesel yield using GC under a fixed reaction condition by varying the other parameter, which includes the amount of dopant loading and calcination temperature. The optimisation of catalytic performance based on the aforementioned parameters is then performed for achieving the highest biodiesel yield. The most favourable dopant concentration and calcination temperature are selected based on the maximum biodiesel yield that can be achieved within a fixed reaction duration.

3.2 Materials and Chemicals

In this research, various types of materials and chemicals are needed to be prepared prior to the experiment. Waste eggshells are chosen as the raw materials to derive CaO catalyst, while the synthesis of doped CaO catalyst is carried out using two different approaches, namely wet impregnation and sol-gel method. All the materials and chemicals used in the preparation of waste eggshells-derived CaO catalyst, synthesis of doped CaO catalyst, transesterification for biodiesel production as well as GC analysis are listed in Table 3.1. It is noted that the analytical grade chemicals are used for standards of GC.

Table 3.1: Materials and Chemicals Used for Research.

Material/Chemical	Composition	Source	Usage
Waste Eggshells	-	Waste from households	Raw material to derive CaO catalyst
Cooking Oil	-	Grocery shop	Feedstock to produce biodiesel by transesterification
Methanol	99.9 %	Merck	Reactant to produce biodiesel by transesterification
Nickel(II) Nitrate Hexahydrate	>99 %	Merck	Precursor to synthesise Ni doped CaO catalyst and NiO doped CaO catalyst
Calcium Nitrate Tetrahydrate	>99 %	Merck	Precursor to synthesise NiO doped CaO catalyst
Citric Acid Monohydrate	>99.5 %	Merck	Catalysing agent in sol-gel method
Ammonia	25 %	Merck	Peptiser in sol-gel method
n-Hexane	99.9 %	Merck	To dilute biodiesel sample
Distilled Water	-	UTAR	To wash off membrane and organic impurities attached to the eggshells
Deionised Water	-	UTAR	To suspend calcined CaO and dissolve metal precursors

Methyl Heptadecanoate	≥99.9 %	Sigma-Aldrich	Internal standard for GC
Methyl Linoleate	≥99.9 %	Sigma-Aldrich	Analytical standard for GC
Methyl Oleate	≥99.9 %	Sigma-Aldrich	Analytical standard for GC
Methyl Palmitate	≥99.9 %	Sigma-Aldrich	Analytical standard for GC
Methyl Stearate	≥99.9 %	Sigma-Aldrich	Analytical standard for GC

3.3 Apparatus, Equipment and Instrument

All the apparatus and equipment used in this research are tabulated in Table 3.2 along with their respective specification and usage.

Table 3.2: Apparatus and Equipment Used for Research.

Apparatus/Equipment	Specification	Usage
Oven	Memmert UNB-400	To dry eggshells, catalyst slurry and gel
Programmable Furnace	Wise Therm FP-03	To calcine powdered eggshells, dried catalyst slurry and gel
Mortar and Pestle	Granite	To grind dried eggshells and calcined chunks into fine powders
Mesh Sieve	2 mm	To filter and separate ground powders into desired size
Beaker	500 mL	To carry out catalyst synthesis
Hot Plate	IKA RCT basic, Heidolph	To heat up reaction mixture to desired temperature while stirring at constant stirring speed
Magnetic Stirrer Bar	PTFE	To ensure even mixing of reaction mixture
Vacuum Pump	-	To filter hydrated catalyst slurry
Filter Funnel	90 mm	To filter hydrated catalyst slurry
Reflux Condenser	Borosilicate glass, coil type, 200 mm	To reflux methanol during transesterification
Round Bottom Flask	Three-neck, 500 mL	To conduct transesterification of cooking oil
Water Bath	-	To maintain reaction temperature during transesterification

The instrument required for catalyst and biodiesel characterisation are summarised in Table 3.3.

Table 3.3: Instrument Used for Research.

Instrument	Specification	Usage
X-ray Diffractometer (XRD)	Shimadzu XRD-600	To determine crystalline substances present and crystallite size of catalyst
Scanning Electron Microscope (SEM)	Hitachi S-3400N	To analyse surface topography and morphology of catalyst
Energy Dispersive X-ray (EDX) Spectrometer	Hitachi S-3400N	To identify elemental composition of catalyst
Temperature-Programmed Desorption (TPD)	Thermo Fisher Scientific TPDRO 1100	To determine basicity of catalyst
Gas Chromatograph (GC)	Perkin Elmer Clarus 500	To determine FAMEs present in biodiesel sample
Thermogravimetric Analyser (TGA)	Perkin Elmer STA 8000	To study thermal stability of catalyst

3.4   Project Flow Chart

```
┌─────────────────────────────────────────────────────────────┐
│                          Start                              │
└─────────────────────────────────────────────────────────────┘
                              ↓
┌─────────────────────────────────────────────────────────────┐
│ Literature review on the synthesis of doped CaO nanocatalyst │
│ for biodiesel production                                    │
└─────────────────────────────────────────────────────────────┘
                              ↓
┌─────────────────────────────────────────────────────────────┐
│ Preparation of Ni doped CaO nanocatalyst with different Ni   │
│ loadings at constant calcination temperature via wet         │
│ impregnation method                                         │
└─────────────────────────────────────────────────────────────┘
                              ↓
┌─────────────────────────────────────────────────────────────┐
│ Preparation of NiO doped CaO nanocatalyst with different NiO │
│ loadings at constant calcination temperature via sol-gel     │
│ method                                                      │
└─────────────────────────────────────────────────────────────┘
                              ↓
┌─────────────────────────────────────────────────────────────┐
│ Preliminary study on dopant type in synthesising doped CaO   │
│ nanocatalyst                                                │
└─────────────────────────────────────────────────────────────┘
                              ↓
┌─────────────────────────────────────────────────────────────┐
│                    Catalyst Chacterisation                  │
│  1. XRD analysis to determine the crystalline substances    │
│     present and crystallite size of catalyst               │
│  2. SEM analysis to study the surface topography and        │
│     morphology of catalyst                                  │
│  3. EDX analysis to determine the elemental composition of  │
│     catalyst                                                │
│  4. TPD analysis to study the basicity of catalyst         │
│  5. TGA to determine the decomposition temperature of       │
│     catalyst                                                │
└─────────────────────────────────────────────────────────────┘
                              ↓
┌─────────────────────────────────────────────────────────────┐
│ Transesterification of cooking oil and methanol with         │
│ synthesised catalyst                                        │
└─────────────────────────────────────────────────────────────┘
                              ↓
┌─────────────────────────────────────────────────────────────┐
│           GC analysis to determine biodiesel yield          │
└─────────────────────────────────────────────────────────────┘
                              ↓
┌─────────────────────────────────────────────────────────────┐
│ Parameter studies on transesterification catalysed by doped  │
│ CaO nanocatalyst                                            │
└─────────────────────────────────────────────────────────────┘
```

```
          ⬇
┌─────────────────────────────────────────────────────────┐
│      Identification of optimum parameter for catalyst synthesis      │
└─────────────────────────────────────────────────────────┘
                          ⬇
┌─────────────────────────────────────────────────────────┐
│                      Thesis write-up                      │
└─────────────────────────────────────────────────────────┘
```

Figure 3.1: Project Flow Chart of Research.

3.5 Catalyst Preparation

The CaO nanocatalyst derived from waste eggshells is treated for properties modification. Besides, there are two synthesis methods investigated in this research to produce doped CaO nanocatalysts, where the preparation steps for both methods are quite different, which are outlined in the following sections.

3.5.1 Synthesis of CaO Nanocatalyst via Hydration-Dehydration Method

In this research, the CaO derived from waste eggshells is used as the catalyst. The eggshells are first washed with distilled water to remove the membrane attached to the eggshells. The rinsed eggshells are left in the oven overnight at 80 ℃ to dry off any remaining water. The dried eggshells are then crushed and grinded into fine powders using mortar and pestle before being calcined in the furnace at 900 ℃ for 3 hours under atmospheric condition. The calcined eggshells are denoted as C-CaO and kept in the desiccator to prevent direct contact with carbon dioxide and moisture from the atmosphere.

The calcined eggshell powders are then proceeded with hydration-dehydration treatment. The CaO catalyst is refluxed in water at 60 ℃ for 4 hours. The hydrated catalyst slurry is then filtered using vacuum pump and dried in the oven overnight at 80 ℃ to completely remove the water. The dried slurry is subsequently dehydrated by calcining in the furnace at 600 ℃ for 3 hours to change the hydroxide form to an oxide form, where the latter being the active form for transesterification reaction. The calcined catalyst is kept in the desiccator to minimise its exposure time to the atmosphere for limiting the possible site contamination by carbon dioxide and water.

3.5.2 Synthesis of Ni Doped CaO Nanocatalyst via Wet Impregnation Method

In this study, the CaO nanocatalyst is derived from waste eggshells which are obtained from household wastes. The waste eggshells are washed several times with distilled water in order to remove the shell membrane or any organic impurities attached to the eggshells. The cleaned eggshells are dried in the oven overnight at 80 ℃ to remove the moisture on the surface. The dried eggshells are then crushed and grinded into fine powders using mortar and pestle before being filtered through mesh sieve. The powdered eggshells are placed in the furnace for calcination at 900 ℃ for 3 hours under atmospheric condition. The calcined eggshells are denoted as C-CaO and kept in the desiccator to prevent direct contact with carbon dioxide and moisture from the atmosphere.

In this research, $Ni(NO_3)_2$ is used as the dopant source and 100 g of Ni/CaO is chosen as the basis for catalyst synthesis. The mass of $Ni(NO_3)_2$ required to produce the desired Ni loading on CaO is tabulated in Table 3.4.

Table 3.4: Mass of $Ni(NO_3)_2$ and CaO Required for Wet Impregnation Method.

Catalyst	Mass of $Ni(NO_3)_2$ (g)	Mass of CaO (g)
1 wt% Ni/CaO	3.11	96.89
2 wt% Ni/CaO	6.23	93.77
3 wt% Ni/CaO	9.34	90.66
4 wt% Ni/CaO	12.45	87.55
5 wt% Ni/CaO	15.57	84.43

For 1 wt% Ni/CaO, approximately 96.89 g of calcined CaO is suspended in 200 mL of deionised water in a glass beaker. After that, about 3.11 g of $Ni(NO_3)_2$ is dissolved in 50 mL of deionised water before adding to the CaO-containing solution. The resulting slurry is stirred on the hot plate for 4 hours continuously at 80 ℃, followed by drying in the oven overnight at 80 ℃. After calcining the dried slurry in the furnace at 600 ℃ for 4 hours, the calcined doped catalyst is kept in the desiccator (Kaur and Ali, 2014).

Based on Table 3.4, a series of Ni doped CaO nanocatalyst is prepared by varying the Ni concentration from 1 to 5 wt% at constant calcination

temperature of 600 ℃, which is denoted as x-Ni/CaO-T, where x and T represent the Ni concentration (wt%) and calcination temperature (℃) respectively. In short, there will be a total of five samples required in this study.

3.5.3 Synthesis of NiO Doped CaO Nanocatalyst via Sol-Gel Method

Unlike wet impregnation method, the CaO nanocatalyst is synthesised directly from reagent-grade chemical in sol-gel method instead of being derived from biomass. In this research, $Ni(NO_3)_2 \cdot 6H_2O$ is used as the source of NiO before doping onto CaO derived from $Ca(NO_3)_2 \cdot 4H_2O$ and 100 g of NiO/CaO is chosen as the basis for catalyst synthesis. In other words, $Ca(NO_3)_2 \cdot 4H_2O$ and $Ni(NO_3)_2 \cdot 6H_2O$ are used as the precursors for CaO and NiO respectively. The mass of $Ni(NO_3)_2 \cdot 6H_2O$ and $Ca(NO_3)_2 \cdot 4H_2O$ required to produce the desired NiO loading on CaO are tabulated in Table 3.5.

Table 3.5: Mass of $Ni(NO_3)_2 \cdot 6H_2O$ and $Ca(NO_3)_2 \cdot 4H_2O$ Required for Sol-Gel Method.

Catalyst	Mass of $Ni(NO_3)_2 \cdot 6H_2O$ (g)	Mass of $Ca(NO_3)_2 \cdot 4H_2O$ (g)
1 wt% NiO/CaO	3.89	96.11
2 wt% NiO/CaO	7.79	92.21
3 wt% NiO/CaO	11.68	88.32
4 wt% NiO/CaO	15.58	84.42
5 wt% NiO/CaO	19.47	80.53

For 1 wt% NiO/CaO, approximately 3.89 g of $Ni(NO_3)_2 \cdot 6H_2O$ is blended with about 96.11 g of $Ca(NO_3)_2 \cdot 4H_2O$. Both the metal nitrate precursors are then mixed with $C_6H_8O_7 \cdot H_2O$ at a total metal precursor/acid molar ratio of 1:3, where the citric acid is used as a catalysing agent which is responsible for the formation of stable dispersion of colloidal particles. The mixture is dissolved in deionised water as solvent in a glass beaker at a total metal precursor/water molar ratio of 1:45, which is followed by vigorous stirring at 400 rpm on the hot plate under the temperature of 90 ℃ for 3 hours to form a wet gel. After that, the ammonia solution is added to the mixture at a total metal precursor/ammonia molar ratio of 1:3, leading to the formation of

solid precursor suspended in the solution, where the ammonia solution is served as a peptiser to convert the precipitate into colloidal sol. The mass of citric acid as well as the volume of deionised water and ammonia solution required are computed based on their respective molar ratios, as shown in Table 3.6.

Table 3.6: Amount of Other Relevant Chemicals for Sol-Gel Method.

Chemical	Molar Ratio (mol/mol)	Mass Required (g)
Citric Acid	1:3	119.60
		Volume Required (mL)
Deionised Water	1:45	159.35
Ammonia	1:3	17.11

The resulting gel is dried in the oven overnight at 80 ℃, followed by the calcination in the furnace at 600 ℃ for 4 hours. The chunks produced from calcination is then ground and sieved into fine powders before being kept in the desiccator (Mohadesi, Hojabri and Moradi, 2014).

Based on Table 3.5, a series of NiO doped CaO nanocatalyst is prepared by varying the NiO concentration from 1 to 5 wt% at constant calcination temperature of 600 ℃, which is denoted as y-NiO/CaO-T, where y and T represent the NiO concentration (wt%) and calcination temperature (℃) respectively. In short, there will be a total of five samples required in this study.

3.6   Transesterification of Cooking Oil for Biodiesel Production

The experimental set-up for transesterification reaction consists of a three-neck round bottom flask, a reflux condenser, a pump, a heating mantle or hot plate and a magnetic stirrer bar. The transesterification of cooking oil will be carried out in the three-neck round bottom flask, where the cooking oil, methanol and doped CaO nanocatalyst are introduced to the flask and heated to the desired temperature using the heating mantle/hot plate. The magnetic stirrer bar is used to ensure a constant mixing condition for the reaction at the desired stirring speed, while the reflux condenser is required to condense any methanol vapor released during the reaction. It is necessary to prevent the methanol vapor formed during the reaction from escaping to the atmosphere as it may cause the

loss of reactant. The pump is coupled with the reflux condenser to cool the water supply.

The procedure is started off with the addition of methanol to cooking oil using a methanol-to-cooking oil molar ratio of 10:1 before pouring into the three-neck round bottom flask. The mixture is then heated to 60 ℃ by employing the heating mantle/hot plate, while the constant stirring speed is set at 400 rpm throughout the reaction. 5 wt% of doped CaO nanocatalyst is added into the mixture where the three-neck round bottom flask is securely stoppered to minimise the exposure to surrounding air. The transesterification process is allowed to proceed for 3 hours, where about 3 mL of the reaction mixture is withdrawn using transfer pipette to be collected as sample for every 1 hour during the reaction to determine the biodiesel yield. The reaction is repeated for the CaO nanocatalyst doped with different loadings at constant calcination temperature to study the effect of dopant concentration on biodiesel yield. The operating conditions employed for biodiesel production are tabulated in Table 3.7.

Table 3.7: Operating Conditions and Parameters for Transesterification.

Condition/Parameter	Specification
Temperature (℃)	60
Reaction Duration (minute)	180
Methanol-to-Cooking Oil Molar Ratio (mol/mol)	10:1
Catalyst Loading (wt%)	5
Stirring Speed (rpm)	400

In this research, the volume of cooking oil used is fixed at 200 mL for every experimental run, whereas the volume of methanol required is predetermined based on the methanol-to-cooking oil molar ratio of 10:1. Besides, the mass of doped CaO nanocatalyst which corresponds to 5 wt% of catalyst loading is calculated in accordance with the mass of cooking oil employed. Table 3.8 summarises the volume of cooking oil and methanol as well as the mass of doped CaO nanocatalyst that are necessary to be used for transesterification.

Table 3.8: Amount of Relevant Materials and Chemicals for Transesterification.

Material/Chemical	Amount Required
Cooking Oil	200 mL
Methanol	88 mL
Doped CaO Nanocatalyst	8.702 g

3.7 Catalyst Characterisation

In this research, instrumental analysis is carried out to study both the physical and chemical properties of synthesised CaO nanocatalyst by employing the analytical instrument stated in Section 3.3. Each of the analysis techniques will be further described and elaborated in the following sections.

3.7.1 X-ray Diffraction (XRD) Analysis

XRD is used to identify the compounds present in the synthesised catalyst. The condition of sample is very crucial as it may affect the result of XRD. First and foremost, the sample holder should be fully filled with the powdered catalyst, where a glass piece is used to smear and pack the catalyst uniformly on the sample holder. Pressure is applied in order to ensure that the surface of catalyst in the sample holder is completely smooth and flat for the diffraction of x-ray. After the sample preparation, the XRD analysis is executed using x-ray diffractometer which employs Cu K-α radiation with wavelength of 1.54 Å at 40 kV to create different diffraction patterns. The catalyst sample is scanned with wavelength in the range of 0.5 to 2 Å and 2θ in the range of 20° to 80° at the scanning rate of 2° per minute.

3.7.2 Scanning Electron Microscopy (SEM) Analysis

The surface feature and morphology of synthesised catalyst are analysed using scanning electron microscope. A small amount of catalyst sample is adhered onto the surface of carbon tape which is fixed on the aluminium sample holder with a diameter of 15 mm. The catalyst sample is then coated with palladium and gold by placing the sample holder in the sputter coater to reduce the thermal destruction from energetic electron beams as well as inhibit charging for a clear resolution. The analysis is initiated by placing the sample holder into the scanning electron microscope once the inner environment becomes vacuum.

The accelerating voltage is fixed at 15 kV, while the micrographs of CaO nanocatalyst at different magnifications including *1000x, 2000x* and *5000x* are taken by the electron detector where the images are displayed on the connected computer. The image capturing should be done within a short period to prevent the charging of catalyst sample by electron beams which will affect the resolution of image formed.

3.7.3   Energy Dispersive X-ray (EDX) Spectroscopy Analysis

The energy dispersive X-ray spectrometer is used to study the elemental composition of synthesised catalyst, where it is an essential part of SEM. In other words, SEM is normally equipped with an EDX detector. The EDX analysis is developed based on the fact that every element in the synthesised catalyst exhibits a unique irradiation which represents different sets of peaks. The accelerating voltage is set at 15 kV, which is similar to SEM. The measurement on the intensity of peaks corresponding to the elements present in the synthesised catalyst is carried out automatically.

3.7.4   Temperature-Programmed Desorption (TPD) of CO_2 Analysis

CO_2-TPD is used to analyse the basicity and basic strength distribution of synthesised doped CaO nanocatalyst. Before running the CO_2-TPD, the catalyst is pre-treated with the flow of nitrogen to clean the surface of catalyst at the temperature of 150 ℃ with a duration of 30 minutes. The temperature is increased linearly at a rate of 10 ℃ per minute and the nitrogen flow is fixed at 20 mL per minute. After the pre-treatment, the temperature is brought down to room temperature before a stream of pure CO_2 is introduced into the reactor. The flow rate of CO_2 is adjusted to 20 mL per minute and held for 1 hour, which is followed by the flushing of system by nitrogen for 30 minutes. After that, the desorption of CO_2 is carried out with helium at a flow rate of 25 mL per minute, while the temperature is increased at a linear rate of 10 ℃ per minute from 30 to 900 ℃.

3.7.5   Thermogravimetric Analysis (TGA)

The thermal stability of synthesised catalyst is investigated using TGA, where it is heated from 30 ℃ to 800 ℃ at a ramping rate of 20 ℃ per minute under nitrogen flow. The inert purge gas (nitrogen) is channelled into the furnace and flows over the catalyst in order to ensure that the catalyst only reacts to temperature during decomposition. TGA is expected to be conducted for 2 hours and 10 minutes, including the cool down period which lasts for about 45 minutes.

3.8   Biodiesel Characterisation

The biodiesel produced by transesterification between cooking oil and methanol in the presence of synthesised catalyst is analysed using gas chromatography to determine the resulting yield acquired.

3.8.1   Gas Chromatography (GC) Analysis

GC is used to analyse the concentration of FAME in the sample collected during the transesterification. A capillary inlet and flame ionisation detector are attached with the GC, where Nukol^{TM} FUSED SILICA with dimension of 30 m × 0.53 mm × 0.5 μm is used as the capillary column. Helium is used as the carrier gas in GC analysis, where the flow rate is set at 3 mL per minute. The temperature of oven is set and maintained at 220 ℃.

The internal and external standards are prepared prior to the analysis. The internal standard is prepared by diluting methyl heptadecanoate with sufficient amount of hexane to yield a mixture with a concentration of 4 g/L. The external standards are prepared by the dilution of methyl linoleate, methyl oleate, methyl palmitate and methyl stearate with hexane to yield mixtures with concentration of 10 g/L respectively. After that, 250 μL of each external standard is mixed with 250 μL of internal standard separately, where 1 μL of each mixture is then injected into the GC separately for analysis. The objective of this step is to determine the peak locations of the respective methyl ester as well as the peak area ratio of methyl linoleate, methyl oleate, methyl palmitate and methyl stearate respectively to peak area of internal standard that gives concentration of 10 g/L. The retention time of peak location for each methyl ester are tabulated in Table 3.9.

Table 3.9: Retention Time for Different Types of FAME.

Type of FAME	Molecular Weight (g/mol)	Retention Time (min)
Methyl Heptadecanoate	284.48	13.27
Methyl Linoleate	294.47	15.88
Methyl Oleate	296.49	15.02
Methyl Palmitate	270.45	12.17
Methyl Stearate	298.50	14.65

The analysis of FAME is performed in a similar manner, where 130 μL of internal standard is mixed with 20 μL of the sample collected, which is followed by the injection of 1 μL of the mixture into GC. The concentration for each methyl ester present in the sample can be calculated by comparing the ratio of respective methyl ester peak area of the FAME sample to the internal standard of FAME sample. Based on the concentration of FAME calculated, the biodiesel yield from transesterification can be estimated using Equation 3.1.

$$Yield = \frac{Actual\ mass\ of\ methyl\ ester\ in\ sample}{Theoretical\ mass\ of\ methyl\ ester\ produced} \times 100\ \% \quad (3.1)$$

CHAPTER 4

RESULTS AND DISCUSSION

4.1 Preliminary Study on Dopant Type in Synthesising Doped CaO Nanocatalyst for Biodiesel Production

Prior to the characterisation and parameters optimisation studies, a preliminary study was carried out to determine the more desirable and efficient dopant in order to produce a cost-effective doped CaO catalyst with excellent catalytic properties. The activity of doped CaO catalysts were investigated by synthesising via two methods that are commonly employed in biodiesel production industry, namely wet impregnation and sol-gel method, where Ni and NiO were used as the dopants to be incorporated into CaO respectively. It is noted that both the doped CaO catalysts were synthesised using the similar parameter, in which 1 wt% of dopant was incorporated to CaO before being calcined at 600 ℃. The screening process was then carried out to determine the catalytic performance of both doped CaO catalysts in terms of biodiesel yield, with the aim to select the more effective doped CaO catalyst in transesterification reaction for biodiesel production. The biodiesel yield obtained from the transesterification catalysed by doped CaO catalysts which were synthesised using two different methods are tabulated in Table 4.1.

Table 4.1: Biodiesel Yield Obtained from Transesterification Catalysed by Doped CaO Catalysts.

Catalyst	Synthesis Method	Biodiesel Yield (%)		
		1st Hour	2nd Hour	3rd Hour
Ni/CaO	Wet Impregnation	72.34	85.96	94.19
NiO/CaO	Sol-Gel	66.75	71.02	79.73

Figure 4.1 illustrates the comparison on the biodiesel yield achieved in transesterification reaction catalysed by Ni doped CaO and NiO doped CaO catalysts.
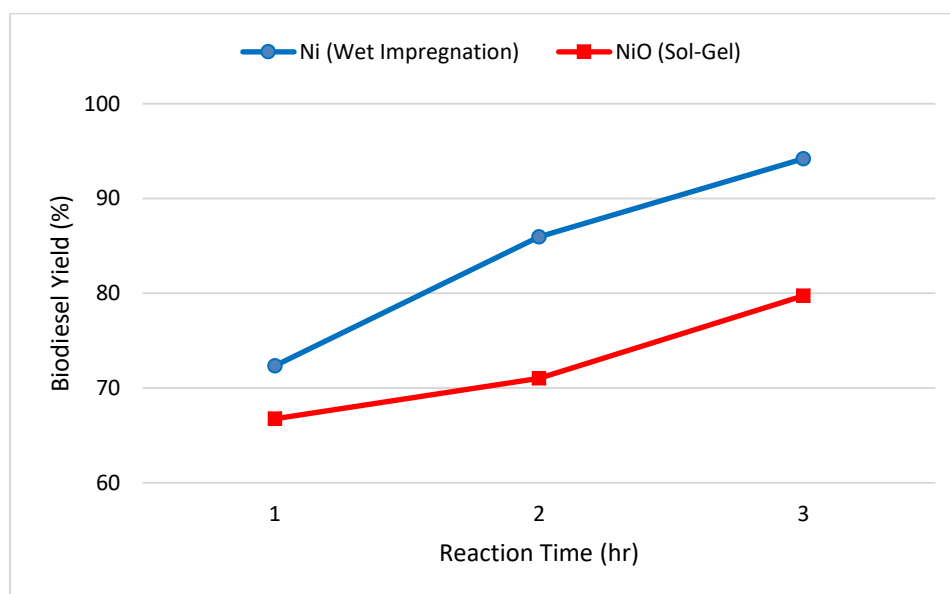
Figure 4.1: Effect of Type of Dopants on Biodiesel Yield.

It is observed that the biodiesel yield achieved for both Ni/CaO and NiO/CaO catalysts increased steadily with reaction time. Ni/CaO catalyst exhibited a relatively higher biodiesel yield of 94.19 % after three hours of reaction as compared to NiO/CaO catalyst with 79.73 % of biodiesel yield achieved. Furthermore, NiO/CaO catalyst showed a slow increase in biodiesel yield, in which there was only 12.98 % increment from the first hour to the third hour of reaction time. It is confirmed that NiO/CaO catalyst possessed a lower catalytic activity with comparatively low reaction rate and biodiesel yield. The activity of CaO-based catalyst was found to be highly dependent on both the basicity and surface area. By referring to Kumar, Abida and Ali (2016), the 1 wt% Ni doped CaO recalcined at 650 ℃ which was synthesised via wet impregnation constituted a total basicity of 12.4 mmol/g which was sufficiently high, implying that more basic sites were available on catalyst surface to catalyse the transesterification. Besides, it possessed a considerably high surface area of 14.7 m^2/g, allowing for more binding sites for the reactants during the reaction, and thus a high reaction rate was expected.

According to Tahvildari, et al. (2015), the CaO catalyst doped via sol-gel method could only achieve a maximum biodiesel yield up to 94.37% under optimum conditions after prolonged transesterification spanning for 6 hours. Moreover, the average particle size of aforementioned catalyst was about 61 nm,

which was considerably large. The larger CaO nanoparticles tended to reduce the specific surface area of catalyst, which in turn led to a decline in the catalytic activity towards transesterification, as evident from the extended duration required to produce the highest possible biodiesel yield. In another research done by Mohadesi, Hojabri and Moradi (2014), the transesterification catalysed by doped CaO catalyst which was synthesised via sol-gel method required a relatively longer duration of 8 hours in order to produce up to 82.1 % of biodiesel yield.

Thus, it is suggested that the CaO catalyst doped with Ni via wet impregnation exhibits a better catalytic activity than the CaO catalyst doped with NiO via sol-gel method. In addition, Ni/CaO renders a lesser production cost as the CaO compound is derived from natural resources, which are waste eggshells instead of commercial chemical, $Ca(NO_3)_2$ which is used as the catalyst precursor for NiO/CaO. Ni was therefore selected as the more effective dopant for CaO catalyst. The doped catalysts synthesised at different Ni loading and calcination temperature were characterised in terms of physical and chemical properties using XRD, SEM, EDX, CO_2-TPD and TGA. Lastly, the effects of Ni dosage and calcination temperature on the catalytic activity of doped catalysts were studied and optimised.

4.2 Characterisation Studies of Undoped and Doped CaO Nanocatalysts

The physicochemical properties of both undoped and doped CaO catalysts were analysed using the characterisation techniques, which include X-ray diffraction (XRD) analysis, scanning electron microscopy (SEM) coupled with energy dispersive X-ray (EDX) spectroscopy analysis, temperature-programmed desorption of CO_2 (CO2-TPD) analysis and thermogravimetric analysis (TGA). The crystalline compounds present in the catalyst were identified using XRD, besides obtaining the crystallite size of catalyst which was calculated using Debye-Scherrer equation. The surface feature and morphology of catalyst were observed through the scanning of electron beams on the catalyst sample using SEM, while the elemental composition of catalyst was determined using EDX. The basicity of catalyst was determined through the amount of carbon dioxide

adsorbed on the catalyst using CO_2-TPD, whereas the thermal stability of catalyst was investigated using TGA. The undoped CaO is referred to as the neat CaO synthesised via calcination; the undoped CaO that has undergone thermal hydration-dehydration treatment is denoted as treated CaO; while the undoped CaO that has impregnated with Ni dopant and undergone re-calcination is denoted as doped CaO. The details of Ni doped CaO synthesised via wet impregnation are tabulated in Table 4.2. It is noted that only one catalyst sample was selected for TGA in the current study as every FYP student was only entitled to one TGA analytical slot.

Table 4.2: Catalyst Notations with Their Respective Parameters.

Catalyst Notation	Dopant Loading (wt%)	Calcination Temperature (℃)
1-Ni/CaO-600		600
1-Ni/CaO-700		700
1-Ni/CaO-800	1	800
1-Ni/CaO-900		900
2-Ni/CaO-600	2	
3-Ni/CaO-600	3	
4-Ni/CaO-600	4	600
5-Ni/CaO-600	5	

4.2.1 X-ray Diffraction (XRD) Analysis

XRD analysis is carried out to identify the crystalline compounds present as well as to determine the crystallite size for all the synthesised catalysts, including undoped CaO and Ni doped CaO. The XRD pattern is plotted based upon 2θ angles in the range of 20° to 80° with the scanning rate of 2° per minute. The 2θ values of diffraction peak which correspond to the respective crystalline compounds present in undoped CaO and Ni doped CaO catalysts are identified using JCPDS database, where the emergence of sharp peak in XRD profile indicates the formation of highly crystalline materials. The findings on diffraction data by various researchers are summarised in Table 4.3, where it is then compared with the 2θ values indicating the emergence of crystalline compounds for each of the synthesised catalyst as tabulated in Table 4.4.

Table 4.3: Crystalline Compounds with Their Corresponding 2θ Values.

Crystalline Compound	2θ (°)	Reference
NiO	43.2	Kumar, Abida and Ali (2016)
$CaNi_4O_8$	37.6	
$Ca(OH)_2$	62.4	
CaO	32.2	Yoosuk, et al. (2010)
	37.4	
	53.9	
$Ca(OH)_2$	54.2	
$CaCO_3$	29.4	
	36.2	
	47.5	
CaO	64.2	Chen, et al. (2016)
	67.4	
$Ca(OH)_2$	28.6	
	34.1	
	46.9	
	50.7	
$CaCO_3$	44.7	Maneerung, et al. (2016)
$CaCO_3$	56.2	Roschat, et al. (2018)
$Ca(OH)_2$	51.2	Asikin-Mijan, Lee and Taufiq-Yap (2015)
$CaCO_3$	48.3	

Table 4.4: Comparison of 2θ Values of Synthesised Catalysts with Literature by Researchers.

Crystalline Compound	2θ (°)	Catalyst									
		Undoped CaO	Treated CaO	1-Ni/CaO-600	1-Ni/CaO-700	1-Ni/CaO-800	1-Ni/CaO-900	2-Ni/CaO-600	3-Ni/CaO-600	4-Ni/CaO-600	5-Ni/CaO-600
CaO	32.2	32.2	32.2	32.2	32.2	32.2	32.2	32.2	32.2	32.2	32.2
	37.4	37.4	37.4	37.4	37.4	37.4	37.4	37.4	37.4	37.4	37.4
	53.9	53.9	53.9	53.9	53.9	53.9	53.9	53.9	53.9	53.9	53.9
	64.2	64.2	64.2	64.2	64.2	64.2	64.2	64.2	64.2	64.2	64.2
	67.4	67.4	67.4	67.3	67.4	67.4	67.4	67.4	67.4	67.5	67.4
$CaCO_3$	29.4	29.4	29.4	29.4	29.4	29.4	-	29.4	29.4	29.5	29.4
	36.2	-	36.0	36.0	36.0	-	-	36.0	36.0	36.0	-
	44.7	-	-	44.6	-	-	-	-	-	-	-
	47.5	-	47.5	47.6	47.5	-	-	47.5	47.5	47.6	47.5
	48.3	48.5	48.5	48.6	48.6	-	-	48.5	48.5	48.6	48.5
	56.2	-	-	-	-	-	-	56.3	-	-	-
$Ca(OH)_2$	28.6	-	-	28.6	-	-	-	-	-	-	-
	34.1	-	-	34.2	-	-	-	34.1	34.0	34.1	-
	46.9	-	-	47.1	47.2	-	-	47.2	47.2	47.1	-

	50.7	-	-	50.7	-	-	-	-	-	-	-
	51.2	-	-	51.1	-	-	-	-	-	-	-
	54.2	-	54.1	54.2	54.2	54.2	54.2	-	-	54.4	54.1
	62.4	-	-	62.5	-	-	-	-	-	-	-
NiO	**43.2**	-	-	43.2	43.2	-	-	43.2	43.2	43.2	43.1
$CaNi_4O_8$	**37.6**	-	-	37.7	37.6	-	-	-	-	37.8	-

The XRD profiles of both neat CaO and treated CaO catalysts are combined in a single graph as illustrated in Figure 4.2.
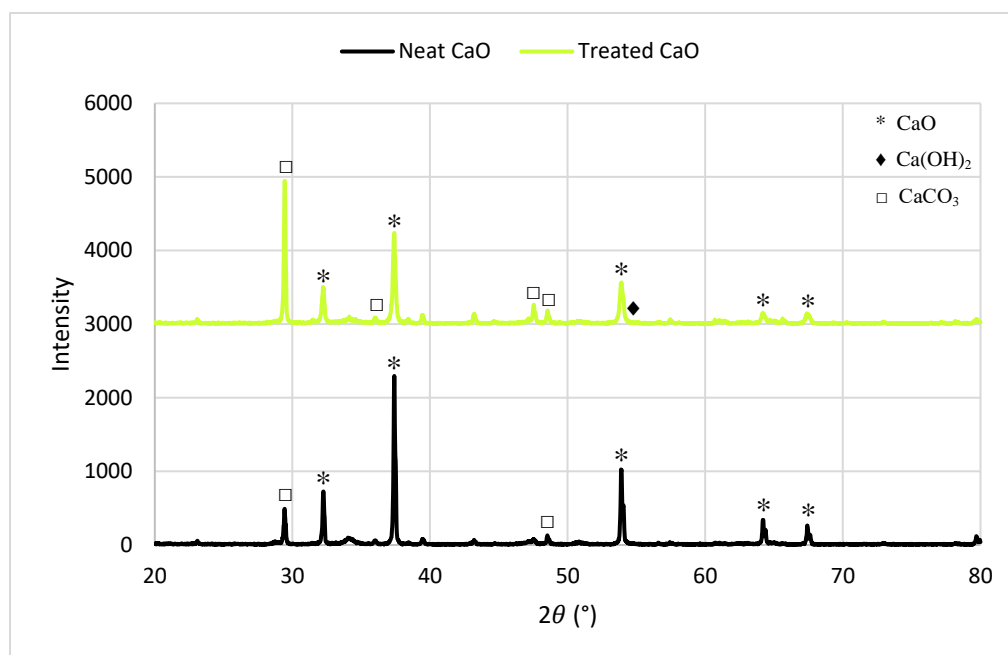
Figure 4.2: Comparison of XRD Profiles of Neat CaO and Treated CaO.

By referring to Figure 4.2, it is observed that the pure CaO derived from eggshells is mostly composed of CaO in cubic phase, which is revealed by the high intensity peaks at 2θ of 32.2°, 37.4°, 53.9°, 64.2° and 67.4°, with the presence of $CaCO_3$ as minor phase. The sharp peaks indicate that the eggshells are highly crystallised after being calcined at 900 ℃ with the transformation of carbonates in eggshells into CaO catalyst. However, the characteristic peaks of cubic CaO become less intense, which denotes the prominent decrease in the amount of CaO after further recalcining the hydrated CaO catalyst at a lower temperature of 600 ℃. In other words, the re-calcination temperature is not sufficiently high to decompose the carbonates into oxides completely, leading to a poorly crystalline structure of treated CaO catalyst.

The partial decomposition of $CaCO_3$ into CaO during the re-calcination of treated CaO is further supported by the minor characteristic peaks of $CaCO_3$ at 2θ of 36.0°, 47.5° and 48.5°, with the most intense $CaCO_3$ peak being emerged at 2θ of 29.4°. Besides, the formation of $CaCO_3$ phase might be due to the physisorption of CO_2 on the catalyst surface upon the exposure to the

atmosphere during catalyst synthesis. Meanwhile, the amount of $CaCO_3$ present in eggshell-derived CaO is insignificant, as evident from the appearance of low intensity peaks at 2θ of 29.4° and 48.5°.

Furthermore, it is observed that $Ca(OH)_2$ is formed in minimal amount upon the hydration-dehydration treatment of neat CaO, which is indicated by the characteristic peak at 2θ of 54.1°. The presence of hydroxide phase in minor intensity is mostly ascribed to the hydroxylation reaction which is taken place in between water and CaO phases during catalyst synthesis process, where the surface hydration proceeds deeply into the bulk, converting CaO that presents in hydrated catalyst into $Ca(OH)_2$ with a lower degree of crystallinity than that of commercial $Ca(OH)_2$. It is also inferred that the partial thermal decomposition of $Ca(OH)_2$ into CaO is occurred, where the remaining water present in the hydrated CaO are not completely removed during the calcination process, which is suggested to be owing to a relatively lower calcination temperature of 600 ℃.

The XRD profiles of undoped CaO and 1 wt% Ni doped CaO catalysts recalcined at the temperature ranging from 600 ℃ to 900 ℃ are combined in a single graph as illustrated in Figure 4.3.
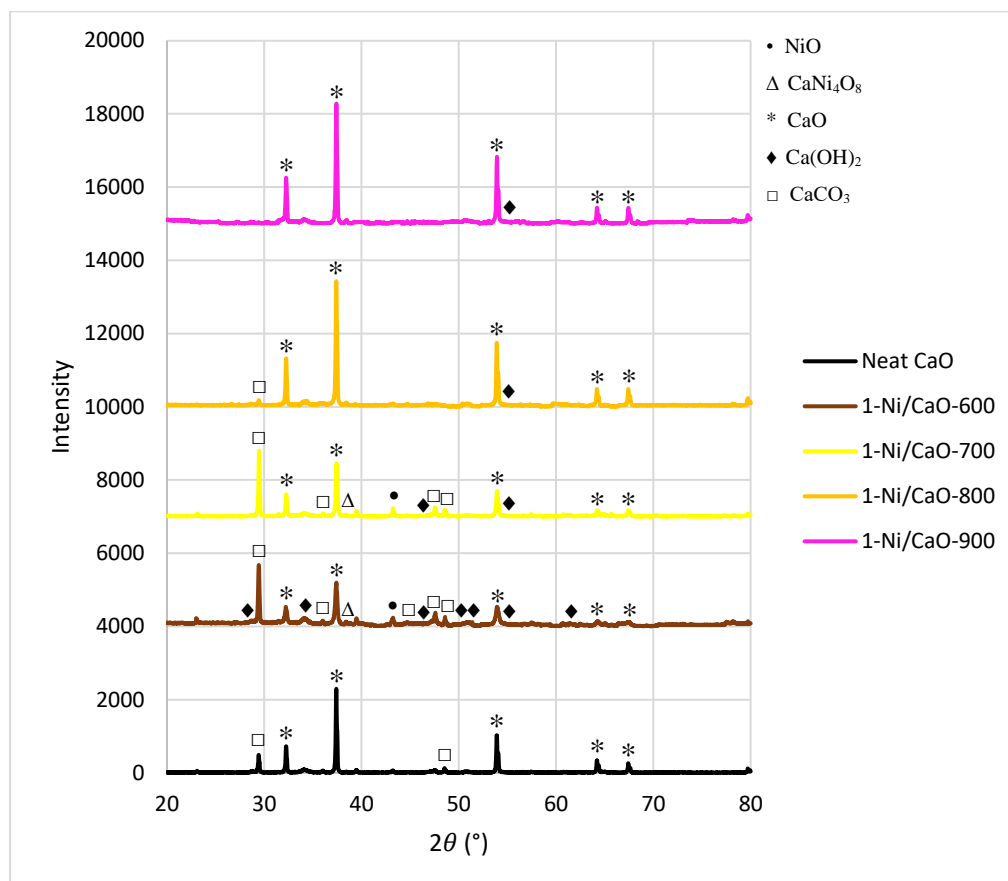
Figure 4.3: Comparison of XRD Profiles of Neat CaO and 1 wt% Ni/CaO Calcined at 600-900 ℃.

It is noticed that the incorporation of 1 wt% Ni dopant to CaO catalyst does not cause any shifting or changes in the XRD profile of parent CaO, but with notable difference in the intensity of several peaks as well as the appearance of new characteristic peak denoting the formation of Ni-Ca compound.

For 1 wt% Ni doped CaO which is recalcined at the temperature ranging from 600 ℃ to 900 ℃, cubic CaO is observed to be the major phase, which is denoted by the characteristic peaks at 2θ of 32.2°, 37.4°, 53.9°, 64.2° and 67.4°. The intensity of CaO peaks is substantially increased with the calcination temperature from 600 ℃ to 900 ℃, where it is observed that $CaCO_3$ were decomposed into CaO at a higher rate under a higher calcination temperature of

800 °C and above. It is noticed that the formation of $CaCO_3$ characterised by the peaks at 2θ of 29.4°, 36.0°, 47.6° and 48.6° is more noticeable in 1-Ni/CaO-700 followed by 1-Ni/CaO-600, whereas 1-Ni/CaO-800 exhibits a characteristic peak of $CaCO_3$ at 2θ of 29.4° in extremely low intensity, implying that the $CaCO_3$ phase present in the catalyst is not completely converted into the CaO phase. Furthermore, the presence of $CaCO_3$ especially in 1 wt% Ni doped CaO recalcined at 600 °C and 700 °C is most probably caused by the reaction of CaO with atmospheric CO_2 while synthesising the catalyst. No peaks corresponding to $CaCO_3$ is observed in XRD pattern of 1-Ni/CaO-900, which implies that a complete thermal decomposition of $CaCO_3$ into cubic CaO phase is taken place at the calcination temperature of 900 °C.

According to Kumar, Abida and Ali (2016), calcination is a crucial process that transforms the Brønsted basic sites ($Ca(OH)_2$) into Lewis basic sites (CaO), where the latter basic sites are reported to be more active during transesterification reaction. A minor phase of hexagonal $Ca(OH)_2$ supported by the peak at 2θ of 54.2° is observed as evident from the XRD patterns of 1 wt% Ni doped CaO recalcined at the temperature ranging from 600 °C to 900 °C, where the formation of $Ca(OH)_2$ is suggested to be attributed to the reaction of CaO with water which is utilised as the reaction medium during wet impregnation process. Moreover, the catalysts tend to undergo partial thermal decomposition of $Ca(OH)_2$ into CaO, causing the compound to present in minor intensity in the catalyst. Besides, it is also observed that 1-Ni/CaO-600 exhibits more characteristic peaks of $Ca(OH)_2$ as compared to other synthesised catalysts, which is most probably owing to the lower temperature for calcination.

The XRD profiles of undoped CaO and doped CaO catalysts recalcined at 600 ℃ with the amount of Ni dopant ranging from 1 wt% to 5 wt% are combined in a single graph as illustrated in Figure 4.4.
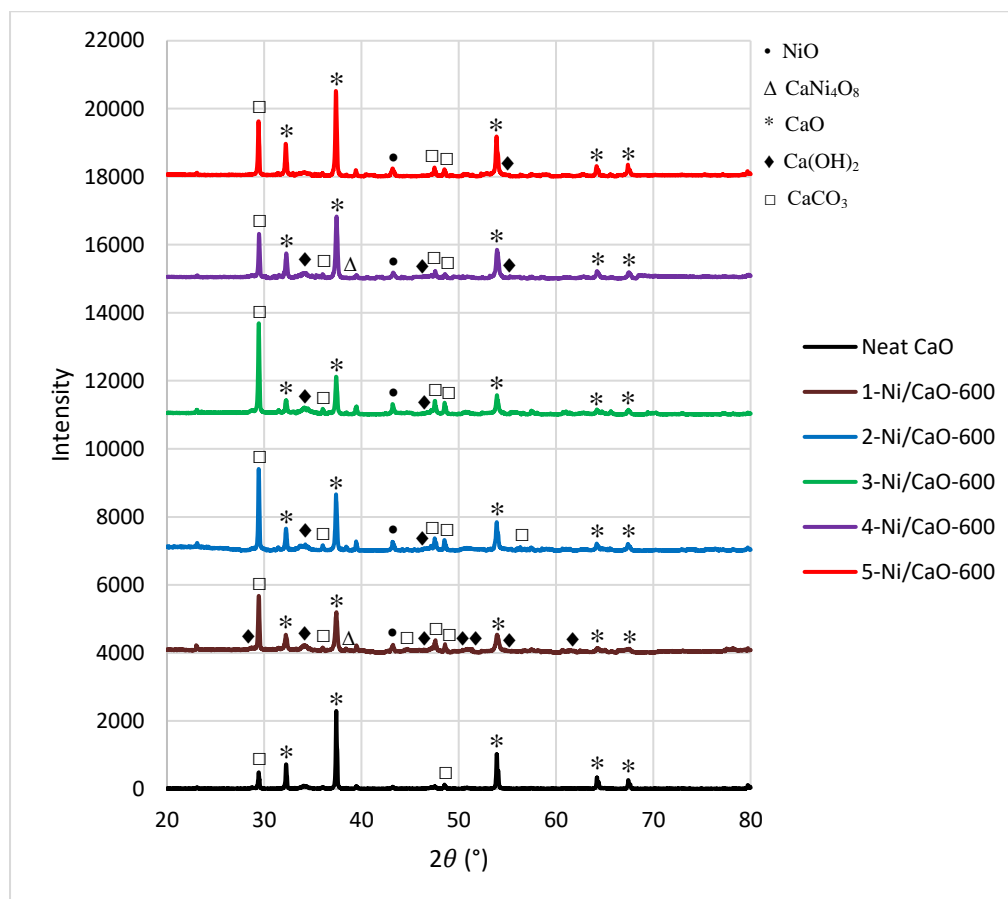
Figure 4.4: Comparison of XRD Profiles of Neat CaO and 1-5 wt% Ni/CaO Calcined at 600 ℃.

It is observed that the XRD pattern of parent CaO is not altered or shifted with the doping of Ni and the increment in Ni loading, but with remarkable difference in the intensity of several peaks as well as the appearance of new characteristic peak denoting the formation of Ni-Ca compound.

For Ni doped CaO recalcined at 600 ℃ with Ni loading of 1 wt%, 2 wt% and 3 wt%, most of the peaks indicating the emergence of CaO are presented at a relatively lower intensity than the characteristic peaks of $CaCO_3$. The peak at 2θ of 29.4° which indicates the presence of $CaCO_3$, is significant especially in the XRD profiles of 2-Ni/CaO-600 and 3-Ni/CaO-600, where the high $CaCO_3$ amount is most probably attributed to the reaction with carbon dioxide upon the

exposure of catalyst to the air during the wet impregnation process in order to dope Ni^{2+} ion into the calcined CaO. Besides, it is further inferred that the removal efficiency of carbon dioxide during the re-calcination which is conducted at 600 °C is relatively lower as compared to the initial calcination which is carried out at 900 °C.

The characteristic peak of cubic CaO at 2θ of 37.4° becomes more definite in the XRD profiles of 4-Ni/CaO-600 and 5-Ni/CaO-600 as compared to 1-Ni/CaO-600, 2-Ni/CaO-600 and 3-Ni/CaO-600. Meanwhile, the intensity of $CaCO_3$ characteristic peaks at 2θ of 36.0°, 47.5° and 48.5° as well as the CaO characteristic peaks at 2θ of 32.2°, 53.9°, 64.2° and 67.4° remain almost similar regardless of the amount of Ni doped in CaO catalysts. Furthermore, there are a few peaks characterising the presence of $Ca(OH)_2$ with immensely low intensity in most of the CaO catalysts doped with different Ni loadings. Hence, the formation of $Ca(OH)_2$ is deduced to be caused by the chemisorption of H_2O on CaO surface upon the exposure of catalyst to the moisture in the atmosphere during catalyst synthesis, cooling process after calcination, storage as well as handling of catalyst, resulting in slightly low rate of reverse reaction.

Moreover, upon the doping of Ni^{2+} ion into the crystal lattice of CaO, the doped catalyst exhibits a new diffraction peak at 2θ of 43.2°, which supports the formation of NiO in cubic phase. NiO is emerged in the XRD profiles of almost all synthesised catalysts due to the fact that Ni^{2+} attracts electrons of O^{2-} strongly since it has a relatively high electronegativity of 1.91 kJ/mol based on Pauling scale. In addition, Ni^{2+} possesses a small ionic radius (83 pm) which allows it to be incorporated into the lattice structure of CaO easily (Boro, et al., 2014). There is a sharp decrease in the crystalline peaks of CaO at 2θ of 32.2°, 37.4°, 53.9°, 64.2° and 67.4° with the increase in dopant loading from 2 wt% to 3 wt%, implying that the phase dispersion of NiO becomes saturated which eventually covers the CaO phase of catalyst. In other words, the increase in Ni dopant impregnated to CaO is expected to compress the crystal structure of CaO due to the formation of NiO phase, and thus suppressing the peak intensity of CaO.

Still, the intensity of NiO peak is lower than those of CaO peaks, which is most probably owing to the low amount of Ni dopant impregnated into CaO

catalyst. According to Kumar, Abida and Ali (2016), the insignificant characteristic peak of NiO indicates that Ni^{2+} is well dispersed on the surface of CaO. The intensity of NiO phase should be as low as possible because NiO will tend to affect the regular CaO structure due to poor distribution of Ni dopant in CaO. It is observed that there is no peak corresponding to NiO phase in the XRD profiles of 1-Ni/CaO-800 and 1-Ni/CaO-900, indicating a high degree of Ni^{2+} dispersion in CaO. It is further inferred that Ca^{2+} sites have been substituted by Ni^{2+}, leading to the formation of Ni/CaO in a single cubic phase. Besides, it is expected that the NiO phase in the doped CaO catalyst will increase with the Ni loading above 5 wt%.

It is noticed that the diffraction peak at 2θ of 37.8° is emerged only in 1-Ni/CaO-600, 1-Ni/CaO-700 and 4-Ni/CaO-600 among all the doped CaO catalysts, implying the formation of $CaNi_4O_8$ phase which mainly due to the interaction between Ni dopant and CaO carrier. It is suggested that CaO is not able to retain its structure with the formation of Ni containing phase. Similar to NiO phase, the $CaNi_4O_8$ complex present in the catalyst is detected only in minor intensity as compared to the major CaO phases. The amount of $CaNi_4O_8$ formed is suggested to be increased with the amount of Ni^{2+} ion doped, which eventually causes the peak to become more intense due to more prominent formation of complex crystal structure.

The crystallite size of synthesised catalysts is calculated using Debye-Scherrer equation based on the most intense peak in XRD profile, as tabulated from Table 4.5 to Table 4.14.

Table 4.5: Crystallite Size of Undoped CaO.

Peak No.	2θ (°)	θ (°)	FWHM (°)	FWHM (rad)	d-spacing (Å)	Crystallite Size (nm)
1	29.4160	14.7080	0.1488	0.0026	3.0340	54.50
2	32.2341	16.1171	0.1415	0.0025	2.7749	57.07
3	37.3897	18.6949	0.1398	0.0024	2.4032	60.29
4	53.8952	26.9476	0.1443	0.0025	1.6998	61.50
5	64.1962	32.0981	0.1436	0.0025	1.4497	64.72
Average						59.62

Table 4.6: Crystallite Size of Treated CaO.

Peak No.	2θ (°)	θ (°)	FWHM (°)	FWHM (rad)	d-spacing (Å)	Crystallite Size (nm)
1	29.4230	14.7115	0.1301	0.0023	3.0333	61.61
2	32.2070	16.1035	0.1908	0.0033	2.7771	43.23
3	37.3660	18.6830	0.1849	0.0032	2.4047	45.21
4	47.5208	23.7604	0.1397	0.0024	1.9118	62.40
5	53.8739	26.9370	0.2130	0.0037	1.7004	41.55
Average						50.80

Table 4.7: Crystallite Size of 1-Ni/CaO-600.

Peak No.	2θ (°)	θ (°)	FWHM (°)	FWHM (rad)	d-spacing (Å)	Crystallite Size (nm)
1	29.4170	14.7085	0.1558	0.0027	3.0339	52.48
2	32.2097	16.1049	0.2339	0.0041	2.7769	34.79
3	37.3731	18.6866	0.2338	0.0041	2.4043	35.29
4	47.5530	23.7765	0.1670	0.0029	1.9106	51.65
5	53.9138	26.9569	0.2750	0.0048	1.6992	32.03
Average						41.25

Table 4.8: Crystallite Size of 1-Ni/CaO-700.

Peak No.	2θ (°)	θ (°)	FWHM (°)	FWHM (rad)	d-spacing (Å)	Crystallite Size (nm)
1	29.4502	14.7251	0.1351	0.0024	3.0305	59.05
2	32.2463	16.1232	0.1559	0.0027	2.7738	52.84
3	37.4034	18.7017	0.1593	0.0028	2.4024	51.68
4	47.5414	23.7707	0.1382	0.0024	1.9111	62.40
5	53.9091	26.9546	0.1675	0.0029	1.6994	53.02
Average						55.80

Table 4.9: Crystallite Size of 1-Ni/CaO-800.

Peak No.	2θ (°)	θ (°)	FWHM (°)	FWHM (rad)	d-spacing (Å)	Crystallite Size (nm)
1	32.2303	16.1152	0.1478	0.0026	2.7752	54.87
2	37.3876	18.6938	0.1490	0.0026	2.4034	55.65
3	53.8930	26.9465	0.1490	0.0026	1.6999	59.14
4	64.1908	32.0954	0.1626	0.0028	1.4498	57.78
5	67.4138	33.7069	0.1589	0.0028	1.3881	58.84
Average						57.26

Table 4.10: Crystallite Size of 1-Ni/CaO-900.

Peak No.	2θ (°)	θ (°)	FWHM (°)	FWHM (rad)	d-spacing (Å)	Crystallite Size (nm)
1	32.2374	16.1187	0.1565	0.0027	2.7746	52.84
2	37.3962	18.6981	0.1503	0.0026	2.4028	55.65
3	53.9077	26.9539	0.1489	0.0026	1.6994	59.14
4	64.2031	32.1016	0.1550	0.0027	1.4495	59.93
5	67.4263	33.7132	0.1584	0.0028	1.3878	58.85
Average						57.28

Table 4.11: Crystallite Size of 2-Ni/CaO-600.

Peak No.	2θ (°)	θ (°)	FWHM (°)	FWHM (rad)	d-spacing (Å)	Crystallite Size (nm)
1	29.4184	14.7092	0.1275	0.0022	3.0337	64.41
2	32.2164	16.1082	0.1596	0.0028	2.7763	50.95
3	37.3675	18.6838	0.1668	0.0029	2.4046	49.89
4	47.5082	23.7541	0.1474	0.0026	1.9123	57.59
5	53.8778	26.9389	0.1777	0.0031	1.7003	49.59
Average						54.49

Table 4.12: Crystallite Size of 3-Ni/CaO-600.

Peak No.	2θ (°)	θ (°)	FWHM (°)	FWHM (rad)	d-spacing (Å)	Crystallite Size (nm)
1	29.4161	14.7081	0.1383	0.0024	3.0340	59.04
2	32.2245	16.1123	0.1945	0.0034	2.7757	41.96
3	37.3774	18.6887	0.1732	0.0030	2.4040	48.23
4	47.5180	23.7590	0.1526	0.0027	1.9119	55.46
5	53.8948	26.9474	0.2012	0.0035	1.6998	43.93
Average						49.72

Table 4.13: Crystallite Size of 4-Ni/CaO-600.

Peak No.	2θ (°)	θ (°)	FWHM (°)	FWHM (rad)	d-spacing (Å)	Crystallite Size (nm)
1	29.4517	14.7259	0.1660	0.0029	3.0304	48.87
2	32.2445	16.1223	0.2023	0.0035	2.7740	40.76
3	37.4039	18.7020	0.2098	0.0037	2.4023	39.11
4	53.9175	26.9588	0.2328	0.0040	1.6991	38.44
5	64.2166	32.1083	0.2268	0.0040	1.4492	40.45
Average						41.53

Table 4.14: Crystallite Size of 5-Ni/CaO-600.

Peak No.	2θ (°)	θ (°)	FWHM (°)	FWHM (rad)	d-spacing (Å)	Crystallite Size (nm)
1	29.3964	14.6982	0.1495	0.0026	3.0359	54.50
2	32.1938	16.0969	0.1634	0.0029	2.7782	49.19
3	37.3536	18.6768	0.1612	0.0028	2.4055	51.67
4	53.8600	26.9300	0.1785	0.0031	1.7008	49.59
5	64.1549	32.0775	0.1829	0.0032	1.4505	50.55
Average						51.10

Table 4.15 summarises the average crystallite size obtained for each of the synthesised catalyst based upon the five most distinct diffraction peaks in XRD profile.

Table 4.15: Average Crystallite Size of Synthesised Catalysts.

Catalyst	Average Crystallite Size (nm)
Undoped CaO	59.62
Treated CaO	50.80
1-Ni/CaO-600	41.25
1-Ni/CaO-700	55.80
1-Ni/CaO-800	57.26
1-Ni/CaO-900	57.28
2-Ni/CaO-600	54.49
3-Ni/CaO-600	49.72
4-Ni/CaO-600	41.53
5-Ni/CaO-600	51.10

The crystallite size of all the synthesised catalysts fall in the nanometer range, which signifies that both neat CaO and Ni doped CaO are nanocatalysts. The pure CaO possesses the largest crystallite size among all the synthesised catalysts, which is 59.62 nm, where the bulky structure is attributed to the non-effective synthesising method in reducing the particle size. The crystallite size of neat CaO is reduced by 8.82 nm after being treated via hydration-dehydration method, which is attributed to the hydroxylation reaction between CaO and water while synthesising the catalyst, resulting in the formation of $Ca(OH)_2$. It is further supported by the research done by Yoosuk, et al. (2010), where the removal of water molecules adsorbed on the catalyst lattice during the dehydration at 600 °C tends to fracture the crystallites of catalyst, which in turn leads to the formation of smaller crystallite size. As a result, the surface area-to-volume ratio of treated CaO is maximised, causing a significant increase in the reaction rate and efficiency as the catalytic performance of catalyst is enhanced by a larger active surface area that is exposed for the reaction to take place. Thus, it can be inferred that the hydration-dehydration treatment of neat

CaO is able to allow the formation of more active sites, besides improving the physicochemical properties such as textural properties which is supported by SEM analysis, as well as an increased basicity as evident from CO_2-TPD analysis.

It is noticed that the crystallite size of catalyst is reduced significantly upon the incorporation of Ni dopant into CaO, with 1-Ni/CaO-600 that encounters the largest reduction of 30.81 % after doping process, which is equivalent to 18.37 nm. It is inferred that the lattice structure of host CaO is disrupted by foreign Ni^{2+} impurities, which eventually causes the reduction of crystallite size. Among all the doped catalysts, the 1 wt% Ni doped CaO recalcined at 900 ℃ possesses the largest crystallite size, which is 57.28 nm, while the smallest crystallite size of 41.25 nm is presented by the 1 wt% Ni doped CaO recalcined at 600 ℃. According to Table 4.15, the crystallite size of 1 wt% Ni doped CaO catalyst is increased with the increase in calcination temperature from 600 ℃ to 900 ℃, where a total increase of 16.03 nm or 38.86 % is observed. The crystallite size increment is attributed to the sintering of Ni/CaO nanoparticles after being calcined at a higher temperature, and thus causing the particles to be agglomerated into lumps. The larger crystallite size of 1 wt% Ni doped CaO recalcined at a higher temperature is further supported by the changes in intensity and width of the main characteristic peak of CaO phase at 2θ of 37.4° in XRD patterns. For 1 wt% Ni doped CaO recalcined from 600 ℃ to 900 ℃, the peak in XRD diffractogram becomes more intense and narrower.

Besides, it is further deduced that the sintering effect becomes more prominent at the calcination temperature above 800 ℃, where both 1-Ni/CaO-800 and 1-Ni/CaO-900 catalysts possess a relatively large crystallite size. By referring to Taufiq-Yap, Nurul Suziana and Hussein (2010), a higher surface area is attributed to a smaller crystallite size or vice versa, where there will be an increase in the number of active sites per unit mass of catalyst. Hence, it can be inferred that the larger crystallite size exhibited by both the aforementioned catalysts tends to reduce the surface area of catalyst substantially. As a result, the number of binding sites available for catalytic reaction in the catalyst is subsequently reduced with the increase of calcination temperature beyond 800

°C. Thus, the catalytic performance of both 1-Ni/CaO-800 and 1-Ni/CaO-900 in transesterification reaction are declined due to the formation of aggregates, as supported by the low basicity achieved during CO_2-TPD analysis, which are 2297.58614 $\mu mol\ CO_2/g$ and 1787.5270 $\mu mol\ CO_2/g$ respectively, and thus resulting in low biodiesel yield.

On the other hand, the doped catalyst experiences a remarkable increase in crystallite size by 13.24 nm upon the increment in Ni loading from 1 wt% to 2 wt%. A reduction of 12.96 nm in crystallite size is observed with a subsequent increase in Ni loading from 3 wt% to 4 wt%. Hence, in terms of dopant amount, both 1-Ni/CaO-600 and 4-Ni/CaO-600 catalysts are reported to exhibit a relatively small crystallite size, which is about 41 nm. It is further inferred that both the 1 wt% and 4 wt% Ni doped CaO recalcined at 600 °C constitute a higher surface area as compared to other synthesised catalysts. As mentioned previously, the surface area of catalyst is the key factor that determines the number of active sites present in the catalyst, which in turn controlling the activity of catalyst towards transesterification. Therefore, both 1-Ni/CaO-600 and 4-Ni/CaO-600 are suggested to carry more active sites per unit mass of catalyst owing to an increased surface area that are exposed for the reaction to take place, leading to a higher catalytic performance in biodiesel production. It is deduced that a maximum of 4 wt% Ni^{2+} can be doped into CaO to assure a high surface area for better catalytic activity. In addition, the outstanding performance of 1-Ni/CaO-600 and 4-Ni/CaO-600 catalysts in catalysing the transesterification reaction is further evinced by a relatively high basicity obtained from CO_2-TPD analysis, which are 2561.33291 $\mu mol\ CO_2/g$ and 2458.54746 $\mu mol\ CO_2/g$ respectively.

The effect of crystallite size on the catalytic activity towards transesterification is significant only up to certain extent. It was reported by Trejo-Zárraga, et al. (2018) that the reaction rates possessed by the heterogeneous catalyst with two different particle sizes of 1 mm and 100 μm were only differed by a slight delay of 15 minutes reaction time for the larger particles. It is inferred that the rate of conversion to biodiesel is kinetically controlled rather than limited by intraparticle mass transfer. On the other hand, according to another research done by Kumar and Ali (2013), the biodiesel yield

is reported to decrease from 99 % to 42 % when the crystallite size of doped CaO is increased from 23 nm to 75 nm. In short, it is concluded that the catalytic performance of catalyst is fairly dependent on the crystallite size in most of the application employing the doped catalyst for biodiesel production.

4.2.2 Scanning Electron Microscopy (SEM) Analysis

The surface morphology of synthesised catalysts including CaO catalyst as well as Ni doped CaO catalysts are analysed using SEM. Figure 4.5 shows the SEM micrographs of neat CaO and treated CaO catalysts.
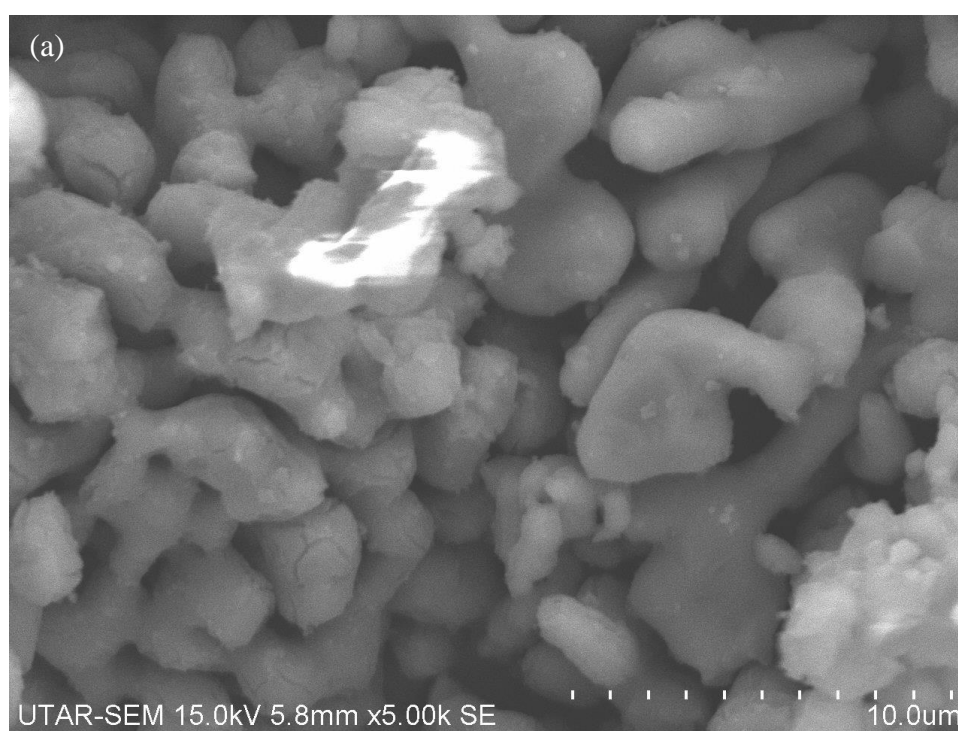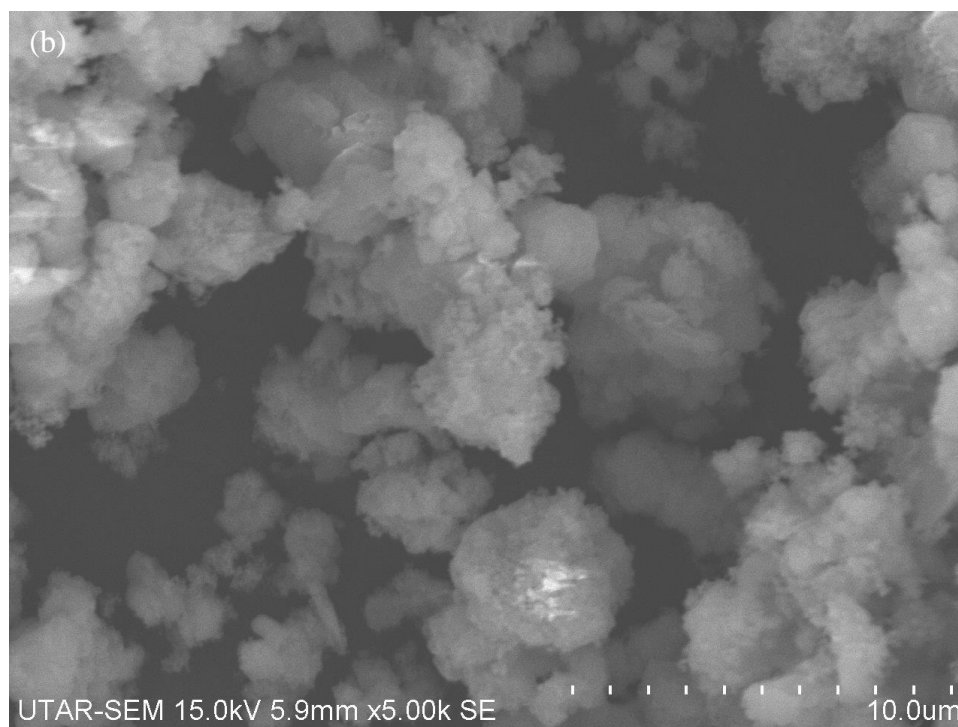
Figure 4.5: SEM Micrographs of (a) Undoped CaO and (b) Treated CaO at 5000x Magnification.

The pure CaO catalyst exhibits a coral-shaped structure with large and uniform-sized particles, which is analogous to the morphology and surface feature observed by Pongtonglor, et al. (2011). It is observed that the catalyst constitutes a fairly rough and porous surface. According to Tangboriboon, Kunanuruksapong and Sirivat (2012), the porous structure of catalyst is attributed to the release of CO_2 upon being thermally decomposed at 900 ℃ during calcination, and thus generating porous channels. The porous nature exhibited by the catalyst is suggested to be the main factor for assuring a high catalytic performance during transesterification reaction.

By referring to Figure 4.5, the morphology of CaO catalyst appears to be comprised of a highly textured structure with a relatively rougher and more porous surface after undergoing hydration-dehydration treatment followed by subsequent re-calcination at 600 ℃. Moreover, the particles residing on the surface of treated CaO catalyst are smaller in size as compared to pre-treated CaO catalyst. It is inferred that the highly porous structure with smaller particle size tends to increase the surface area of catalyst exposed to the reactants, leading to a higher reaction rate. Hence, it can be deduced that the modification

of neat CaO catalyst via hydration-dehydration treatment has considerably improved the physicochemical properties of the resulting catalyst.

Figure 4.6 shows the SEM micrographs of 1 wt% Ni doped CaO catalysts recalcined at 600 ℃ and 700 ℃.
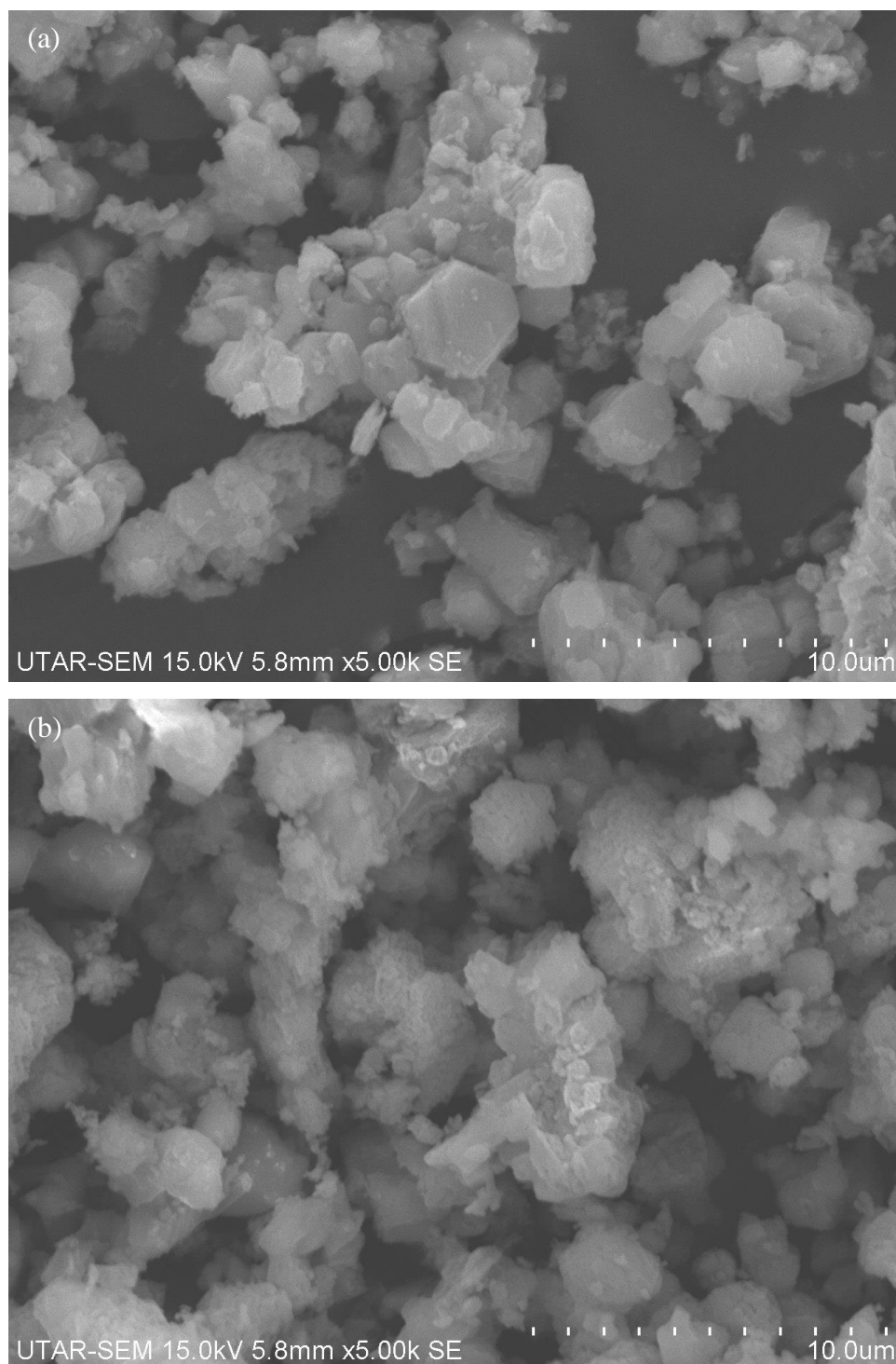
Figure 4.6: SEM Micrographs of (a) 1-Ni/CaO-600 and (b) 1-Ni/CaO-700 at 5000x Magnification.

The increase in calcination temperature from 600 ℃ to 700 ℃ only causes a slight change in the surface morphology, where both catalysts are observed to be composed of hexagonal, plate-like particles and irregular-shaped clusters with rough and porous surface. The catalyst surface is comprised of relatively small aggregates of variable morphologies, in which the smaller size of aggregates is able to provide a higher specific surface area for the reaction to occur. The spherical particles indicating Ni dopant are not significantly observed, where it is inferred that those particles are well dispersed on CaO surface. This variation in shape of particles may be owing to the heavy clustering of Ni/CaO nanoparticles during wet impregnation and calcination. The 1 wt% Ni doped CaO catalyst exhibits a more prominent clusters of particles at the calcination temperature of 700 ℃ as compared to 600 ℃, which is possibly due to particles agglomeration at a higher temperature.

Figure 4.7 shows the SEM micrographs of 1 wt% Ni doped CaO catalysts recalcined at 800 ℃ and 900 ℃.
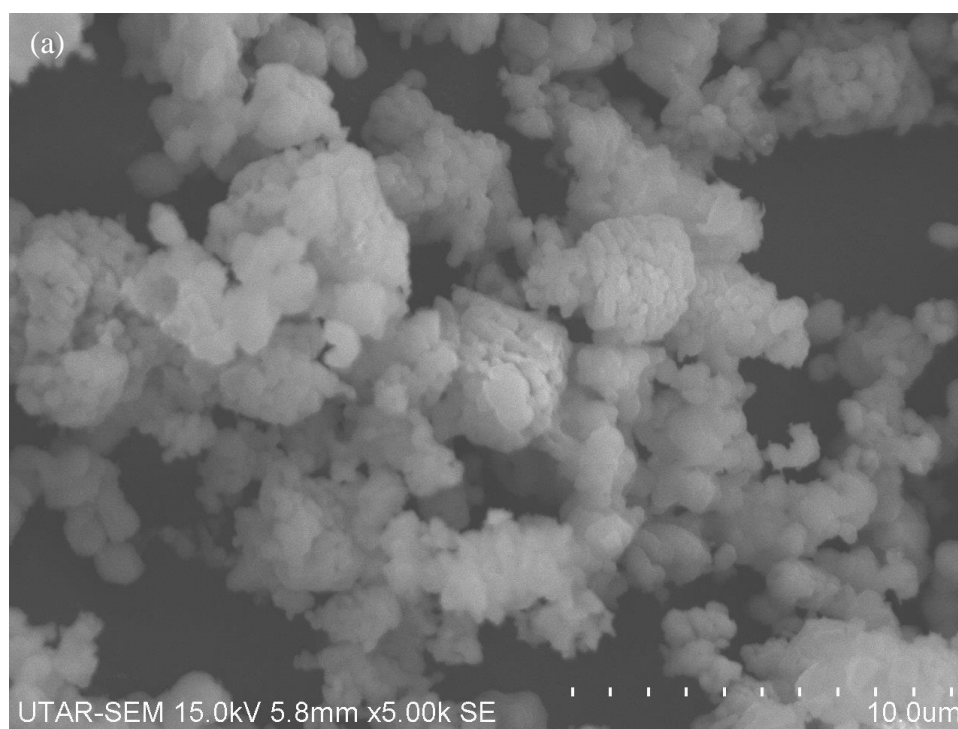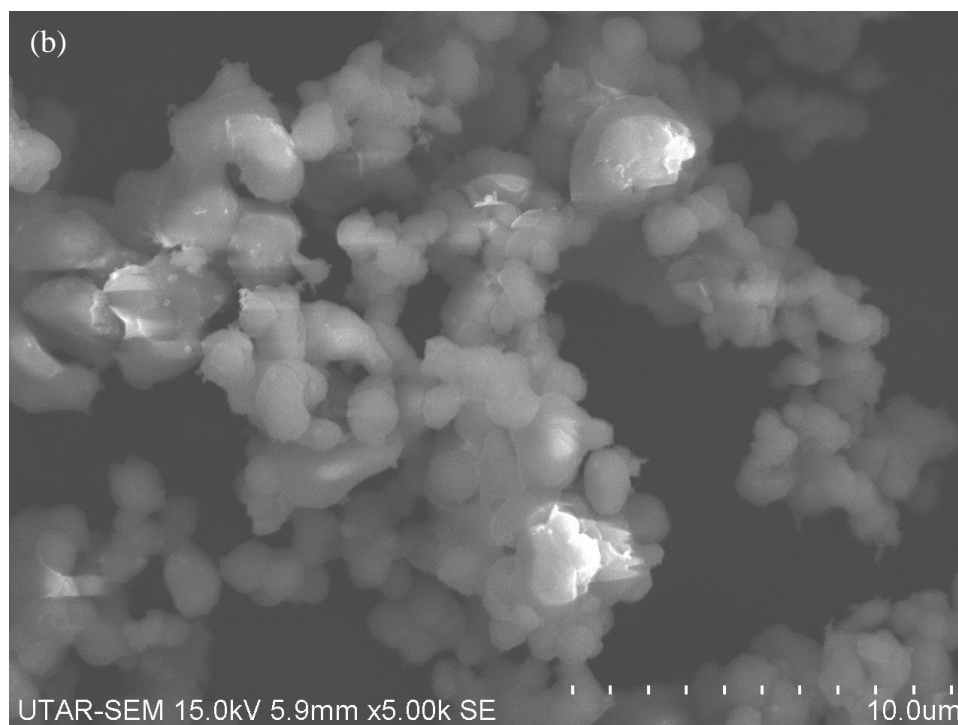
Figure 4.7: SEM Micrographs of (a) 1-Ni/CaO-800 and (b) 1-Ni/CaO-900 at 5000x Magnification.

By referring to Figure 4.7, it can be observed that the higher calcination temperature above 800 ℃ poses significant effect on the surface morphology of catalyst. Unlike 1-Ni/CaO-600 and 1-Ni/CaO-700 catalysts which exhibit a porous structure with highly rough surface, the 1 wt% Ni doped CaO catalysts recalcined at 800 ℃ and 900 ℃ show distinctive agglomeration of the particles, giving rise to the reduction in the number of active sites on catalyst surface. By comparing both the catalysts, the 1 wt% Ni doped CaO catalyst recalcined at 900 ℃ constitutes a more severe formation of particle aggregates in view of a more notable clusters of particles, forming spherical structures which are smoother and more defined. Thus, it is deduced that the sintering effect has taken place on the rough surface of catalyst upon the exposure to higher calcination temperature, which eventually causes the particle size to increase after being agglomerated into lumps, leading to reduced specific surface area for the catalytic reaction.

Figure 4.8 shows the SEM micrographs of Ni doped CaO catalysts recalcined at 600 ℃ with dopant loading of 2 wt% and 3 wt%.
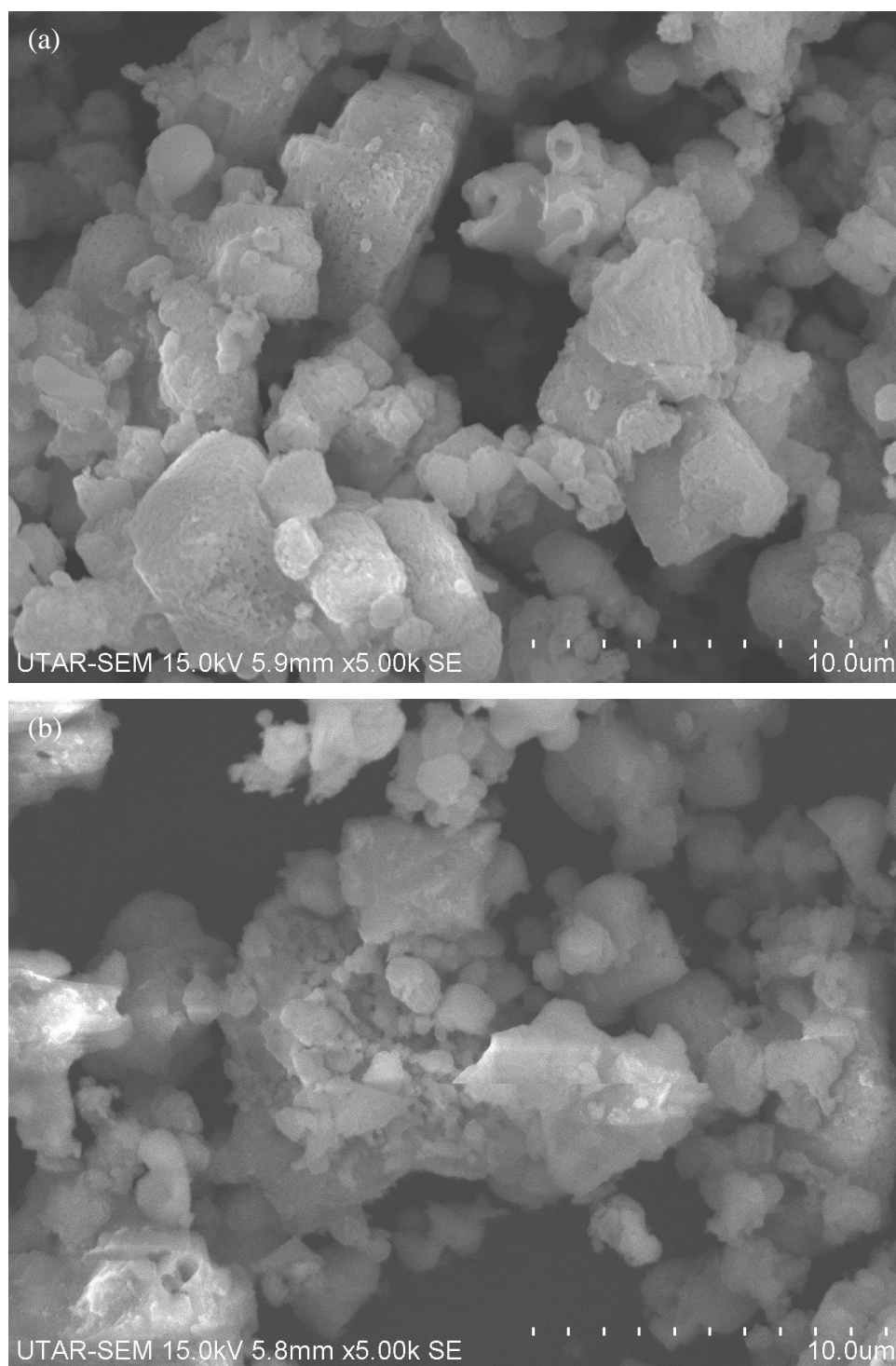
Figure 4.8: SEM Micrographs of (a) 2-Ni/CaO-600 and (b) 3-Ni/CaO-600 at 5000x Magnification.

There are relatively more spherical particles on the catalyst surface as compared to 1 wt% Ni doped CaO catalyst, indicating the increment of dopant content. The spherical shape particles cover almost the entire catalyst surface, where these particles are revealed to be the active Ni species. According to Borah, et al. (2019), the particle size decreases along with the increase in the amount of Ni dopant impregnated to CaO catalyst, which is predominantly due to the disruption of CaO carrier lattice by foreign Ni^{2+} impurities. The 3 wt% Ni doped CaO catalyst depicts the clusters of finer and smaller particles if compared with 2 wt% Ni doped CaO catalyst. Unlike 2 wt% Ni doped CaO catalyst which exhibits a moderately porous structure with coarse surface along with the combination of irregular-shaped and cubic clusters of particles, the surface morphology of 3 wt% Ni doped CaO catalyst appears to be composed of spherical, plate-like and non-uniform sized clusters of particles with fine and porous surface.

Figure 4.9 shows the SEM micrographs of Ni doped CaO catalysts recalcined at 600 ℃ with dopant loading of 4 wt% and 5 wt%.
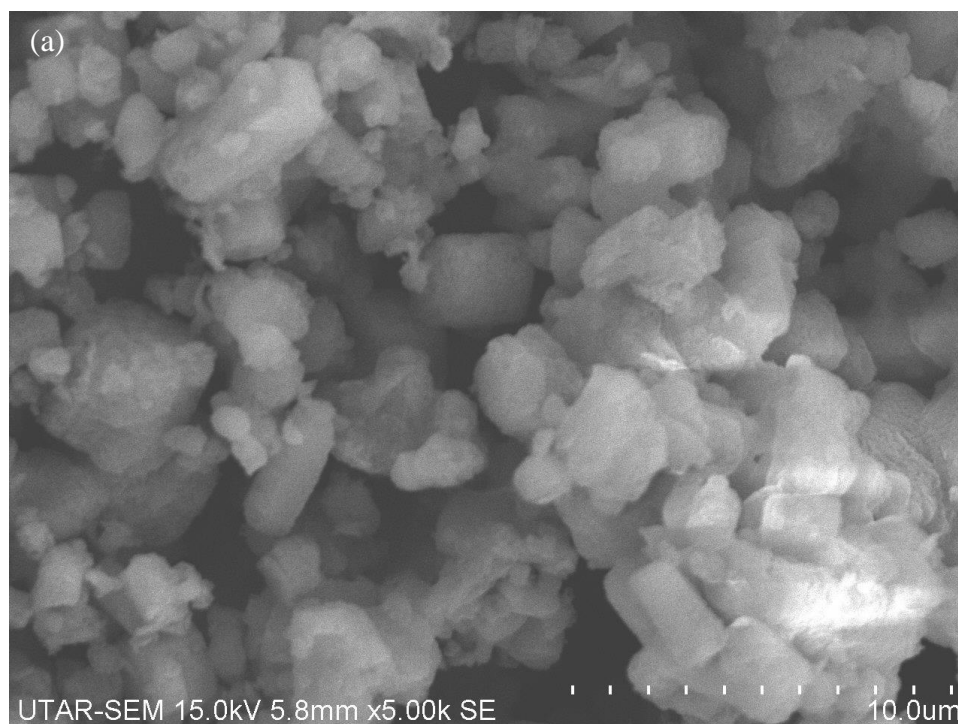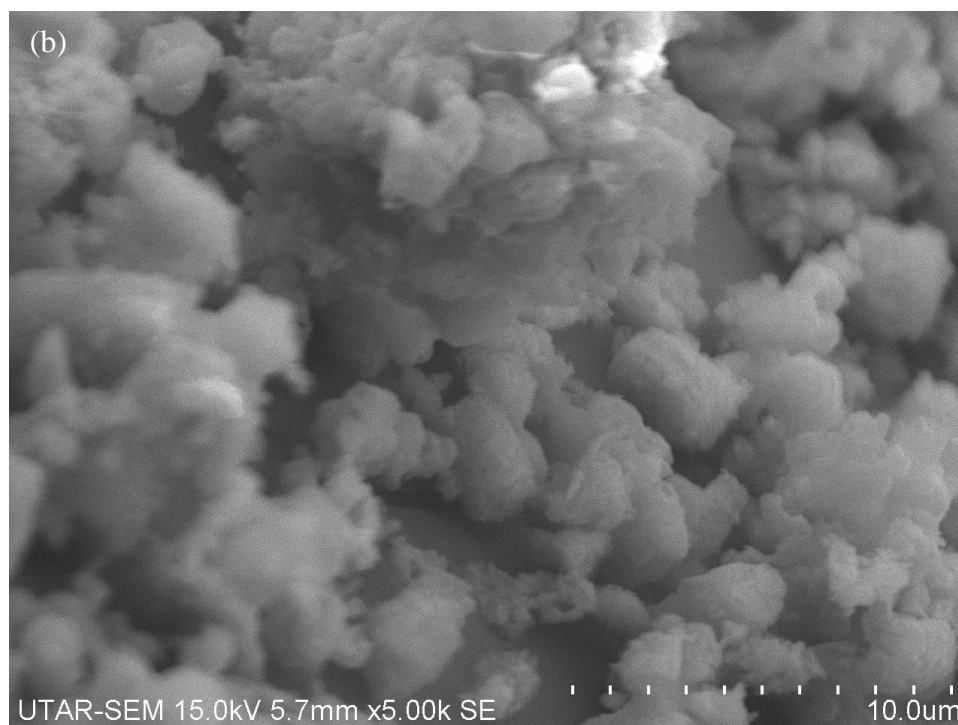
Figure 4.9: SEM Micrographs of (a) 4-Ni/CaO-600 and (b) 5-Ni/CaO-600 at 5000x Magnification.

There is no much difference in the surface feature between 4 wt% and 5 wt% Ni doped CaO catalysts, where the agglomerates of hexagonal, cubic and irregular-shaped particles are formed on the catalyst surface. It is inferred that the irregularities in the Ni impregnated CaO catalysts might be due to the formation of clusters of NiO and $CaNi_4O_8$ during calcination as a result of poor dispersion of Ni particles on CaO surface. Both the 4 wt% and 5 wt% Ni doped CaO catalysts exhibits a porous structure with a considerably rough surface, but the surface porosity is observed to be decreased with the increase in amount of Ni dopant impregnated to CaO as the 1 wt% and 2 wt% Ni doped CaO catalysts constitute a relatively more porous structure. Hence, it can be deduced that the catalytic sites available for the reaction to take place are reduced with the decrease in the surface area of CaO catalyst upon being incorporated with Ni dopant. Besides, it is also observed that the particle size changes from large cluster shape in 2 wt% and 3 wt% Ni doped CaO catalysts to the moderate crystalline shape in 4 wt% and 5 wt% Ni doped CaO catalysts, which is supported by the findings done by Borah, et al. (2019).

The comparison on the surface morphology of both undoped and doped CaO catalysts is made, where the undoped CaO catalyst presents a coral-shaped structure with a larger particle size as compared to the doped CaO catalysts. It is suggested that the impregnation of Ni dopant to CaO has prominently altered the morphology and surface feature of catalyst. Upon the substitution of continuous coral-shaped structure accompanied by larger particles with the irregular-shaped structure accompanied by smaller particles, the doped CaO catalysts constitute an increased specific surface area, resulting in more active sites available to expedite the reaction, which in turn enhances the catalytic activity in biodiesel production.

4.2.3   Energy Dispersive X-ray (EDX) Spectroscopy Analysis

EDX analysis is performed on the synthesised catalysts in order to verify the elemental composition of neat CaO as well as Ni doped CaO catalysts. The data are collected at three different spots on each catalyst to obtain an average value for both weight and atomic percentages. The weight percentage and atomic percentage of each element present in the synthesised catalysts are tabulated from Table 4.16 to Table 4.25.

Table 4.16: Elemental Composition of Undoped CaO.

Run	wt%			at%		
	Ca	O	C	Ca	O	C
1	60.64	36.96	2.40	37.61	57.42	4.97
2	59.30	39.07	1.62	36.47	60.20	3.33
3	60.41	38.01	1.58	37.54	59.17	3.28
Average	60.12	38.01	1.87	37.21	58.93	3.86

Table 4.17: Elemental Composition of Treated CaO.

Run	wt%			at%		
	Ca	O	C	Ca	O	C
1	67.78	28.49	3.73	44.71	47.08	8.21
2	66.19	29.88	3.92	42.94	48.57	8.50
3	65.78	31.54	2.68	42.78	51.40	5.82
Average	66.58	29.97	3.44	43.48	49.02	7.51

Table 4.18: Elemental Composition of 1-Ni/CaO-600.

Run	wt%				at%			
	Ca	O	C	Ni	Ca	O	C	Ni
1	54.01	38.89	6.15	0.94	31.29	56.44	11.90	0.37
2	49.70	43.08	4.68	2.54	28.40	61.68	8.93	0.99
3	55.07	35.00	9.11	0.82	31.70	50.48	17.50	0.32
Average	52.93	38.99	6.65	1.43	30.46	56.20	12.78	0.56

Table 4.19: Elemental Composition of 1-Ni/CaO-700.

Run	wt%				at%			
	Ca	O	C	Ni	Ca	O	C	Ni
1	64.27	31.61	3.12	1.00	41.58	51.24	6.73	0.44
2	60.67	34.22	4.28	0.83	37.63	53.17	8.85	0.35
3	68.30	26.49	3.26	1.94	46.50	45.18	7.42	0.90
Average	64.41	30.77	3.55	1.26	41.90	49.86	7.67	0.56

Table 4.20: Elemental Composition of 1-Ni/CaO-800.

Run	wt%				at%			
	Ca	O	C	Ni	Ca	O	C	Ni
1	49.87	39.16	10.08	0.89	27.37	53.84	18.47	0.33
2	50.44	45.18	3.75	0.63	28.57	64.10	7.09	0.24
3	63.61	31.25	4.49	0.65	40.43	49.76	9.53	0.28
Average	54.64	38.53	6.11	0.72	32.12	55.90	11.70	0.28

Table 4.21: Elemental Composition of 1-Ni/CaO-900.

Run	wt%				at%			
	Ca	O	C	Ni	Ca	O	C	Ni
1	52.40	39.48	7.20	0.92	29.78	56.22	13.65	0.36
2	63.70	32.18	3.12	1.00	40.98	51.87	6.70	0.44
3	61.67	34.48	2.33	1.53	39.32	55.07	4.95	0.66
Average	59.26	35.38	4.22	1.15	36.69	54.39	8.43	0.49

Table 4.22: Elemental Composition of 2-Ni/CaO-600.

Run	wt%				at%			
	Ca	O	C	Ni	Ca	O	C	Ni
1	66.24	28.63	3.18	1.95	44.18	47.84	7.09	0.89
2	63.00	31.21	4.02	1.77	40.43	50.18	8.61	0.78
3	65.44	30.15	2.97	1.44	43.09	49.74	6.52	0.65
Average	64.89	30.00	3.39	1.72	42.57	49.25	7.41	0.77

Table 4.23: Elemental Composition of 3-Ni/CaO-600.

Run	wt%				at%			
	Ca	O	C	Ni	Ca	O	C	Ni
1	74.72	20.14	1.77	3.37	56.02	37.82	4.43	1.72
2	53.78	38.04	3.90	4.29	32.59	57.75	7.88	1.77
3	66.05	29.46	2.64	1.85	44.05	49.22	5.88	0.84
Average	64.85	29.21	2.77	3.17	44.22	48.26	6.06	1.44

Table 4.24: Elemental Composition of 4-Ni/CaO-600.

Run	wt%				at%			
	Ca	O	C	Ni	Ca	O	C	Ni
1	48.96	42.18	4.93	3.93	28.17	60.81	9.47	1.54
2	63.87	29.53	3.24	3.35	42.31	49.01	7.17	1.52
3	59.85	31.87	3.76	4.52	38.53	51.40	8.08	1.98
Average	57.56	34.53	3.98	3.93	36.34	53.74	8.24	1.68

Table 4.25: Elemental Composition of 5-Ni/CaO-600.

Run	wt%				at%			
	Ca	**O**	**C**	**Ni**	**Ca**	**O**	**C**	**Ni**
1	54.31	32.32	8.52	4.84	32.52	48.47	17.03	1.98
2	50.48	40.19	3.17	6.16	30.42	60.68	6.37	2.53
3	61.00	30.74	5.09	3.17	38.81	49.00	10.82	1.38
Average	55.26	34.42	5.59	4.72	33.92	52.72	11.41	1.96

The average elemental compositions for each of the synthesised catalyst are tabulated in Table 4.26.

Table 4.26: Average Elemental Composition of Synthesised Catalysts.

Catalyst	Composition (wt%)			
	Calcium	**Oxygen**	**Carbon**	**Nickel**
Undoped CaO	60.12	38.01	1.87	-
Treated CaO	66.58	29.97	3.44	-
1-Ni/CaO-600	52.93	38.99	6.65	1.43
1-Ni/CaO-700	64.41	30.77	3.55	1.26
1-Ni/CaO-800	54.64	38.53	6.11	0.72
1-Ni/CaO-900	59.26	35.38	4.22	1.15
2-Ni/CaO-600	64.89	30.00	3.39	1.72
3-Ni/CaO-600	64.85	29.21	2.77	3.17
4-Ni/CaO-600	57.56	34.53	3.98	3.93
5-Ni/CaO-600	55.26	34.42	5.59	4.72

By referring to Table 4.26, it is known that all the synthesised catalysts including neat, treated and doped CaO are predominantly comprised of calcium as the major component, ranging from 52.93 wt% to 66.58 wt%. The treated CaO constitutes a higher Ca content as compared to pure CaO, where the composition of calcium in the catalyst increases by 6.46 wt% from 60.12 wt% after hydration-dehydration treatment. Meanwhile, the O content decreases significantly from 38.01 wt% to 29.97 wt%. The modification of undoped CaO through hydration-dehydration process is inferred to cause an increase in the

functional group of CaO due to higher Ca content, which denotes that there are more active sites available for the reaction to take place, and thus constituting a better catalytic activity. On the other hand, the carbon present in the treated catalyst experiences a slight increment of 1.57 wt% if compared with undoped catalyst. Besides, the undoped CaO accounts for a relatively higher Ca content as compared to Ni doped CaO, with the exception of 1-Ni/CaO-700, 2-Ni/CaO-600 and 3-Ni/CaO-600, along with a higher O content apart from 1-Ni/CaO-600 and 1-Ni/CaO-800. In addition, the amount of carbon in the catalyst is increased from 1.87 wt% to a maximum of 6.65 wt% upon the doping of Ni to CaO carrier.

After the impregnation of Ni dopant into CaO catalyst, the Ca content of catalyst is reduced from 60.12 wt% to the lowest of 52.93 wt%, which is attained by 1-Ni/CaO-600 even though it is composed of the highest O content of 38.99 wt%. On the other hand, 3-Ni/CaO-600 constitutes the lowest O content of 29.21 wt%. The Ni content for each of the catalyst shows deviation from the actual amount of Ni dopant impregnated, where 1-Ni/CaO-600 possesses the most remarkable aberration, which is 0.43 wt% higher than the initial amount intended. The other catalysts also experience some slight deviation of Ni content from the actual doping amount. The deviation is most probably due to the improper distribution of dopant during the wet impregnation process. Similar to undoped catalyst, all the doped catalysts mainly consist of calcium and oxygen, indicating the presence of active sites which in turn determines the catalytic performance of CaO catalyst. It is inferred that the number of active sites present in all the doped CaO catalysts are high with low $CaCO_3$ content, as there is a high Ca content ranging from 52.93 wt% to 64.89 wt%, high O content ranging from 29.21 wt% to 38.99 wt% alongside low C content ranging from 2.77 wt% to 6.65 wt%.

By comparing the carbon content for all the synthesised catalysts, undoped CaO shows the lowest C content, which is 1.87 wt%, whereas the highest C content is represented by 1-Ni/CaO-600, which is 6.65 wt%. The presence of carbon may be induced by the direct exposure of catalyst to the atmosphere while delivering and transferring the catalyst, either for drying, calcination or storing. It was reported by Kumar and Ali (2012) that the doped catalyst poses a smaller crystallite size after impregnation process, resulting in

more carbon dioxide in the air to react with the active sites of catalyst to form carbonate owing to the high reactivity of CaO catalyst in the air. By referring to Table 4.26, the 1 wt% Ni doped CaO recalcined at 600 ℃ constitutes the highest C content among the synthesised catalysts, which is in line with the finding results. Furthermore, it is deduced that neat CaO has encountered the least contamination by carbon dioxide among the synthesised catalysts.

Furthermore, the calcination temperature is also one of the factors that affects the C content in the doped CaO catalyst. It is presumed that the calcination temperature is not sufficiently high to remove the adsorbed carbon dioxide from the catalyst surface. Hence, the low calcination temperature is the reason behind the low Ca content and high O content possessed by 1-Ni/CaO-600 mainly due to high C content resulted during the wet impregnation process. In addition, the C content in doped catalyst decreases with the increase in the Ni concentration while incorporating Ni dopant to the lattice structure of CaO catalyst.

4.2.4 Temperature-Programmed Desorption (TPD) of CO_2 Analysis

TPD analysis is carried out to study the basicity for all the synthesised catalysts. Carbon dioxide is used as the adsorbed gas in CO_2-TPD to detect the number of basic sites present in the catalyst, where the basicity of synthesised catalysts is determined based on the amount of CO_2 adsorbed on the active sites of catalyst. TCD measures the concentration of desorbed CO_2 and quantifies the density of basic sites at the desorption temperature of CO_2. The amount of CO_2 adsorbed on the catalyst which is equivalent to the number of active sites that can form carbonate and the desorption temperature of CO_2 for each of the synthesised catalyst are tabulated in Table 4.27.

Table 4.27: TPD Results of Synthesised Catalysts.

Catalyst	Desorption Temperature of CO_2 (°C)	Amount of CO_2 Adsorbed ($\mu mol\ CO_2/g$)
Undoped CaO	730	1599.53140
Treated CaO	754	2134.92701
1-Ni/CaO-600	774	2561.33291
1-Ni/CaO-700	760	2539.86270
1-Ni/CaO-800	761	2297.58614
1-Ni/CaO-900	743	1787.52703
2-Ni/CaO-600	756	2725.44643
3-Ni/CaO-600	771	2957.16087
4-Ni/CaO-600	760	2458.54746
5-Ni/CaO-600	740	1524.13100

The TPD profile presents CO_2 desorption peak at certain temperature, where it refers to the temperature at which CO_2 starts to desorb from the catalyst surface. The CO_2 desorption temperature is used as an indicator of the basic strength of catalyst. According to Roschat, et al. (2018), the basic sites present on the catalyst surface are considered to be weak with CO_2 desorption peak emerging below 300 °C, whereas the peak above 600 °C is attributed to CO_2 desorption from strong basic sites. Meanwhile, the active sites are moderately basic with the desorption temperature of CO_2 ranging from 300 °C to 600 °C. Thus, it is inferred that all the synthesised catalysts are strongly basic. Besides, the desorption temperature of CO_2 exhibited by the desorption peak in TPD profile carries the information on the optimum calcination temperature for catalyst synthesis.

The TPD profiles of both neat CaO and treated CaO catalysts are combined in a single graph as illustrated in Figure 4.10.
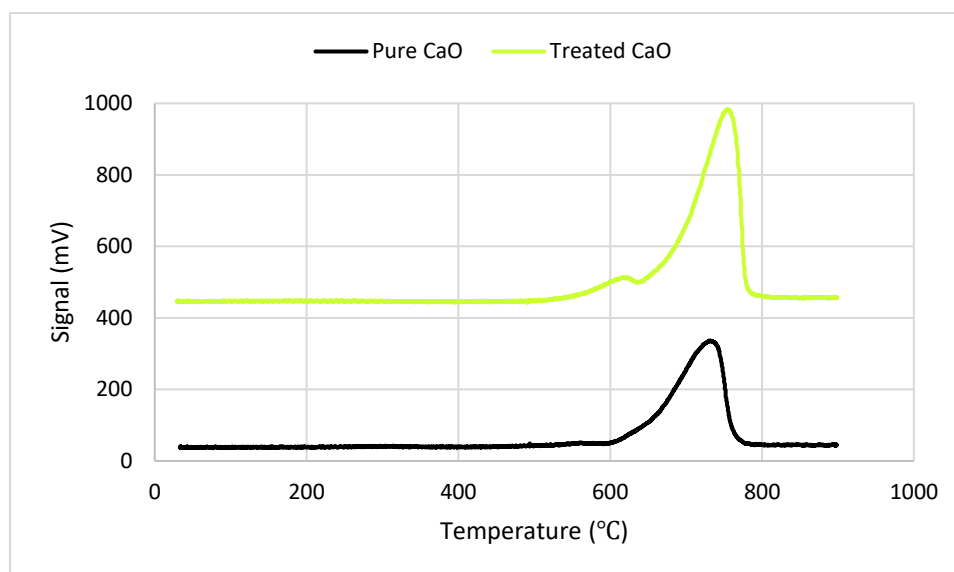
Figure 4.10: Comparison of TPD Profiles of Neat CaO and Treated CaO.

The treated CaO possesses a relatively higher basicity than undoped CaO with an increment of 535.4 $\mu mol\ CO_2/g$ which is equivalent to 33.47 %. It is in line with the research done by Roschat, et al. (2018), where various types of neat CaO including commercial CaO, eggshell-derived CaO, river snail shell-derived CaO and golden apple snail shell-derived CaO constitute a total basicity of 424.8 $\mu mol\ CO_2/g$, 215.5 $\mu mol\ CO_2/g$, 165.4 $\mu mol\ CO_2/g$ and 188.9 $\mu mol\ CO_2/g$ respectively. The basicity of those CaO catalysts are less basic as compared to hydration-dehydration treated CaO with a total basicity of 874.7 $\mu mol\ CO_2/g$. It is further evidenced in another research done by Yoosuk, et al. (2010), in which the CaO that has been treated with hydration and subsequent thermal dehydration at 600 ℃ possesses a higher concentration of strong basic sites than natural calcite-derived CaO, as evident from the total basicity of 1532.4 $\mu mol\ CO_2/g$ and 505.7 $\mu mol\ CO_2/g$ respectively, where the treated CaO is three times more basic than neat CaO obtained from the calcination of calcite.

By referring to Figure 4.10, the undoped CaO and treated CaO exhibit the desorption peaks at 730 ℃ and 754 ℃ respectively, where the CO_2 desorption at high temperature is suggested to be associated with the strong

interaction of CO_2 with active sites of catalyst which is highly basic. According to Roschat, et al. (2018), the hydration-dehydration treatment generates a higher surface area which correlates with the basic sites of catalyst. There is a significant number of gaseous H_2O molecules from $Ca(OH)_2$ removed during the calcination of hydrated catalyst, and hence creates more porosity. The expulsion of H_2O from the lattice is expected to fracture the crystallites, which is associated with the formation of more basic sites (Yoosuk, et al., 2010). Besides, the active sites generated by the calcination of hydrated catalyst at 600 ℃ possess a higher basicity than those produced from the calcination of eggshell-derived CaO at 900 ℃. Thus, it is deduced that the CaO catalyst renders a higher catalytic activity after hydration-dehydration treatment as it is able to increase the basicity of catalyst to a large extent, where a large number of strong basic sites are provided by a higher surface area.

By referring to Table 4.27, it is inferred that the impregnation of Ni dopant to CaO catalyst generates new active sites in view of the interaction between the active carrier (CaO) and doping component (Ni) at high calcination temperature ranging from 600 ℃ to 900 ℃. It was evident from the basicity of Ni doped CaO catalyst which is relatively higher than neat CaO catalyst except for 5 wt% Ni doped CaO recalcined at 600 ℃. The 3 wt% Ni doped CaO recalcined at 600 ℃ achieves the highest basicity of 2957.16087 $\mu mol\ CO_2/g$, which is equivalent to 84.88 % increment as compared to 1599.53140 $\mu mol\ CO_2/g$ achieved by the undoped CaO catalyst. In other words, the doped catalyst carries more active sites as compared to the undoped catalyst, and thus promotes a higher catalytic activity towards transesterification.

The TPD profiles of undoped CaO and 1 wt% Ni doped CaO catalysts recalcined at the temperature ranging from 600 ℃ to 900 ℃ are combined in a single graph as illustrated in Figure 4.11.
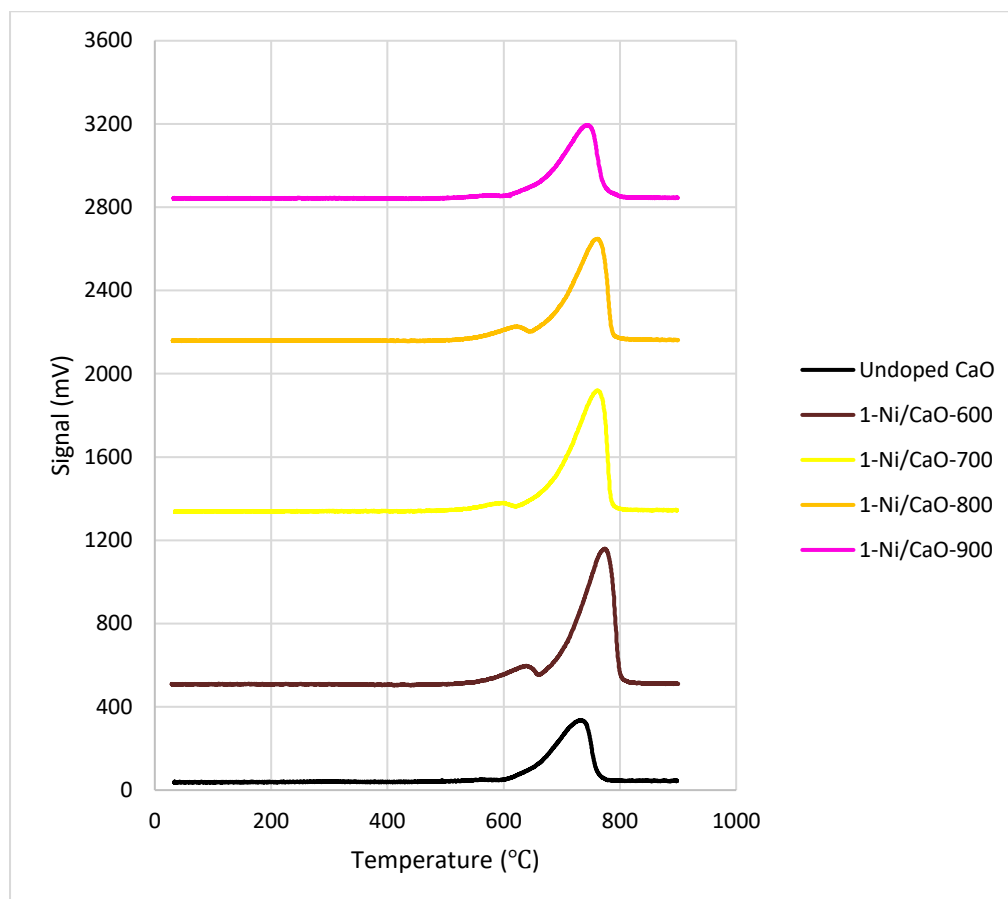
Figure 4.11: Comparison of TPD Profiles of Neat CaO and 1 wt% Ni/CaO Calcined at 600-900 ℃.

The CO_2 desorption temperature as indicated by the desorption peak at 774 ℃, 760 ℃, 761 ℃ and 743 ℃ in TPD curve correspond to 1 wt% Ni doped CaO catalysts recalcined at 600 ℃, 700 ℃, 800 ℃ and 900 ℃ respectively. As mentioned previously, the emergence of desorption peak at high temperature above 600 ℃ is attributed to the interaction of CO_2 with highly basic active sites on catalyst surface. Hence, it is evident that the strong basic sites are formed in the aforementioned catalysts.

In spite of the fact that every synthesised catalyst possesses strong adsorption sites, where there is no much difference in the basic strength of catalyst, the basicity or the number of basic sites present on the catalyst surface

can be varied with the change in parameter such as calcination temperature. Among all the CaO catalysts doped with 1 wt% Ni, the 1 wt% Ni doped CaO recalcined at 600 ℃ achieves the highest basicity of 2561.33291 $\mu mol\ CO_2/g$. It is revealed that the basicity of CaO-based catalyst is predominantly attributed to the strong basicity of Lewis base, which is composed of metal-O groups (-O-), where it has been reported as the strong basic sites for transesterification. Thus, it is inferred that there is an increase in Lewis basic sites due to the formation of CaO phase upon the thermal decomposition of carbonates into corresponding oxides at high temperature. The basicity of 1-Ni/CaO-600 is said to be enhanced, which is mainly ascribed to the formation of strong Lewis basic sites on CaO surface when being calcined at 600 ℃. Besides, a sufficiently high calcination temperature is required in order to facilitate the interaction between carrier and active component for the formation of new active sites.

However, it is found that the basicity of 1 wt% Ni doped CaO is slightly reduced by increasing the calcination temperature from 600 ℃ to 700 ℃ with a total reduction of 21.47021 $\mu mol\ CO_2/g$. The 1 wt% Ni doped CaO encounters a significant drop in basicity by 10.3 % and 30.21 % after being calcined at 800 ℃ and 900 ℃ respectively as compared to 600 ℃. The reduction of basicity is further supported by the decrease in the intensity of CO_2 desorption peak in TPD profile, with the least distinct CO_2 desorption peak exhibited by 1-Ni/CaO-900. With the increase in calcination temperature from 600 ℃ to 900 ℃, it implies that there will be a relatively lesser basic sites on catalyst surface. Besides, it is also evidenced by Kumar, Abida and Ali (2016), where the total basicity of 1 wt% Ni doped CaO drops by 2.4 mmol/g when the calcination temperature is increased from 650 ℃ to 950 ℃. The modest decline in the basicity of 1 wt% Ni doped CaO is most probably due to the sintering of Ni/CaO particles at a significantly higher temperature, leading to particle agglomeration. The resulting larger particles tend to cause the catalytic surface area to decrease, which in turn lead to the lower number of basic sites on catalyst surface. The amount of CO_2 adsorbed becomes apparently lower as the increase in calcination temperature tends to diminish the number of CO_2 adsorption sites. Thus, it is inferred that the decline in catalytic activity is attributed to the reduction in basicity at a higher calcination temperature.

The TPD profiles of undoped CaO and doped CaO catalysts recalcined at 600 ℃ with the amount of Ni dopant ranging from 1 wt% to 5 wt% are combined in a single graph as illustrated in Figure 4.12.
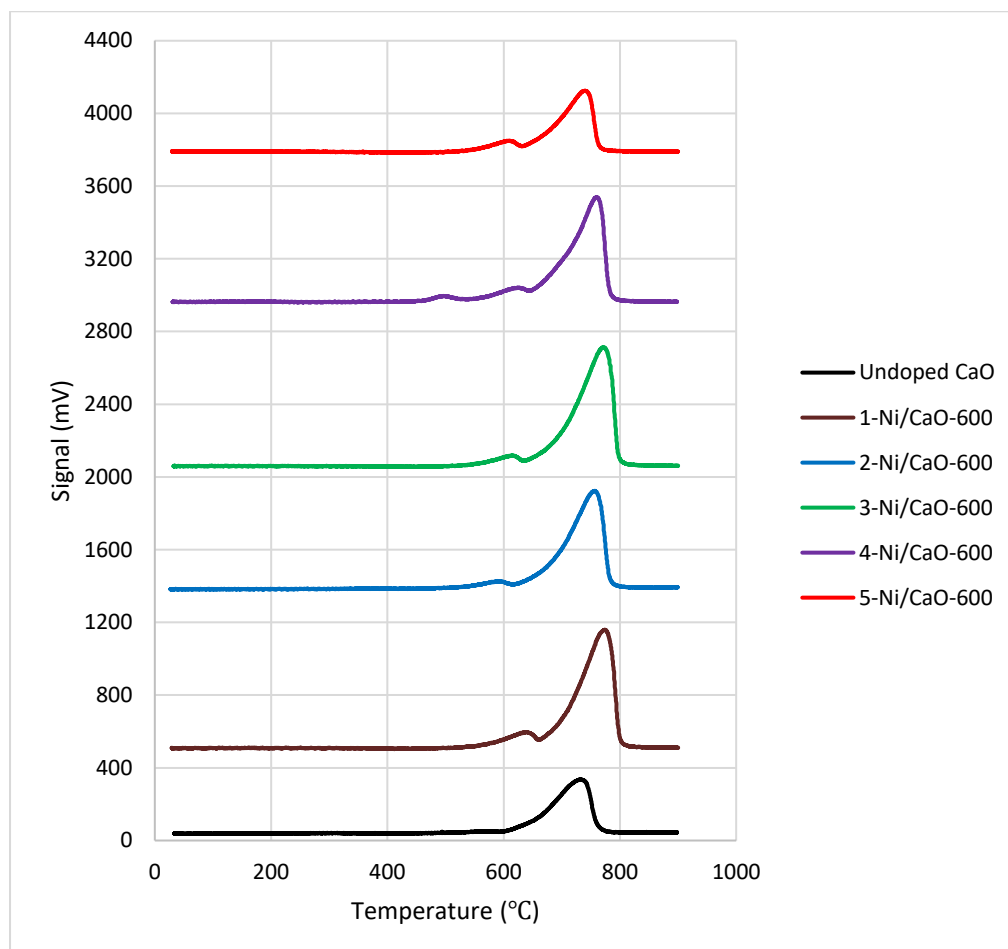
Figure 4.12: Comparison of TPD Profiles of Neat CaO and 1-5 wt% Ni/CaO Calcined at 600 ℃.

The doped CaO catalysts recalcined at 600 ℃ with Ni loading of 1 wt%, 2 wt%, 3 wt%, 4 wt% and 5 wt% exhibit a CO_2 desorption peak at 774 ℃, 756 ℃, 771 ℃, 760 ℃ and 740 ℃ respectively. Since the desorption temperature of CO_2 is higher than 600 ℃, the active sites with high basic strength are suggested to present in the aforementioned catalysts for CO_2 adsorption.

Similar to calcination temperature, the variation of dopant loading has a direct impact on the basicity or the number of basic sites on catalyst surface even though the CO_2 adsorption sites of all synthesised catalysts possess nearly similar basic strength. The basicity of Ni doped CaO recalcined at 600 ℃ is

observed to increase by 395.82796 $\mu mol\ CO_2/g$ with the addition of Ni dopant to CaO from 1 wt% to 3 wt%. By further increasing the Ni dosage from 3 wt% to 5 wt%, the basicity of Ni doped CaO catalyst decreases prominently by 1433.02987 $\mu mol\ CO_2/g$.

It is realised that an increase in basicity by 15.45 % with a successive increase of Ni concentration in CaO from 1 wt% to 3 wt% is ascribed to the presence of NiO and CaO as active species. Besides, the enhancement on the basicity of catalyst is attributed to the formation of Lewis basic sites on CaO surface upon the impregnation of Ni dopant to CaO. A maximum basicity of 2957.16087 $\mu mol\ CO_2/g$ is attained by 3 wt% Ni doped CaO, where it is deduced that the number of Lewis basic sites is increased with the increase in Ni concentration up to 3 wt% as evident from the increase in basicity. The basicity of Ni doped CaO is reduced abruptly by 48.46 % with an increase of Ni loading from 3 wt% to 5 wt%, where it desorbs a relatively lower amount of adsorbed CO_2. It implies that the increase in Ni loading on CaO surface tends to obstruct the adsorption of CO_2 on the active sites. Hence, it is known that a further increase in Ni amount incorporated does not improve the basicity of catalyst to any further extent. Furthermore, it is also inferred that the CaO species are reduced due to overloading of Ni on CaO surface, where the excess Ni remains as residual bulk phase on composite, leading to a reduced synergetic interaction between the metallic ions of CaO and NiO. Since the dominant species are only associated with Ni, the total basicity of catalyst is decreased due to a reduction in the number of basic sites, leading to a decline in catalytic activity towards transesterification.

Since Ni is supported on CaO, it is evenly dispersed on CaO surface as long as the Ni content is lower than a threshold with mono-molecular layer. The Ni dopant will eventually cover the active sites of catalyst upon the impregnation of Ni above the threshold value, which in turn causes the catalytic activity to reduce. In this case, it is further inferred that 3 wt% is the threshold value of Ni loading with high catalytic performance towards transesterification.

The TPD profiles of all the synthesised catalysts are combined for comparison as illustrated in Figure 4.13.
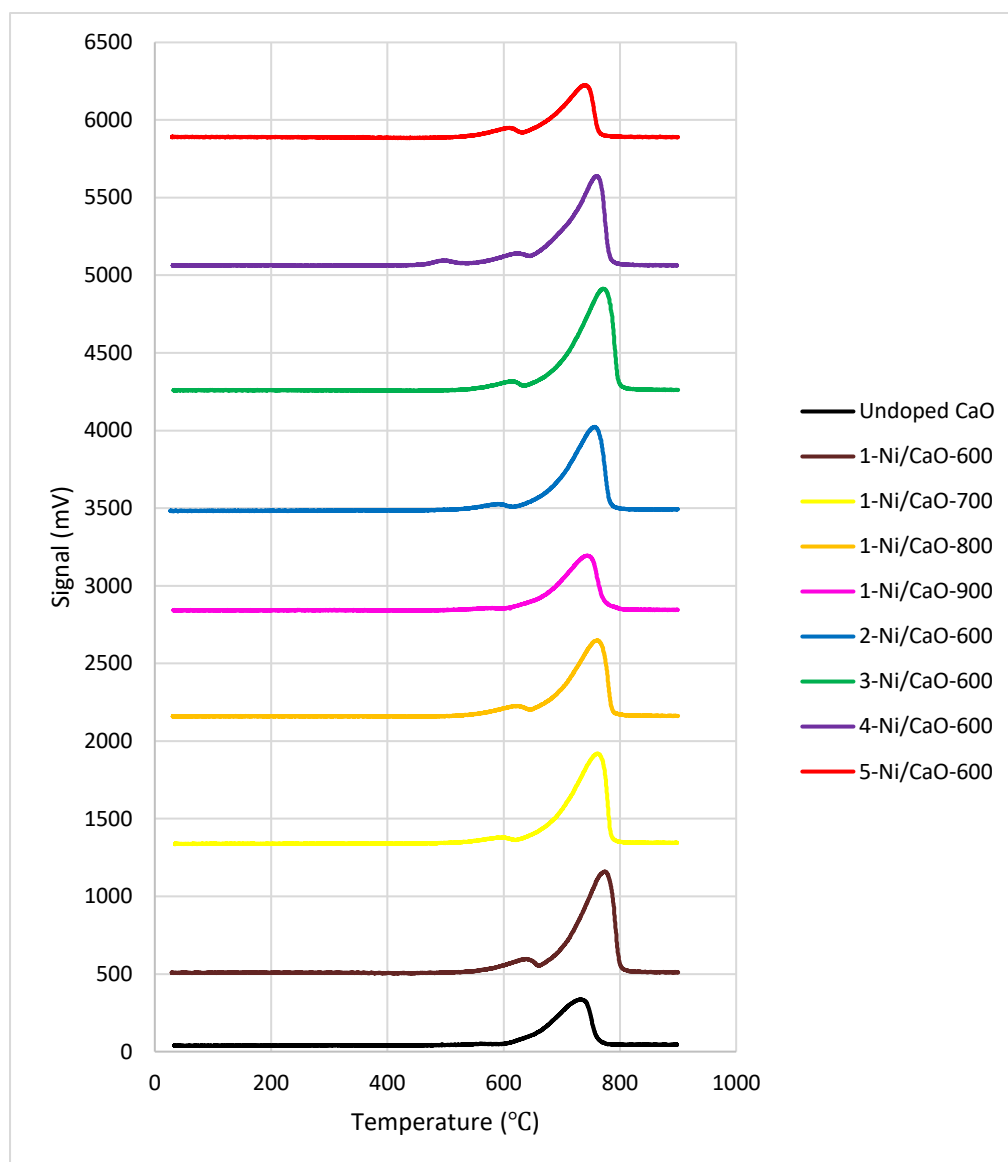
Figure 4.13: Comparison of TPD Profiles of Synthesised Catalysts.

It is found that 3-Ni/CaO-600 renders the maximum basicity with the highest number of basic sites among the synthesised catalysts, where 2957.16087 $\mu mol/g$ of CO_2 is being adsorbed on catalyst surface, followed by 1-Ni/CaO-600 with a total basicity of 2561.33291 $\mu mol\ CO_2/g$. The TPD result is consistent with the research done by Kumar, Abida and Ali (2016), where both 1 wt% and 3 wt% Ni doped CaO recalcined at 650 ℃ possess the highest basicity of 12.4 mmol/g among all the synthesised catalysts. Both 3-Ni/CaO-

600 and 1-Ni/CaO-600 constitute a maximum CO_2 adsorption, which is indicated by the desorption peak at 771 ℃ and 774 ℃ respectively. Moreover, by referring to Figure 4.13, both the aforementioned catalysts possess the most intense CO_2 desorption peaks as compared to other synthesised catalysts, implying the high availability of strong basic sites on catalyst surface for CO_2 adsorption. Thus, both 3-Ni/CaO-600 and 1-Ni/CaO-600 catalysts are expected to exhibit an enhanced catalytic activity for biodiesel production.

On the other hand, the undoped CaO exhibits the lowest basicity with the least number of basic sites, where only 1599.53140 $\mu mol/g$ of CO_2 is being adsorbed on catalyst surface. Besides, the undoped CaO exhibits the least intense CO_2 desorption peak at 730 ℃ among all the synthesised catalysts, where it is inferred that the undoped CaO accounts for the least catalytic performance towards transesterification. Meanwhile, these TPD results are further assured by the biodiesel yield acquired from the transesterification catalysed by both 3-Ni/CaO-600 and 1-Ni/CaO-600 catalysts are higher than undoped CaO catalyst.

Hence, by evaluating and analysing all the TPD results acquired, it can be concluded that the doped catalysts are highly basic in nature as compared to the parent catalyst, but the basicity tends to reduce at higher calcination temperature and dopant loading. Based on the intense desorption band emerged in the TPD profile, the optimum calcination temperature for synthesising Ni doped CaO catalyst is suggested to fall between 730 ℃ to 780 ℃ in order to enhance the rate of transesterification reaction for biodiesel production. It is further inferred that the strong basic sites occupy on the catalyst surface since all the synthesised catalysts exhibit intense CO_2 desorption peak.

The transesterification activity is dependent on the number of basic sites present on catalyst surface which is equivalent to the basicity. In other words, the basic sites on catalyst surface act as the active center for transesterification. The catalyst with a greater basicity is more favourable as the higher number of basic sites is suggested to be provided by a larger surface area. Since the surface area of CaO-based catalyst possesses a direct impact on its catalytic activity, the surface area which is sufficiently high will provide more accessible active sites, which in turn enhance the biodiesel yield. However, the doped CaO catalyst

does not solely depend on the basicity in determining its catalytic performance, as evident from the lower biodiesel yield produced for 3-Ni/CaO-600 as compared to 1-Ni/CaO-600 despite the fact that the former catalyst possesses a higher basicity.

According to Lee, et al. (2014), basicity plays a key role in determining the activity of catalyst, but the other possible factors such as surface area, crystallite size and pore size of catalyst should not be neglected. It is proved by Kumar, Abida and Ali (2016) that although the total basicity of 0.5 wt% Ni doped CaO catalyst is increased from 9.9 mmol/g to 12.3 mmol/g by increasing the calcination temperature from 650 ℃ to 950 ℃, the biodiesel yield achieved in the transesterification reaction catalysed by Ni doped CaO is found to decrease from 99 % to less than 90 %. Thus, it is inferred that the catalytic activity depends on the surface area of catalyst instead of basicity as 0.5-Ni/CaO-950 possesses a lower surface area of 3.9 m^2/g as compared to 0.5-Ni/CaO-650 with the surface area of 14.7 m^2/g. The particle agglomeration is said to be taken place at a relatively higher calcination temperature, where the sintering of catalyst particles will eventually reduce the catalytic performance of Ni doped CaO catalyst for biodiesel production. In another research done by Abdullah, Wibowo and Zakaria (2011), the transesterification catalysed by heterogeneous catalyst with a surface area of 78 m^2/g has achieved 60.1 % of conversion, whereas the conversion is reduced to 45.6 % for heterogeneous catalyst with a lower surface area of 42 m^2/g even though both catalysts possess the same basicity.

4.2.5 Thermogravimetric Analysis (TGA)

The CaO catalyst derived from waste eggshells with the incorporation of Ni dopant via wet impregnation process is analysed using TGA. It is carried out to determine the thermal stability of catalyst by identifying the temperature at which it starts to decompose. Only one of the synthesised catalysts, 1-Ni/CaO-600 is analysed due to the limited number of slots available for FYP. The TGA thermogram for 1 wt% Ni doped CaO recalcined at 600 ℃ is illustrated in Figure 4.14.
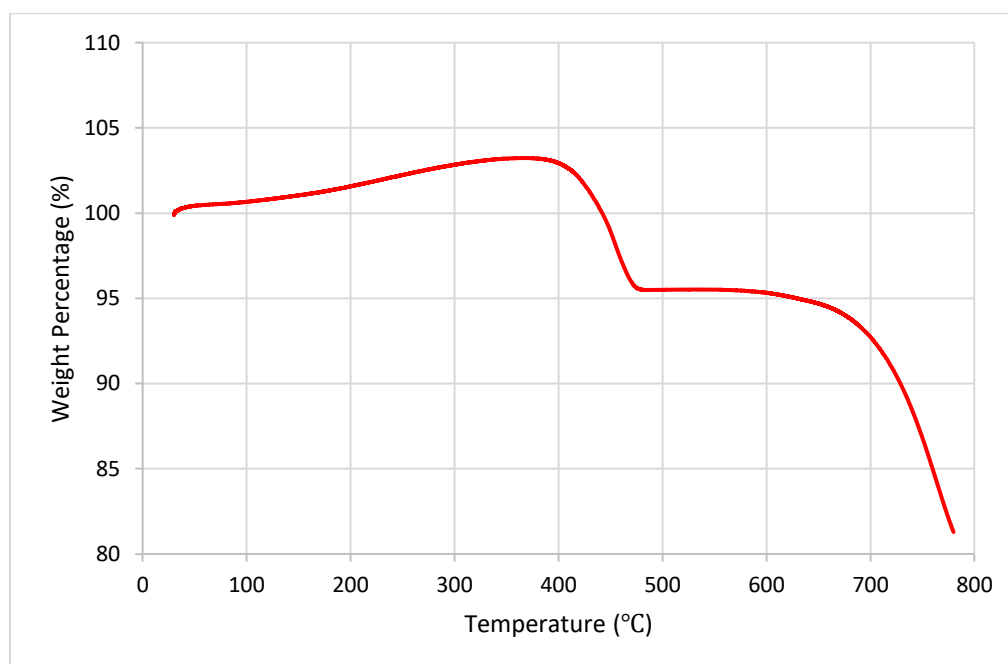
Figure 4.14: TGA Thermogram of 1-Ni/CaO-600.

Initially, the catalyst possesses a slight degradation with a total weight loss of about 7.26 wt% at the temperature ranging from 370 ℃ to 470 ℃, implying that all $Ca(OH)_2$ are thermally decomposed into CaO and H_2O, as stated by Krishnamurthy, Sridhara and Ananda-Kumar (2019). From the minor degradation peak, it can be inferred that the presence of $Ca(OH)_2$ is mainly attributed to the partial thermal decomposition of $Ca(OH)_2$ into CaO during calcination process. $Ca(OH)_2$ is most likely formed during wet impregnation process, where H_2O is used as the reaction medium and tends to react with CaO. Furthermore, it is also deduced that H_2O is chemisorbed on CaO surface upon

the exposure of catalyst to the moisture in the atmosphere during catalyst synthesis, cooling process after calcination and storage of catalyst.

Besides, there is a significant weight loss of approximately 14.23 wt% from 530 ℃ to 780 ℃, which indicates the removal of CO_2 during the thermal decomposition of $CaCO_3$ to CaO, as evident from the major degradation peak in TGA curve. The substantial weight reduction symbolises that the decomposition is completed at 780 ℃ by releasing CO_2 simultaneously, as claimed by Rahman, et al. (2019). The partial decomposition of $CaCO_3$ into CaO during calcination process is the main reason behind the presence of $CaCO_3$ with a relatively larger amount as compared to $Ca(OH)_2$ due to the fact that the calcination temperature of 600 ℃ is not sufficiently high to decompose all the carbonates into oxides completely. Meanwhile, it is inferred that the physisorption of atmospheric CO_2 on CaO surface when in contact with the atmosphere during catalyst synthesis tends to form small crystallites of $CaCO_3$.

By referring to Risso, et al. (2018), the CaO-based catalyst can be partially or rapidly deactivated by the moisture and CO_2 present in the air. Hence, it is suggested that the calcination temperature of 780 ℃ is feasible in synthesising Ni doped CaO catalyst using wet impregnation method with complete decomposition of $CaCO_3$ into CaO. It is further supported by the TGA findings done by Abdelhady, et al. (2020), where the catalyst should be calcined at a temperature above 700 ℃ in order to transform $CaCO_3$ in waste shells to CaO. The TGA result acquired in this research is in good agreement with TPD result, where CO_2 starts to desorb from catalyst surface at 774 ℃. Both the TGA and TPD findings are summarised in Table 4.28.

Table 4.28: Comparison of TGA and TPD Results.

Analysis Technique	Component Analysed	Analysis Result
TGA	Decomposition Temperature of $CaCO_3$	780 ℃
TPD	Desorption Temperature of CO_2	774 ℃

4.3   Parameter Studies on Transesterification Reaction Catalysed by Undoped and Doped CaO Nanocatalysts

The catalytic performance of both neat CaO and doped CaO catalysts are tested in the transesterification of cooking oil with methanol to produce biodiesel, where the catalysts are synthesised by means of two experimental designs:

(i)   Different calcination temperature at constant dopant dosage.

(ii)   Different dopant dosage at constant calcination temperature.

After the transesterification which is carried out at 60 ℃ for 3 hours, the concentration of FAMEs present in the biodiesel at every hour are analysed using GC, where the main FAMEs produced are methyl palmitate, methyl stearate, methyl oleate and methyl linoleate. The biodiesel yield obtained from transesterification reaction catalysed by undoped CaO, treated CaO and doped CaO catalysts at varying Ni loadings are tabulated in Table 4.29. The effects of two parameters related to catalytic activity, which include the dopant loading and calcination temperature on the biodiesel yield are investigated in order to determine the optimum conditions for transesterification reaction.

Table 4.29: Biodiesel Yield Obtained from Transesterification Reaction Catalysed by Various Types of Catalysts.

Catalyst	Biodiesel Yield (%)		
	1st Hour	2nd Hour	3rd Hour
Undoped CaO	63.77	68.13	72.14
Treated CaO	71.83	76.92	87.79
1-Ni/CaO-600	72.34	85.96	94.19
1-Ni/CaO-700	63.87	85.62	92.84
1-Ni/CaO-800	62.76	76.51	73.24
1-Ni/CaO-900	67.62	69.21	60.63
2-Ni/CaO-600	65.44	81.43	92.49
3-Ni/CaO-600	65.10	77.17	67.87
4-Ni/CaO-600	68.55	72.50	77.73
5-Ni/CaO-600	78.15	79.36	72.20

The biodiesel yield produced as a function of reaction time for all the synthesised catalysts are illustrated in Figure 4.15.
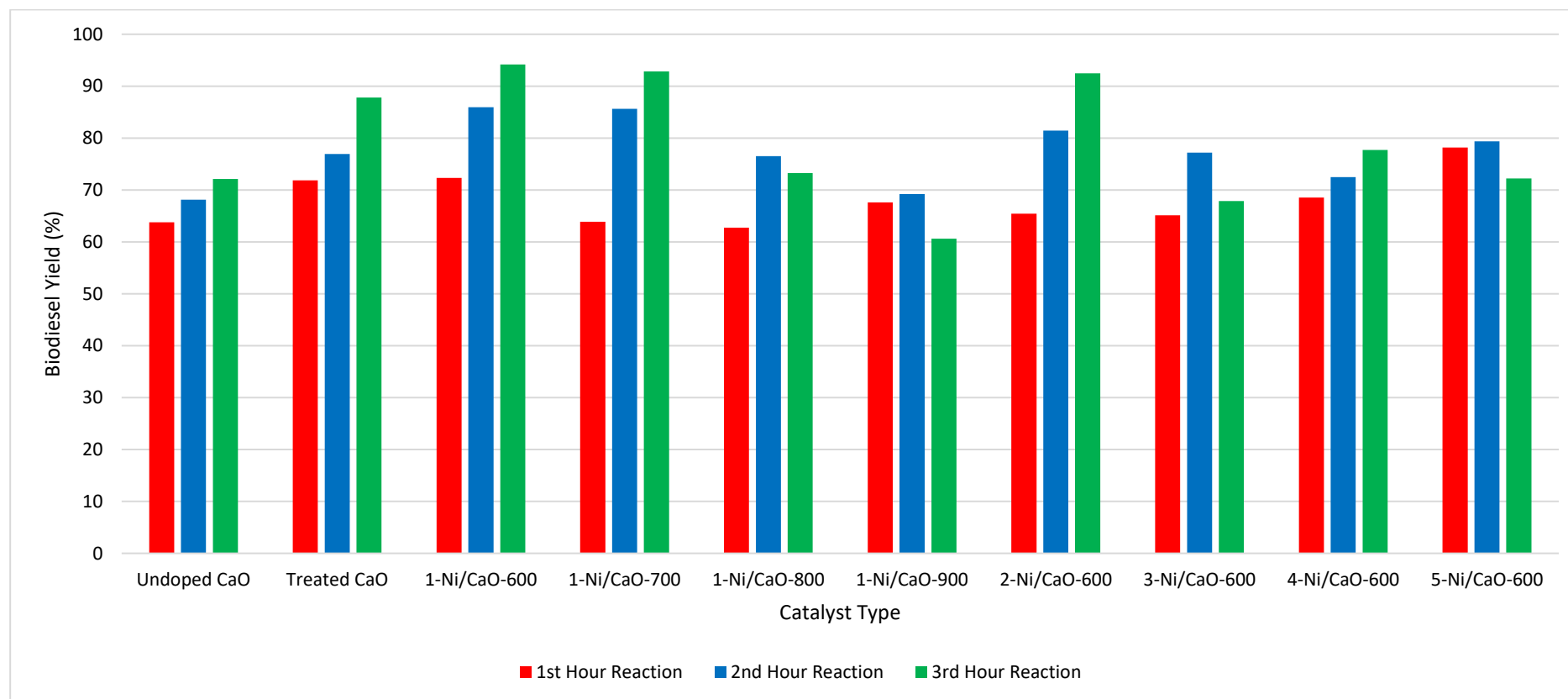
Figure 4.15: Biodiesel Yield Obtained Using Different Types of Catalysts.

According to Mathiyazhagan and Ganapathi (2011), the transesterification reaction is slow at the beginning owing to the mixing and dispersion of methanol and cooking oil, as evident from the biodiesel yield which falls below 80 % during the first hour of reaction for every synthesised catalyst. The biodiesel yield produced by undoped CaO is generally lower than Ni doped CaO, where the highest biodiesel yield that can be achieved by CaO with no impregnation of Ni dopant is 72.14 % after three hours of reaction. Both the pure CaO and hydration-dehydration treated CaO exhibit a steady increase in biodiesel yield with reaction time, where the treated CaO attains a relatively higher biodiesel yield of 87.79 % than pure CaO after the third hour of reaction.

In terms of dopant loading, most of the Ni doped CaO possess a better catalytic performance as compared to neat CaO, except for 3 wt% Ni doped CaO whereby it achieves a comparatively lower biodiesel yield than undoped CaO at the third hour of reaction. The biodiesel yield produced by 1-Ni/CaO-600, 2-Ni/CaO-600 and 4-Ni/CaO-600 show an increasing trend with reaction time, with the highest biodiesel yield achieved after three hours of reaction, which are 94.19 %, 92.49 % and 77.73 % respectively. As for 3-Ni/CaO-600 and 5-Ni/CaO-600, the biodiesel yield drops dramatically after the second hour of reaction, which is mostly attributed to the soap formation in view of the prolonged transesterification reaction. The speculation is further supported by Daniyan, et al. (2015) that about two hours of reaction is sufficient to drive the base-catalysed transesterification towards completion with an optimum conversion of palm oil to biodiesel, which is 80 %. It is then followed by a notable decline in biodiesel yield at the third hour of reaction with the formation of soap and gel, and thus obstructing the separation of ester layer. Hence, it is inferred that the equilibrium is achieved after two hours of reaction beyond which it results in a reduced biodiesel yield.

In terms of calcination temperature, the catalytic performance of Ni doped CaO is relatively better than pure CaO, except for Ni doped CaO recalcined at 800 ℃ and 900 ℃. Both 1-Ni/CaO-800 and 1-Ni/CaO-900 achieve a comparatively lower biodiesel yield as compared to undoped CaO during the first hour and third hour of reaction respectively. The biodiesel yield produced by both 1-Ni/CaO-600 and 1-Ni/CaO-700 increases steadily with reaction time,

resulting in the highest biodiesel yield after three hours of reaction, which are 94.19 % and 92.84 % respectively. On the other hand, 1-Ni/CaO-800 and 1-Ni/CaO-900 are the catalysts that exhibit a relatively poorer catalytic performance, where both the aforementioned catalysts encounter an abrupt decline in the biodiesel yield after the second hour of reaction. It is claimed that the biodiesel yield decreases with reaction time after the equilibrium is attained, where it is most probably due to saponification when the transesterification reaction is carried out for a longer time. Besides, a prolonged reaction might give rise to the backward reaction as transesterification is reversible in nature, which eventually causes the glycerol and biodiesel to recombine, resulting in loss of esters (Mathiyazhagan and Ganapathi, 2011). In short, the presence of reversible reaction alongside side reaction tend to cause the decline of biodiesel yield upon reaching the equilibrium after two hours of reaction. Still, the transesterification catalysed by most of the Ni doped CaO is deduced to achieve the equilibrium conversion after three hours of reaction.

In overall, 2-Ni/CaO-600 and 1-Ni/CaO-700 show the best catalytic performance due to the remarkable increase in biodiesel yield from the first hour to the third hour of reaction, where the biodiesel yield is increased from 65.44 % to 92.49 % for 2-Ni/CaO-600, while 1-Ni/CaO-700 possesses an increase in biodiesel yield from 63.87 % to 92.84 %. However, among all the synthesised catalysts, 1-Ni/CaO-600 exhibits the highest reaction rate in biodiesel production with the increment in biodiesel yield from 72.34 % during the first hour of reaction to 85.96 % during the second hour of reaction, which eventually results in the highest biodiesel yield of 94.19 % after the third hour of reaction. Thus, 1-Ni/CaO-600 is suitable to be used in biodiesel production for long term as it is able to achieve a relatively higher biodiesel yield within a short period of time, besides maintaining a stable catalytic performance throughout the 3-hour transesterification reaction as compared to other doped catalysts.

4.3.1 Effect of Hydration-Dehydration Treatment on Biodiesel Yield

Figure 4.16 illustrates the biodiesel yield produced at every hour of reaction with a total duration of three hours for both the pure CaO and treated CaO catalysts.

Figure 4.16: Comparison between Neat CaO and Treated CaO on Biodiesel Yield.

The pure CaO possesses a linear increase in biodiesel yield over the reaction of three hours, accounting for a total increment of 8.37 %. After undergoing hydration-dehydration treatment, the biodiesel yield achieved by CaO are notably improved with reaction time, resulting in a total increment of 15.96 %. Besides, the treated CaO also exhibits a relatively higher reaction rate as compared to neat CaO especially after the second hour of reaction, which in turn gives rise to the highest biodiesel yield of 87.79 % at the third hour of reaction. The results obtained can be further confirmed and verified by Roschat, et al. (2018), where the hydration-dehydration treated CaO is able to produce more than 96 % of biodiesel after one hour. Compared to hydration-dehydration treated CaO, the transesterification reaction catalysed by waste shell-derived CaO results in a biodiesel yield which is lower than 68 % after two hours of reaction when both the CaO catalysts are operated under the same reaction conditions. It is revealed that the treated CaO shows a better catalytic activity than pure CaO derived from natural $CaCO_3$ sources as the treated CaO catalyst

consists of small particles with a higher porosity and surface area, which correspond to the higher amount of basic sites as compared to the pure CaO catalyst. Hence, the hydration-dehydration treatment is proved to be one of the favourable methods to enhance the catalytic properties and activity of CaO for biodiesel production.

By referring to Yoosuk, et al. (2010), the highly active CaO is generated after the reconstruction of decomposed calcite by hydrating the catalyst, followed by subsequent calcination. The carbonates are first decomposed during the first calcination prior to the hydration of CaO formed, and thus creating Brønsted base sites. The second calcination is carried out on the hydrated CaO with Brønsted base sites, where it shows a higher catalytic activity in transesterification reaction as compared to the decomposed calcite after first calcination. Besides, the aforementioned activity results are consistent with the order of basicity, in which the treated CaO possesses a greater number of strong basic sites than the pre-treated CaO. The finding correlates to the TPD results, where the basicity of treated CaO is 535.4 $\mu mol\ CO_2/g$ higher than that of pure CaO, implying that the treated CaO after the calcination of 600 ℃ has a higher number of basic sites as compared to the CaO derived from natural carbonates after the calcination of 900 ℃.

Hence, it is affirmed that the activity of CaO in the transesterification is strongly dependent on its basicity as the catalytic activity of hydration-dehydration treated CaO is mainly enhanced due to high amount of basic sites. Besides possessing a high number of basic sites for transesterification reaction, it is also inferred that the hydration-dehydration of calcined calcite is feasible to generate the CaO with excellent physicochemical properties.

4.3.2   Effect of Dopant Loading on Biodiesel Yield

Figure 4.17 illustrates the biodiesel yield produced at every hour of reaction with a total duration of three hours, in which the reaction is catalysed by the neat CaO and doped CaO catalysts recalcined at 600 ℃ with Ni loadings varying from 1 wt% to 5 wt%.
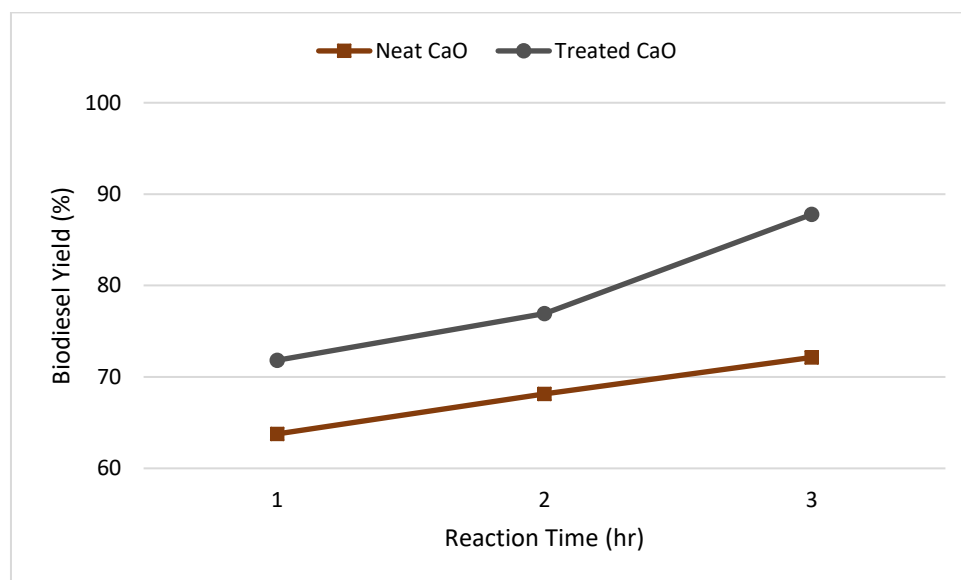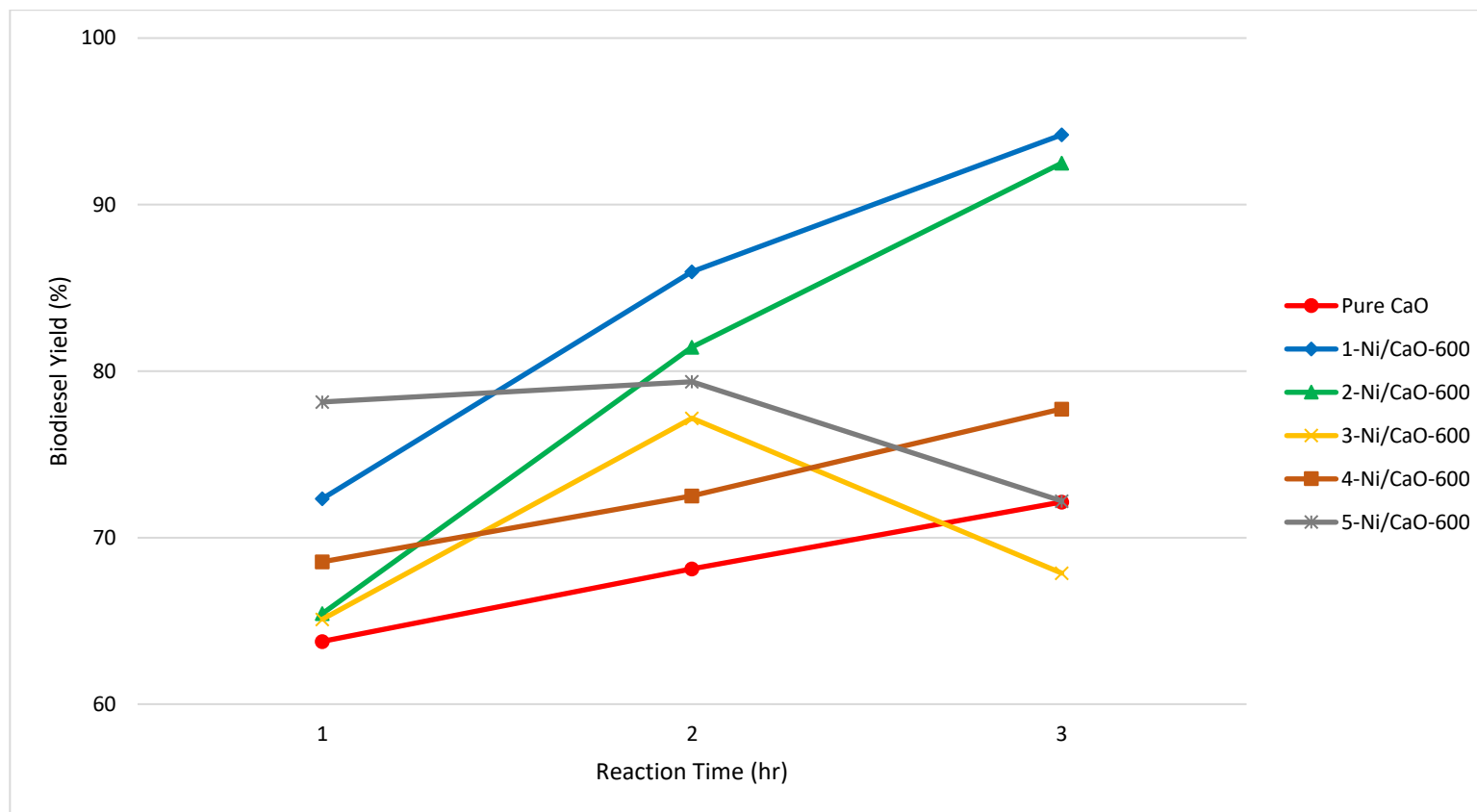
Figure 4.17: Comparison between Neat CaO and 1-5 wt% Ni/CaO Calcined at 600 ℃ on Biodiesel Yield.

The pure CaO is found to exhibit poor activity towards transesterification, which is denoted by a relatively low basicity of 1599.53140 $\mu mol\ CO_2/g$ according to TPD result. It is supported by Kaur and Ali (2014), where the biodiesel yield obtained from the transesterification catalysed by pure CaO shows a significant decline despite of the fact that it possesses basic sites on its surface in the form of oxygen anions, which is most probably due to a lower basic strength possessed by the active sites. Hence, the neat CaO is impregnated with various concentration of Ni dopant in order to increase the basicity, which in turn enhances the catalytic activity in terms of biodiesel yield.

The catalytic performance of CaO is suggested to be improved with the impregnation of Ni dopant as it is observed that the biodiesel yield produced by employing doped CaO catalysts are mostly higher than neat CaO. During the first hour of reaction, the neat CaO possesses the lowest biodiesel yield of 63.77 % as compared to the doped CaO, while the highest biodiesel yield of 78.15 % is attained by 5-Ni/CaO-600. The biodiesel yield increases steadily over the reaction time for neat CaO, 1-Ni/CaO-600, 2-Ni/CaO-600 and 4-Ni/CaO-600. 1-Ni/CaO-600 and 2-Ni/CaO-600 show a relatively higher production rate in biodiesel, with 8.23 % and 11.06 % respectively as observed from second hour to third hour of reaction.

On the other hand, the biodiesel yield achieved for 5-Ni/CaO-600 is slightly increased by 1.21 % at the first hour of reaction, followed by a notable decline of 7.16 % at the second hour of reaction despite of the fact that it shows the highest biodiesel yield initially. For 3-Ni/CaO-600, it shows a higher rate of increase in biodiesel yield than 5-Ni/CaO-600 at the first hour of reaction, which is 12.07 %, before encountering a significant reduction of 9.3 % at the second hour of reaction. Eventually after three hours of reaction, 3-Ni/CaO-600 achieves the lowest biodiesel yield of 67.87 % among all the synthesised catalysts. Meanwhile, 1-Ni/CaO-600 constitutes the highest biodiesel yield, with 85.96 % and 94.19 % achieved at the second hour and third hour of reaction respectively.

Both 1-Ni/CaO-600 and 2-Ni/CaO-600 exhibit an excellent catalytic performance in the transesterification, as evident from the biodiesel yield achieved. Meanwhile, 2-Ni/CaO-600 shows the best overall catalytic activity

among other synthesised catalysts as it accounts for the largest increase in biodiesel yield of 27.05 % from the first hour to the third hour of reaction. Nevertheless, 1-Ni/CaO-600 is suitable to be used in biodiesel production for long term as it is able to achieve a high biodiesel yield within two hours under mild operating conditions. Thus, it is inferred that the catalytic activity of CaO is enhanced by incorporating the Ni dopant up to 2 wt%, as evident from the higher biodiesel yield produced. A further increase in the Ni loading beyond 2 wt% does not improve the biodiesel yield, in which a prominent decrease in biodiesel yield is observed. In other words, the enhancement in catalytic performance of CaO is limited by the amount of Ni dopant impregnated. It is revealed that undoped CaO and 3-Ni/CaO-600 exhibit the lower catalytic performance in the transesterification, which is supported by a relatively lower biodiesel yield achieved.

The remarkable decline in biodiesel yield after the second hour of reaction observed in 3-Ni/CaO-600 and 5-Ni/CaO-600 can be explained by Le Chatelier's principle due to the reversibility of transesterification reaction. According to Le Chatelier's principle, if a dynamic equilibrium is disturbed by the change in environment, the position of equilibrium will move to counteract the change. Since the concentration of reactants (cooking oil and methanol) decrease, while the concentration of products (FAME and glycerol) increase with reaction time during transesterification, the product side with a relatively higher concentration tends to convert the product back to the reactant to offset the change before achieving dynamic equilibrium. The equilibrium position will keep on moving leftwards, where more products will be reacted to replace the reactants that have been removed. Hence, the concentration of biodiesel will be reduced due to backward reaction.

The effect of amount of Ni dopant impregnated to CaO on biodiesel yield is illustrated in Figure 4.18.
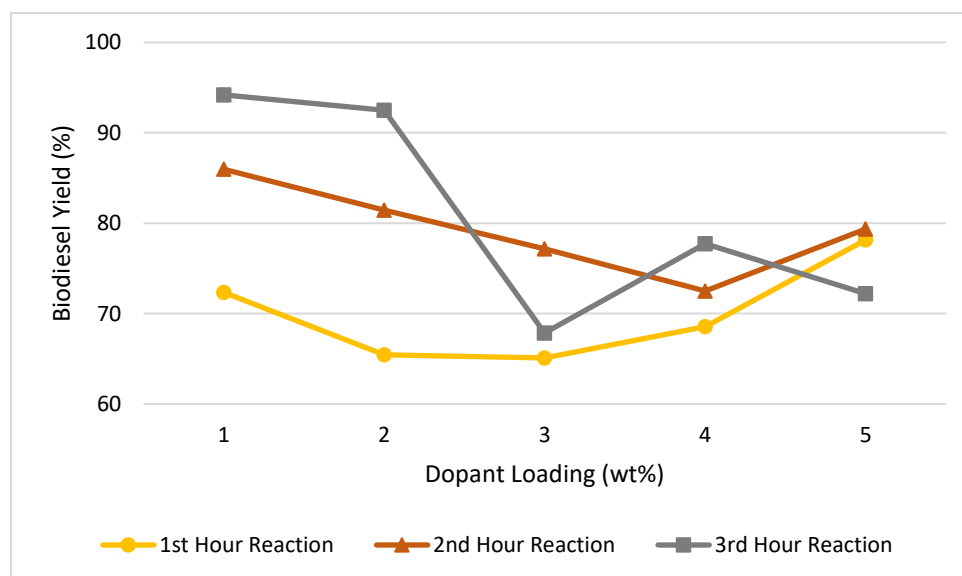
Figure 4.18: Effect of Dopant Loading on Biodiesel Yield.

At the first hour of reaction, the biodiesel yield decreases gradually by 6.9 % when the amount of Ni impregnated to CaO is increased from 1 wt% to 2 wt%, which is followed by an insignificant reduction of 0.34 % by increasing the Ni loading from 2 wt% to 3 wt%. By further increasing the Ni dosage from 3 wt% to 5 wt%, the biodiesel yield increases steadily by 13.05 % with a maximum biodiesel yield of 78.15 % attained at 5 wt% of Ni loading. As for the second hour of reaction, the doped catalyst exhibits a linear decrease in the biodiesel yield from 85.96 % to 72.5 % by increasing the Ni loading from 1 wt% to 4 wt%. A subsequent increase in the biodiesel yield of 6.86 % is observed with the increase in the amount of Ni dopant impregnated from 4 wt% to 5 wt%. Meanwhile, the doped catalyst possesses an unstable change in biodiesel yield at the third hour of reaction, where it shows a slight reduction in biodiesel yield of 1.7 % with the increase of Ni loading up to 2 wt%. An abrupt decline in the biodiesel yield of 24.62 % is noticed with the increase of Ni amount from 2 wt% to 3 wt%. The biodiesel yield is then increased prominently by 9.86 % upon increasing the Ni loading to 4 wt%, before possessing a gradual decrease of 5.53 % with a subsequent increase in the amount of Ni dopant impregnated to 5 wt%.

The performance of Ni doped eggshell-derived CaO with different Ni loadings are evaluated in which the highest biodiesel yield is achieved with 1 wt% of Ni loading, where 72.34 %, 85.96 % and 94.19 % are achieved at the first hour, second hour and third hour of reaction time respectively. According to Boro, Konwar and Deka (2014), the initial increase in biodiesel yield is most probably owing to the incorporation of Ni^{2+} ions into the CaO framework, which in turn improves the basicity of neat CaO, as evident from a higher basicity acquired for 1 wt% Ni doped CaO than undoped CaO, which are 2561.33291 $\mu mol\ CO_2/g$ and 1599.53140 $\mu mol\ CO_2/g$ respectively. By referring to Kumar and Ali (2013), the catalytic activity is enhanced with a higher basicity as the basic sites of CaO-based catalyst serve as the active center for transesterification reaction. Besides, the effects arisen from the formation of CaO, NiO and $CaNi_4O_8$ phases in the crystal lattice of CaO upon the doping of Ni lead to a higher catalytic activity towards transesterification. It is further supported by Boro, et al. (2014) that the increase in biodiesel yield with the impregnation of Ni dopant is most probably ascribed to the presence of CaO and NiO which act as active species during the reaction.

However, the activity of Ni doped CaO starts to drop slightly when the Ni loading is increased up to 2 wt%, where a subsequent increase in the amount of Ni dopant impregnated can no longer improve the biodiesel yield. It is inferred that the overloading of Ni on CaO surface is the possible reason for the decline in biodiesel yield, where the excess Ni loading is most likely to cover the basic sites on catalyst surface, which eventually impedes the interaction of catalyst with reactants (Boro, et al., 2014). According to Borah, et al. (2019), the structural distortion of parent catalyst becomes apparent due to excess Ni loading, which in turn results in a relatively lower surface. Besides, it is also inferred that the Ni-Ca compound does not actively involve in the reaction, which in turn adversely affect the catalytic performance of catalyst in terms of biodiesel yield. It is further evinced by Nasar Mansir, et al. (2018) that the transesterification reaction is dependent on the number of basic sites present in the catalyst as well as their strength. The outcomes of CO_2-TPD analysis support the finding results whereby the biodiesel yield is reduced with the

increase in Ni loading from 2 wt% to 5 wt% due to the decrement in total basicity of 1201.31543 $\mu mol\ CO_2/g$.

It can be deduced that an appropriate Ni loading on CaO is one of the key factors that enhances the activity of catalyst in transesterification. Hence, it is optimal to incorporate the Ni dopant varying from 1 wt% to 2 wt% to CaO catalyst in order to augment the Lewis basic sites on catalyst surface for a better catalytic activity towards transesterification, beyond which it can neither improved the basicity nor activity of Ni doped CaO.

4.3.3 Effect of Calcination Temperature on Biodiesel Yield

Figure 4.19 illustrates the biodiesel yield produced at every hour of reaction with a total duration of three hours, in which the reaction is catalysed by the neat CaO and 1 wt% Ni doped CaO catalysts recalcined at the temperature varying from 600 ℃ to 900 ℃.
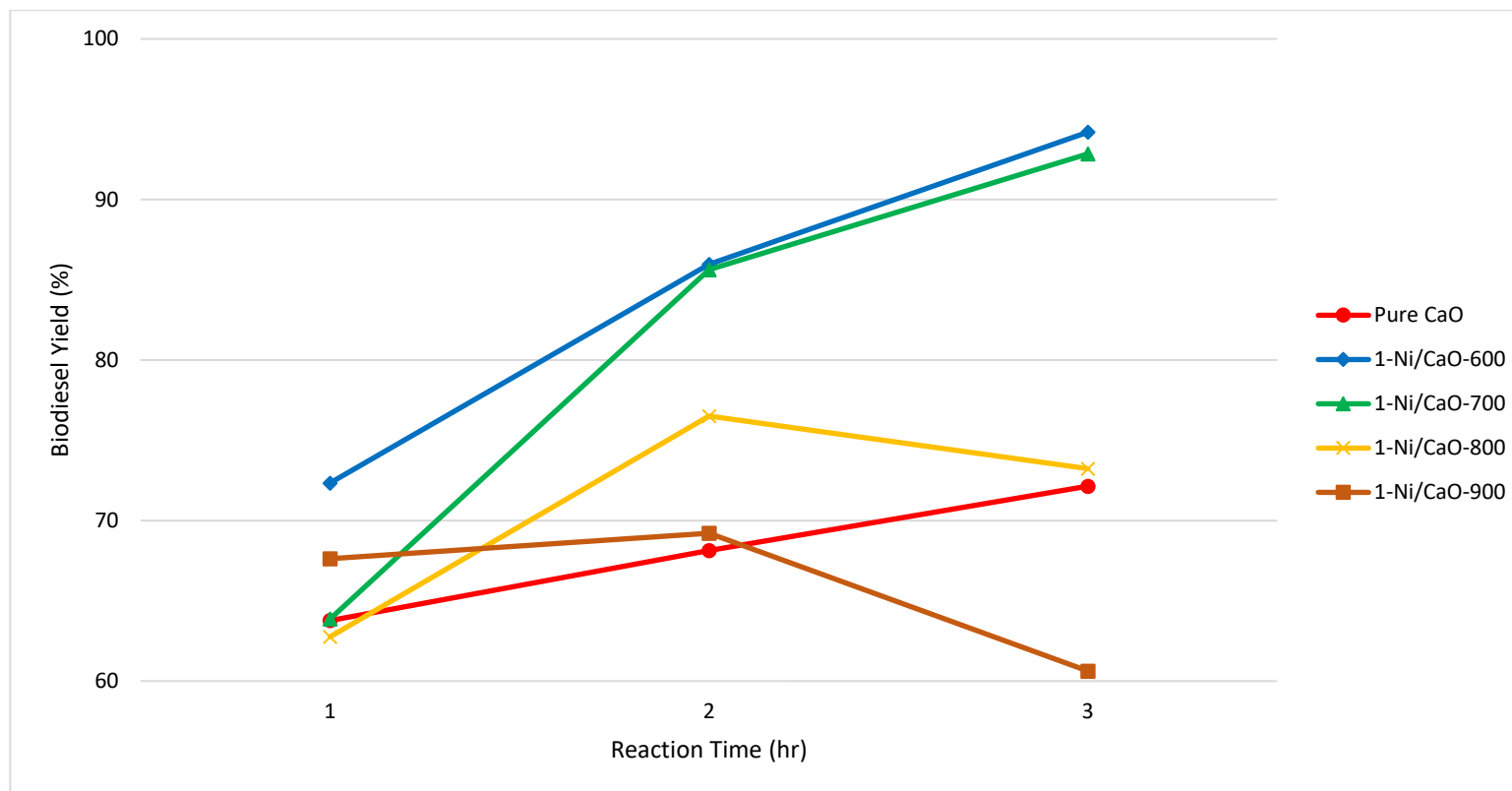
Figure 4.19: Comparison between Neat CaO and 1 wt% Ni/CaO Calcined at 600-900 ℃ on Biodiesel Yield.

The biodiesel yield obtained from the transesterification catalysed by neat CaO increases linearly with the reaction time. Nevertheless, the pure CaO possesses a relatively lower biodiesel yield as compared to doped CaO catalysts, implying the enhanced catalytic performance of CaO upon the incorporation of Ni dopant, except for 1-Ni/CaO-900 where the biodiesel yield achieved by undoped CaO is significantly higher. The biodiesel yield increases steadily over the reaction of 3 hours for 1-Ni/CaO-600, where the biodiesel yield achieved is the highest among the synthesised catalysts. Meanwhile, 1-Ni/CaO-700 shows a significant increase in biodiesel yield from first hour to third hour of reaction even though the biodiesel yield achieved by 1-Ni/CaO-700 is relatively lower than 1-Ni/CaO-600 after three hours of reaction.

On the other hand, the biodiesel yield achieved by 1-Ni/CaO-800 is prominently increased by 13.75 % in spite of the fact that it constitutes the lowest biodiesel yield of 62.76 % among other synthesised catalysts at the first hour of reaction. For 1-Ni/CaO-900, it only possesses a slight increase in biodiesel yield of 1.59 % at the first hour of reaction, before encountering an abrupt decline of 8.58 % at the second hour of reaction, resulting in the lowest biodiesel yield of 60.63 % among the synthesised catalysts at the third hour of reaction.

Both 1-Ni/CaO-600 and 1-Ni/CaO-700 are revealed as the best catalysts which present the most outstanding catalytic performance. Both the aforementioned catalysts show a relatively higher biodiesel yield especially after the second hour of reaction. Still, 1-Ni/CaO-700 possesses the best overall catalytic activity among other synthesised catalysts, as evident from the largest increase in biodiesel yield of 28.97 % from the first hour to the third hour of reaction. Meanwhile, 1-Ni/CaO-600 is feasible to be used in biodiesel production for long term as it is able to achieve a high biodiesel yield within a short period of time under mild operating conditions. Hence, it is inferred that the calcination temperature ranging from 600 ℃ to 700 ℃ is optimal to enhance the catalytic activity of Ni doped CaO, where a subsequent increase in the calcination temperature beyond 700 ℃ leads to a remarkable decline in the biodiesel yield. In other words, the enhancement in catalytic performance of Ni doped CaO is restrained by the calcination temperature. On the other hand, the

undoped CaO and 1-Ni/CaO-900 possess the lower catalytic performance towards the transesterification as the biodiesel yield achieved by both catalysts are comparatively lower as compared to other synthesised catalysts.

There is a notable decrease in the biodiesel yield after the second hour of reaction for 1-Ni/CaO-800 and 1-Ni/CaO-900 on account of the reversibility of transesterification, as explained by Le Chatelier's principle. The reversible reaction tends to reduce the biodiesel yield, which is most probably attributed to the recombination of glycerol and FAMEs after prolonged reaction. Besides, the saponification is suggested to be taken place along with backward reaction, where the formation of soap will eventually increase the viscosity of reaction mixture, and thus affecting the rate of mass transfer for the reactants to bind with the active sites on catalyst surface.

The effect of calcination temperature on biodiesel yield is illustrated in Figure 4.20.
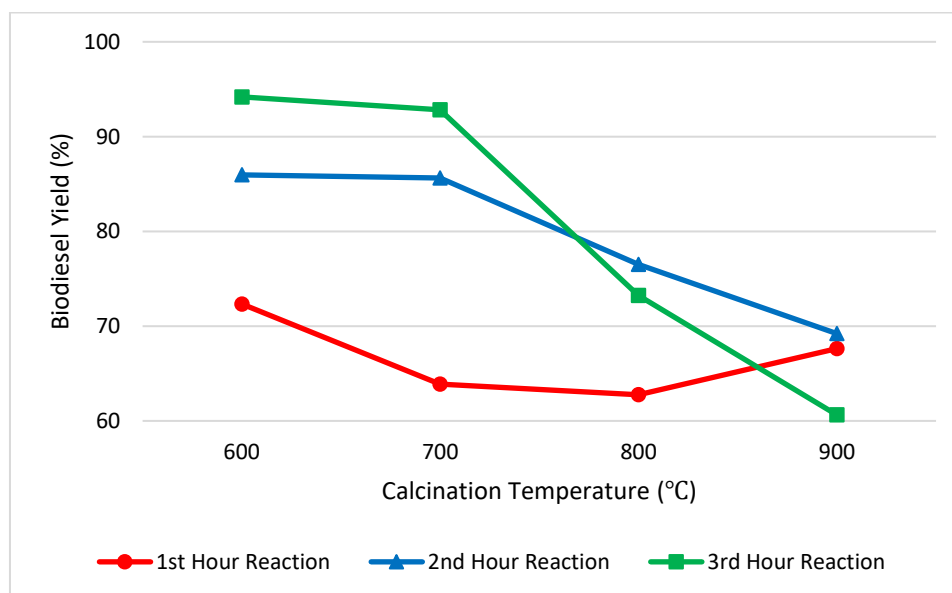
Figure 4.20: Effect of Calcination Temperature on Biodiesel Yield.

During the first hour of reaction, the biodiesel yield is reduced gradually by 8.47 % with the increase of calcination temperature from 600 ℃ to 700 ℃. A slight decline in the biodiesel yield of 1.11 % is observed upon the increment of calcination temperature from 700 ℃ to 800 ℃, followed by a stable increase of 4.86 % at the calcination temperature of 900 ℃. As for the second hour of

reaction, the doped catalyst possesses a mere decline in biodiesel yield of 0.34 % when the calcination temperature is increased from 600 ℃ to 700 ℃, beyond which it exhibits a linear decrease of 16.41%, resulting in the lowest biodiesel yield of 69.21 % at the calcination temperature of 900 ℃. Meanwhile during the third hour of reaction, the doped catalyst shows the similar decreasing trend as the second hour of reaction. A slight reduction in the biodiesel yield of 1.35 % is noticed with the increase of calcination temperature from 600 ℃ to 700 ℃, followed by an abrupt decline in biodiesel yield to a large extent, which is 32.21 % with a subsequent increase in calcination temperature from 700 ℃ to 900 ℃. Eventually, the remarkably higher rate of decline in biodiesel yield during the third hour of reaction has resulted in the lowest biodiesel yield of 60.63 % among all the synthesised catalysts.

The performance of Ni doped eggshell-derived CaO which are calcined at different temperatures are evaluated in which the highest biodiesel yield is achieved with the calcination temperature of 600 ℃, where 72.34 %, 85.96 % and 94.19 % are achieved at the first hour, second hour and third hour of reaction time respectively. By referring to Kaur and Ali (2014), the high biodiesel yield achieved at a high calcination temperature of 600 ℃ is mainly attributed to the formation of strong Lewis basic sites on catalyst surface as a result of the thermal decomposition of hydroxides into corresponding oxides during calcination process. According to Kumar and Ali (2013), the Brønsted base ($Ca(OH)_2$) is the dominant species at the calcination temperature below 550 ℃, while the Lewis base (CaO) becomes predominant in Ni doped CaO catalyst at 550 ℃ or above, where it is in line with the XRD results acquired. It is further reported that the Lewis basic sites exhibit a better activity towards transesterification reaction as they are more basic than the corresponding Brønsted basic sites. Besides, it is inferred that the calcination temperature of 600 ℃ is sufficiently high to promote a high surface area for Ni doped CaO, resulting in a high concentration of Lewis base on catalyst surface, which in turn improves the catalytic activity.

However, the activity of Ni doped CaO starts to drop slightly with the increase of calcination temperature up to 700 ℃, where a further increase in the calcination temperature can no longer enhance the catalytic performance, which

is denoted by either an undesired biodiesel yield attained after prolonged reaction or more time required to drive the reaction towards completion. The doped catalyst possesses a relatively lower activity towards transesterification as the basicity tends to reduce at a higher calcination temperature, as claimed by Kumar, Abida and Ali (2016). By referring to the TPD results obtained, the basicity of Ni doped CaO is reduced by 773.80588 $\mu mol\ CO_2/g$ upon increasing the calcination temperature from 600 ℃ up to 900 ℃, which is indicated by a reduced number of basic sites on catalyst surface. Furthermore, the doped catalyst also encounters a prominent decrease in surface area, which is predominantly attributed to the sintering of Ni/CaO particles, and thus causing the increase in particle size. The sintering effect becomes more significant especially at 900 ℃, which is further supported by the increase in crystallite size of 16.03 nm, as evident from the XRD results acquired. The surface area reduction due to immensely high calcination temperature is accompanied by the decrease of active sites on catalyst surface, which is in accordance with the impact due to the decline in basicity.

It can be inferred that the calcination temperature is the critical parameter in determining the catalytic performance of Ni doped CaO in transesterification. Thus, it is feasible to perform the calcination at the temperature ranging from 600 ℃ to 700 ℃ in order to ensure the presence of a substantial number of basic sites on the catalyst surface which are accessible for the reactants, beyond which it can no longer enhance the catalytic activity of Ni doped CaO.

4.3.4 Parameters Optimisation

The biodiesel yield produced as a function of reaction time for all types of CaO catalysts are illustrated in Figure 4.21.
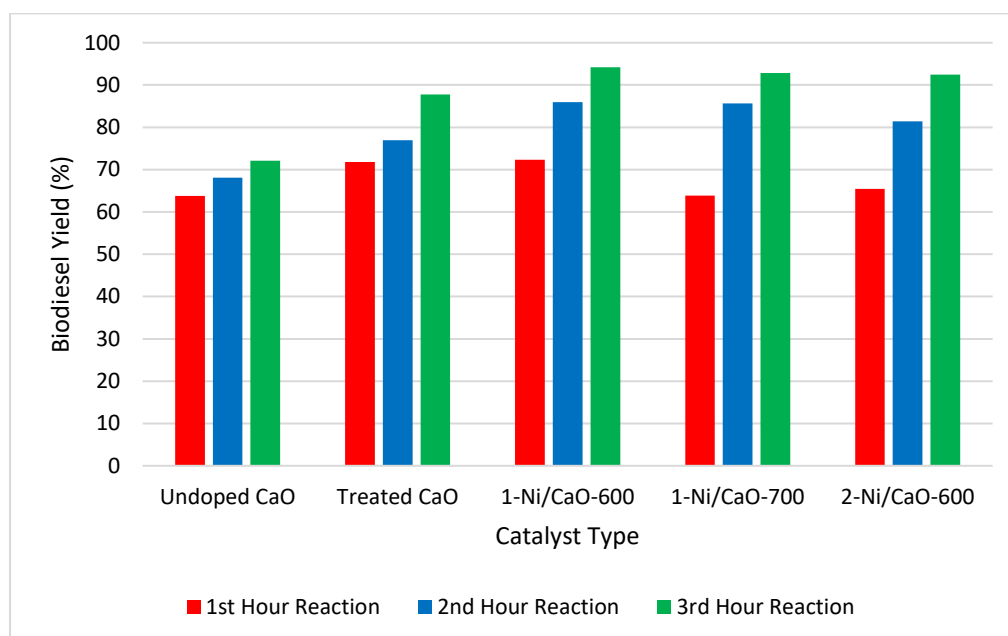
Figure 4.21: Comparison of Biodiesel Yield Achieved in Transesterification Reaction Catalysed by Undoped CaO, Treated CaO and Ni Doped CaO.

The catalytic performance of CaO in biodiesel production is significantly improved after undergoing the hydration-dehydration treatment, as evident from the researches done by Roschat, et al. (2018) and Yoosuk, et al. (2010). Besides, the impregnation of Ni dopant to CaO is imperative as the biodiesel yield produced by Ni doped CaO is relatively higher than pure CaO, implying an enhanced catalytic activity towards transesterification reaction. Yet, the catalytic performance of doped CaO is dependent on the amount of Ni dopant impregnated. The biodiesel yield increases with the Ni loading only up to certain extent before encountering a gradual decline beyond the optimum Ni loading, as reported by Boro, Konwar and Deka (2014) and Boro, et al. (2014). Moreover, the calcination temperature is also one of the parameters that affects the catalytic performance of Ni doped CaO. The Ni doped CaO exhibits an improved biodiesel yield with the initial increase of calcination temperature, where a further increase above optimum calcination temperature can no longer enhance the catalytic activity. Meanwhile, the elucidation is tally with the findings from the researches done by Kaur and Ali (2014) and Kumar, Abida and Ali (2016). In present study, 2 wt % Ni doped CaO and Ni doped CaO recalcined at 700 ℃ exhibit the best overall catalytic performance in terms of dopant loading and

calcination temperature respectively, as evident from the prominent increase in biodiesel yield over the three-hour transesterification reaction.

Although 2-Ni/CaO-600 and 1-Ni/CaO-700 possess the best overall catalytic performance, the biodiesel yield produced by the aforementioned catalysts at every hour of reaction time are not as high as 1-Ni/CaO-600, where the latter catalyst is reported to achieve the highest biodiesel yield after three hours of reaction. Besides, the catalytic activity of 1-Ni/CaO-600 is relatively better and more stable even at the first hour of reaction, where the biodiesel yield is maintained above 70 % after the first hour of reaction. In short, 1-Ni/CaO-600 is the most feasible catalyst to be used in biodiesel production for long term as it is able to attain a sufficiently high biodiesel yield within a short period of time under mild operating conditions. In other words, the optimum parameters of catalyst synthesis for transesterification reaction are summarised in Table 4.30.

Table 4.30: Optimum Parameters of Catalyst Synthesis for Biodiesel Production.

Parameter	Optimum Value
Dopant Loading	1 wt%
Calcination Temperature	600 ℃

Moreover, the catalytic performance of Ni doped CaO is also dependent on the doping methods. There are several ways to incorporate the metal dopant to CaO catalyst, which include wet impregnation, incipient wetness impregnation, sol-gel method and co-precipitation. Wet impregnation is chosen as the catalyst synthesis method in this research owing to the low cost incurred. Apart from this consideration, it is inferred that the catalytic performance of Ni doped CaO can be enhanced by other doping methods. Furthermore, the research is potential to be proceeded by investigating other catalyst synthesis parameters affecting the catalytic activity towards transesterification such as type of metal dopant incorporated to CaO and calcination duration as well as reaction parameters such as catalyst loading, methanol-to-oil molar ratio, reaction temperature and reaction duration in order to achieve a more promising biodiesel yield than the current synthesised catalysts.

CHAPTER 5

CONCLUSION AND RECOMMENDATION

5.1   Conclusion

The catalytic performance of waste eggshells-derived CaO doped with Ni via wet impregnation as well as the commercial reagents-derived CaO doped with NiO via sol-gel method are first investigated for preliminary study. The Ni doped CaO catalyst is ultimately selected because the use of waste eggshells as catalyst source for biodiesel production not only provides the environmentally benign and cost-effective way to recycle those wastes due to the fact that it can minimise various problems related to the disposal of those wastes, but also facilitates in lowering the biodiesel production cost to make biodiesel competitive with fossil-based diesel fuel. Moreover, Ni doped CaO has proved in producing a relatively higher biodiesel yield than NiO doped CaO. A series of Ni doped CaO are then prepared by varying the calcination temperature and Ni loading in CaO, where the synthesised catalysts are subsequently used to produce biodiesel from transesterification reaction. Both the undoped and doped CaO catalysts are characterised by employing XRD, SEM, EDX, CO_2-TPD and TGA, where it is inferred that the physicochemical properties of CaO catalyst have been improved by the impregnation of Ni dopant.

From XRD analysis, the high intensity peaks exhibited by the synthesised CaO catalysts at 2θ of 32.2°, 37.4°, 53.9°, 64.2° and 67.4° indicate the presence of highly crystalline CaO in cubic phase. The new diffraction peaks at 2θ of 37.8° and 43.2° for Ni doped CaO catalysts support the formation of $CaNi_4O_8$ and NiO phase respectively. The crystallite size of CaO catalysts is reduced after the impregnation of Ni dopant based on the calculation using Debye-Scherrer equation. SEM analysis reveals the alteration of morphology and surface feature of synthesised catalysts following the incorporation of Ni dopant to CaO catalyst, where it changes from a coral-shaped structure with larger particles to irregular-shaped structure with smaller particles. Meanwhile, EDX analysis shows that the synthesised CaO catalysts mainly comprise of calcium and oxygen, where the CaO compound is equivalent to the active sites

present in the catalyst. Upon the impregnation of Ni dopant, the active CaO species is reduced, as evident from the lower Ca and O content in doped CaO catalysts. On the other hand, the active Ni species is increased with the amount of dopant impregnated to CaO catalyst. Furthermore, CO_2-TPD analysis evinces that the impregnation of Ni dopant has enhanced the basicity of CaO catalyst, besides resulting in the formation of numerous strong basic sites. The reactivity of doped CaO catalysts towards transesterification is also improved in line with the increase of basicity, as confirmed by the biodiesel yield produced. Last but not least, TGA correlates the temperature at which $CaCO_3$ is completely decomposed into CaO alongside the release of CO_2 with the temperature at which CO_2 starts to desorb from CaO surface acquired from TPD analysis, where both the analysis results are used to determine the feasible calcination temperature in synthesising Ni doped CaO catalyst.

The activity of catalyst is found to be a function of basicity and crystallite size, which in turn depends on the concentration of Ni dopant and calcination temperature. The catalyst synthesised with 1 wt% Ni in CaO followed by calcination at 600 ℃ (1-Ni/CaO-600) is highly active owing to a relatively higher basicity as supported by TPD analysis, denoting a better catalytic activity towards methanolysis of cooking oil. Besides, it is also revealed as the best catalyst in terms of specific surface area due to the fact that it exists in the nanocrystalline form and possesses the smallest crystallite size among the synthesised catalysts as evident from XRD analysis, which in turn providing more access to the reactants for reaction to take place on the active sites. In addition, the formation of a relatively smaller aggregates on catalyst surface further demonstrates the presence of a higher surface area as apparent from SEM analysis, which eventually enhancing its catalytic performance in biodiesel production.

The catalytic performance of synthesised catalysts towards transesterification reaction is investigated, in which the Ni doped CaO shows a better catalytic activity as compared to undoped CaO in terms of biodiesel yield. The initial increase in both dopant loading and calcination temperature slightly reduce the biodiesel yield, and any further increase above optimum amount of dopant impregnated and calcination temperature can no longer improve the

catalytic performance in transesterification reaction. Under the optimum conditions of 1 wt% Ni dopant loading and 600 ℃ calcination temperature, a maximum biodiesel yield of 94.19 % is produced after three hours of reaction.

5.2   Recommendation for Future Work

This research is not able to reveal the optimum operating parameters and their interactions completely as well as in a wider scale owing to the unavailability of BET instrument and limited number of slots for TPD and TGA instrument in order to carry out the characterisation on the synthesised catalysts. Hence, several recommendations are suggested for further improvement in order to conduct this research in a more thorough way.

First and foremost, all the synthesised catalysts should be stored in a completely airtight container before placing in the desiccator to prevent the adsorption of carbon dioxide and moisture from the atmosphere to catalyst surface, which will cause the formation of $CaCO_3$ and $Ca(OH)_2$ respectively. The presence of carbonates and hydroxides in both undoped and doped CaO catalysts are detected in XRD analysis, where it is inferred that the number of active sites is reduced subsequent to the occupying of $CaCO_3$ and $Ca(OH)_2$ on catalyst surface, which in turn adversely affects the catalytic performance of synthesised catalysts. Besides, the catalyst sample is suggested to be scanned with a lower rate in X-ray diffractometer especially for the doped catalysts with a comparatively smaller amount of Ni dopant impregnated as the presence of Ni dopant in CaO catalyst might be overlooked in view of rapid scanning. Hence, the scanning rate of XRD is recommended to be adjusted, which is lower than $2°$ per minute for a more precise and accurate analysis result.

Furthermore, the characterisation on the synthesised catalysts as well as the transesterification catalysed by both undoped and doped catalysts should be carried out as soon as possible after synthesising the catalysts. The amount of carbon dioxide and moisture present in the catalyst is increased due to prolonged storage period as the continuous contact of catalyst with the air tends to reduce its catalytic performance. Based on the experimental results concerning the biodiesel yield obtained from transesterification, there is still room for improvement on the activity of doped CaO catalyst. Thus, a further study should

be conducted on other parameters for catalyst synthesis that affect the catalytic performance, including doping method, type of metal dopant incorporated to CaO and re-calcination duration in order to activate more active sites of doped CaO catalyst, which in turn enhancing its catalytic activity.

Other than that, the operating parameters for transesterification reaction such as catalyst loading, methanol-to-oil molar ratio, reaction temperature and reaction duration should be carried out in order to determine the optimum operating conditions for transesterification reaction in a more comprehensive way. In addition, the reusability of catalyst should be also studied in order to reduce the overall processing cost of a chemical reaction by determining the life cycle as well as the onset of degradation denoting the activity loss, besides minimising the cost of biodiesel production, where the transesterification is performed under optimised reaction conditions after parameters optimisation.

REFERENCES

Abbah, E.C., Nwandikom, G.I., Egwuonwu, C.C. and Nwakuba, N.R., 2017. Effect of reaction temperature on the yield of biodiesel from neem seed oil. *American Journal of Energy Science ,* 4(2), pp. 5-9.

Abdelhady, H.H., Elazab, H.A., Ewais, E.M., Saber, M. and El-Deab, M.S., 2020. Efficient catalytic production of biodiesel using nano-sized sugar beet agro-industrial waste. *Fuel,* Volume 261, p. 116481.

Abdullah, A. Z., Wibowo, T. Y., and Zakaria, R., 2011. Effect of tetramethyl ammonium hydroxide on the activity of LiOH-intercalated montmorillonite catalyst in the transesterification of methyl laurate with glycerol. *Chemical Engineering Journal,* 167(1), pp. 328-334.

Abdullah, A., Salamatinia, B., Mootabadi, H. and Bhatia, S., 2009. Current status and policies on biodiesel industry in Malaysia as the world's leading producer of palm oil. *Energy Policy,* Volume 37, pp. 5440-5448.

Adewale, P., Dumont, M.J. and Ngadi, M., 2015. Recent trends of biodiesel production from animal fat wastes and associated production techniques. *Renewable and Sustainable Energy Reviews,* Volume 45, pp. 574-588.

Aguilar, D.H., Torres-Gonzalez, L.C., Torres-Martinez, L.M., Lopez, T. and Quintana, P., 2001. Thin ZrO2 sol–gel films for catalytic applications. *Journal of Solid State Chemistry,* Volume 158, p. 349.

Ahmad, A.L.,Yasin, N.H.M., Derek, C.J.C. and Lim, J.K., 2011. Microalgae as a sustainable energy source for biodiesel production: a review. *Renewable and Sustainable Energy Reviews,* 15(1), pp. 584-593.

Alhassan, F.H., Yunus, R., Rashid, U., Sirat, K., Islam, A., Lee, H.V. and Taufiq-Yap, Y.H., 2013. Production of biodiesel from mixed waste vegetable oils using Ferric hydrogen sulphate as an effective reusable heterogeneous solid acid catalyst. *Applied Catalysis A: General,* Volume 456, pp. 182-187.

Alonso, D.M., Mariscal, R., Granados, M.L. and Maireles-Torres, P., 2009. Biodiesel preparation using Li/CaO catalysts: Activation process and homogeneous contribution. *Catalysis Today,* Volume 143, pp. 167-171.

Amani, H., Ahmad, Z., Asif, M. and Hameed, B.H., 2014. Transesterification of waste cooking palm oil by MnZr with supported alumina as a potential heterogeneous catalyst. *Journal of Industrial and Engineering Chemistry,* Volume 20, pp. 4437-4442.

Ambat, I., Srivastava, V. and Sillanpää, M., 2018. Recent advancement in biodiesel production methodologies using various feedstock: A review. *Renewable and Sustainable Energy Reviews,* Volume 90, pp. 356-369.

Aranda, D.A.G., Santos, R.T.P., Tapanes, N.C.O., Ramos, A.L.D. and Antunes, O.A.C., 2007. Acid-catalyzed homogeneous esterification reaction for biodiesel production from palm fatty acids. *Catalysis Letters ,* Volume 122, pp. 20-25.

Aransiola, E.F., Ojumu, T.V., Oyekola, O.O., Madzimbamuto, T.F. and Ikhu-Omoregbe, D.I.O., 2014. A review of current technology for biodiesel production: state of the art. *Biomass & Bioenergy,* Volume 61, pp. 276-197.

Asikin-Mijan, N., Lee, H. V. and Taufiq-Yap, Y. H., 2015. Synthesis and catalytic activity of hydration-dehydration treated clamshell derived CaO for biodiesel production. *Chemical Engineering Research and Design,* Volume 102, p. 368–377.

Atabani, A.E., Silitonga, A.S., Ong, H.C., Mahlia, T.M.I., Masjuki, H.H., Badruddin, I.A. and Fayaz, H., 2013. Non-edible vegetable oils: A critical evaluation of oil extraction, fatty acid compositions, biodiesel production, characteristics, engine performance and emissions production. *Renewable and Sustainable Energy Reviews,* Volume 18, pp. 211-245.

Atadashi, I.M., Aroua, M.K., Abdul-Aziz, A.R. and Sulaiman, N.M.N., 2013. The effects of catalysts in biodiesel production: A review. *Journal of Industrial and Engineering Chemistry,* Volume 19, pp. 14-26.

Avhad, M.R. and Marchetti, J.M., 2015. A review on recent advancement in catalytic materials. *Renewable and Sustainable Energy Reviews,* Volume 50, pp. 696-718.

Azizul Hakim, Wan Nor Roslam, Maratun Najiha, Muhammad Rahimi, Mohamed Wahab and Mohd Ambar, 2015. Temperature Programmed Desorption of Carbon Dioxide for Activated Carbon Supported Nickel Oxide: The Adsorption and Desorption Studies. *Advanced Materials Research,* Volume 1087, pp. 45-49.

Azman, A., Rahman, A., Bakar, N., Hanaffi, F. and Khamis, A., 2011. Study of renewable energy potential in Malaysia. *Renewable and Sustainable Energy Reviews,* Volume 15, pp. 170-176.

Bai, H., Shen, X., Liu, X. and Liu, S., 2009. Synthesis of porous CaO microsphere and its application in catalyzing transesterification reaction for biodiesel. *Transactions of Nonferrous Metals Society of China ,* Volume 19, pp. 674-677.

Banković–Ilić, I.B., Miladinović, M.R., Stamenković, O.S. and Veljković, V.B., 2017. Application of nano CaO–based catalysts in biodiesel synthesis. *Renewable and Sustainable Energy Reviews,* Volume 72, pp. 746-760.

Banković–Ilić, I.B., Stamenković, O.S. and Veljković, V.B., 2012. Biodiesel production from non-edible plant oils. *Renewable and Sustainable Energy Reviews,* Volume 16, pp. 3621-3647.

Banković–Ilić, I.B., Stojković, I.J., Stamenković, O.S., Veljković, V.B. and Hung, Y.T., 2014. Waste animal fats as feedstocks for biodiesel production. *Renewable and Sustainable Energy Reviews,* Volume 32, pp. 238-254.

Baroutian, S., Aroua, M.K., Raman, A.A. and Sulaiman, N.M., 2009. RBD Palm Olein-Based Methyl/Ethyl Esters. *Journal of Oil Palm Research,* Volume 21, pp. 659-666.

Baskar, G. and Aiswarya, R., 2015. Nano catalyst for transesterification of fatty acids into biodiesel. *Journal of Nanobiotechnology ,* Volume 1, pp. 1-4.

Baskar, G. and Aiswarya, R., 2016. Trends in catalytic production of biodiesel from various feedstocks. *Renewable and Sustainable Energy Reviews,* Volume 57, pp. 496-504.

Baskar, G., Selvakumari, I.A.E. and Aiswarya, R., 2018. Biodiesel production from castor oil using heterogeneous Ni doped ZnO nanocatalyst. *Bioresource Technology,* Volume 250, pp. 793-798.

Baumert, K., Herzog, T. and Jonathan, P., 2005. Navigating the numbers greenhouse gas data and international climate policy. *United States of America: World Resources Institute,* Volume 37, pp. 5440-5448.

Bensebaa, F., 2013. Nanoparticle fundamentals. *Interface Science and Technology,* Volume 19, pp. 1-84.

Borah, M.J., Das, A., Das, V., Bhuyan, N. and Deka, D., 2019. Transesterification of waste cooking oil for biodiesel production catalyzed by Zn substituted waste egg shell derived CaO nanocatalyst. *Fuel,* Volume 242, pp. 345-354.

Borges, L.D., Moura, N.N., Costa, A.A., Braga, P.R.S., Dias, J.A., Dias, S.C.L., Macedo, J.L. and Ghesti, G.F., 2013. Investigation of biodiesel production by HUSY and Ce/HUSY zeolites: Influence of structural and acidity parameters. *Applied Catalysis A: General,* Volume 450, pp. 114-119.

Borges, M.E. and Díaz, L., 2012. Recent development on heterogeneous catalysts for biodiesel production by oil esterification and transesterification reactions: A review. *Renewable and Sustainable Energy Reviews,* Volume 18, pp. 2839-2849.

Boro, J., Deka, D. and Thakur, A.J., 2012. A review on solid oxide derived from waste shells as catalyst for biodiesel production. *Renewable and Sustainable Energy Reviews,* Volume 16, pp. 904-910.

Boro, J., Konwar, L. J. and Deka, D., 2014. Transesterification of non edible feedstock with lithium incorporated egg shell derived CaO for biodiesel production. *Fuel Processing Technology,* Volume 122, pp. 72-78.

Boro, J., Konwar, L.J., Thakur, A.J. and Deka, D., 2014. Ba doped CaO derived from waste shells of T striatula (TS-CaO) as heterogeneous catalyst for biodiesel production. *Fuel,* Volume 129, pp. 182-187.

Borugadda, V.B. and Goud, V.V., 2012. Biodiesel production from renewable feedstocks: Status and opportunities. *Renewable and Sustainable Energy Reviews,* Volume 16, p. 4763–4784.

Brito, J.Q.A., Silva, C.S., Almeida, J.S., Korn, M.G.A., Korn, M. and Teixeira, L.S.G., 2012. Ultrasound-assisted synthesis of ethyl esters from soybean oil via homogeneous catalysis. *Fuel Proessing Technology,* Volume 95, pp. 33-36.

Buasri, A., Chaiyut, N., Loryuenyong, V., Wongweang, C. and Khamsrisuk, S., 2013. Application of eggshell wastes as a heterogeneous catalyst for biodiesel production. *Renewable and Sustainable Energy Reviews,* 1(2), pp. 7-13.

Casanave, D., Duplan, J.L. and Freund, E., 2007. Diesel fuels from biomass. *Pure and Applied Chemistry,* 79(11), pp. 2071-2081.

Chakraborty, R., Bepari, S. and Banerjee, A., 2011. Application of calcined waste fish (Labeo rohita) scale as low-cost heterogeneous catalyst for biodiesel synthesis. *Bioresource Technology,* Volume 102, pp. 3610-3618.

Chen, C.L., Huang, C.C., Tran, D.T. and Chang, J.S., 2012. Biodiesel synthesis via heterogeneous catalysis using modified strontium oxides as the catalysts. *Bioresource Technology,* Volume 113, pp. 8-13.

Chen, G., Shan, R., Shi, J., and Yan, B. , 2014. Ultrasonic-assisted production of biodiesel from transesterification of palm oil over ostrich eggshell-derived CaO catalysts. *Bioresource Technology,* Volume 171, pp. 428-432.

Chen, G.Y., Shan, R., Yan, B.B., Shi, J.F., Li, S.Y., and Liu, C.Y., 2016. Remarkably enhancing the biodiesel yield from palm oil upon abalone shell-derived CaO catalysts treated by ethanol. *Fuel Processing Technology,* Volume 143, pp. 110-117.

Chen, K.S., Lin, Y.C., Hsu, K.H. and Wang, H.K., 2012. Improving biodiesel yields from waste cooking oil by using sodium methoxide and a microwave heating system. *Energy,* Volume 38, pp. 151-156.

Chongkhong, S., Tongurai, C. and Chetpattananondh, P, 2009. Continuous esterification for biodiesel production from palm fatty acid distillate using economical process. *Renewable Energy,* 34(4), pp. 1059-1063.

Chung, K.H., Kim, J. and Lee, K.Y., 2009. Biodiesel production by transesterification of duck tallow with methanol on alkali catalysts. *Biomass & Bioenergy,* Volume 33, pp. 155-158.

Correia, L.M., Saboya, R.M.A., Campbelo, N.S., Cecilia, J.A., Rodríguez-Castellón, E., Cavalcante, C.L. and Vieira, R.S., 2014. Characterization of calcium oxide catalysts from natural sources and their application in the transesterification of sunflower oil. *Bioresource Technology,* Volume 151, pp. 207-213.

Costa, A.A., Braga, P.R.S., Macedo, J.L., Dias, J.A. and Dias, S.C.L., 2012. Structural effects of WO3 incorporation on USY zeolite and application to free

fatty acids esterification. *Microporous and Mesoporous Materials,* Volume 147, pp. 142-148.

Daniyan, I.A., Adeodu, A.O., Dada, O.M. and Adewumi, D.F., 2015. Effects of Reaction Time on Biodiesel Yield. *Journal of Bioprocessing and Chemical Engineering,* 3(2), pp. 1-3.

Danks, A. E., Hall, S. R. and Schnepp, Z., 2016. The evolution of 'sol–gel' chemistry as a technique for materials synthesis. *Materials Horizons,* 3(2), pp. 91-112.

Dawodu, F.A., Ayodele, O., Xin, J., Zhang, S. and Yan, D., 2014. Effective conversion of non-edible oil with high free fatty acid into biodiesel by sulphonated carbon catalyst. *Applied Energy,* Volume 114, pp. 819-826.

Degirmenbasi, N., Coskun, S., Boz, N. and Kalyon, D.M., 2015. Biodiesel synthesis from canola oil via heterogeneous catalysis using functionalized CaO nanoparticles. *Fuel,* Volume 153, pp. 620-627.

Demirbas, A. and Demirbas, I., 2007. Importance of rural bioenergy for developing countries. *Energy Conversion and Management,* Volume 48, pp. 2386-2398.

Demirbas, M.F., Balat, M. and Balat, H., 2009. Potential contribution of biomass to the sustainable energy development. *Energy Conversion and Management,* Volume 50, pp. 1746-1760.

Demirbas, A., 2005. Biodiesel production from vegetable oils via catalytic and noncatalytic supercritical methanol transesterification methods. *Progress in Energy and Combustion Science,* Volume 31, pp. 466-487.

Demirbas, A., 2006. Biodiesel Production via Non-Catalytic SCF Method and Biodiesel Fuel Characteristics. *Energy Conversion and Management,* Volume 47, pp. 2271-2282.

Demirbas, A., 2007. Importance of biodiesel as transportation fuel. *Energy Policy,* Volume 35, pp. 4661-4670.

Demirbas, A., 2008. *Biodiesel: a realistic fuel alternative for diesel,* London: Springer.

Demirbas, A., 2008. New liquid biofuels from vegetable oils via catalytic pyrolysis. *Energy Education Science and Technology ,* Volume 21, pp. 1-59.

Demirbas, A., 2009. Biofuels securing the planet's future energy needs. *Energy Conversion and Management,* 50(9), pp. 2239-2249.

Demirbas, A., 2009. Production of biodiesel fuels from linseed oil using methanol and ethanol in non-catalytic SCF conditions. *Biomass & Bioenergy,* 33(1), pp. 113-118.

Demirbas, A., 2009. Progress and recent trends in biodiesel fuels. *Energy Conversion and Management,* Volume 50, pp. 14-34.

Dennis, Y.C.,Leung, X.W. and Leung M.K.H., 2010. A review on biodiesel production using catalyzed transesterification. *Applied Energy,* Volume 87, pp. 1083-1095.

Deraz, N., 2018. The comparative jurisprudence of catalysts preparation methods: I.precipitation and impregnation methods. *Journal of Industrial and Environmental Chemistry ,* 2(1), pp. 19-21.

Dias, A.P.S., Bernardo, J., Felizardo, P. and Correia, M.J.N., 2012. Biodiesel production over thermal activated cerium modified Mg-Al hydrotalcites. *Energy,* Volume 41, pp. 344-353.

Dias, J.M., Alvim-Ferraz, M.C.M. and Almeida, M.F., 2008. Comparison of the performance of different homogeneous alkali catalysts during transesterification of waste and virgin oils and evaluation of biodiesel quality. *Fuel,* Volume 87, pp. 3572-3578.

Dodić, S.N., Popov, S.D., Dodić, J.M., Ranković, J.A., Zavargo, Z.Z. and Golušin, M.T., 2010. A overview of biomass energy utilization in Vojvodina. *Renewable and Sustainable Energy Reviews,* Volume 14, pp. 550-553.

Dossin, T.F., Reyniers, M.F., Berger, R.J. and Marin, G.B., 2006. Simulation of heterogeneously MgO-catalyzed transesterification for fine-chemical and biodiesel industrial production. *Applied Catalysis B: Environmental,* Volume 67, pp. 136-148.

Edgar, L., Yijun, L., Dora, L.E., Kaewta, S., David, B.A. and Goodwin, J.G., 2005. Synthesis of biodiesel via acid catalysis. *Industrial and Engineering Chemistry Research,* Volume 44, pp. 5353-5363.

Fadhil, A.B. and Ali, L.H., 2013. Alkaline-catalyzed transesterification of Silurus triostegus Heckel fish oil: optimization of transesterification parameters. *Renewable Energy,* Volume 60, pp. 481-488.

Farag, H.A., El-Maghraby, A. and Taha, N.A., 2011. Optimization of factors affecting esterification of mixed oil with high percentage of free fatty acid. *Fuel Processing Technology,* Volume 92, pp. 507-510.

Fernandes, D.M., Serqueira, D.S., Portela, F.M., Assunção, R.M.N., Munoz, R.A.A. and Terrones, M.G.H., 2012. Preparation and characterization of methylic and ethylic biodiesel from cottonseed oil and effect of tert-butylhydroquinone on its oxidative stability. *Fuel,* Volume 97, pp. 658-661.

Filho, C.A.A. and Murzin, D.Y., 2018. A structure sensitivity approach to temperature programmed desorption. *Applied Catalysis A: General,* Volume 550, pp. 48-56.

Freedman, B., Pryde, E.H. and Mounts, T.L., 1984. Variables affecting the yields of fatty esters from transesterified vegetable oils. *Journal of the American Oil Chemists Society,* Volume 61, p. 1638–1643.

Furuta, S., Matsuhashi, H. and Arata, K., 2006. Biodiesel fuel production with solid amorphous-zirconia catalysis in fixed bed reactor. *Biomass & Bioenergy,* Volume 30, pp. 870-873.

Galchar, J., 2017. Production of biodiesel using Nano Catalysts, Review study. *Journal of Engineering Development and Research,* 5(1), pp. 485-488.

García-Sancho, C., Moreno-Tost, R., Mérida-Robles, J.M., Santamaría-González, J., Jiménez-López, A. and Maireles-Torres, P., 2011. Niobium-containing MCM-41 silica catalysts for biodiesel production. *Applied Catalysis B: Environmental,* Volume 108-109, pp. 161-167.

Gardy, J., Hassanpour, A., Lai, X., Mukhtar Ahmed and Mohammad Rehan, 2017. Biodiesel production from used cooking oil using a novel surface functionalised TiO2 nano-catalyst. *Applied Catalysis B: Environmental,* Volume 207, pp. 297-310.

Gashaw, A. and Lakachew, A., 2014. Production of biodiesel from non edible oil and its properties. *International Journal of Environmental Science and Technology,* Volume 3, pp. 1544-1562.

Gotch, A.J., Reeder, A.J. and McCormick, A., 2009. Study of heterogeneous base catalysts for biodiesel production. *Journal of Undergraduate Chemistry Research,* 8(9), pp. 22-26.

Granados, M.L., Poves, M.D.Z., Alonso, D.M., Mariscal, R., Galisteo, F.C., Moreno-Tost, R., Santamaría, J. and Fierro, J.L.G., 2007. Biodiesel from sunflower oil by using activated calcium oxide. *Applied Catalysis B: Environmental ,* Volume 73, pp. 317-326.

Guan, G., Kusakabe, K., Sakurai, N. and Moriyama, K., 2009. Transesterification of vegetable oil to biodiesel fuel using acid catalysts in the presence of dimethyl ether. *Fuel,* Volume 88, pp. 81-86.

Gui, M.M., Lee, K.T. and Bhatia, S., 2008. Feasibility of edible oil vs. non-edible oil vs. waste edible oil as biodiesel feedstock. *Energy,* 33(11), pp. 1646-1653.

Gurunathan, B. and Ravi, A., 2015. Biodiesel production from waste cooking oil using copper doped zinc oxide nanocomposite as heterogeneous catalyst. *Bioresource Technology,* Volume 188, pp. 124-127.

Hanh, H.D., Dong, N.T., Okitsu, K., Nishimura, R. ang Maeda, Y., 2009. Biodiesel production by esterification of oleic acid with short-chain alcohols under ultrasonic irradiation condition. *Renewable Energy,* Volume 34, pp. 780-783.

Hannon, M., Gimpel, J., Tran, M., Rasala, B. and Mayfield, S., 2010. Biofuels from algae: challenges and potential. *Biofuels ,* 1(5), pp. 763-784.

Harsha-Hebbar, H.R., Math, M.C. and Yatish, K.V., 2018. Optimization and kinetic study of CaO nano-particles catalyzed biodiesel production from Bombax ceiba oil. *Energy,* Volume 143, pp. 25-34.

Hattori, H., 1995. Heterogeneous basic catalysis. *Chemical Reviews ,* Volume 95, pp. 537-558.

Helwani, Z., Othman, M.R., Aziz, N., Fernando, W.J.N and Kim, J., 2009. Solid heterogeneous catalysts for transesterification of triglycerides with methanol: A review. *Applied Catalysis A: General,* 363(1), pp. 1-10.

Hernandez-Hipolito, P., Garcia-Castillejos, M., Martinez-Klimova, E., Juarez-Flores, N., Gomez-Cortes, A. and Klimova, T.K., 2014. Biodiesel production with nanotubular sodium titanate as a catalyst. *Catalysis Today,* Volume 220-222, pp. 4-11.

Hideki, F., Akihiko, K. and Hideo, N., 2001. Biodiesel fuel production by transesterification of oils: review. *Journal of Bioscience and Bioengineering,* Volume 92, p. 405.

Hoora, M., Ong, H.C., Masjuki, H.H., Zeynab, A., Harrison, M.D., Wang, C.T., Kusumo, F. and Azham, A., 2018. Rice bran oil based biodiesel production using calcium oxide catalyst derived from Chicoreus brunneus shell. *Energy,* Volume 144, pp. 10-19.

Hossain, A., Sharif, B.M., Salleh, A., Boyce, A.N. and Chowdhury, P., 2008. Biodiesel production from algae as renewable energy. *American Journal of Biochemistry and Biotechnology,* 4(3), pp. 250-254.

Hossein, A., Anwar, J., Haslenda, H. and Elham, H., 2018. A source of renewable energy in Malaysia, why biodiesel?. *Renewable and Sustainable Energy Reviews,* Volume 35, pp. 244-257.

Hu, S., Guan, Y., Wang, Y. and Han, H., 2011. Nano–magnetic catalyst KF/CaO–Fe3O4 for biodiesel production. *Applied Energy,* Volume 88, pp. 2685-2690.

Hu, S., Wen, L., Wang, Y., Zheng, X. and Han, H., 2012. Gas–liquid countercurrent integration process for continuous biodiesel production using a microporous solid base KF/CaO as catalyst. *Bioresource Technology,* Volume 123, pp. 413-418.

Issariyakul, T. and Dalai, A.K., 2014. Biodiesel from vegetable oils. *Renewable and Sustainable Energy Reviews,* Volume 31, pp. 446-471.

Janaun, J. and Ellis, N., 2010. Perspectives on biodiesel as a sustainable fuel. *Renewable and Sustainable Energy Reviews,* Volume 14, pp. 1312-1320.

Jeon, H., Kim, D.J., Kim, S.J. and Kim, J.H., 2013. Synthesis of mesoporous MgO catalyst templated by a PDMS–PEO comb-like copolymer for biodiesel production. *Fuel Processing Technology,* Volume 116, pp. 325-331.

Jiang, W., Lu, H.F., Qi, T., Yan, S.L. ang Liang, B., 2010. Preparation, application, and optimization Zn/Al complex oxides for biodiesel production under sub-critical conditions.. *Biotechnology Advances,* 28(5), pp. 620-627.

Jiang, Y., Lu, J., Sun, K., Ma, L. and Ding, J., 2013. Esterification of oleic acid with ethanol catalyzed by sulfonated cation exchange resin: experimental and kinetic studies. *Energy Conversion and Management,* Volume 76, pp. 980-985.

Jiménez López, A., Jiménez-Morales, I., Santamaría-González, J. and Maireles-Torres, P., 2011. Biodiesel production from sunflower oil by tungsten oxide supported on zirconium doped MCM-41 silica. *Journal of Molecular Catalysis A: Chemical,* Volume 335, pp. 205-209.

Jitputti, J., Kitiyanan, B., Rangsunvigit, P., Bunyakiat, K., Attanatho, L. and Jenvanitpanjakul, P., 2006. Transesterification of crude palm kernel oil and crude coconut oil by different solid catalysts. *Chemical Engineering Journal,* Volume 116, pp. 61-66.

Johnston, M. and Holloway, T., 2018. A global comparison of national biodiesel production potentials. *Environmental Science & Technology,* Volume 41, pp. 7967-7973.

Kamel, D.A., Farag, H.A., Amin, N.K., Zatout, A.A. and Ali, R.M., 2018. Smart utilization of jatropha (Jatropha curcas Linnaeus) seeds for biodiesel production: optimization and mechanism. *Industrial Crops and Products,* Volume 111, pp. 407-413.

Karavalakis, G., Anastopoulos, G. and Stournas, S., 2011. Tetramethylguanidine as an efficient catalyst for transesterification of waste frying oils. *Applied Energy,* Volume 88, pp. 3645-3650.

Karavalakis, G., Anastopoulos, G., Karonis, D. and Stournas, S., 2010. Biodiesel production using tetramethyl- andbenzyltrimethyl ammonium hydroxides as strong base catalysts. *Fuel Processing Technology,* Volume 91, pp. 1585-1590.

Karmakar, A., Karmakar, S. and Mukherjee, S., 2010. Properties of various plants and animals feedstocks for biodiesel production. *Bioresource Technology,* Volume 101, pp. 7201-7210.

Karmakar, B. and Halder, G., 2019. Progress and future of biodiesel synthesis: Advancements in oil extraction and conversion technologies. *Energy Conversion and Management,* Volume 182, pp. 307-339.

Kathlene, J., Rajesh, G., Charan, M.L. and Kumar, D.A., 2008. Solid acid catalyzed biodiesel production from waste cooking oil. *Applied Catalysis B: Environmental,* Volume 85, pp. 86-91.

Kaur, M. and Ali, A., 2011. Lithium ion impregnated calcium oxide as nanocatalyst for the biodiesel production from karanja and jatropha oils. *Renewable Energy,* Volume 36, pp. 2866-2871.

Kaur, M. and Ali, A., 2014. Potassium fluoride impregnated CaO/NiO: an efficient heterogeneous catalyst for transesterification of waste cottonseed oil. *European Journal of Lipid Science and Technology,* Volume 116, pp. 80-88.

Kaur, N. and Ali, A., 2014. Kinetics and reusability of Zr/CaO as heterogeneous catalyst for the ethanolysis and methanolysis of Jatropha crucas oil. *Fuel Processing Technology,* Volume 119, pp. 173-184.

Kawashima, A., Matsubara, K. and Honda, K., 2008. Development of heterogeneous base catalysts for biodiesel productionv. *Bioresource Technology,* Volume 99, pp. 3439-3443.

Kawashima, A., Matsubara, K. and Honda, K., 2009. Acceleration of catalytic activity of calcium oxide for biodiesel production. *Bioresource Technology,* Volume 100, pp. 696-700.

Keera, S.T., Sabagh, S.M. and Taman, A.R., 2011. Transesterification of vegetable oil to biodiesel fuel using alkaline catalyst. *Fuel,* Volume 90, pp. 42-47.

Kesić, Ž., Lukić, I., Zdujić, M., Mojović, L. and Skala, D., 2016. Calcium oxide based catalysts for biodiesel production: a review. *Chemical Industry and Chemical Engineering Quarterly ,* Volume 22, pp. 391-408.

Komor, P. and Bazilian, M., 2005. Renewable energy policy goals, programs, and technologies. *Energy Policy,* Volume 33, pp. 1873-1881.

Konwar, L.J., Boro, J. and Deka, D., 2014. Review on latest developments in biodiesel production using carbon-based catalysts. *Renewable and Sustainable Energy Reviews,* Volume 29, pp. 546-564.

Kouzu, M., Tsunomori, M., Yamanaka, S. and Hidaka, J., 2010. Solid base catalysis of calcium oxide for a reaction to convert vegetable oil into biodiesel. *Advanced Powder Technology ,* Volume 21, pp. 488-494.

Krishnamurthy, K.N., Sridhara, S.N. and Ananda-Kumar, C.S., 2019. Optimization and kinetic study of biodiesel production from Hydnocarpus wightiana oil and dairy waste scum using snail shell CaO nano catalyst. *Renewable Energy,* Volume 146, pp. 280-296.

Kumar, D. and Ali, A., 2010. Nanocrystalline lithium ion impregnated calcium oxide as Nanocrystalline lithium ion impregnated calcium oxide as seed oil. *Energy & Fuels,* Volume 24, pp. 2091-2097.

Kumar, D. and Ali, A., 2012. Nanocrystalline K–CaO for the transesterification of a variety of feedstocks: structure, kinetics and catalytic properties. *Biomass & Bioenergy,* Volume 46, pp. 459-468.

Kumar, D. and Ali, A., 2013. Transesterification of low–quality triglycerides over a Zn/CaO heterogeneous catalyst: kinetics and reusability studies. *Energy & Fuels,* Volume 27, pp. 3758-3768.

Kumar, D., Abida, K., and Ali, A., 2016. Aminolysis of triglycerides using nanocrystalline nickel doped CaO as an efficient solid catalyst. *RSC Advances,* 6(71), pp. 66822-66832.

Kumar, M. and Sharma, M.P. , 2016. Selection of potential oils for biodiesel production. *Renewable and Sustainable Energy Reviews,* Volume 56, p. 1129–1138.

Kung, H. and Kung, M., 2007. Nanotechnology and Heterogeneous Catalysis. In: B. Zhou, S. Han, R. Raja & G. Somorjai, eds. *Nanotechnology in Catalysis.* New York: Springer Science+Business Media, pp. 1-11.

Kusdiana, D. and Saka, S., 2004. Effects of water on biodiesel fuel production by supercritical methanol treatment. *Bioresource Technology,* Volume 91, p. 289–295.

Lam, M.K., Lee, K.T. and Mohamed, A.R., 2010. Homogeneous, heterogeneous and enzymatic catalysis for transesterification of high free fatty acid oil (waste cooking oil) to biodiesel: a review. *Biotechnology Advances,* Volume 28, pp. 500-518.

Lapham, D.P. and Lapham, J.L., 2019. BET surface area measurement of commercial magnesium stearate by krypton adsorption in preference to nitrogen adsorption. *International Journal of Pharmaceutics,* Volume 568, p. 118522.

Lee, H., Juan, J., Binti Abdullah, N., Nizah MF, R., and Taufiq-Yap, Y., 2014. Heterogeneous base catalysts for edible palm and non-edible Jatropha-based biodiesel production. *Chemistry Central Journal,* 8(1), pp. 1-9.

Lee, H.V., Juan, J.C., Yun-Hin, T.Y. and Ong, H.C., 2016. Environment-friendly heterogeneous alkaline-based mixed metal oxide catalysts for biodiesel production. *Energies,* 9(8), p. 611.

Lee, F., 2019. *APEC Energy Demand and Supply Outlook 7th Edition 2019,* Tokyo: Asia Pacific Energy Research Centre.

Leung, D.Y.C., Wu, X. and Leung, M.K.H., 2010. A review on biodiesel production using catalyzed transesterification. *Applied Energy,* Volume 87, pp. 1083-1095.

Li, J., Fu, Y.J., Qu, X.J., Wang, W., Luo, M., Zhao, C.J. and Zu, Y.G., 2012. Biodiesel production from yellow horn (Xanthoceras sorbifolia Bunge.) seed oil using ion exchange resin as heterogeneous catalyst. *Bioresource Technology,* Volume 108, pp. 112-118.

Li, Y., Qiu, F., Yang, D., Sun, P. and Li, X., 2012. Transesterification of soybean oil and analysis of bioproduct. *Food and Bioproducts Processing ,* Volume 90, pp. 135-140.

Li, Y., Zhang, X.D., Sun, L., Xu, M., Zhou, W.G. and Liang, X.H., 2010. Solid superacid catalyzed fatty acid methyl esters production from acid oil. *Applied Energy,* Volume 87, pp. 2369-2373.

Liu, C., Lv, P., Yuan, Z., Yan, F. and Luo, W., 2010. The nanometer magnetic solid base catalyst for production of biodiesel. *Renewable Energy,* Volume 35, pp. 1531-1536.

López, J.M., Gómez, Á., Aparicio, F. and Javier-Sánchez, F., 2009. Comparison of GHG emissions from diesel, biodiesel and natural gas refuse trucks of the City of Madrid. *Applied Energy,* Volume 86, pp. 610-615.

Ma, F. and Hanna, M.A., 1999. Biodiesel production: a review. *Bioresource Technology,* Volume 70, pp. 1-15.

Macario, A. and Giordano, G., 2013. Catalytic conversion of renewable sources for biodiesel production: a comparison between biocatalysts and inorganic catalysts. *Catalysis Letters,* Volume 143, pp. 159-168.

MacLeod, C.S., Harvey, A.P., Lee, A.F. and Wilson, K., 2008. Evaluation of the activity and stability of alkali-doped metal oxide catalysts for application to an intensified method of biodiesel production. *Chemical Engineering Journal,* Volume 135, pp. 63-70.

Mahdavi, M., Abedini, E. and Darabi, A.H., 2015. Biodiesel synthesis from oleic acid by Nano-catalyst (ZrO2/Al2O3) under high voltage conditions. *RSC Advances,* 5(68), pp. 55027-55032.

Mahesh, S.E., Ramanathan, A., Begum, K.M.M.S. and Narayanan, A., 2015. Biodiesel production from waste cooking oil using KBr impregnated CaO as catalyst. *Energy Conversion and Management,* Volume 91, pp. 442-450.

Mahlia, T., Abdulmuin, M., Alamsyah, T. and Mukhlishien, D., 2001. An alternative energy source from palm wastes industry for Malaysia and Indonesia. *Energy Conversion and Management,* Volume 42, pp. 2109-2118.

Maneerung, T., Kawi, S., Dai, Y., and Wang, C.H., 2016. Sustainable biodiesel production via transesterification of waste cooking oil by using CaO catalysts prepared from chicken manure. *Energy Conversion and Management,* Volume 123, pp. 487-497.

Mangesh, K.G., Ajay, D.K., Charan, M.L. and Narayan, N.S., 2006. Transesterification of karanja (Pongamia pinnata) oil by solid basic catalysts. *European Journal of Lipid Science and Technology,* Volume 108, pp. 389-397.

Marchetti, J. and Errazu, A., 2008. Esterification of free fatty acids using sulfuric acid as catalyst in the presence of triglycerides. *Biomass & Bioenergy,* 32(9), pp. 892-895.

Marchetti, J.M. and Errazu, A.F., 2008. Esterification of free fatty acids using sulfuric acid as catalyst in the presence of triglycerides. *Biomass & Bioenergy,* Volume 32, pp. 892-895.

Marinković, D.M., Stanković, M.V., Veličković, A.V., Avramović, J.M., Miladinović, M.R., Stamenković, O.O., Veljković, V.B. and Jovanović, D.M., 2016. Calcium oxide as a promising heterogeneous catalyst for biodiesel

production: Current state and perspectives. *Renewable and Sustainable Energy Reviews,* Volume 56, pp. 1387-1408.

Mata, T.M., Martins, A.A. and Caetano, N.S., 2010. Microalgae for biodiesel production and other applications: a review. *Renewable and Sustainable Energy Reviews,* 14(1), pp. 217-232.

Mathiyazhagan, M. and Ganapathi, A., 2011. Factors Affecting Biodiesel Production. *Research in Plant Biology,* 1(2), pp. 1-5.

Mbaraka, I.K. and Shanks, B.H., 2006. Conversion of oils and fats using advanced mesoporous heterogeneous catalysts. *Journal of the American Oil Chemists' Society,* Volume 83, pp. 79-91.

Meher, L.C., Kulkarni, M.G., Dalai, A.K. and Naik, S.N., 2006. Transesterification of karanja (Pongamia pinnata) oil by solid basic catalysts. *European Journal of Lipid Science and Technology,* 108(5), pp. 389-397.

Meher, L.C., Naik, S.N. and Das, L.M., 2004. Methanolysis of Pongamia Pinnata (Karanja) oil for production of biodiesel. *Journal of Scientific and Industrial Research,* Volume 63, pp. 913-918.

Meher, L.C., Sagar, D.V. and Naik, S.N., 2006. Technical aspects of biodiesel production by transesterification: a review. *Renewable and Sustainable Energy Reviews,* Volume 10, pp. 248-268.

Melero, J.A., Bautista, L.F., Morales, G., Iglesias, J. and Sánchez-Vázquez, R., 2010. Biodiesel production from crude palm oil using sulfonic acid-modified mesostructured catalysts. *Chemical Engineering Journal,* Volume 161, pp. 323-331.

Miao, X., Li, R. and Yao, H., 2009. Effective acid-catalyzed transesterification for biodiesel production. *Energy Conversion and Management,* Volume 50, pp. 2680-2684.

Mikhaylov, R.V., Nikitin, K.V., Glazkova, N.I. and Kuznetsov, V.N., 2018. Temperature-programmed desorption of CO_2, formed by CO photooxidation on TiO_2 surface. *Journal of Photochemistry & Photobiology A: Chemistry,* Volume 360, pp. 255-261.

Mohadesi, M., Hojabri, Z. and Moradi, G., 2014. Biodiesel production using alkali earth metal oxides catalyst synthesized by sol-gel method. *Biofuel Research Journal,* Volume 1, pp. 30-33.

Mohammed Takase, Zhang, M., Feng, W., Chen, Y., Zhao, T., Cobbina, S.J., Yang, L. and Wu, X., 2014. Application of zirconia modified with KOH as heterogeneous solid base catalyst to new non-edible oil for biodiesel. *Energy Conversion and Management,* Volume 80, pp. 117-125.

Mota, C.J.A., Pinto, B.P., Lima, A.L., 2017. *Glycerol: a versatile renewable feedstock for the chemical industry,* Brazil: Springer International Publishing.

Narkhede, N. and Patel, A., 2013. Biodiesel production by esterification of oleic acid and transesterification of soybean oil using a new solid acid catalyst comprising 12-tungstosilicic acid and zeolite Hβ. *Industrial & Engineering Chemistry Research ,* Volume 52, pp. 13637-13644.

Nasar Mansir, Teo, S.H., Umer Rashid and Yun Hin Taufiq-Yap, 2018. Efficient waste Gallus domesticus shell derived calcium-based catalyst for. *Fuel,* Volume 211, pp. 67-75.

Nautiyal, P., Subramanian, K.A. and Dastidar, M.G., 2014. Kinetic and thermodynamic studies on biodiesel production from Spirulina platensis algae biomass using single stage extraction–transesterification process. *Fuel,* Volume 135, pp. 228-234.

Ngo, H.L., Zafiropoulos, N.A., Foglia,T.A., Samulski,E.T. and Lin, W., 2008. Efficient two-step synthesis of biodiesel from greases. *Energy Fuel,* Volume 22, pp. 626-634.

Nor Azyan, F.A.Z., Sarina, S. and Parveen, J., 2018. Thermally Produced Nano Catalyst for Biodiesel Production: A Review. *Journal of Advanced Research in Fluid Mechanics and Thermal Sciences,* 52(2), pp. 139-147.

Nurfitri, I., Maniam, G.P., Hindryawati, N., Yusoff, M.M. and Ganesan, S., 2013. Potential of feedstock and catalysts from waste in biodiesel preparation: A review. *Energy Conversion and Management,* Volume 74, pp. 395-402.

Oh, T.H., Pang, S.Y. and Chua, S.C., 2018. Energy policy and alternative energy in Malaysia: issues and challenges for sustainable growth. *Renewable and Sustainable Energy Reviews,* Volume 14, pp. 1241-1252.

Omer, A., 2018. Energy, environment and sustainable development. *Renewable and Sustainable Energy Reviews,* Volume 12, pp. 2265-2300.

Park, J.Y., Wang, Z.M., Kim, D.K. and Lee, J.S., 2010. Effects of water on the esterification of free fatty acids by acid catalysts. *Renewable Energy ,* Volume 35, pp. 614-618.

Patel, A., Brahmkhatri, V. and Singh, N., 2013. Biodiesel production by esterification of free fatty acid over sulfated zirconia. *Renewable Energy,* Volume 51, pp. 227-233.

Paul, A.M., Patel, J. and Prem, R.A., 2014. Algae Oil: a sustainable renewable fuel of future. *Biotechnology Research International,* Volume 2014, pp. 1-8.

Pergo, C. and Villa, P., 1997. Catalyst preparation methods. *Catalysis Today ,* Volume 34, pp. 281-305.

Philippot, K. and Serp, P., 2013. Concepts in Nanocatalysis. In: P. Serp & K. Philippot, eds. *Nanomaterials in Catalysis.* Weinheim, Germany: Wiley–VCH Verlag GmbH & Co. KGaA, pp. 1-54.

Pongtonglor, P., Hoonnivathana, E., Limsuwan, P., Limsuwan, S. and Naemchanthara, K., 2011. Utilization of Waste Eggshells as Humidity Adsorbent. *Journal of Applied Sciences,* 11(21), pp. 3659-3662.

Poonjarernsilp, C., Sano, N. and Tamon, H., 2014. Hydrothermally sulfonated single-walled carbon nanohorns for use as solid catalysts in biodiesel production by esterification of palmitic acid. *Applied Catalysis B: Environmental,* Volume 147, pp. 726-732.

Predojević, Z., 2008. The production of biodiesel from waste frying oils: A comparison of different purification steps. *Fuel,* 87(17-18), pp. 3522-3528.

Rahman, W.U., Fatima, A., Anwer, A.H., Athar, M., Khan, M.Z., Khan, N.A. and Halder, G., 2019. Biodiesel synthesis from eucalyptus oil by utilizing waste egg shell derived calcium based metal oxide catalyst. *Process Safety and Environmental Protection,* Volume 122, pp. 313-319.

Ramadhas, A. S., Jayaraj, S. and Muraleedharan C., 2005. Biodiesel production from high FFA rubber seed oil. *Fuel,* Volume 84, pp. 335-340.

Rashid, U. and Anwar, F., 2008. Production of biodiesel through base-catalyzed transesterification of safflower oil using an optimized protocol. *Energy & Fuels,* Volume 22, pp. 1306-1312.

Rashtizadeh, E., Farzanesh, F. and Talebpour, Z., 2014. Synthesis and characterization of Sr3Al2O6 nanocomposite as catalyst for biodiesel production. *Bioresource Technology,* Volume 154, pp. 32-37.

Reddy, C.R.V., Oshel, R. and Verkade, J.G., 2006. Room–temperature conversion of soybean oil and poultry fat to biodiesel catalyzed by nanocrystalline calcium oxides. *Energy & Fuels,* Volume 20, pp. 1310-1314.

Rezaei, R., Mohadesi, M. and Moradi, G.R., 2013. Optimization of biodiesel production using waste mussel shell catalyst. *Fuel,* Volume 109, pp. 534-541.

Risso, R., Ferraz, P., Meireles, S., Fonseca, I. and Vital, J., 2018. Highly active CaO catalysts from waste shells of egg, oyster and clam for biodiesel production. *Applied Catalysis A, General,* Volume 567, pp. 56-64.

Roschat, W., Kacha, M., Yoosuk, B., Sudyoadsuk, T. and Promarak, V., 2012. Biodiesel production based on heterogeneous process catalyzed by solid waste coral fragment. *Fuel,* Volume 98, pp. 194-202.

Roschat, W., Phewphong, S., Thangthong, A., Moonsin, P., Yoosuk, B., Kaewpuang, T. and Promarak, V., 2018. Catalytic performance enhancement of CaO by hydration-dehydration process for biodiesel production at room temperature. *Energy Conversion and Management,* Volume 165, pp. 1-7.

Rubio-Caballero, J.M., Santamaría-González, J., Mérida-Robles, J., Moreno-Tost, R., Alonso-Castillo, M.L., Vereda-Alonso, E., Jiménez-López, A. and Maireles-Torres, P., 2013. Calcium zincate derived heterogeneous catalyst for biodiesel production by ethanolysis. *Fuel,* Volume 105, pp. 518-522.

Saka, S. and Kusdiana, D., 2001. Biodiesel fuel from rapeseed oil as prepared in supercritical methanol. *Fuel ,* Volume 80, pp. 225-231.

Santiago-Torres, N., Romero-Ibarra, I.C. and Pfeiffer, H., 2014. Sodium zirconate (Na2ZrO3) as a catalyst in a soybean oil transesterification reaction for biodiesel production. *Fuel Processing Technology,* Volume 120, pp. 34-39.

Satoshi, F., Hiromi, M. and Arata-Kazushi, A., 2004. Biodiesel fuel production with solid super acid catalysis in fixed bed reactor under atmospheric pressure. *Catalysis Communications,* Volume 5, pp. 721-723.

Scott, S.A., Davey, M.P. and Dennis, J.S., 2010. Biodiesel from algae: challenges and prospects. *Current Opinion in Biotechnology,* 21(3), p. 277–286.

Semwal, S., Arora, A.K., Badoni, R.P. and Tuli, D.K., 2011. Biodiesel production using heterogeneous catalysts. *Bioresource Technology,* Volume 102, pp. 2151-2161.

Shahraki, H., Entezari, M.H. and Goharshadi, E.K., 2015. Sono-synthesis of biodiesel from soybean oil by KF/γ-Al2O3 as a nano-solid-base catalyst. *Ultrasonics Sonochemistry,* Volume 23, pp. 266-274.

Sharifah, H., Nur Hanis, H., Azman, A., Roslan, U., Hafizan, J., Helena, K. and Azizah, E., 2017. A review of biomass-derived heterogeneous catalyst for a sustainable biodiesel production. *Renewable and Sustainable Energy Reviews,* Volume 70, pp. 1040-1051.

Sharma, S., Saxena, V., Baranwal, A., Chandra, P. and Pandey, L.M., 2018. Engineered nanoporous materials mediated heterogeneous catalysts and their implications in biodiesel production. *Materials Science for Energy Technologies,* Volume 1, pp. 11-21.

Sharma, Y.C. and Singh, B., 2009. Development of biodiesel: current scenario. *Renewable and Sustainable Energy Reviews,* Volume 13, pp. 1646-1651.

Sharma, Y.C., Singh, B. and Upadhyay, S.N. , 2008. Advancements in development and characterization of biodiesel: a review. *Fuel,* Volume 87, pp. 2355-2373.

Shu, Q., Gao, J., Nawaz, Z.,Liao, Y.,Wang, D. and Wang, J., 2010. Synthesis of biodiesel from waste vegetable oil with large amounts of free fatty acids using a carbon-based solid acid catalyst. *Applied Energy,* Volume 87, pp. 2589-2596.

Sindra, H., Sumbal, G., Tariq, M., Umar, N. and Hadayatullah, F., 2016. Biodiesel Production by using CaO-Al2O3 Nano Catalyst. *International Journal of Engineering Research & Science,* Volume 2, pp. 43-49.

Singh, B., Gulde, A., Rawat, I. and Bux, F., 2014. Towards a sustainable approach for development of biodiesel from plant and microalgae. *Renewable and Sustainable Energy Reviews,* Volume 29, pp. 216-245.

Singh, J. and Gu, S., 2010. Commercialization potential of microalgae for biofuels production. *Renewable and Sustainable Energy Reviews,* Volume 14, p. 1367.

Singh, S.P. and Singh, D., 2010. Biodiesel production through the use of different sources and characterization of oils and their esters as the substitute of diesel: a review. *Renewable and Sustainable Energy Reviews,* Volume 14, pp. 200-216.

Smith, S.M., Oopathum, C., Weeramongkhonlert, V., Smith, C.B., Chaveanghong, S., Ketwong, P. and Boonyuen, S., 2013. Transesterification of soybean oil using bovine bone waste as new catalyst. *Bioresource Technology,* Volume 143, pp. 686-690.

Soriano, N.U., Venditti, R. and Argyropoulos, D.S., 2009. Biodiesel synthesis via homogeneous Lewis acid-catalyzed transesterification. *Fuel,* Volume 88, pp. 560-565.

Su, C.H., 2013. Kinetic study of free fatty acid esterification reaction catalyzed by recoverable and reusable hydrochloric acid. *Bioresource Technology,* Volume 130, pp. 522-528.

Su, C.H., 2013. Recoverable and reusable hydrochloric acid used as a homogeneous catalyst for biodiesel production. *Applied Energy,* Volume 104, pp. 503-509.

Suarez, P.A.Z., Meneghetti, P.S.M., Meneghetti, M.R. and Wolf, C.R., 2007. Transformation of triglycerides into fuels, polymers and chemicals: some applications of catalysis in oleo chemistry. *Química Nova,* Volume 30, pp. 667-676.

Sulaiman, F., Abdullah, N., Gerhauser, H. and Shariff, A., 2011. An outlook of Malaysian energy,oil palm industry and its utilization of wastes as useful resources. *Biomass & Bioenergy,* Volume 35, pp. 3775-3786.

Sumathi, S., Chai, S. and Mohamed, A., 2018. Utilization of oil palm as a source of renewable energy in Malaysia. *Renewable and Sustainable Energy Reviews,* Volume 12, pp. 2404-2421.

Suryaputra, W., Winata, I., Indraswati, N. and Ismadji, S., 2013. Waste capiz (Amusium cristatum) shell as a new heterogeneous catalyst for biodiesel production. *Renewable Energy,* Volume 50, pp. 795-799.

Tahvildari, K., Anaraki, Y.N., Fazaeli, R., Mirpanji, S. and Delrisch, E., 2015. The study of CaO and MgO heterogenic nano-catalyst coupling on transesterification reaction efficacy in the production of biodiesel from reycled cooking oil. *Journal of Environmental Health Science & Engineering,* 13(73), pp. 1-9.

Takagaki, A., Toda, M., Okamura, M., Kondo, J.N., Hayashi, S., Domen, K. and Hara, M., 2006. Esterification of higher fatty acids by a novel strong solid acid. *Catalysis Today,* Volume 116, pp. 157-161.

Tan, K.T., Lee, K.T. and Mohamed, A.R., 2010. Effects of free fatty acids, water content and co-solvent on biodiesel production by supercritical methanol reaction. *Journal of Supercritical Fluids,* Volume 53, pp. 88-91.

Tangboriboon, N., Kunanuruksapong, R., and Sirivat, A., 2012. Preparation and properties of calcium oxide from eggshells via calcination. *Materials Science-Poland,* 30(4), pp. 313-322.

Tangy, A., Pulidindi, I.N., Perkas, N. and Gedanken, A., 2017. Continuous flow through a microwave oven for the large-scale production of biodiesel from waste cooking oil. *Bioresource Technology,* Volume 224, pp. 333-341.

Tariq, M., Ali, S. and Khalid, N., 2012. Activity of homogeneous and heterogeneous catalysts, spectroscopic and chromatographic characterization of biodiesel: a review. *Renewable and Sustainable Energy Reviews,* Volume 16, pp. 6303-6316.

Taufiq-Yap, Y. H., Nurul Suziana, N. M., and Hussein, M. Z., 2010. Influences of the Various Metal Dopants for the Nanosized Vanadium Phosphate Catalysts. *Catalysis Letters,* 141(1), pp. 136-148.

Thiam, L.C. and Bhatia, S., 2008. Catalytic processes towards the production of biofuels in a palm oil and oil palm biomass-based biorefinery. *Bioresource Technology,* Volume 99, pp. 7911-7922.

Tonetto, G.M. and Marchetti, J.M., 2010. Transesterification of soybean oil over Me/Al2O3 (Me=Na, Ba, Ca and K) catalysts and monolith K/Al2O3-cordierite. *Topics in Catalysis,* 53(11), pp. 755-762.

Trejo-Zárraga, F., Jesús Hernández-Loyo, F., Chavarría-Hernández, J.C. and Sotelo-Boyás, R., 2018. Kinetics of Transesterification Processes for Biodiesel Production. *Biofuels - State of Development,* pp. 149-179.

Uzun, B.B., Kılıç, M., Özbay, N., Pütün, A.E. and Pütün, E., 2012. Biodiesel production from waste frying oils: optimization of reaction parameters and determination of fuel properties. *Energy,* Volume 44, pp. 347-351.

Vicente, G., Martínez, M. and Aracil, J., 2007. Optimization of integrated biodiesel production part I: a study of the biodiesel purity and yields. *Bioresource Technology,* Volume 98, pp. 1724-1733.

Vieira, S.S., Magriotis, Z.M., Santos, N.A., Saczk, A.A., Hori, C.E. and Arroyo, P.A., 2013. Biodiesel production by free fatty acid esterification using Lanthanum (La3+) and HZSM-5 based catalysts. *Bioresource Technology,* Volume 133, pp. 248-255.

Viola, E., Blasi, A., Valerio, V., Guidi, I., Zimbardi, F., Braccio, G. and Giordano, G., 2012. Biodiesel from fried vegetable oils via transesterification by heterogeneous catalysis. *Catalysis Today,* Volume 179, pp. 185-190.

Viriya-empikul, N., Krasae, P., Nualpaeng, W., Yoosuk, B. and Faungnawakij, K., 2012. Biodiesel Production over Ca-Based Solid Catalyst Derived from Industrial Waste. *Fuel,* Volume 92, pp. 239-244.

Vitiyaa Selva Kumar, Lee, Z.H., Sim, J.H., Law, S.C. and Abdul Rahman Mohamed, 2019. Improved CO2 Sorption Performance of Calcium Oxide (CaO) Sorbent with Nickel Oxide Additive. *IOP Conf. Series: Earth and Environmental Science,* 268(012026), pp. 1-7.

Wang, L. and Yang, J., 2007. Transesterification of soybean oil with nano-MgO or not in supercritical and subcritical methanol. *Fuel,* Volume 86, pp. 328-333.

Wang, S.H., Wang, Y.B., Dai, Y.M. and Jehng, J.M., 2012. Preparation and characterization of hydrotalcite-like compounds containing transition metal as a solid base catalyst for the transesterification. *Applied Catalysis A: General,* Volume 439-440, pp. 135-141.

Wang, Y., Hu, S., Guan, Y., Wen, L. and Han, H., 2009. Preparation of mesoporous nanosized KF/CaO–MgO catalyst and its application for biodiesel production by transesterification. *Catalysis Letters,* Volume 131, pp. 574-578.

Wei, C., May, C.Y. and Board, M.P.O., 2018. Palm biodiesel development and its social and environment impacts in Malaysia. *Policy Dialogue on Biofuels in Asia: Benefits and Challenges,* Volume 14, p. 27.

Wen, L., Wang, Y., Lu, D., Hu, S. ang Han, H., 2010. Preparation of KF/CaO nanocatalyst and its application in biodiesel production from Chinese tallow seed oil. *Fuel,* Volume 89, pp. 2267-2271.

Xie, W. and Wang, T., 2013. Biodiesel production from soybean oil transesterification using tin oxide-supported WO3 catalysts. *Fuel Processing Technology,* Volume 109, pp. 150-155.

Xie, W. and Yang, D., 2012. Transesterification of soybean oil over WO3 supported on AlPO4 as a solid acid catalyst. *Bioresource Technology,* Volume 119, pp. 60-65.

Xue, J., Grift, T.E. ang Hansen, A.C., 2011. Effect of biodiesel on engine performances and emissions. *Renewable and Sustainable Energy Reviews,* Volume 15, pp. 1098-1116.

Yao, J., Ji, L., Sun, P., Zhang, L. and Xu, N., 2010. Low boiling point organic amine-catalyzed transesterification of cottonseed oil to biodiesel with trace amount of KOH as co-catalyst. *Fuel,* Volume 89, pp. 3871-3875.

Yong, W., Shiyi, O., Pengzhan, L., Feng, X. and Shuze, T., 2006. Comparison of two different processes to synthesize biodiesel by waste cooking oil. *Journal of Molecular Catalysis A: Chemical,* Volume 252, pp. 107-112.

Yoosuk, B., Udomsap, P., Puttasawat, B. and Krasae, P., 2010. Modification of calcite by hydration–dehydration method for heterogeneous biodiesel production process: The effects of water on properties and activity. *Chemical Engineering Journal,* Volume 162, pp. 135-141.

Yusuf, C., 2007. Biodiesel from microalgae. *Biotechnology Advances,* Volume 25, pp. 294-306.

Zabeti, M., Daud, W.M.A.W and Aroua, M.K., 2009. Activity of solid catalysts for biodiesel production: a review. *Fuel Processing Technology,* Volume 90, pp. 770-777.

Zabeti, M., Daud, W.M.A.W. and Aroua, M.K., 2009. Optimization of the Activity of CaO/Al2O3 Catalyst for Biodiesel Production Using Response Surface Methodology. *Applied Catalysis A: General,* 366(1), pp. 154-159.

Zhang, Y., Dube, M.A., McLean, D.D. and Kates, M., 2003. Biodiesel production from waste cooking oil: 1. Process design and technological assessment. *Bioresource Technology,* Volume 89, pp. 1-16.

Zhang, Y., Wong, W.T. and Yung, K.F., 2014. Biodiesel production via esterification of oleic acid catalyzed by chlorosulfonic acid modified zirconia. *Applied Energy,* Volume 116, pp. 191-198.

Zhao, L., Qui, W. and Stagg-Williams, S.M., 2013. Transesterification of canola oil catalyzed by tansesterification of canola oil catalyzed by nanopowder calcium oxide. *Fuel Processing Technology,* Volume 114, pp. 154-162.

APPENDICES

APPENDIX A: Experimental Procedures for Synthesising CaO-based Catalyst

Table A-1: Procedures for Treating Undoped CaO Catalyst via Hydration-Dehydration Method.

Step 1: Preparation of waste eggshell-derived CaO catalyst		
①**Washing** The waste eggshells are washed several times with distilled water.	②**Drying** The rinsed eggshells are dried in the oven overnight at 80 ℃.	③**Crushing and Grinding** The dried eggshells are then crushed and grinded into fine powders using mortar and pestle.

Step 1: Preparation of waste eggshell-derived CaO catalyst	
④Calcination The powdered eggshells are calcined in the furnace at 900 ℃ for 3 hours.	⑤Storing The calcined eggshells are kept in the crucible which is sealed with parafilm before placing it in the desiccator.

Step 2: Modification of undoped CaO catalyst
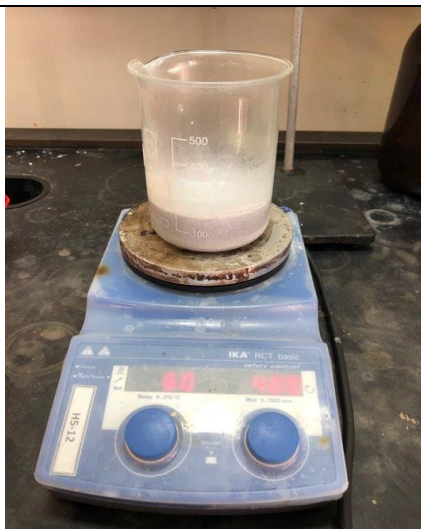
①**Hydration** 100 g of calcined CaO is refluxed in water with constant stirring speed on the hot plate at 60 ℃ for 4 hours.	②**Drying** The resulting slurry is filtered and dried in the oven overnight at 80 ℃.	③**Dehydration** The dried slurry is calcined in the furnace at 600 ℃ for 3 hours.	④**Storing** The calcined catalyst is kept in the crucible which is sealed with parafilm before placing it in the desiccator.

Table A-2: Procedures for Synthesising Ni Doped CaO Catalyst via Wet Impregnation Method.

Step 1: Preparation of waste eggshell-derived CaO catalyst

①Washing	**②Drying**	**③Crushing and Grinding**
The waste eggshells are washed several times with distilled water.	The cleaned eggshells are dried in the oven overnight at 80 ℃.	The dried eggshells are then crushed and grinded into fine powders using mortar and pestle.

Step 1: Preparation of waste eggshell-derived CaO catalyst

④Calcination

The powdered eggshells are placed in the furnace for calcination at 900 ℃ for 3 hours.

⑤Storing

The calcined eggshells are kept in the crucible which is sealed with parafilm before placing it in the desiccator.

Step 2: Synthesis of Ni doped CaO catalyst
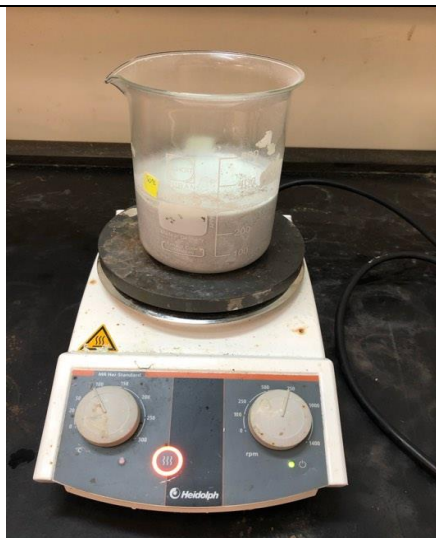
①**Wet Impregnation**	②**Drying**	③**Re-calcination**	④**Storing**
For 1 wt% Ni/CaO, approximately 96.89 g of calcined CaO and 3.11 g of $Ni(NO_3)_2$ are dissolved in deionised water, followed by mixing and stirring on the hot plate for 4 hours continuously at 80 ℃.	The resulting slurry is dried in the oven overnight at 80 ℃.	The dried slurry is recalcined in the furnace at 600 ℃ for 4 hours.	The calcined doped catalyst is kept in the crucible which is sealed with parafilm before placing it in the desiccator.
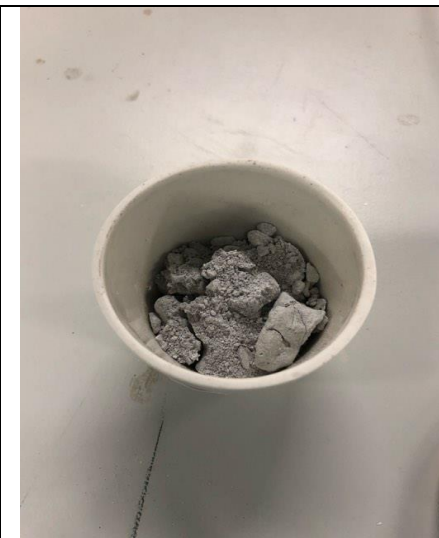
Table A-3: Procedures for Synthesising NiO Doped CaO Catalyst via Sol-Gel Method.
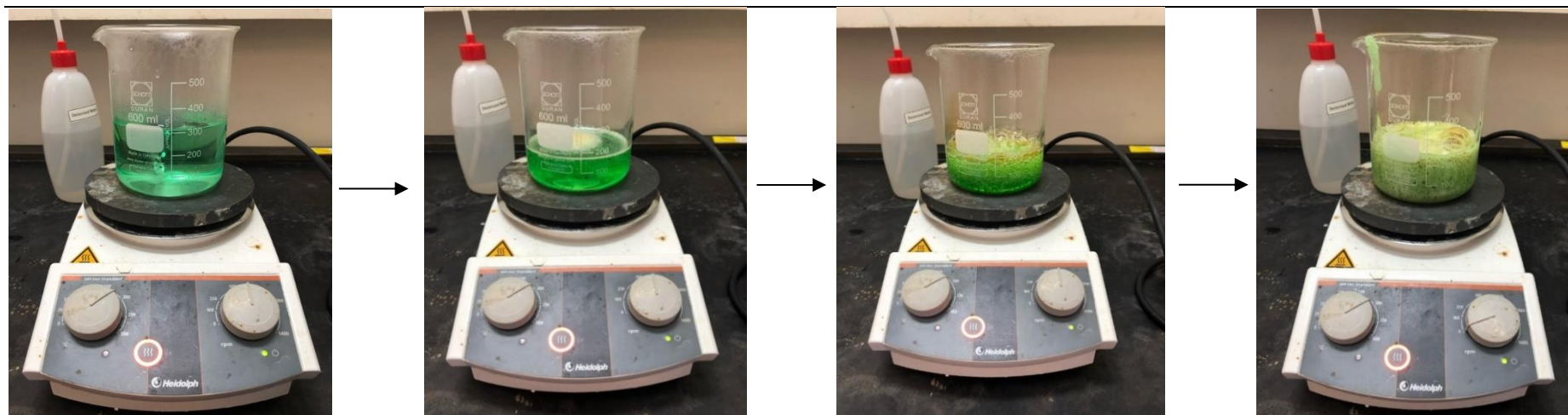
For 1 wt% NiO/CaO,

Step 1:

The predetermined amount of metal nitrate precursors and citric acid monohydrate are mixed before dissolving in deionised water as follows:

$Ni(NO_3)_2 \cdot 6H_2O = 3.89$ g

$Ca(NO_3)_2 \cdot 4H_2O = 96.11$ g

$C_6H_8O_7 \cdot H_2O = 119.60$ g
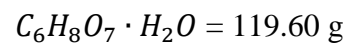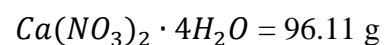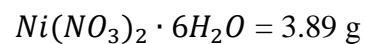
Deionised water = 159.35 mL

Step 2:

The mixture is stirred vigorously on the hot plate at 90 ℃ for 3 hours.

Step 3:

Approximately 17.11 mL of ammonia solution is added as a peptiser to the mixture.

Step 4:

The resulting gel is transferred immediately to the crucible before solidifying.

Step 5:

The gel is dried in the oven overnight at 80 ℃.

Step 6:

The dried product is sent to the furnace for calcination at 600 °C for 4 hours.

Step 7:

The calcined doped catalyst is kept in the crucible which is sealed with parafilm before placing it in the desiccator.

APPENDIX B: Experimental Set-Up for Transesterification Reaction

Figure B-1: Experimental Set-Up for Transesterification Reaction with Heating Mantle.
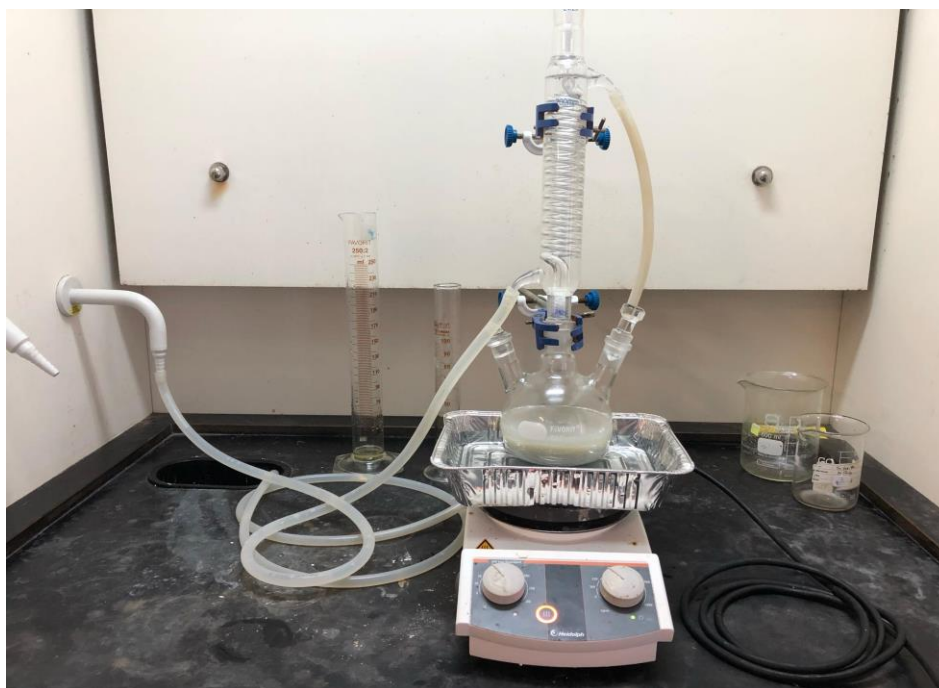
Figure B-2: Alternative Experimental Set-Up for Transesterification Reaction with Hot Plate.

APPENDIX C: Sample Calculation for Amount of Doped Catalyst Required

①Wet Impregnation Method

Basis: 100 g Ni/CaO

$Molecular\ weight\ of\ nickel(II)\ nitrate, Ni(NO_3)_2$

$= 58.69 + 2[14.01 + 3(16)]$

$= 182.71\ g/mol$

$Molecular\ weight\ of\ nickel, Ni = 58.69\ g/mol$

$$Percentage\ of\ Ni\ by\ weight\ in\ Ni(NO_3)_2 = \frac{58.69\ g/mol}{182.71\ g/mol} \times 100\ \%$$

$$= 32.12\ wt\%$$

For 1 wt% Ni doped CaO,

$$\frac{32.12}{100} = \frac{1\ g}{x_1}$$

$Mass\ of\ Ni(NO_3)_2, x_1 = 3.11\ g$

$Mass\ of\ CaO, y_1 = 96.89\ g$

For 2 wt% Ni doped CaO,

$$\frac{32.12}{100} = \frac{2\ g}{x_2}$$

$Mass\ of\ Ni(NO_3)_2, x_2 = 6.23\ g$

$Mass\ of\ CaO, y_2 = 93.77\ g$

For 3 wt% Ni doped CaO,

$$\frac{32.12}{100} = \frac{3\ g}{x_3}$$

$Mass\ of\ Ni(NO_3)_2, x_3 = 9.34\ g$

$Mass\ of\ CaO, y_3 = 90.66\ g$

For 4 wt% Ni doped CaO,

$$\frac{32.12}{100} = \frac{4\ g}{x_4}$$

Mass of $Ni(NO_3)_2, x_4 = 12.45\ g$

Mass of $CaO, y_4 = 87.55\ g$

For 5 wt% Ni doped CaO,

$$\frac{32.12}{100} = \frac{5\ g}{x_5}$$

Mass of $Ni(NO_3)_2, x_5 = 15.57\ g$

Mass of $CaO, y_5 = 84.43\ g$

②Sol-Gel Method

Basis: 100 g NiO/CaO

Molecular weight of calcium nitrate tetrahydrate, $Ca(NO_3)_2 \cdot 4H_2O$

$= 40.08 + 2[14.01 + 3(16)] + 4[2(1.01) + 16]$

$= 236.18\ g/mol$

Molecular weight of nickel(II)nitrate hexahydrate, $Ni(NO_3)_2 \cdot 6H_2O$

$= 58.69 + 2[14.01 + 3(16)] + 6[2(1.01) + 16]$

$= 290.83\ g/mol$

Molecular weight of nickel(II) oxide, $NiO = 58.69 + 16$

$$= 74.69\ g/mol$$

Percentage of NiO by weight in $Ni(NO_3)_2 \cdot 6H_2O$

$$= \frac{74.69\ g/mol}{290.83\ g/mol} \times 100\ \%$$

$= 25.68\ wt\%$

For 1 wt% NiO doped CaO,

$$\frac{25.68}{100} = \frac{1\ g}{x_1}$$

Mass of $Ni(NO_3)_2 \cdot 6H_2O, x_1 = 3.89\ g$

Mass of $Ca(NO_3)_2 \cdot 4H_2O, y_1 = 96.11\ g$

For 2 wt% NiO doped CaO,

$$\frac{25.68}{100} = \frac{2\ g}{x_2}$$

$Mass\ of\ Ni(NO_3)_2 \cdot 6H_2O, x_2 = 7.79\ g$

$Mass\ of\ Ca(NO_3)_2 \cdot 4H_2O, y_2 = 92.21\ g$

For 3 wt% NiO doped CaO,

$$\frac{25.68}{100} = \frac{3\ g}{x_3}$$

$Mass\ of\ Ni(NO_3)_2 \cdot 6H_2O, x_3 = 11.68\ g$

$Mass\ of\ Ca(NO_3)_2 \cdot 4H_2O, y_3 = 88.32\ g$

For 4 wt% NiO doped CaO,

$$\frac{25.68}{100} = \frac{4\ g}{x_4}$$

$Mass\ of\ Ni(NO_3)_2 \cdot 6H_2O, x_4 = 15.58\ g$

$Mass\ of\ Ca(NO_3)_2 \cdot 4H_2O, y_4 = 84.42\ g$

For 5 wt% NiO doped CaO,

$$\frac{25.68}{100} = \frac{5\ g}{x_5}$$

$Mass\ of\ Ni(NO_3)_2 \cdot 6H_2O, x_5 = 19.47\ g$

$Mass\ of\ Ca(NO_3)_2 \cdot 4H_2O, y_5 = 80.53\ g$

Note that

$Total\ mass\ of\ metal\ precursors\ [Ni(NO_3)_2 \cdot 6H_2O + Ca(NO_3)_2 \cdot 4H_2O]$
$= 100\ g$

$Mole\ of\ total\ metal\ precursor$
$$= \frac{Total\ mass\ of\ metal\ precursors}{Total\ molecular\ weight\ of\ metal\ precursors}$$
$$= \frac{100\ g}{(236.18 + 290.83)\ g/mol}$$
$$= 0.1897\ mol$$

Molar ratio of total metal precursor/acid $= 1:3$

$$\text{Mole of } C_6H_8O_7 \cdot H_2O = 0.1897 \, mol \times 3$$
$$= 0.5691 \, mol$$

$$\text{Molecular weight of } C_6H_8O_7 \cdot H_2O = 6(12.01) + 10(1.01) + 8(16)$$
$$= 210.16 \, g/mol$$

Mass of $C_6H_8O_7 \cdot H_2O$
$= \text{Mole of } C_6H_8O_7 \cdot H_2O \ \times \text{Molecular weight of } C_6H_8O_7 \cdot H_2O$
$= 0.5691 \, mol \times 210.16 \, g/mol$
$= 119.60 \, g$

Molar ratio of total metal precursor/water $= 1:45$

$$\text{Mole of deionised } H_2O = 0.1897 \, mol \times 45$$
$$= 8.5365 \, mol$$

$$\text{Molecular weight of deionised } H_2O = 2(1.01) + 16$$
$$= 18.02 \, g/mol$$

Mass of deionised H_2O
$= \text{Mole of deionised } H_2O \ \times \text{Molecular weight of deionised } H_2O$
$= 8.5365 \, mol \times 18.02 \, g/mol$
$= 153.83 \, g$

Volume of deionised H_2O
$$= \frac{\text{Mass of deionised } H_2O}{\text{Density of } H_2O \, @ \, 90 \, ^\circ C \, (Kumar, Abida \ and \ Ali, 2016)}$$
$$= \frac{153.83 \, g}{965.34 \, kg/m^3} \times \frac{1 \, kg}{1000 \, g} \times \frac{1000 \, L}{1 \, m^3} \times \frac{1000 \, mL}{1 \, L}$$
$$= 159.35 \, mL$$

$Molar\ ratio\ of\ total\ metal\ precursor/ammonia = 1:3$

$Mole\ of\ NH_3 = 0.1897\ mol \times 3$

$$= 0.5691\ mol$$

$Molecular\ weight\ of\ NH_3 = 14.01 + 3(1.01)$

$$= 17.04\ g/mol$$

$Mass\ of\ NH_3 = Mole\ of\ NH_3\ \times Molecular\ weight\ of\ NH_3$

$$= 0.5691\ mol \times 17.04\ g/mol$$

$$= 9.697\ g$$

$Volume\ of\ NH_3$

$$= \frac{Mass\ of\ NH_3}{Density\ of\ NH_3\ @\ 90\ ℃\ (Kumar, Abida\ and\ Ali, 2016)}$$

$$= \frac{9.697\ g}{0.5669\ g/mL}$$

$$= 17.11\ mL$$

APPENDIX D: Sample Calculation for Transesterification Reaction

Note that

$Volume\ of\ cooking\ oil\ (palm\ oil\text{-}based) = 200\ mL\ (fixed)$

$Density\ of\ palm\ oil\ @\ 60\ ℃ = 870.2\ kg/m^3$ (Kumar, Abida and Ali, 2016)

$Molecular\ weight\ of\ palm\ oil = 847.3\ g/mol$ (Baroutian, et al., 2009)

$$Mole\ of\ cooking\ oil = \frac{Density\ of\ palm\ oil \times Volume\ of\ cooking\ oil}{Molecular\ weight\ of\ palm\ oil}$$

$$= \frac{870.2\ kg/m^3 \times 200\ mL}{847.3\ g/mol} \times \frac{1000\ g}{1\ kg} \times \frac{1\ m^3}{1000\ L}$$

$$\times \frac{1\ L}{1000\ mL}$$

$$= 0.2054\ mol$$

$Methanol\text{-}to\text{-}oil\ molar\ ratio = 10{:}1$

$1\ mol\ oil : 10\ mol\ methanol$

$0.2054\ mol\ oil : x\ methanol$

$$Mole\ of\ methanol, x = \frac{0.2054 \times 10}{1}$$

$$= 2.054\ mol$$

$$Molecular\ weight\ of\ methanol, CH_3OH = 12.01 + 4(1.01) + 16$$

$$= 32.05\ g/mol$$

$Volume\ of\ methanol$

$$= \frac{Mole\ of\ methanol \times Molecular\ weight\ of\ methanol}{Density\ of\ methanol\ @\ 60\ ℃\ (Kumar, Abida\ and\ Ali, 2016)}$$

$$= \frac{2.054\ mol \times 32.05\ g/mol}{748.08\ kg/m^3} \times \frac{1\ kg}{1000\ g} \times \frac{1000\ L}{1\ m^3} \times \frac{1000\ mL}{1\ L}$$

$$= 88\ mL$$

Catalyst loading $= 5\ wt\%$ with respect to oil

Mass of catalyst

$= Mass\ fraction\ of\ catalyst \times Mole\ of\ cooking\ oil$

$\times Molecular\ weight\ of\ palm\ oil$

$= 0.05\ g/g \times 0.2054\ mol \times 847.3\ g/mol$

$= 8.702\ g$

APPENDIX E: Sample Calculation for Biodiesel Yield

The biodiesel yield can be calculated using the equation as follows:

$$Yield = \frac{Actual\ concentration\ of\ FAME}{Theoretical\ concentration\ of\ FAME} \times 100\ \%$$

The theoretical concentration of FAME can be computed using the information listed below:

- $Volume\ of\ cooking\ oil\ (palm\ oil\text{-}based) = 200\ mL$
- $Volume\ of\ methanol = 88\ mL$
- $Dilution\ factor = \frac{Final\ volume,\ V_f}{Initial\ volume,\ V_i}$

  ➤ $1\ mL\ biodiesel\ sample\ is\ diluted\ with\ 3\ mL\ hexane;\ D_1$

  ➤ $100\ \mu L\ resulting\ sample\ mixture\ is\ diluted\ with\ 200\ \mu L$ $internal\ standard;\ D_2$

  $\therefore Dilution\ factor = D_1 \times D_2$

  $$= \frac{4\ mL}{1\ mL} \times \frac{300\ \mu L}{100\ \mu L}$$

  $$= 4 \times 3 = 12$$

- $Density\ of\ palm\ oil\ @\ 60\ °C = 870.2\ kg/m^3$ (Kumar, Abida and Ali, 2016)
- $Molecular\ weight\ of\ palm\ oil = 847.3\ g/mol$ (Baroutian, et al., 2009)
- $Molecular\ weight\ of\ methyl\ ester$

  $= \frac{Total\ molecular\ weight\ of\ all\ methyl\ esters\ produced}{Total\ methyl\ esters\ produced}$

  ➤ $Molecular\ weight\ of\ methyl\ palmitate = 270.45\ g/mol$

  ➤ $Molecular\ weight\ of\ methyl\ stearate = 298.5\ g/mol$

  ➤ $Molecular\ weight\ of\ methyl\ oleate = 296.5\ g/mol$

  ➤ $Molecular\ weight\ of\ methyl\ linoleate = 294.5\ g/mol$ (Kumar, Abida and Ali, 2016)

$$\therefore Molecular\ weight\ of\ methyl\ ester$$

$$= \frac{(270.45 + 298.5 + 296.5 + 294.5)\ g/mol}{4}$$

$$= 289.99\ g/mol$$

i.   Theoretical Concentration of FAME

$Mass\ of\ cooking\ oil$

$= Density\ of\ palm\ oil \times Volume\ of\ cooking\ oil$

$$= 870.2\ \frac{kg}{m^3} \times 200\ mL\ \times \frac{1\ m^3}{1000\ L} \times \frac{1\ L}{1000\ mL} \times \frac{1000\ g}{1\ kg}$$

$$= 174.04\ g$$
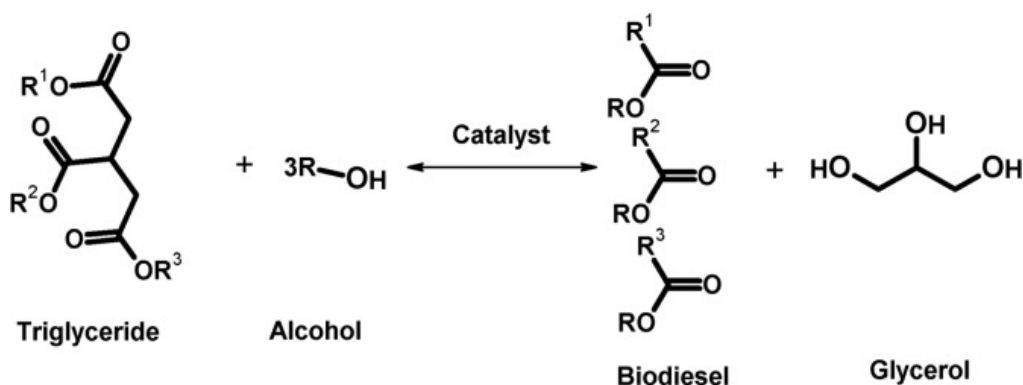
Figure E-1: Schematic Representation of Triglyceride Transesterification.

According to the equation in Figure E-1, one mole of triglyceride will react with three moles of methanol to produce three moles of FAME and one mole of glycerol.

$$Mole\ of\ cooking\ oil = \frac{Mass\ of\ cooking\ oil}{Molecular\ weight\ of\ palm\ oil}$$

$$= \frac{174.04\ g}{847.3\ g/mol}$$

$$= 0.2054\ mol$$

$Mole\ of\ FAME\ produced = 3 \times Mole\ of\ cooking\ oil$

$$= 3 \times 0.2054\ mol$$

$$= 0.6162\ mol$$

$Mass\ of\ FAME\ produced$

$= Mole\ of\ FAME \times Molecular\ weight\ of\ FAME$

$= 0.6162\ mol \times 289.99\ g/mol$

$= 178.70\ g$

$Theoretical\ concentration\ of\ FAME$

$$= \frac{Mass\ of\ FAME}{Volume\ of\ cooking\ oil + Volume\ of\ methanol}$$

$$= \frac{178.70\ g}{(200 + 88)\ mL} \times \frac{1000\ mL}{1\ L}$$

$$= 620.47\ g/L$$

ii.   Actual Concentration of FAME

The peak area of FAMEs present in the biodiesel sample are acquired via gas chromatography analysis before dividing by the peak area of internal standard to obtain the respective ratios, where they are treated as the response factor of FAMEs in internal standard. The concentration of each FAME is computed using the gradient of corresponding calibration curve, which is served as the response factor of FAME in external standard.

By taking transesterification catalysed by 1 wt% Ni doped CaO calcined at 600 °C (1-Ni/CaO-600) at first hour of reaction for sample calculation,

Table E-1: Data for Calculation of Biodiesel Yield.

Catalyst	Reaction Time (hr)	Methyl Ester	Peak Area (µV.s)	Methyl Ester/Internal Standard	Concentration (g/L)
1-Ni/CaO-600	1	Methyl Palmitate	36595.65	3.5288	170.41
		Methyl Stearate	4110.53	0.3964	20.18
		Methyl Oleate	43192.65	4.1650	202.18
		Methyl Linoleate	11291.46	1.0888	56.08
		Methyl Heptadecanoate (IS)	10370.45	-	-

Table E-2: Response Factor of Methyl Esters in External Standard.

Methyl Ester	Response Factor
Methyl Palmitate	0.2485
Methyl Stearate	0.2357
Methyl Oleate	0.2472
Methyl Linoleate	0.2330

$Concentration\ of\ methyl\ ester$

$= \dfrac{Response\ factor\ of\ methyl\ ester\ in\ internal\ standard}{Response\ factor\ of\ methyl\ ester\ in\ external\ standard}$

$\times Dilution\ factor$

$Concentration\ of\ methyl\ palmitate = \dfrac{3.5288}{0.2485} \times 12$

$= 170.41\ g/L$

$Concentration\ of\ methyl\ stearate = \dfrac{0.3964}{0.2357} \times 12$

$= 20.18\ g/L$

$Concentration\ of\ methyl\ oleate = \dfrac{4.1650}{0.2472} \times 12$

$= 202.18\ g/L$

$Concentration\ of\ methyl\ linoleate = \dfrac{1.0888}{0.2330} \times 12$

$= 56.08\ g/L$

$Actual\ concentration\ of\ FAME$

$= Total\ concentration\ of\ FAME$

$= (170.41 + 20.18 + 202.18 + 56.08)\ g/L$

$= 448.85\ g/L$

$$Yield = \frac{Actual\ concentration\ of\ FAME}{Theoretical\ concentration\ of\ FAME} \times 100\ \%$$

$$= \frac{448.85\ g/L}{620.47\ g/L} \times 100\ \%$$

$$= 72.34\ \%$$

The calculation is repeated for other synthesised catalysts as well as for every hour of reaction.

APPENDIX F: Calibration Curves for Methyl Esters
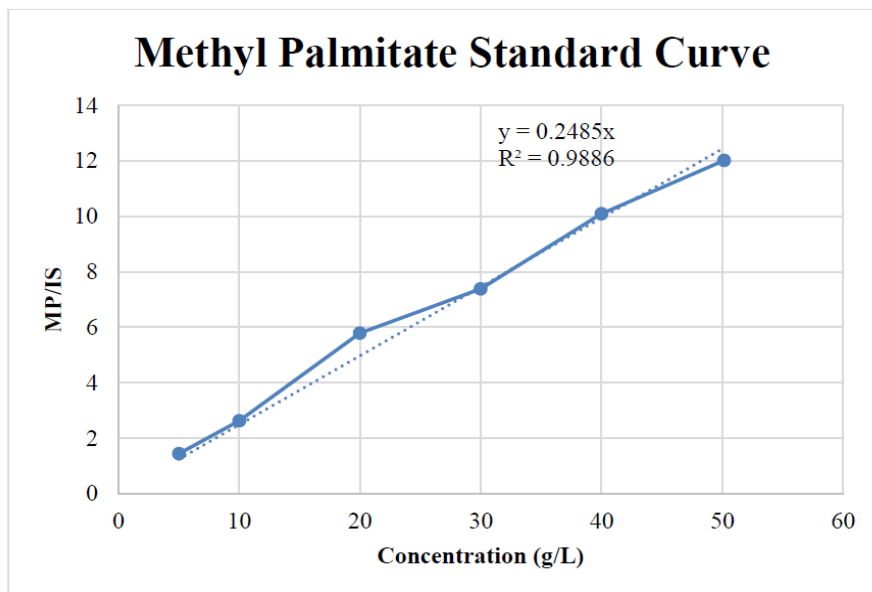
Figure F-1: Standard Curve of Methyl Palmitate.
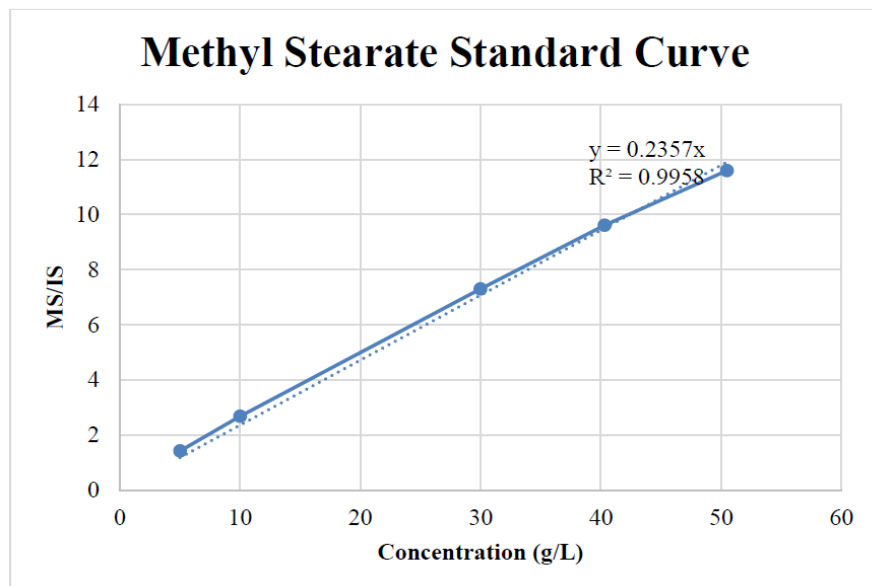
Figure F-2: Standard Curve of Methyl Stearate.
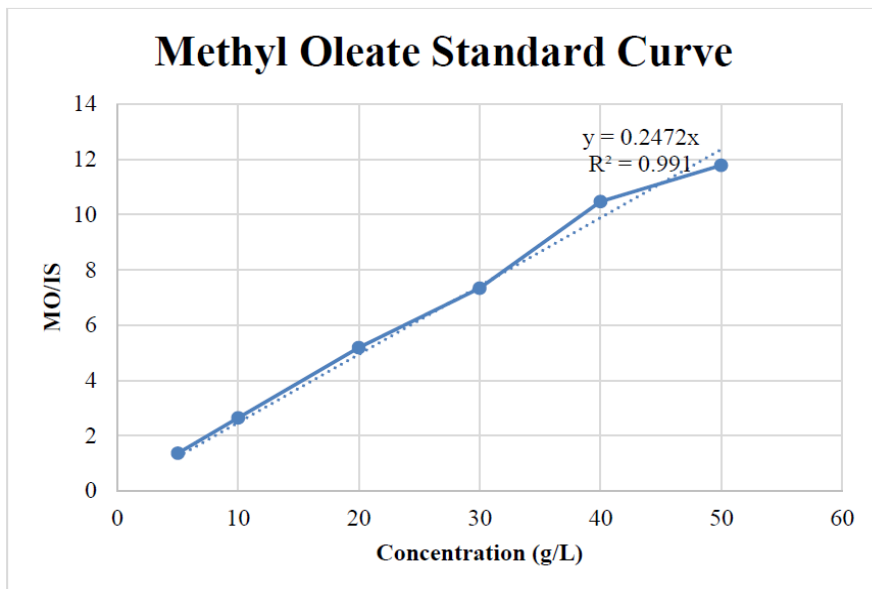
Figure F-3: Standard Curve of Methyl Oleate.
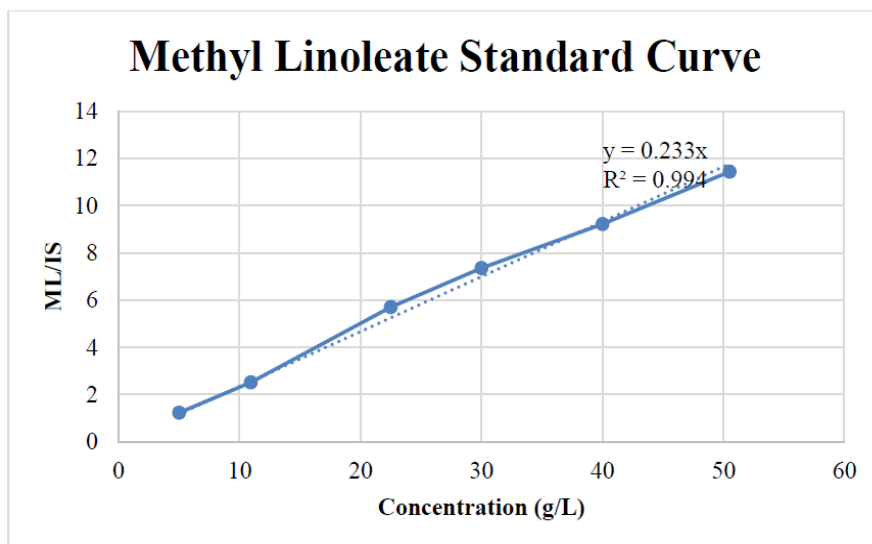
Figure F-4: Standard Curve of Methyl Linoleate.

APPENDIX G: Data from Gas Chromatography Analysis
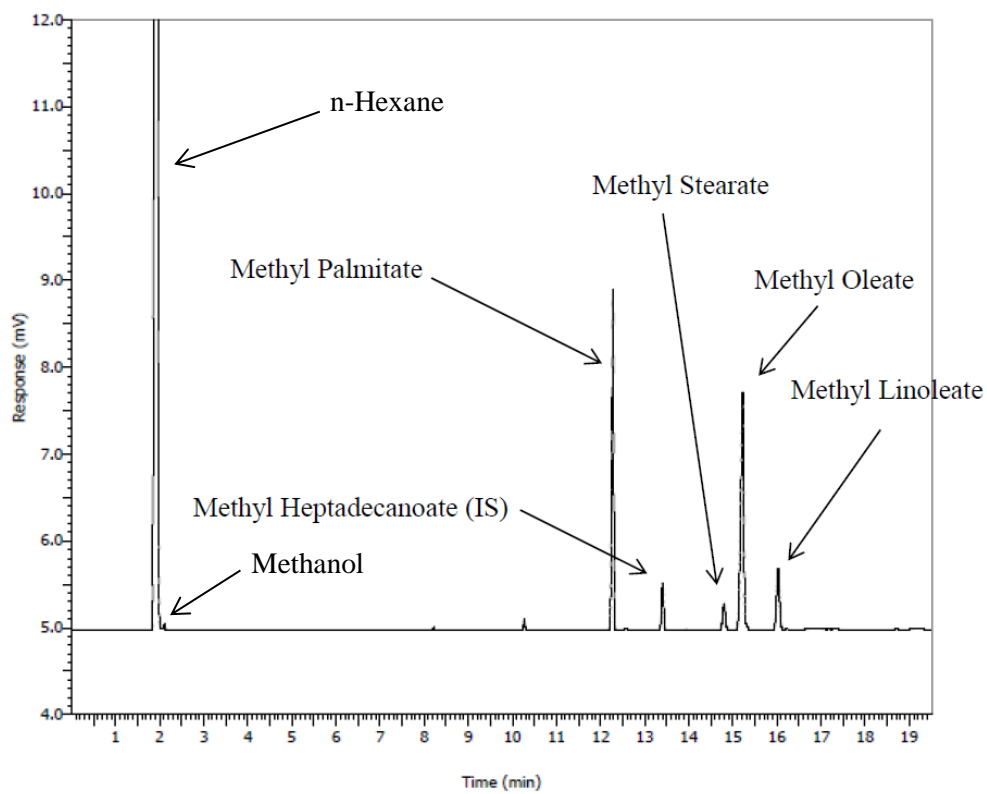
Figure G-1: Peak Locations of FAME from GC Analysis.

Table G-1: Data for Calculation of Biodiesel Yield.

Catalyst	Reaction Time (hr)	Methyl Ester	Peak Area (µV.s)	Methyl Ester/Internal Standard	Concentration (g/L)
1-NiO/CaO-600	1	Methyl Palmitate	29008.81	3.4197	165.14
		Methyl Stearate	5377.18	0.6339	32.27
		Methyl Oleate	20145.85	2.3749	115.29
		Methyl Linoleate	16715.47	1.9705	101.49
		Methyl Heptadecanoate (IS)	8482.84	-	-
					414.18
	2	Methyl Palmitate	9053.19	3.8353	185.21
		Methyl Stearate	836.17	0.3542	18.03
		Methyl Oleate	8982.01	3.8051	184.72
		Methyl Linoleate	2414.48	1.0229	52.68
		Methyl Heptadecanoate (IS)	2360.49	-	-
					440.64
	3	Methyl Palmitate	27481.58	4.2290	204.22
		Methyl Stearate	3791.95	0.5835	29.71
		Methyl Oleate	23888.09	3.6760	178.45
		Methyl Linoleate	10385.23	1.5981	82.31
		Methyl Heptadecanoate (IS)	6498.43	-	-
					494.68

Catalyst	Reaction Time (hr)	Methyl Ester	Peak Area (µV.s)	Methyl Ester/Internal Standard	Concentration (g/L)
Undoped CaO	1	Methyl Palmitate	25764.94	2.4448	118.06
		Methyl Stearate	7368.94	0.6992	35.60
		Methyl Oleate	30795.12	2.9221	141.85
		Methyl Linoleate	20491.92	1.9445	100.14
		Methyl Heptadecanoate (IS)	10538.63	-	-
					395.65
	2	Methyl Palmitate	22020.17	2.2921	110.68
		Methyl Stearate	7643.53	0.7956	40.51
		Methyl Oleate	31116.75	3.2390	157.23
		Methyl Linoleate	21322.53	2.2195	114.31
		Methyl Heptadecanoate (IS)	9606.99	-	-
					422.73
	3	Methyl Palmitate	22032.39	3.5696	172.37
		Methyl Stearate	3573.63	0.5790	29.48
		Methyl Oleate	20672.76	3.3493	162.59
		Methyl Linoleate	9970.45	1.6154	83.19
		Methyl Heptadecanoate (IS)	6172.29	-	-
					447.63

Catalyst	Reaction Time (hr)	Methyl Ester	Peak Area (µV.s)	Methyl Ester/Internal Standard	Concentration (g/L)
Treated CaO	1	Methyl Palmitate	51850.74	3.4541	166.80
		Methyl Stearate	5688.71	0.3790	19.29
		Methyl Oleate	63297.25	4.2166	204.69
		Methyl Linoleate	16002.48	1.0660	54.90
		Methyl Heptadecanoate (IS)	15011.47	-	-
					445.68
	2	Methyl Palmitate	59212.97	4.1049	198.22
		Methyl Stearate	8822.61	0.6116	31.14
		Methyl Oleate	47483.68	3.2918	159.79
		Methyl Linoleate	24674.08	1.7105	88.09
		Methyl Heptadecanoate (IS)	14425.00	-	-
					477.25
	3	Methyl Palmitate	34912.45	4.3862	211.81
		Methyl Stearate	3732.02	0.4689	23.87
		Methyl Oleate	39665.23	4.9834	241.91
		Methyl Linoleate	10372.15	1.3031	67.11
		Methyl Heptadecanoate (IS)	7959.53	-	-
					544.71

Catalyst	Reaction Time (hr)	Methyl Ester	Peak Area (µV.s)	Methyl Ester/Internal Standard	Concentration (g/L)
1-Ni/CaO-600	1	Methyl Palmitate	36595.65	3.5288	170.41
		Methyl Stearate	4110.53	0.3964	20.18
		Methyl Oleate	43192.65	4.1650	202.18
		Methyl Linoleate	11291.46	1.0888	56.08
		Methyl Heptadecanoate (IS)	10370.45	-	-
					448.85
	2	Methyl Palmitate	36607.05	4.2516	205.31
		Methyl Stearate	4025.63	0.4675	23.80
		Methyl Oleate	42282.26	4.9107	238.38
		Methyl Linoleate	11009.46	1.2787	65.85
		Methyl Heptadecanoate (IS)	8610.21	-	-
					533.35
	3	Methyl Palmitate	7277.77	5.0829	245.45
		Methyl Stearate	630.61	0.4404	22.42
		Methyl Oleate	7292.95	5.0935	247.26
		Methyl Linoleate	1926.57	1.3455	69.30
		Methyl Heptadecanoate (IS)	1431.82	-	-
					584.43

Catalyst	Reaction Time (hr)	Methyl Ester	Peak Area (μV.s)	Methyl Ester/Internal Standard	Concentration (g/L)
1-Ni/CaO-700	1	Methyl Palmitate	1139.99	4.5673	220.55
		Methyl Stearate	0.00	0.0000	0.00
		Methyl Oleate	762.11	3.0533	148.22
		Methyl Linoleate	133.50	0.5349	27.55
		Methyl Heptadecanoate (IS)	249.60	-	-
					396.32
	2	Methyl Palmitate	44833.95	4.2273	204.14
		Methyl Stearate	4960.39	0.4677	23.81
		Methyl Oleate	51853.56	4.8892	237.34
		Methyl Linoleate	13577.91	1.2802	65.94
		Methyl Heptadecanoate (IS)	10605.71	-	-
					531.23
	3	Methyl Palmitate	45226.54	4.5602	220.21
		Methyl Stearate	5002.41	0.5044	25.68
		Methyl Oleate	52819.08	5.3258	258.53
		Methyl Linoleate	13787.56	1.3902	71.60
		Methyl Heptadecanoate (IS)	9917.66	-	-
					576.02

Catalyst	Reaction Time (hr)	Methyl Ester	Peak Area (μV.s)	Methyl Ester/Internal Standard	Concentration (g/L)
1-Ni/CaO-800	1	Methyl Palmitate	37342.78	3.9162	189.11
		Methyl Stearate	4052.68	0.4250	21.64
		Methyl Oleate	23375.62	2.4515	119.00
		Methyl Linoleate	11039.08	1.1577	59.62
		Methyl Heptadecanoate (IS)	9535.37	-	-
					389.38
	2	Methyl Palmitate	21500.01	3.7857	182.81
		Methyl Stearate	2182.70	0.3843	19.57
		Methyl Oleate	25373.89	4.4678	216.88
		Methyl Linoleate	6117.49	1.0772	55.48
		Methyl Heptadecanoate (IS)	5679.30	-	-
					474.73
	3	Methyl Palmitate	40466.70	3.4868	168.38
		Methyl Stearate	6851.03	0.5903	30.05
		Methyl Oleate	41412.29	3.5683	173.22
		Methyl Linoleate	18655.24	1.6074	82.79
		Methyl Heptadecanoate (IS)	11605.65	-	-
					454.44

Catalyst	Reaction Time (hr)	Methyl Ester	Peak Area (µV.s)	Methyl Ester/Internal Standard	Concentration (g/L)
1-Ni/CaO-900	1	Methyl Palmitate	33942.01	3.9436	190.43
		Methyl Stearate	3795.39	0.4410	22.45
		Methyl Oleate	25467.26	2.9589	143.64
		Methyl Linoleate	10532.61	1.2237	63.03
		Methyl Heptadecanoate (IS)	8606.89	-	-
					419.55
	2	Methyl Palmitate	42946.73	3.5865	173.19
		Methyl Stearate	8591.78	0.7175	36.53
		Methyl Oleate	38451.73	3.2111	155.88
		Methyl Linoleate	14844.29	1.2396	63.84
		Methyl Heptadecanoate (IS)	11974.66	-	-
					429.44
	3	Methyl Palmitate	43387.04	2.7300	131.83
		Methyl Stearate	12065.50	0.7592	38.65
		Methyl Oleate	26603.82	1.6739	81.26
		Methyl Linoleate	38394.60	2.4158	124.42
		Methyl Heptadecanoate (IS)	15892.89	-	-
					376.16

Catalyst	Reaction Time (hr)	Methyl Ester	Peak Area (µV.s)	Methyl Ester/Internal Standard	Concentration (g/L)
2-Ni/CaO-600	1	Methyl Palmitate	22040.18	3.2499	156.94
		Methyl Stearate	2346.26	0.3460	17.61
		Methyl Oleate	25337.71	3.7362	181.37
		Methyl Linoleate	6600.00	0.9732	50.12
		Methyl Heptadecanoate (IS)	6781.72	-	-
					406.04
	2	Methyl Palmitate	34184.44	3.9620	191.32
		Methyl Stearate	3870.63	0.4486	22.84
		Methyl Oleate	40496.42	4.6936	227.84
		Methyl Linoleate	10598.69	1.2284	63.26
		Methyl Heptadecanoate (IS)	8628.09	-	-
					505.27
	3	Methyl Palmitate	30472.47	4.5609	220.25
		Methyl Stearate	3353.86	0.5020	25.56
		Methyl Oleate	35335.97	5.2888	256.74
		Methyl Linoleate	9251.24	1.3847	71.31
		Methyl Heptadecanoate (IS)	6681.22	-	-
					573.86

Catalyst	Reaction Time (hr)	Methyl Ester	Peak Area (µV.s)	Methyl Ester/Internal Standard	Concentration (g/L)
3-Ni/CaO-600	1	Methyl Palmitate	27474.17	3.2853	158.65
		Methyl Stearate	2880.79	0.3445	17.54
		Methyl Oleate	30715.88	3.6729	178.30
		Methyl Linoleate	8029.82	0.9602	49.45
		Methyl Heptadecanoate (IS)	8362.78	-	-
					403.93
	2	Methyl Palmitate	27922.45	3.9054	188.59
		Methyl Stearate	2808.56	0.3928	20.00
		Methyl Oleate	31159.55	4.3581	211.56
		Methyl Linoleate	8145.84	1.1393	58.68
		Methyl Heptadecanoate (IS)	7149.72	-	-
					478.83
	3	Methyl Palmitate	43886.93	5.9421	286.94
		Methyl Stearate	4726.61	0.6400	32.58
		Methyl Oleate	1621.71	0.2196	10.66
		Methyl Linoleate	13038.39	1.7653	90.92
		Methyl Heptadecanoate (IS)	7385.76	-	-
					421.10

Catalyst	Reaction Time (hr)	Methyl Ester	Peak Area (µV.s)	Methyl Ester/Internal Standard	Concentration (g/L)
4-Ni/CaO-600	1	Methyl Palmitate	32646.10	3.2222	155.60
		Methyl Stearate	6201.15	0.6121	31.16
		Methyl Oleate	30899.61	3.0498	148.05
		Methyl Linoleate	17811.99	1.7581	90.54
		Methyl Heptadecanoate (IS)	10131.52	-	-
					425.36
	2	Methyl Palmitate	22447.04	2.5616	123.70
		Methyl Stearate	6890.91	0.7864	40.04
		Methyl Oleate	31398.99	3.5831	173.94
		Methyl Linoleate	19085.10	2.1779	112.17
		Methyl Heptadecanoate (IS)	8762.96	-	-
					449.84
	3	Methyl Palmitate	20652.82	3.8544	186.13
		Methyl Stearate	8820.35	1.6461	83.81
		Methyl Oleate	1683.87	0.3143	15.26
		Methyl Linoleate	20503.39	3.8265	197.07
		Methyl Heptadecanoate (IS)	5358.25	-	-
					482.26

Catalyst	Reaction Time (hr)	Methyl Ester	Peak Area (µV.s)	Methyl Ester/Internal Standard	Concentration (g/L)
5-Ni/CaO-600	1	Methyl Palmitate	32458.18	3.8097	183.97
		Methyl Stearate	3653.73	0.4289	21.83
		Methyl Oleate	38336.31	4.4997	218.43
		Methyl Linoleate	10038.83	1.1783	60.68
		Methyl Heptadecanoate (IS)	8519.83	-	-
					484.92
	2	Methyl Palmitate	22767.38	3.9947	192.90
		Methyl Stearate	2421.80	0.4249	21.63
		Methyl Oleate	25514.53	4.4767	217.32
		Methyl Linoleate	6697.79	1.1752	60.52
		Methyl Heptadecanoate (IS)	5699.39	-	-
					492.38
	3	Methyl Palmitate	20159.71	3.5513	171.49
		Methyl Stearate	2218.49	0.3908	19.90
		Methyl Oleate	23512.71	4.1419	201.06
		Methyl Linoleate	6121.19	1.0783	55.53
		Methyl Heptadecanoate (IS)	5676.78	-	-
					447.98

Table G-2: Data for Calculation of Biodiesel Yield.

Catalyst	Reaction Time (hr)	Theoretical Concentration of FAME (g/L)	Actual Concentration of FAME (g/L)	Biodiesel Yield (%)
1-NiO/CaO-600	1		414.18	**66.75**
	2	620.47	440.64	**71.02**
	3		494.68	**79.73**
Undoped CaO	1		395.65	**63.77**
	2	620.47	422.73	**68.13**
	3		447.63	**72.14**
Treated CaO	1		445.68	**71.83**
	2	620.47	477.25	**76.92**
	3		544.71	**87.79**
1-Ni/CaO-600	1		448.85	**72.34**
	2	620.47	533.35	**85.96**
	3		584.43	**94.19**
1-Ni/CaO-700	1		396.32	**63.87**
	2	620.47	531.23	**85.62**
	3		576.02	**92.84**
1-Ni/CaO-800	1		389.38	**62.76**
	2	620.47	474.73	**76.51**
	3		454.44	**73.24**
1-Ni/CaO-900	1		419.55	**67.62**
	2	620.47	429.44	**69.21**
	3		376.16	**60.63**

Catalyst	Reaction Time (hr)	Theoretical Concentration of FAME (g/L)	Actual Concentration of FAME (g/L)	Biodiesel Yield (%)
2-Ni/CaO-600	1		406.04	**65.44**
	2	620.47	505.27	**81.43**
	3		573.86	**92.49**
3-Ni/CaO-600	1		403.93	**65.10**
	2	620.47	478.83	**77.17**
	3		421.10	**67.87**
4-Ni/CaO-600	1		425.36	**68.55**
	2	620.47	449.84	**72.50**
	3		482.26	**77.73**
5-Ni/CaO-600	1		484.92	**78.15**
	2	620.47	492.38	**79.36**
	3		447.98	**72.20**

APPENDIX H: GC Analysis Report

It is noted that the GC analysis reports on the FAMEs produced after three hours of transesterification reaction for all the synthesised catalysts will only be attached.

DEFAULT REPORT

Peak #	Time [min]	Area [µV·s]	Height [µV]	Area [%]	Norm. Area [%]	BL	Area/Height [s]
1	1.836	1008059.32	644584.02	91.55	91.55	BB	1.5639
2	2.022	333.74	173.46	0.03	0.03	BB	1.9240
3	8.101	261.70	119.87	0.02	0.02	BB	2.1833
4	10.154	845.32	358.32	0.08	0.08	BB	2.3591
5	12.177	22032.39	8837.80	2.91	2.91	BB	3.6245
6	12.422	140.53	56.11	0.01	0.01	BB	2.5046
7	13.257	6172.29	1791.74	0.56	0.56	BB	3.4449
8	14.655	3573.63	776.11	0.32	0.32	BB	4.6045
9	15.060	20672.76	6236.68	3.60	3.60	BB	6.3612
10	15.781	9970.45	2058.10	0.91	0.91	BB	4.8445
		1101062.13	664992.21	100.00	100.00		
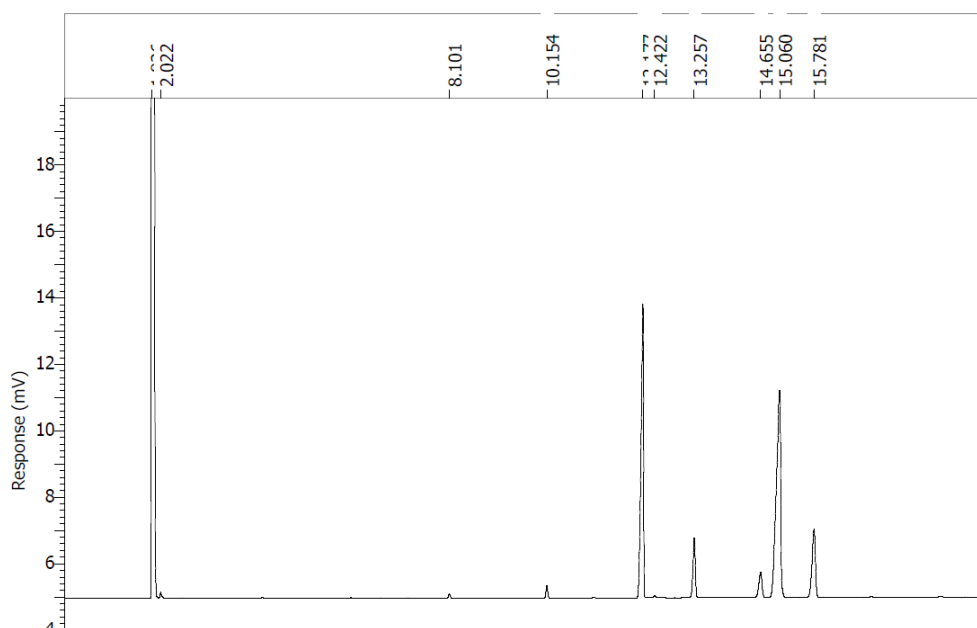
Figure H-1: Peak Report and GC Chromatogram of Undoped CaO.

DEFAULT REPORT

Peak #	Time [min]	Area [µV·s]	Height [µV]	Area [%]	Norm. Area [%]	BL	Area/Height [s]
1	1.830	1185378.51	807084.53	92.36	92.36	BB	1.4687
2	2.019	139.71	100.17	0.01	0.01	BB	1.3947
3	4.174	69.15	36.96	0.01	0.01	BB	1.8710
4	8.136	263.62	116.14	0.02	0.02	BB	2.2699
5	10.199	811.26	333.25	0.06	0.06	BB	2.4344
6	12.242	34912.45	9234.33	2.72	2.72	BB	3.7807
7	12.490	146.37	57.86	0.01	0.01	BB	2.5295
8	13.341	7959.53	2170.83	0.62	0.62	BB	3.6666
9	14.746	3732.02	750.92	0.29	0.29	BB	4.9699
10	15.161	39665.23	6338.27	3.09	3.09	BB	6.2581
11	15.900	10372.15	2075.26	0.81	0.81	BB	4.9980
		1283450.00	828298.51	100.00	100.00		
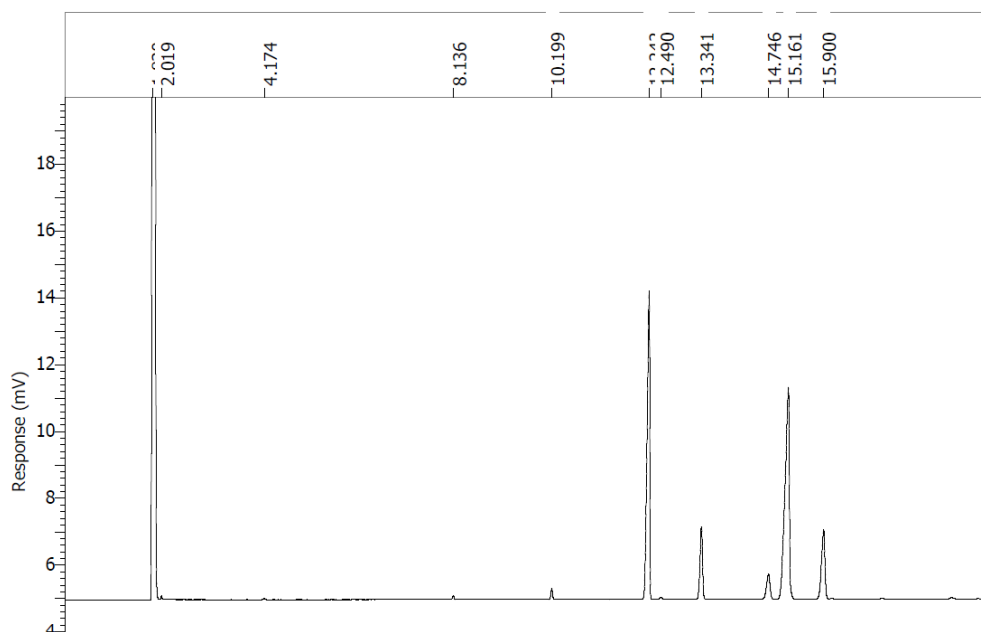
Figure H-2: Peak Report and GC Chromatogram of Treated CaO.

DEFAULT REPORT

Peak #	Time [min]	Area [μV·s]	Height [μV]	Area [%]	Norm. Area [%]	BL	Area/Height [s]
1	1.851	275362.27	239870.37	55.15	55.15	BV	1.1480
2	1.878	205054.98	99341.06	41.07	41.07	VB	2.0642
3	2.034	32.74	26.18	0.01	0.01	BB	1.2507
4	8.127	67.29	32.30	0.01	0.01	BB	2.0831
5	10.184	189.99	83.45	0.04	0.04	BB	2.2766
6	12.173	7277.77	2654.84	1.46	1.46	BB	2.7413
7	13.294	1431.82	441.32	0.29	0.29	BB	3.2444
8	14.670	630.61	161.90	0.13	0.13	BB	3.8950
9	15.043	7292.95	1647.57	1.46	1.46	BB	4.4265
10	15.828	1926.57	412.11	0.39	0.39	BB	4.6749
		499266.99	344671.10	100.00	100.00		
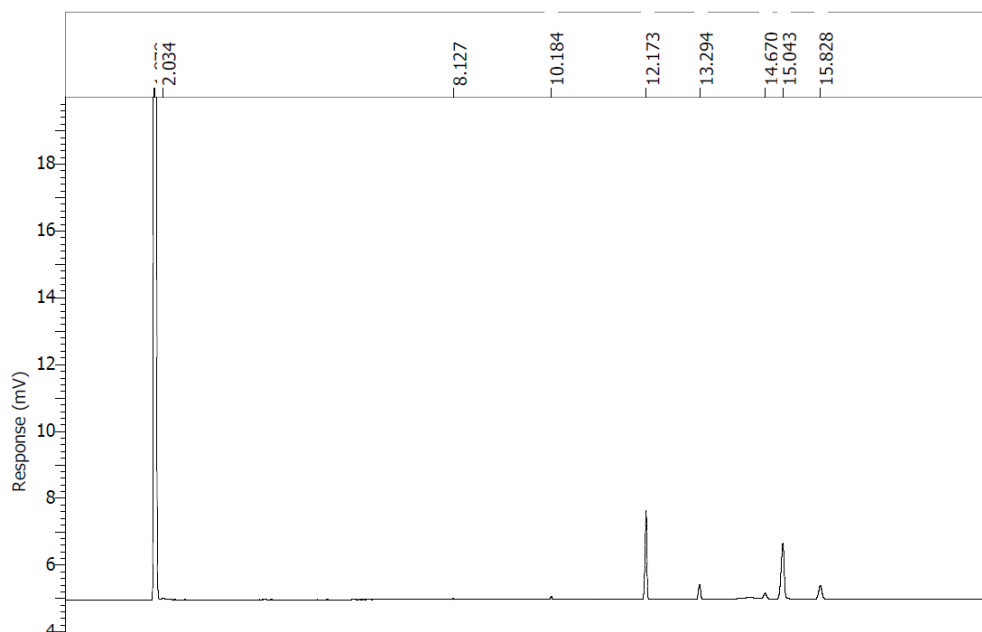
Figure H-3: Peak Report and GC Chromatogram of 1-Ni/CaO-600.

DEFAULT REPORT

Peak #	Time [min]	Area [μV·s]	Height [μV]	Area [%]	Norm. Area [%]	BL	Area/Height [s]
1	1.844	1345755.39	947933.08	91.26	91.26	BB	1.4197
2	2.035	247.61	163.64	0.02	0.02	BB	1.5132
3	4.182	82.56	45.87	0.01	0.01	BB	1.8000
4	8.131	331.60	152.25	0.02	0.02	BB	2.1780
5	10.191	1017.93	434.72	0.07	0.07	BB	2.3416
6	12.245	45226.54	11230.84	3.07	3.07	BB	4.0270
7	12.483	191.03	75.62	0.01	0.01	BB	2.5260
8	13.332	9917.66	2733.99	0.67	0.67	BB	3.6275
9	14.747	5002.41	981.22	0.34	0.34	BB	5.0982
10	15.173	52819.08	7572.65	3.58	3.58	BB	6.9750
11	15.899	13787.56	2668.42	0.93	0.93	BB	5.1669
12	18.556	263.33	50.17	0.02	0.02	BB	5.2488
		1474642.71	974042.46	100.00	100.00		
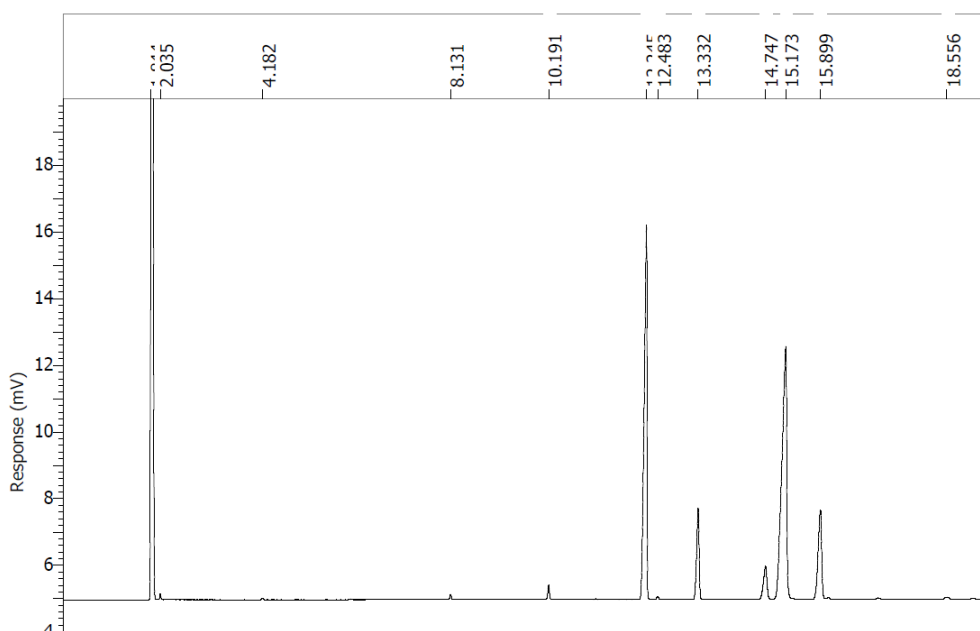
Figure H-4: Peak Report and GC Chromatogram of 1-Ni/CaO-700.

DEFAULT REPORT

Peak #	Time [min]	Area [µV·s]	Height [µV]	Area [%]	Norm. Area [%]	BL	Area/Height [s]
1	1.840	721040.16	756013.79	43.95	43.95	BV	0.9537
2	1.857	744917.13	659217.31	45.41	45.41	VE	1.1300
3	1.903	1955.32	1923.78	0.12	0.12	EB	1.0164
4	2.031	636.83	309.47	0.04	0.04	BB	2.0578
5	4.181	117.30	61.46	0.01	0.01	BB	1.9087
6	6.033	59.72	30.46	0.00	0.00	BB	1.9607
7	8.105	440.13	201.06	0.03	0.03	BB	2.1891
8	10.152	1373.86	578.87	0.08	0.08	BB	2.3734
9	11.134	57.16	26.09	0.00	0.00	BB	2.1910
10	12.208	40466.70	13390.85	3.69	3.69	BB	4.5155
11	12.427	256.77	100.98	0.02	0.02	BB	2.5429
12	13.270	11605.65	3146.61	0.71	0.71	BB	3.6883
13	14.691	6851.03	1286.76	0.42	0.42	BB	5.3243
14	15.113	41412.29	9242.49	4.33	4.33	BB	7.6941
15	15.811	18655.24	3463.29	1.14	1.14	BV	5.3866
16	15.966	227.97	54.76	0.01	0.01	VB	4.1629
17	16.994	202.14	46.60	0.01	0.01	BB	4.3377
18	18.436	472.40	80.42	0.03	0.03	BB	5.8743
		1640447.80	1.45e+06	100.00	100.00		
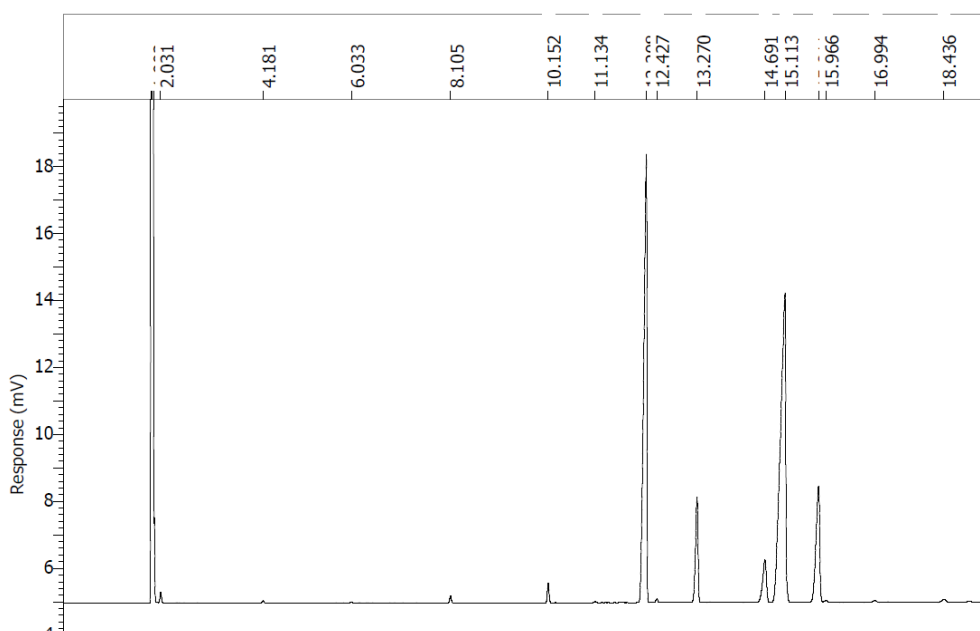
Figure H-5: Peak Report and GC Chromatogram of 1-Ni/CaO-800.

DEFAULT REPORT

Peak #	Time [min]	Area [µV·s]	Height [µV]	Area [%]	Norm. Area [%]	BL	Area/Height [s]
1	1.821	1479454.58	984404.53	82.78	82.78	BB	1.5029
2	4.165	172.13	91.36	0.01	0.01	BB	1.8840
3	6.029	119.64	58.17	0.01	0.01	BB	2.0568
4	8.109	931.69	414.24	0.05	0.05	BB	2.2491
5	10.167	2778.22	1108.56	0.16	0.16	BB	2.5061
6	11.150	116.28	47.22	0.01	0.01	BB	2.4625
7	12.273	43387.04	19255.63	6.34	6.34	BB	5.8885
8	12.464	479.05	181.13	0.03	0.03	BB	2.6448
9	13.307	15892.89	3886.42	0.89	0.89	BB	4.0893
10	14.785	12065.50	1857.52	0.68	0.68	BV	6.4955
11	15.218	26603.82	12680.92	7.08	7.08	VB	9.9838
12	15.900	38394.60	5420.83	1.87	1.87	BE	6.1604
13	16.025	427.28	110.72	0.02	0.02	EB	3.8591
14	17.041	433.11	90.84	0.02	0.02	BB	4.7681
15	18.488	912.74	143.25	0.05	0.05	BB	6.3714
		1787168.58	1.03e+06	100.00	100.00		
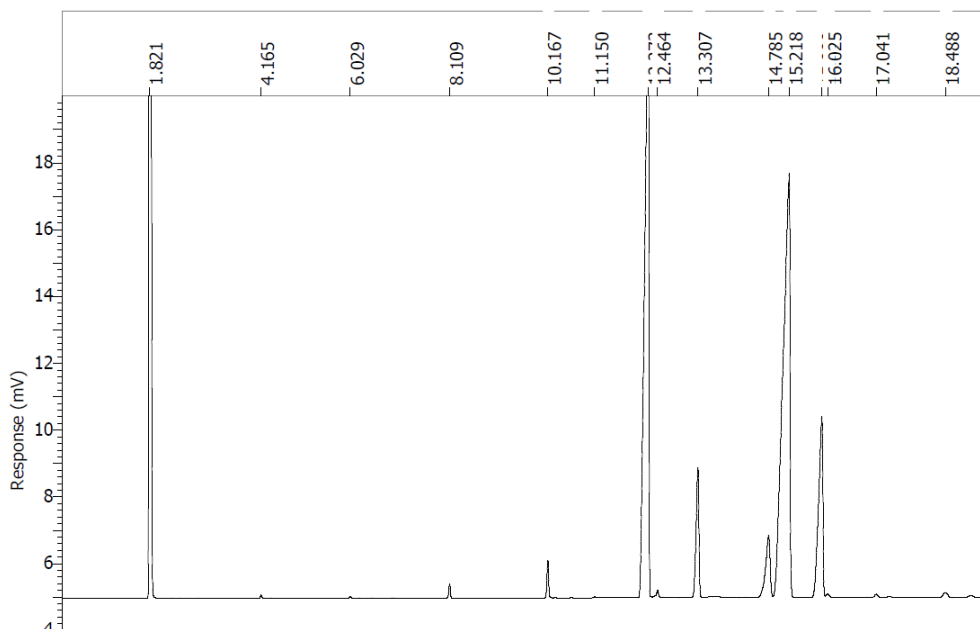
Figure H-6: Peak Report and GC Chromatogram of 1-Ni/CaO-900.

DEFAULT REPORT

Peak #	Time [min]	Area [µV·s]	Height [µV]	Area [%]	Norm. Area [%]	BL	Area/Height [s]
1	1.831	847473.44	692747.55	77.21	77.21	BE	1.2234
2	1.866	163108.97	74057.45	14.86	14.86	EV	2.2025
3	2.018	754.99	416.82	0.07	0.07	VB	1.8113
4	4.174	65.32	35.66	0.01	0.01	BB	1.8318
5	8.106	246.19	110.44	0.02	0.02	BB	2.2292
6	10.156	717.83	302.48	0.07	0.07	BB	2.3732
7	12.177	30472.47	8576.36	2.78	2.78	BB	3.5531
8	12.422	125.43	50.10	0.01	0.01	BB	2.5034
9	13.261	6681.22	1908.93	0.61	0.61	BB	3.5000
10	14.650	3353.86	727.90	0.31	0.31	BB	4.6076
11	15.051	35335.97	5856.69	3.22	3.22	BB	6.0334
12	15.780	9251.24	1877.55	0.84	0.84	BB	4.9273
		1097586.92	786667.94	100.00	100.00		
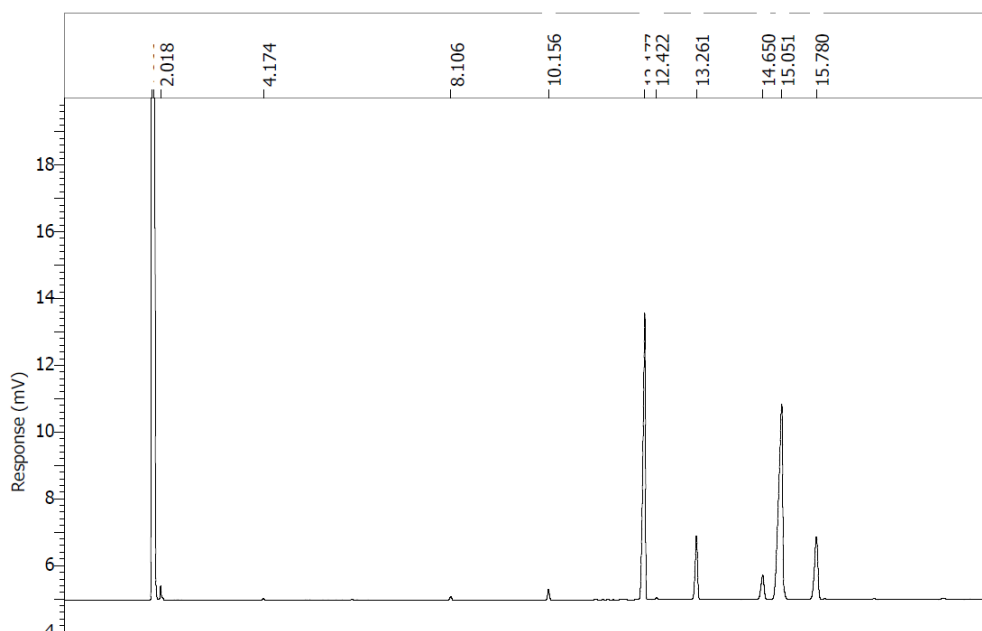
Figure H-7: Peak Report and GC Chromatogram of 2-Ni/CaO-600.

DEFAULT REPORT

Peak #	Time [min]	Area [µV·s]	Height [µV]	Area [%]	Norm. Area [%]	BL	Area/Height [s]
1	1.847	1174048.04	747632.43	94.15	94.15	BV	1.5704
2	2.034	624.45	306.43	0.05	0.05	VB	2.0378
3	4.182	94.14	48.20	0.01	0.01	BB	1.9532
4	8.134	338.20	152.14	0.03	0.03	BB	2.2230
5	10.196	1032.47	429.18	0.08	0.08	BB	2.4057
6	12.251	43886.93	10796.69	3.52	3.52	BB	4.0648
7	12.489	186.99	73.76	0.01	0.01	BB	2.5350
8	13.335	7385.76	1984.89	0.59	0.59	BB	3.7210
9	14.756	4726.61	919.50	0.38	0.38	BB	5.1404
10	15.174	1621.71	362.84	0.13	0.13	BB	4.4695
11	15.913	13038.39	2518.39	1.05	1.05	BB	5.1773
		1246983.68	765224.45	100.00	100.00		
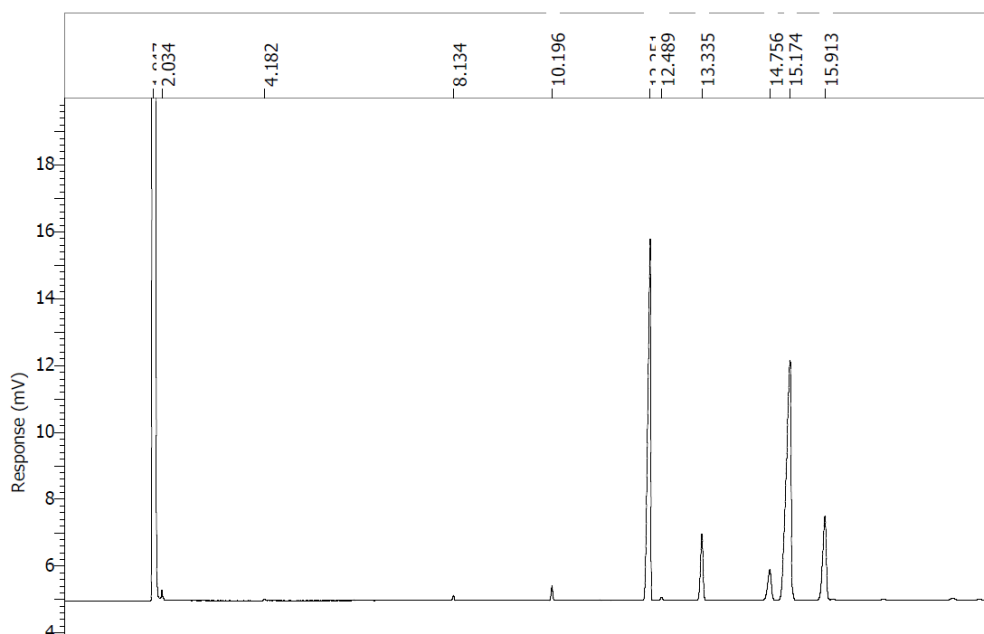
Figure H-8: Peak Report and GC Chromatogram of 3-Ni/CaO-600.

DEFAULT REPORT

Peak #	Time [min]	Area [µV·s]	Height [µV]	Area [%]	Norm. Area [%]	BL	Area/Height [s]
1	1.835	1062554.87	954743.13	50.16	50.16	BV	1.1129
2	1.860	828932.47	703505.59	39.13	39.13	VE	1.1783
3	1.906	2612.13	2513.41	0.12	0.12	EV	1.0393
4	2.027	939.34	460.36	0.04	0.04	VB	2.0405
5	8.114	567.15	257.45	0.03	0.03	BB	2.2029
6	10.161	1915.43	806.26	0.09	0.09	BB	2.3757
7	11.141	82.43	36.10	0.00	0.00	BB	2.2835
8	12.229	20652.82	15056.24	3.52	3.52	BB	4.9583
9	12.441	329.29	128.51	0.02	0.02	BB	2.5625
10	13.288	5358.25	3727.50	0.68	0.68	BB	3.8520
11	14.736	8820.35	1495.49	0.42	0.42	BB	5.8980
12	15.164	1683.87	11176.09	4.56	4.56	BB	8.6510
13	15.852	20503.39	4262.87	1.16	1.16	BV	5.7481
14	15.988	233.57	57.12	0.01	0.01	VB	4.0891
15	17.012	393.89	82.48	0.02	0.02	BB	4.7756
16	18.455	752.08	119.86	0.04	0.04	BB	6.2744
		2118331.32	1.70e+06	100.00	100.00		
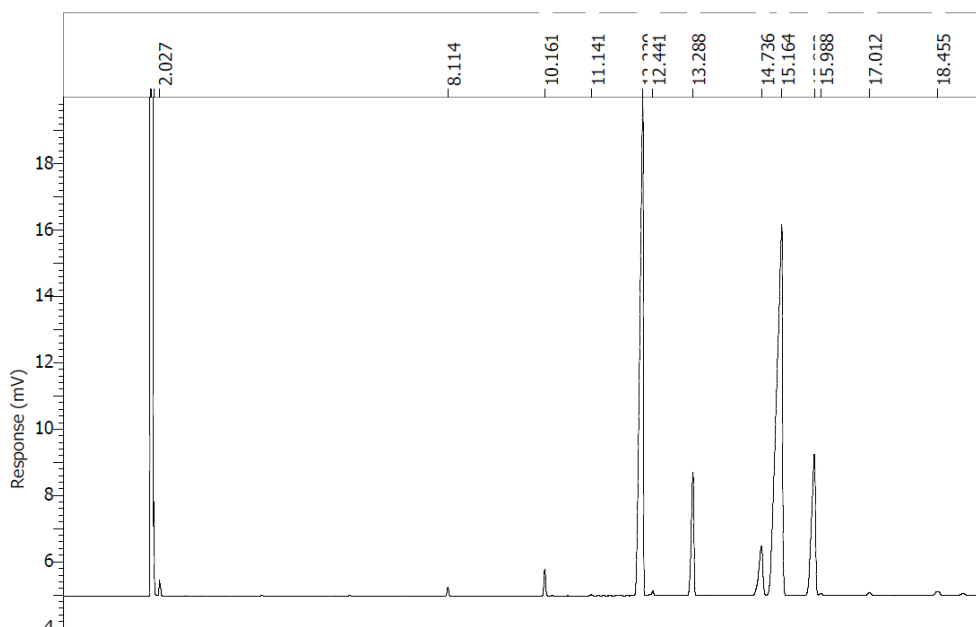
Figure H-9: Peak Report and GC Chromatogram of 4-Ni/CaO-600.

DEFAULT REPORT

Peak #	Time [min]	Area [µV·s]	Height [µV]	Area [%]	Norm. Area [%]	BL	Area/Height [s]
1	1.831	702159.44	647062.24	61.36	61.36	BV	1.0851
2	1.864	382262.69	353273.51	33.41	33.41	VE	1.0821
3	1.906	1300.57	1275.37	0.11	0.11	EB	1.0198
4	2.017	109.58	92.60	0.01	0.01	BB	1.1834
5	4.168	42.53	22.54	0.00	0.00	BB	1.8870
6	8.102	160.90	73.30	0.01	0.01	BB	2.1950
7	10.152	466.53	197.75	0.04	0.04	BB	2.3592
8	12.157	20159.71	6281.01	1.76	1.76	BB	3.2096
9	12.418	76.86	31.67	0.01	0.01	BB	2.4266
10	13.258	5676.78	1631.88	0.50	0.50	BB	3.4787
11	14.635	2218.49	490.78	0.19	0.19	BB	4.5203
12	15.020	23512.71	4417.74	2.05	2.05	BB	5.3223
13	15.769	6121.19	1283.56	0.53	0.53	BB	4.7689
		1144267.99	1.02e+06	100.00	100.00		

Figure H-10: Peak Report and GC Chromatogram of 5-Ni/CaO-600.

APPENDIX I: Sample Calculation for Crystallite Size of Catalyst

The sample calculation is in reference to 1 wt% Ni doped CaO calcined at 600 ℃ (1-Ni/CaO-600), where the average crystallite size of catalyst is obtained based on a total of five distinct peaks in XRD profile.
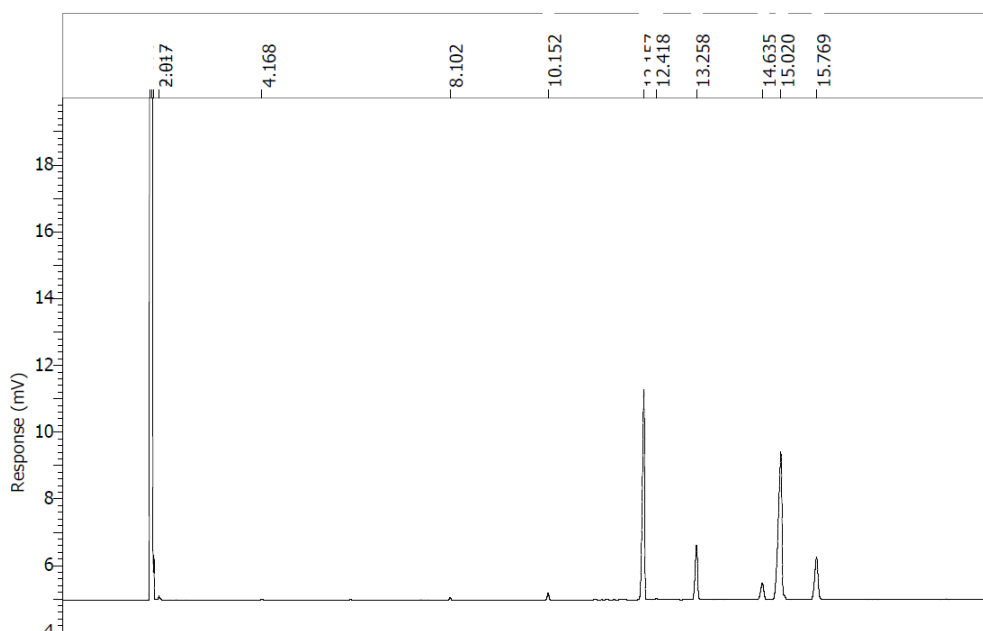
Table I-1: Peak Data for Calculation of Crystallite Size.

Catalyst	Peak No.	2θ (°)	θ (°)	FWHM (°)	FWHM (rad)	d-spacing (Å)
1-Ni/CaO-600	1	29.4170	14.7085	0.1558	0.0027	3.0339
	2	32.2097	16.1049	0.2339	0.0041	2.7769
	3	37.3731	18.6866	0.2338	0.0041	2.4043
	4	47.5530	23.7765	0.1670	0.0029	1.9106
	5	53.9138	26.9569	0.2750	0.0048	1.6992

The X-ray wavelength is first calculated using the equation derived from Bragg's Law as follows:

$$\lambda = 2d\ sin\theta$$

where

λ = wavelength of X-ray

d = lattice interplanar spacing of crystal

θ = angle of incidence; angle between incident X-ray and scatter plane

Hence, the X-ray wavelength for peak number 1 is

$\lambda = 2d\ sin\theta$

$= 2(3.0339)(sin14.7085)$

$= 1.54$ Å

Since 1 Å = 0.1 nm,

$\lambda = 0.154\ nm$

The crystallite size is then calculated using Debye-Scherrer equation as shown below:

$$L = \frac{K\lambda}{\beta cos\theta}$$

where

L = mean size of crystalline domains

K = Scherrer shape factor, typically 0.89

λ = X-ray wavelength

β = peak width; full width at half maximum (FWHM)

θ = angle of maximum diffraction peak; Bragg angle

Thus, the crystallite size for peak number 1 is

$$L = \frac{K\lambda}{\beta cos\theta}$$
$$= \frac{(0.89)(0.154\ nm)}{(0.0027)(cos14.7085)}$$
$$= 52.48\ nm$$

The calculation is then repeated for the remaining peaks before adding up the respective crystallite sizes to obtain an average value, as well as for other synthesised catalysts.

APPENDIX J: XRD Analysis Report

```
# Strongest 3 peaks
  no. peak    2Theta      d      I/I1   FWHM    Intensity  Integrated Int
      no.     (deg)      (A)            (deg)   (Counts)   (Counts)
   1   3     37.3897   2.40322   100   0.13980    1699      13376
   2   6     53.8952   1.69978    51   0.14430     874       7187
   3   2     32.2341   2.77485    31   0.14150     529       4272

# Peak Data List
      peak    2Theta      d      I/I1   FWHM    Intensity  Integrated Int
      no.     (deg)      (A)            (deg)   (Counts)   (Counts)
       1     29.4160   3.03396    19   0.14880     325       2796
       2     32.2341   2.77485    31   0.14150     529       4272
       3     37.3897   2.40322   100   0.13980    1699      13376
       4     39.4472   2.28249     3   0.17890      54        528
       5     48.5261   1.87454     5   0.13650      93        694
       6     53.8952   1.69978    51   0.14430     874       7187
       7     64.1962   1.44965    17   0.14360     289       2424
       8     67.4191   1.38797    13   0.14840     217       1855
       9     79.7093   1.20201     6   0.16230      97        895
```
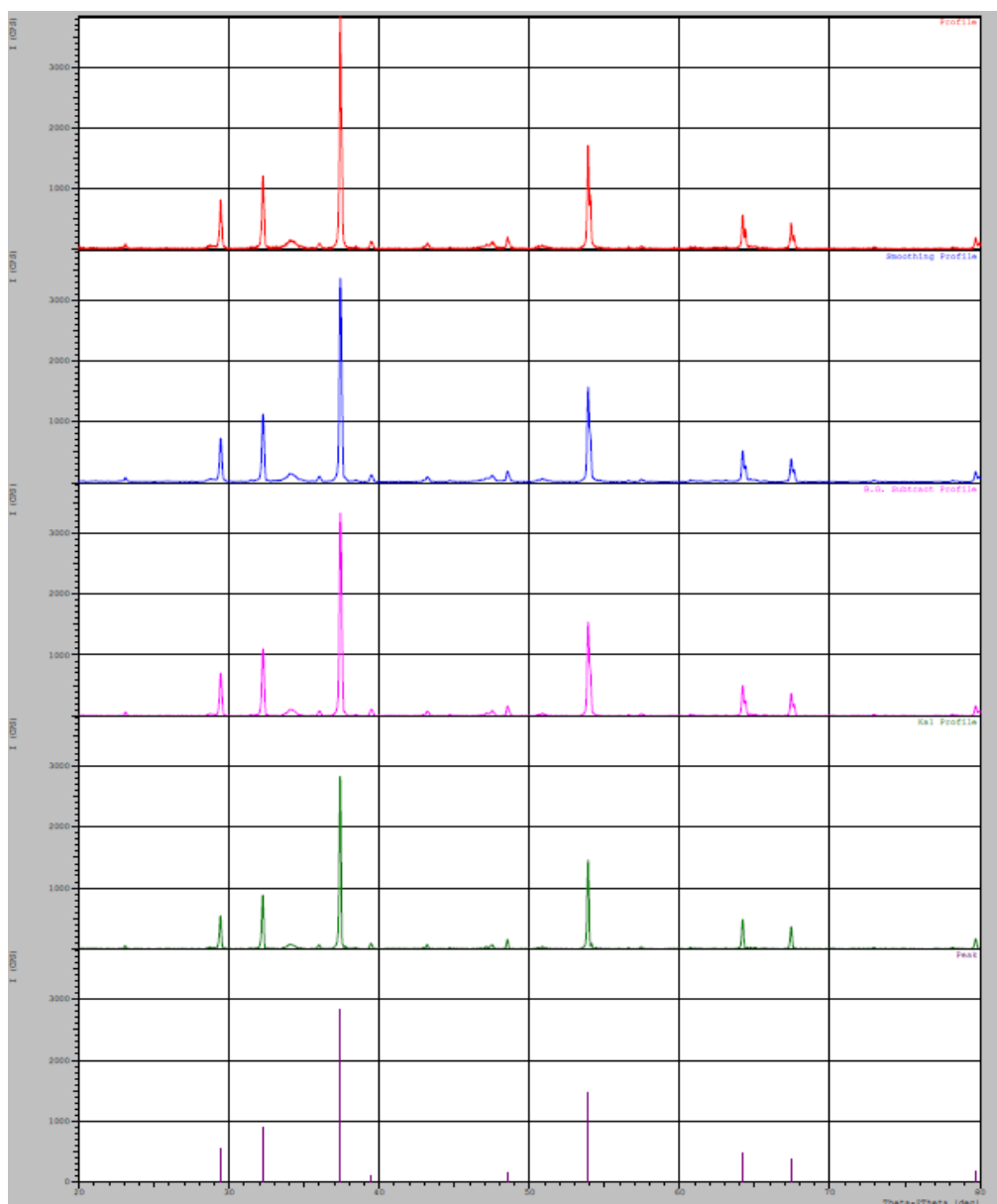

Figure J-1: Peak Report and XRD Diffractogram of Undoped CaO.

```
# Strongest 3 peaks
   no. peak    2Theta       d        I/I1    FWHM      Intensity    Integrated Int
        no.    (deg)        (A)               (deg)    (Counts)     (Counts)
    1    1     29.4230     3.03325    100     0.13010    1457        10917
    2    4     37.3660     2.40469     63     0.18490     912        10504
    3   10     53.8739     1.70040     31     0.21300     447         5048

# Peak Data List
        peak   2Theta       d        I/I1    FWHM      Intensity    Integrated Int
        no.    (deg)        (A)               (deg)    (Counts)     (Counts)
         1     29.4230     3.03325    100     0.13010    1457        10917
         2     32.2070     2.77712     23     0.19080     339         3789
         3     35.9928     2.49323      3     0.14570      49          392
         4     37.3660     2.40469     63     0.18490     912        10504
         5     39.4305     2.28341      6     0.14370      93          774
         6     43.1915     2.09289      7     0.14540      96          794
         7     47.5208     1.91183     13     0.13970     196         1787
         8     48.5278     1.87448      9     0.14830     127         1095
         9     53.6000     1.70845      3     0.11200      48          436
        10     53.8739     1.70040     31     0.21300     447         5048
        11     54.1000     1.69383      5     0.07340      71          505
        12     57.4263     1.60337      3     0.13930      44          343
        13     64.1658     1.45026      8     0.22030     113         1450
        14     65.6182     1.42163      4     0.13070      53          382
        15     67.3927     1.38845      7     0.26040     106         1596
```
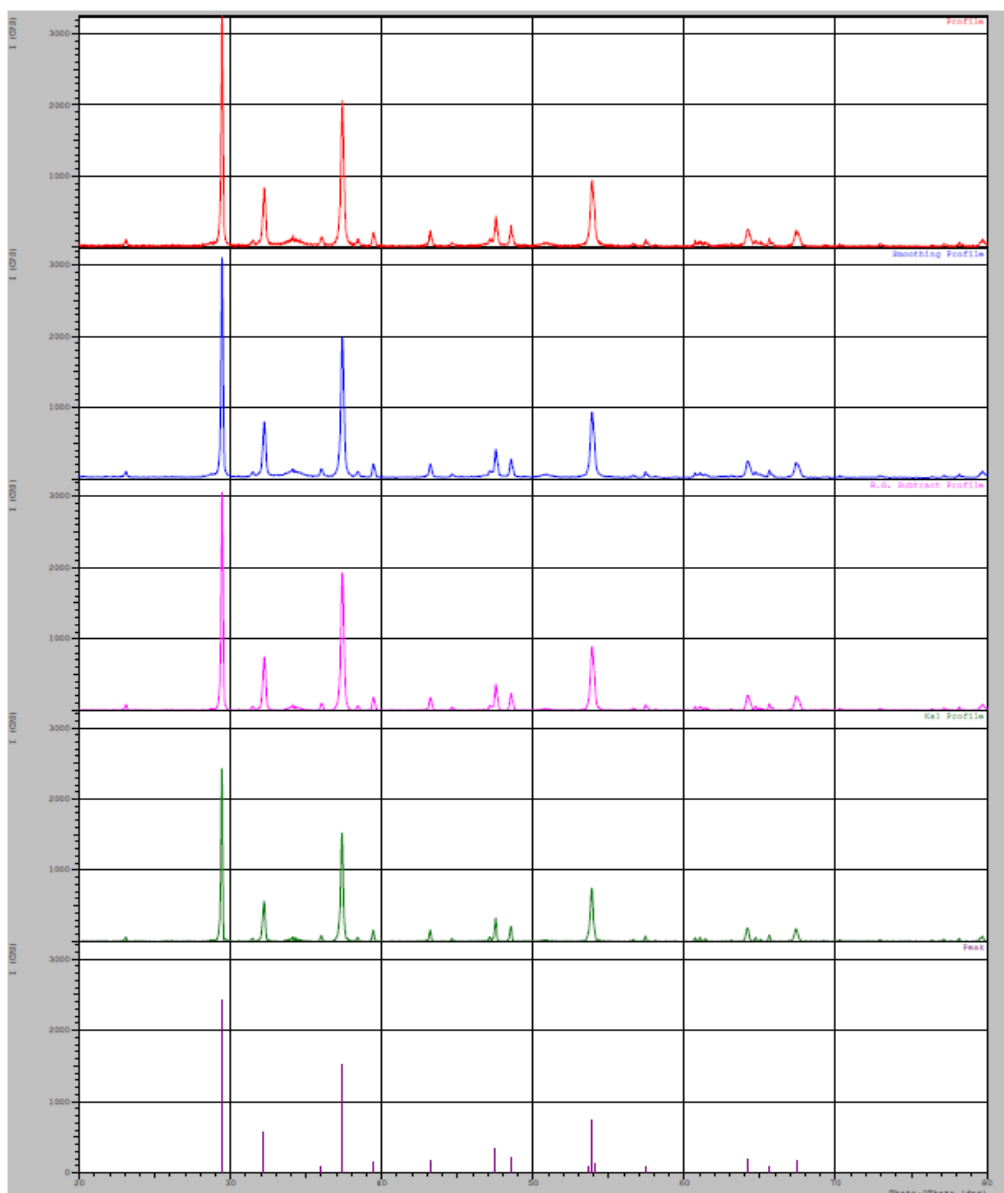

Figure J-2: Peak Report and XRD Diffractogram of Treated CaO.

```
# Strongest 3 peaks
  no. peak    2Theta      d        I/I1   FWHM       Intensity   Integrated Int
       no.    (deg)      (A)              (deg)      (Counts)    (Counts)
   1    3    29.4170    3.03385    100   0.15580     1153        9937
   2   11    37.3731    2.40425     70   0.23380      803        9963
   3   27    53.9138    1.69924     32   0.27500      369        5471

# Peak Data List
       peak   2Theta      d        I/I1   FWHM       Intensity   Integrated Int
       no.    (deg)      (A)              (deg)      (Counts)    (Counts)
        1    23.0466    3.85600      6   0.17330       67         724
        2    28.6265    3.11581      3   0.32300       36         933
        3    29.4170    3.03385    100   0.15580     1153        9937
        4    32.2097    2.77690     25   0.23390      293        4013
        5    33.7800    2.65131      5   0.12500       55         875
        6    33.9600    2.63767      7   0.00000       79           0
        7    34.1600    2.62268      8   0.00000       91           0
        8    34.3800    2.60640      5   0.15600       59        1294
        9    36.0010    2.49268      5   0.14740       63         506
       10    37.0600    2.42384      7   0.14400       84        1226
       11    37.3731    2.40425     70   0.23380      803        9963
       12    37.7400    2.38172      4   0.08800       43         486
       13    38.3920    2.34276      5   0.13600       52         619
       14    39.4629    2.28161     11   0.15120      122        1150
       15    43.0200    2.10084      6   0.09720       68         495
       16    43.2000    2.09250     12   0.18560      136        1413
       17    44.6408    2.02825      3   0.22830       38         688
       18    47.1400    1.92638      4   0.18660       45         814
       19    47.3200    1.91947      6   0.00000       65           0
       20    47.5530    1.91061     20   0.16700      234        2467
       21    48.5614    1.87326     14   0.16510      159        1552
       22    50.4000    1.80915      3   0.19120       40         855
       23    50.6600    1.80048      4   0.00000       41           0
       24    50.8600    1.79386      5   0.00000       60           0
       25    51.0600    1.78731      4   0.36000       46         869
       26    51.3550    1.77773      3   0.13000       37         265
       27    53.9138    1.69924     32   0.27500      369        5471
       28    54.1800    1.69152      7   0.15560       80        1108
       29    57.4702    1.60225      4   0.17550       48         657
       30    60.6376    1.52592      4   0.22190       47         702
       31    61.4375    1.50795      5   0.19500       54        1033
       32    62.4660    1.48558      3   0.14800       39         399
       33    64.2273    1.44902      7   0.32320       81        1622
       34    65.0247    1.43317      4   0.16150       49         517
       35    66.4146    1.40650      6   0.21580       66         730
       36    66.8200    1.39895      4   0.33000       50        1081
       37    67.1400    1.39306      5   0.00000       53           0
       38    67.3000    1.39014      5   0.00000       60           0
       39    67.5200    1.38614      6   0.26000       66        1214
       40    77.5554    1.22992      5   0.22730       53         770
       41    78.1360    1.22223      5   0.23200       56         817
```
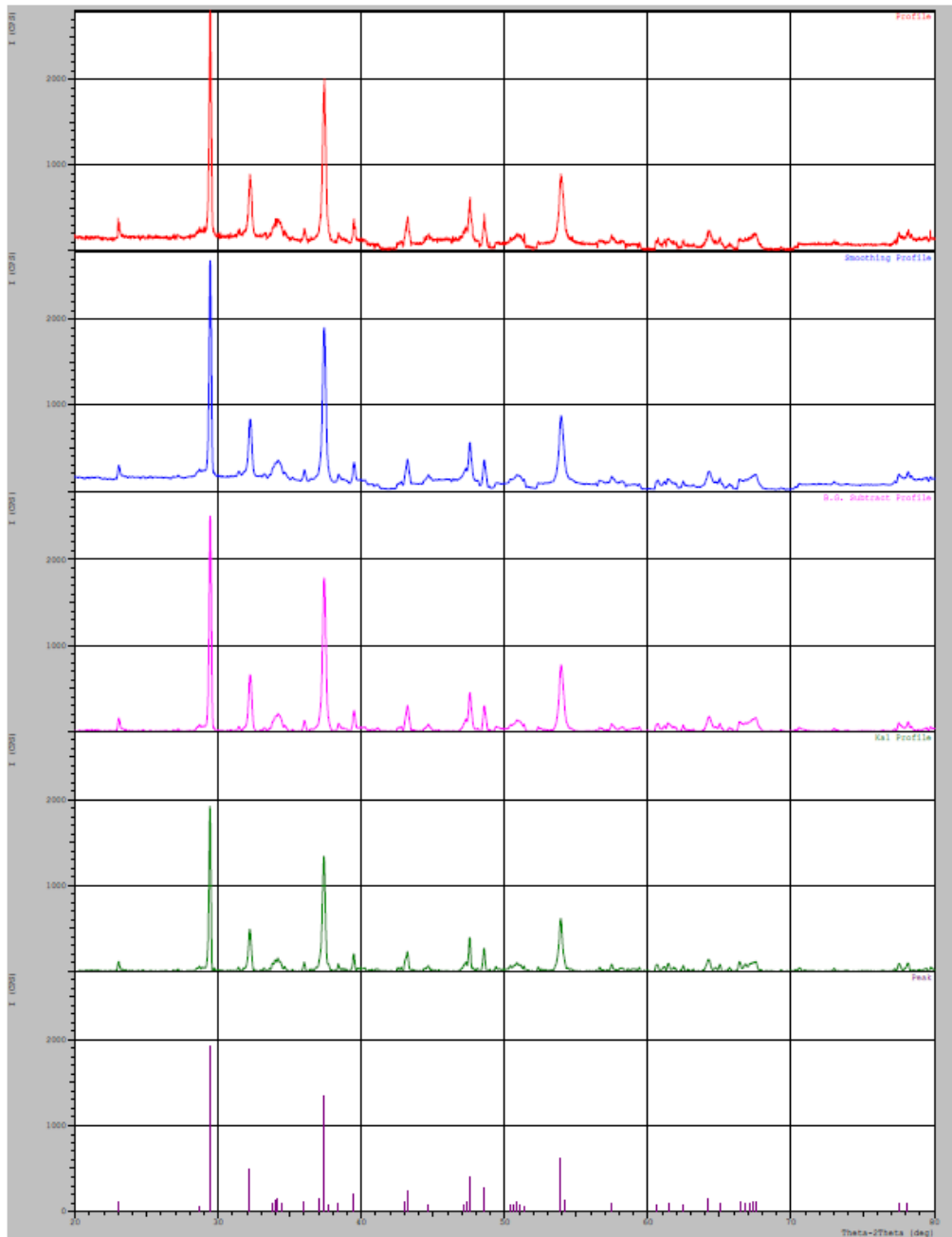
Figure J-3: Peak Report of 1-Ni/CaO-600.

Figure J-4: XRD Diffractogram of 1-Ni/CaO-600.

```
# Strongest 3 peaks
  no. peak    2Theta      d        I/I1   FWHM      Intensity   Integrated Int
       no.    (deg)      (A)              (deg)     (Counts)    (Counts)
    1    2   29.4502   3.03051    100   0.13510      1322        10294
    2    5   37.4034   2.40237     87   0.15930      1145        10667
    3   13   53.9091   1.69938     43   0.16750       571         5145

# Peak Data List
       peak   2Theta      d        I/I1   FWHM      Intensity   Integrated Int
       no.    (deg)      (A)              (deg)     (Counts)    (Counts)
         1   23.1097   3.84562      3   0.11770        41          310
         2   29.4502   3.03051    100   0.13510      1322        10294
         3   32.2463   2.77383     32   0.15590       429         3957
         4   36.0218   2.49128      4   0.12360        52          405
         5   37.4034   2.40237     87   0.15930      1145        10667
         6   37.6400   2.38782      4   0.08000        59          674
         7   39.4667   2.28140      8   0.14190       108          855
         8   43.2243   2.09138     13   0.12090       169         1329
         9   47.1579   1.92569      3   0.15080        41          402
        10   47.5414   1.91105     15   0.13820       196         1607
        11   48.5610   1.87328     11   0.14260       151         1235
        12   53.6400   1.70727      3   0.14000        42          627
        13   53.9091   1.69938     43   0.16750       571         5145
        14   54.1600   1.69210      3   0.06900        44          420
        15   57.4633   1.60243      4   0.13170        47          381
        16   64.1968   1.44964     10   0.19100       132         1537
        17   65.6459   1.42110      4   0.12820        53          405
        18   67.4253   1.38786     11   0.18470       143         1690
        19   79.7076   1.20203      4   0.20190        49          551
```
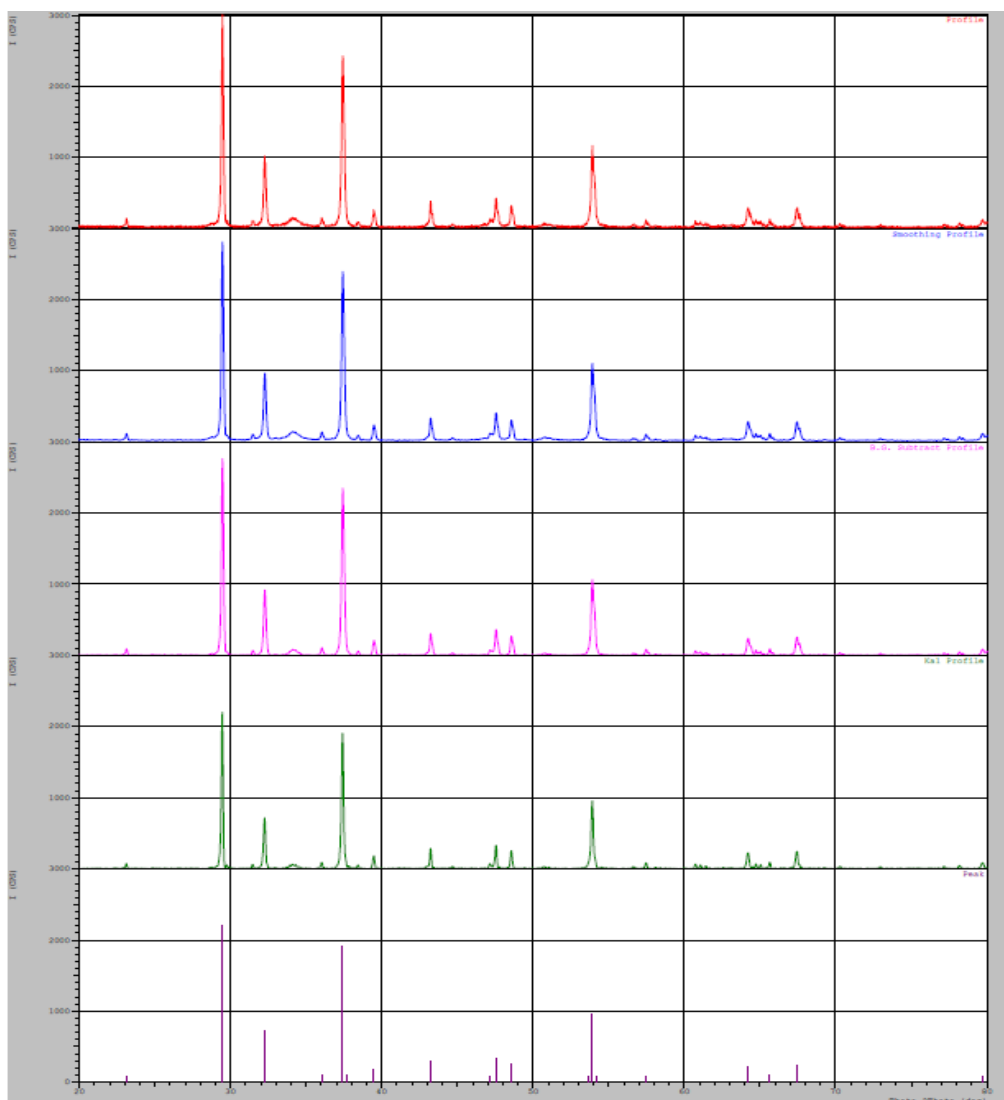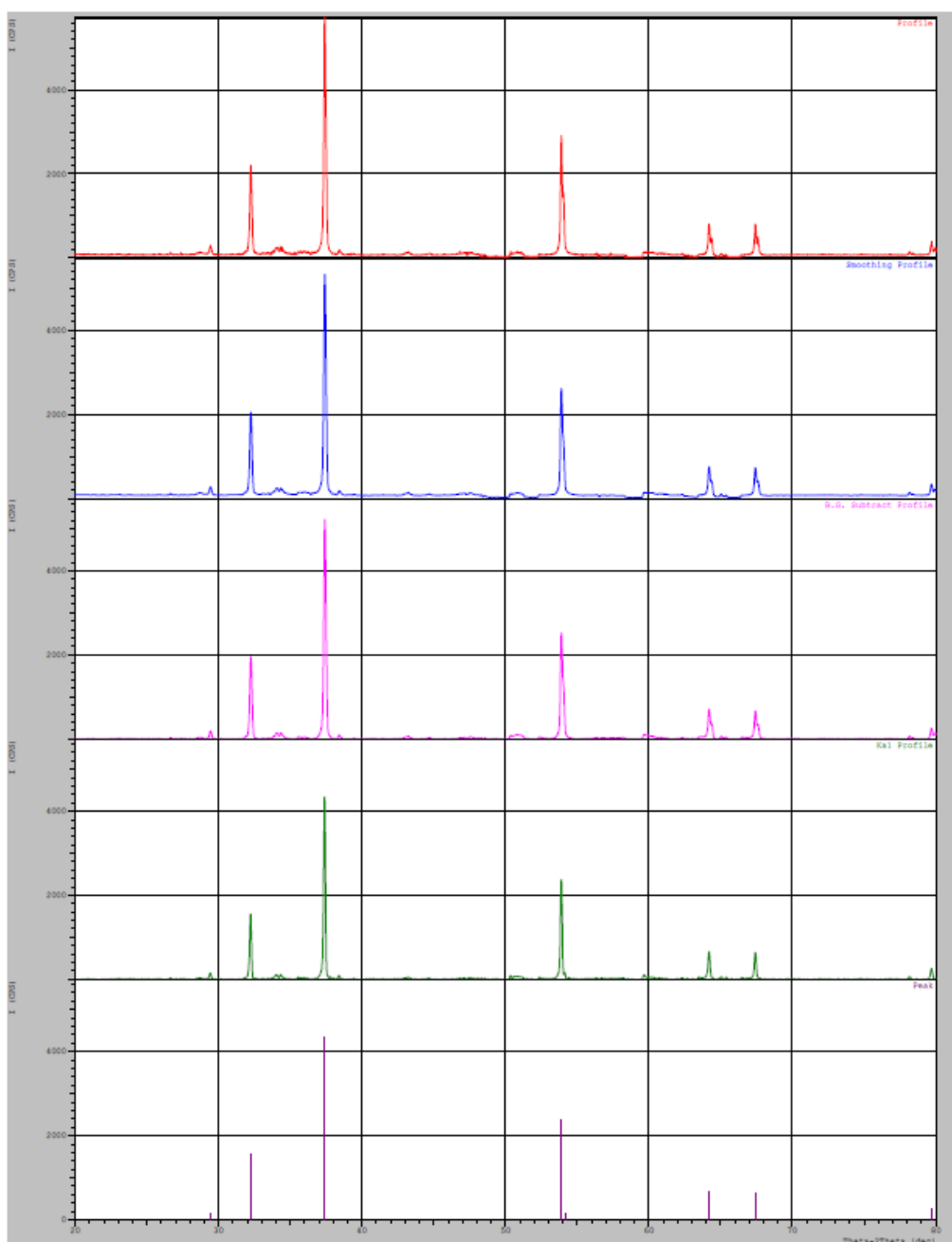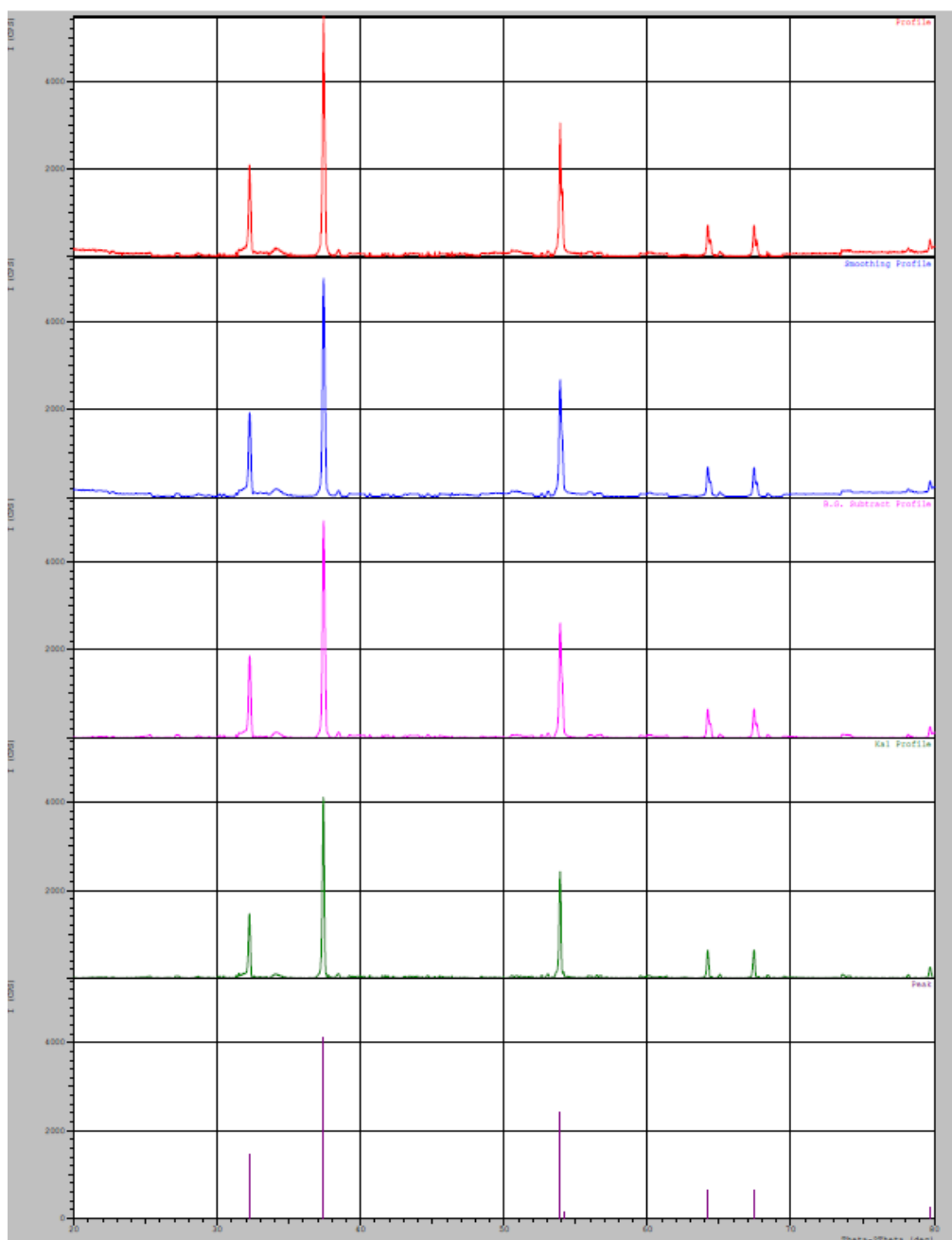

Figure J-5: Peak Report and XRD Diffractogram of 1-Ni/CaO-700.

```
# Strongest 3 peaks
  no. peak    2Theta       d         I/I1   FWHM      Intensity    Integrated Int
       no.    (deg)       (A)               (deg)     (Counts)     (Counts)
   1    3    37.3876    2.40335      100   0.14900     2601         22251
   2    4    53.8930    1.69985       55   0.14900     1425         11965
   3    2    32.2303    2.77517       36   0.14780      933          7974

# Peak Data List
       peak   2Theta       d         I/I1   FWHM      Intensity    Integrated Int
       no.    (deg)       (A)               (deg)     (Counts)     (Counts)
        1    29.4192    3.03363        3   0.15620       86           778
        2    32.2303    2.77517       36   0.14780      933          7974
        3    37.3876    2.40335      100   0.14900     2601         22251
        4    53.8930    1.69985       55   0.14900     1425         11965
        5    54.1600    1.69210        3   0.07140       85           562
        6    64.1908    1.44976       15   0.16260      393          3984
        7    67.4138    1.38807       15   0.15890      382          3731
        8    79.7021    1.20210        6   0.16290      151          1352
```
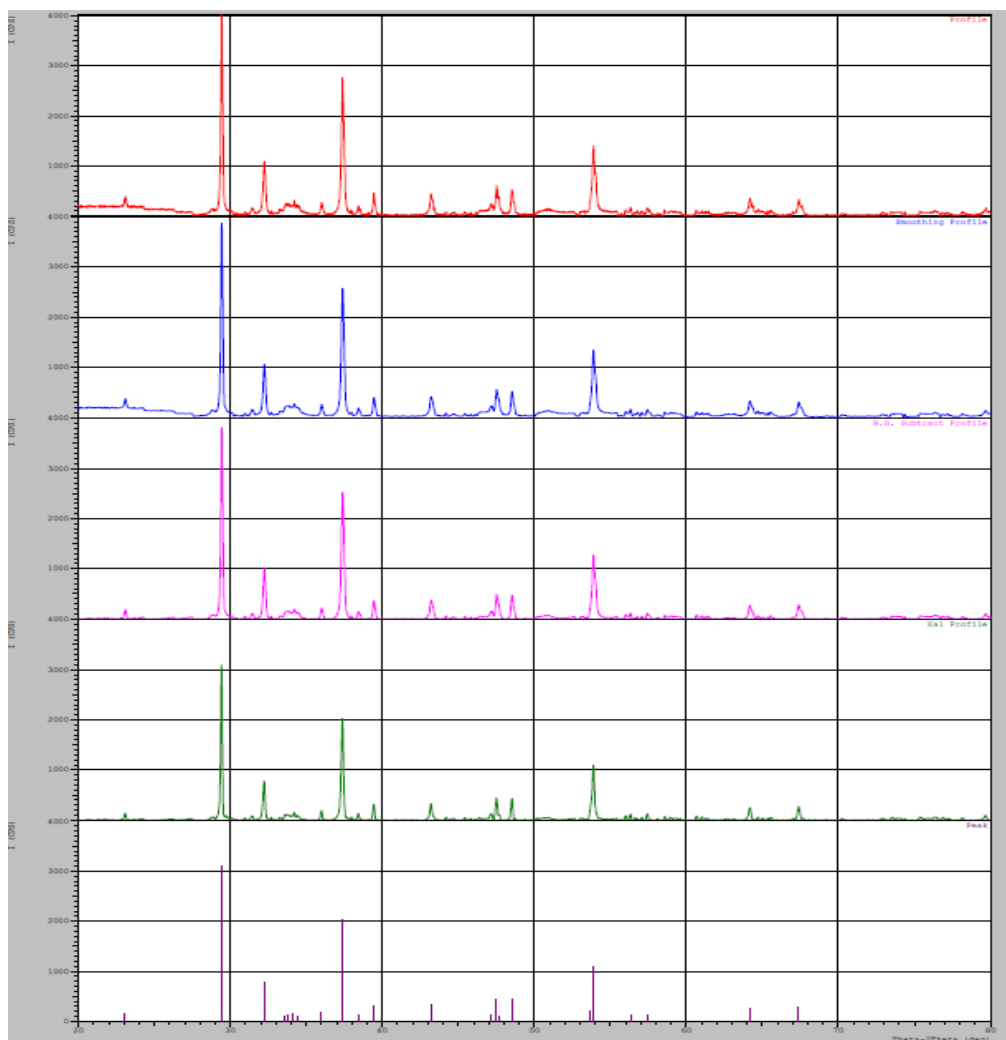

Figure J-6: Peak Report and XRD Diffractogram of 1-Ni/CaO-800.

```
# Strongest 3 peaks
  no. peak    2Theta      d        I/I1   FWHM       Intensity   Integrated Int
       no.    (deg)       (A)             (deg)      (Counts)    (Counts)
   1    2     37.3962     2.40282  100    0.15030    2467        20994
   2    3     53.9077     1.69942   59    0.14890    1453        12418
   3    1     32.2374     2.77457   36    0.15650     879         8305

# Peak Data List
       peak   2Theta      d        I/I1   FWHM       Intensity   Integrated Int
       no.    (deg)       (A)             (deg)      (Counts)    (Counts)
        1     32.2374     2.77457   36    0.15650     879         8305
        2     37.3962     2.40282  100    0.15030    2467        20994
        3     53.9077     1.69942   59    0.14890    1453        12418
        4     54.1600     1.69210    3    0.08640      80          626
        5     64.2031     1.44951   15    0.15500     378         3362
        6     67.4263     1.38784   15    0.15840     379         3512
        7     79.7125     1.20197    6    0.16210     149         1349
```
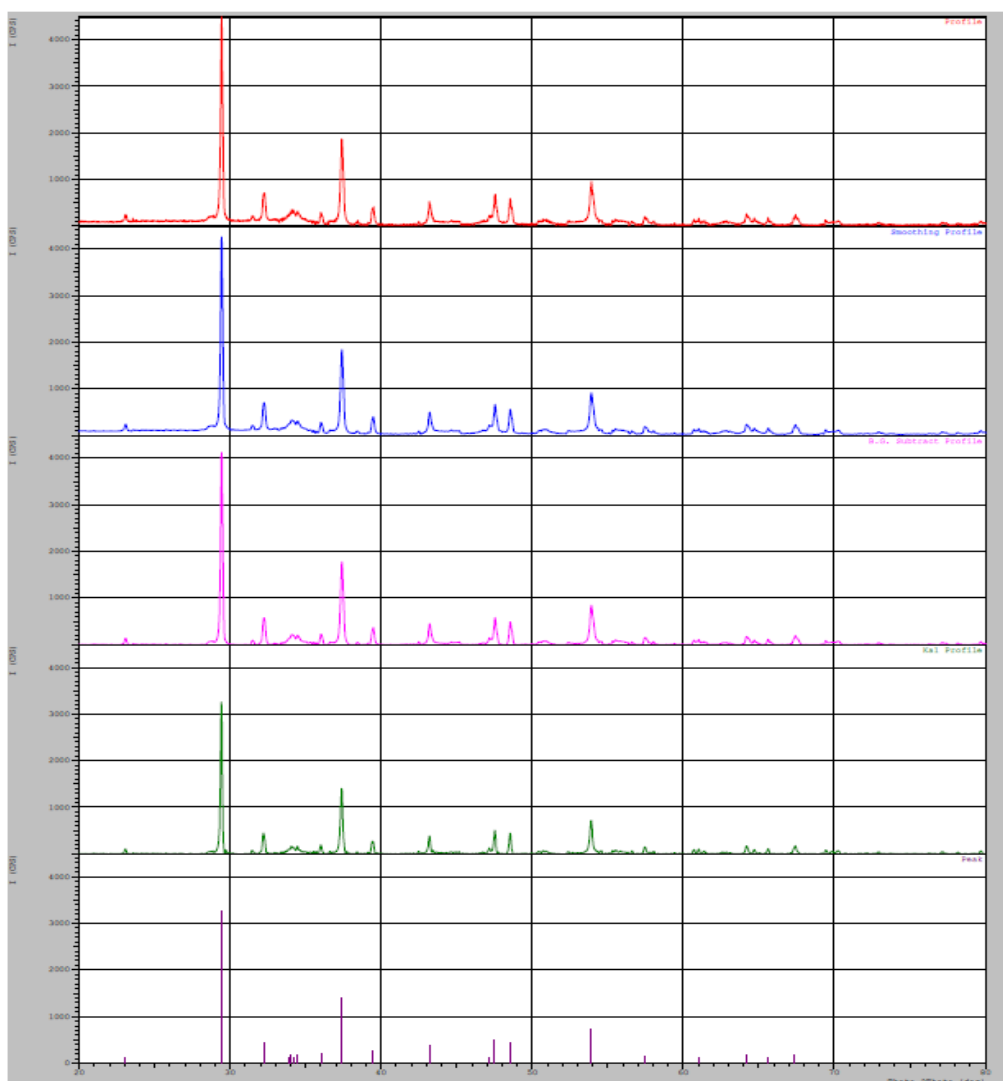

Figure J-7: Peak Report and XRD Diffractogram of 1-Ni/CaO-900.

```
# Strongest 3 peaks
  no. peak   2Theta       d        I/I1   FWHM      Intensity   Integrated Int
       no.   (deg)       (A)              (deg)     (Counts)    (Counts)
    1    2   29.4184   3.03371     100   0.12750      1857        13984
    2    9   37.3675   2.40460      66   0.16680      1218        12417
    3   18   53.8778   1.70029      35   0.17770       659         6796

# Peak Data List
       peak  2Theta       d        I/I1   FWHM      Intensity   Integrated Int
       no.   (deg)       (A)              (deg)     (Counts)    (Counts)
        1    23.0770   3.85099       5   0.12600        85          710
        2    29.4184   3.03371     100   0.12750      1857        13984
        3    32.2164   2.77633      25   0.15960       467         4467
        4    33.6000   2.66510       4   0.16000        68         1088
        5    33.7600   2.65284       4   0.00000        70            0
        6    34.1285   2.62503       5   0.28100        94         1590
        7    34.4339   2.60245       3   0.26350        59          813
        8    35.9914   2.49332       6   0.12440       115          822
        9    37.3675   2.40460      66   0.16680      1218        12417
       10    38.4139   2.34147       4   0.12420        79          640
       11    39.4366   2.28307      10   0.13220       192         1422
       12    43.2011   2.09245      11   0.15770       199         2142
       13    47.1523   1.92591       4   0.20070        78         1138
       14    47.5082   1.91231      14   0.14740       265         2101
       15    47.7200   1.90431       3   0.07340        61          347
       16    48.5188   1.87481      14   0.14030       260         2110
       17    53.6600   1.70668       6   0.09040       119          969
       18    53.8778   1.70029      35   0.17770       659         6796
       19    56.3185   1.63225       4   0.11450        76          500
       20    57.4259   1.60338       4   0.13980        75          749
       21    64.1729   1.45012       8   0.18250       148         1688
       22    67.3878   1.38854       9   0.17780       164         1974
```

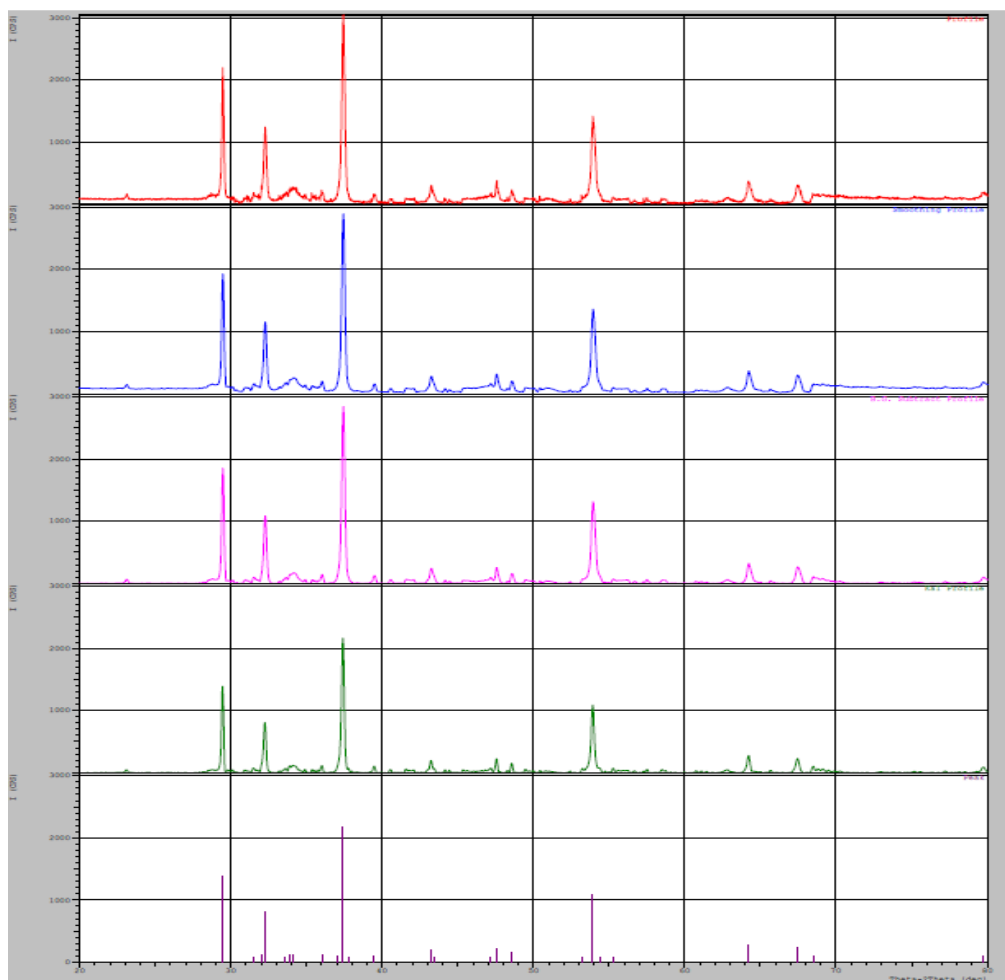

Figure J-8: Peak Report and XRD Diffractogram of 2-Ni/CaO-600.

```
# Strongest 3 peaks
  no. peak    2Theta      d        I/I1   FWHM      Intensity   Integrated Int
       no.    (deg)      (A)              (deg)     (Counts)    (Counts)
    1    2    29.4161    3.03395    100   0.13830     1954        15961
    2    9    37.3774    2.40399     43   0.17320      840         9106
    3   15    53.8948    1.69979     22   0.20120      432         5888

# Peak Data List
       peak   2Theta      d        I/I1   FWHM      Intensity   Integrated Int
       no.    (deg)      (A)              (deg)     (Counts)    (Counts)
        1    23.0611    3.85361      3   0.13770       63          523
        2    29.4161    3.03395    100   0.13830     1954        15961
        3    32.2245    2.77566     14   0.19450      268         2852
        4    33.8800    2.64372      3   0.24000       61         1296
        5    34.0400    2.63166      5   0.00000       99            0
        6    34.2400    2.61674      4   0.00000       72            0
        7    34.4620    2.60039      5   0.18800       98         1640
        8    36.0020    2.49261      6   0.14190      117         1051
        9    37.3774    2.40399     43   0.17320      840         9106
       10    39.4345    2.28319      8   0.19870      161         1809
       11    43.1934    2.09280     12   0.15180      231         2503
       12    47.1625    1.92551      4   0.18500       76         1034
       13    47.5180    1.91193     15   0.15260      302         2596
       14    48.5336    1.87427     14   0.14930      266         2234
       15    53.8948    1.69979     22   0.20120      432         5888
       16    57.4616    1.60247      4   0.18010       87         1040
       17    61.0205    1.51726      3   0.12900       61          968
       18    64.2060    1.44945      5   0.19600      102         1420
       19    65.6177    1.42164      3   0.14450       65          600
       20    67.3866    1.38856      5   0.23170      106         1398
```


Figure J-9: Peak Report and XRD Diffractogram of 3-Ni/CaO-600.

```
# Strongest 3 peaks
   no. peak    2Theta      d        I/I1   FWHM      Intensity   Integrated Int
        no.    (deg)       (A)              (deg)     (Counts)    (Counts)
    1   10     37.4039    2.40234    100   0.20980    1300        14908
    2   1      29.4517    3.03036    64    0.16600    834         7956
    3   19     53.9175    1.69913    50    0.23280    652         8901

# Peak Data List
        peak   2Theta      d        I/I1   FWHM      Intensity   Integrated Int
        no.    (deg)       (A)              (deg)     (Counts)    (Counts)
        1      29.4517    3.03036    64    0.16600    834         7956
        2      31.5128    2.83670    4     0.21430    46          900
        3      32.0200    2.79291    6     0.11740    76          610
        4      32.2445    2.77398    37    0.20230    485         5122
        5      33.6037    2.66482    3     0.20750    43          651
        6      33.9000    2.64220    5     0.21500    66          512
        7      34.1000    2.62716    5     0.59340    71          2171
        8      36.0060    2.49234    5     0.16800    69          772
        9      37.0400    2.42511    5     0.13340    60          986
        10     37.4039    2.40234    100   0.20980    1300        14908
        11     37.7600    2.38050    3     0.15660    42          787
        12     39.4707    2.28118    5     0.16320    64          635
        13     43.2315    2.09105    9     0.19540    118         1355
        14     43.4400    2.08149    3     0.15120    42          338
        15     47.1314    1.92671    3     0.26290    45          1029
        16     47.5545    1.91055    10    0.16470    134         1206
        17     48.5661    1.87309    7     0.15630    92          893
        18     53.2400    1.71915    3     0.14540    42          563
        19     53.9175    1.69913    50    0.23280    652         8901
        20     54.3600    1.68634    4     0.22400    47          1054
        21     55.2715    1.66067    3     0.16090    43          638
        22     64.2166    1.44924    13    0.22680    167         2416
        23     67.4533    1.38735    11    0.27330    137         2147
        24     68.4944    1.36878    5     0.22450    62          1284
        25     79.7430    1.20159    4     0.29400    54          995
```


Figure J-10: Peak Report and XRD Diffractogram of 4-Ni/CaO-600.

```
# Strongest 3 peaks
  no. peak    2Theta       d         I/I1    FWHM     Intensity   Integrated Int
       no.    (deg)       (A)                (deg)    (Counts)    (Counts)
    1   4    37.3536    2.40546     100    0.16120     1903         17321
    2   1    29.3964    3.03593      59    0.14950     1130          9572
    3   9    53.8600    1.70081      49    0.17850      935          9907

# Peak Data List
      peak    2Theta       d         I/I1    FWHM     Intensity   Integrated Int
       no.    (deg)       (A)                (deg)    (Counts)    (Counts)
        1    29.3964    3.03593      59    0.14950     1130          9572
        2    32.1938    2.77823      35    0.16340      662          6530
        3    37.0400    2.42511       5    0.14540       89          1422
        4    37.3536    2.40546     100    0.16120     1903         17321
        5    39.4050    2.28483       7    0.14850      131          1075
        6    43.1480    2.09490       8    0.25860      160          2519
        7    47.4960    1.91277      10    0.14520      190          1814
        8    48.5122    1.87505       8    0.16550      150          1458
        9    53.8600    1.70081      49    0.17850      935          9907
       10    54.1400    1.69267       5    0.15340       87          1565
       11    64.1549    1.45048      13    0.18290      248          2703
       12    67.3844    1.38860      13    0.17680      247          2905
       13    79.6745    1.20245       5    0.20440       92          1175
```
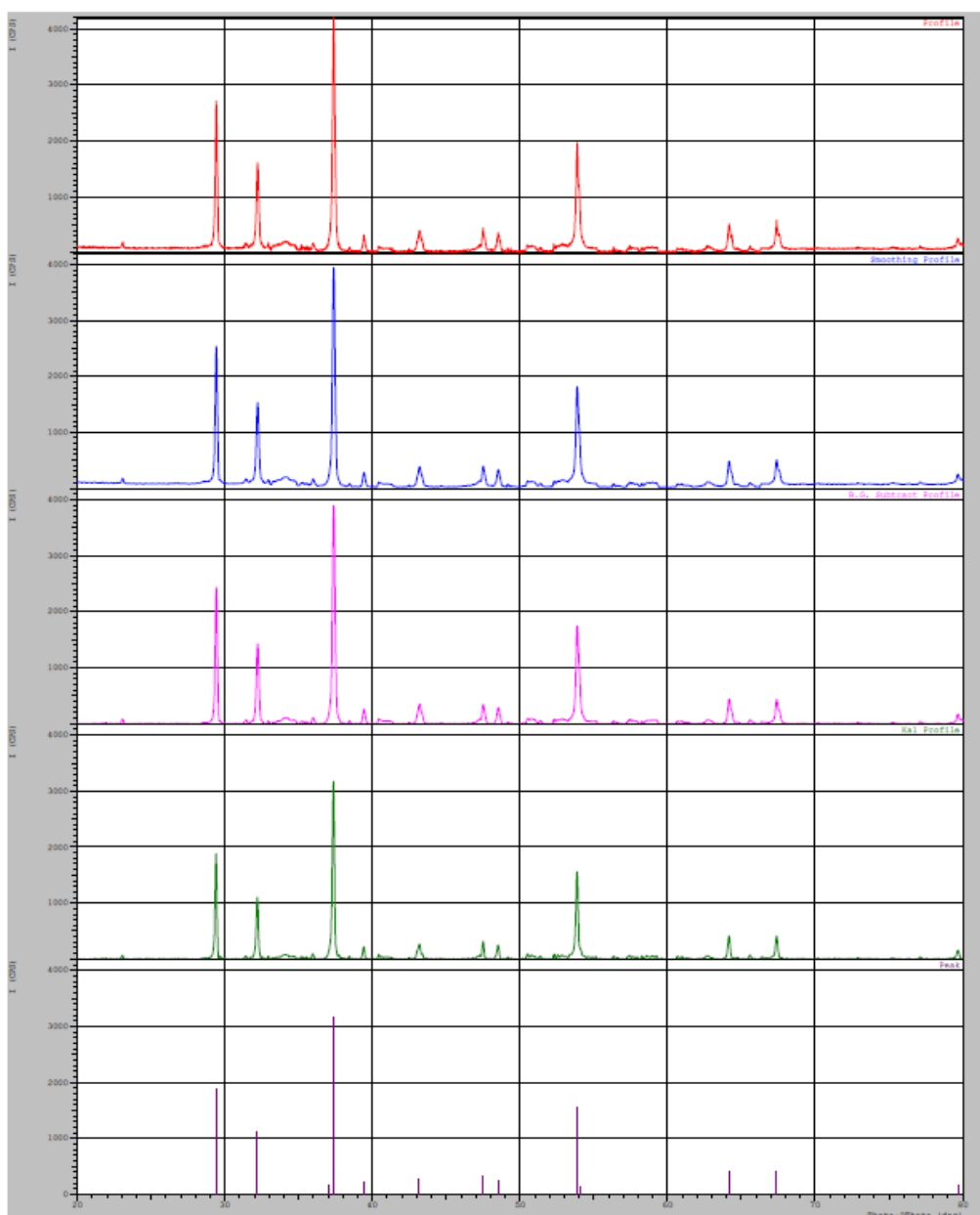

Figure J-11: Peak Report and XRD Diffractogram of 5-Ni/CaO-600.

APPENDIX K: SEM Analysis Report
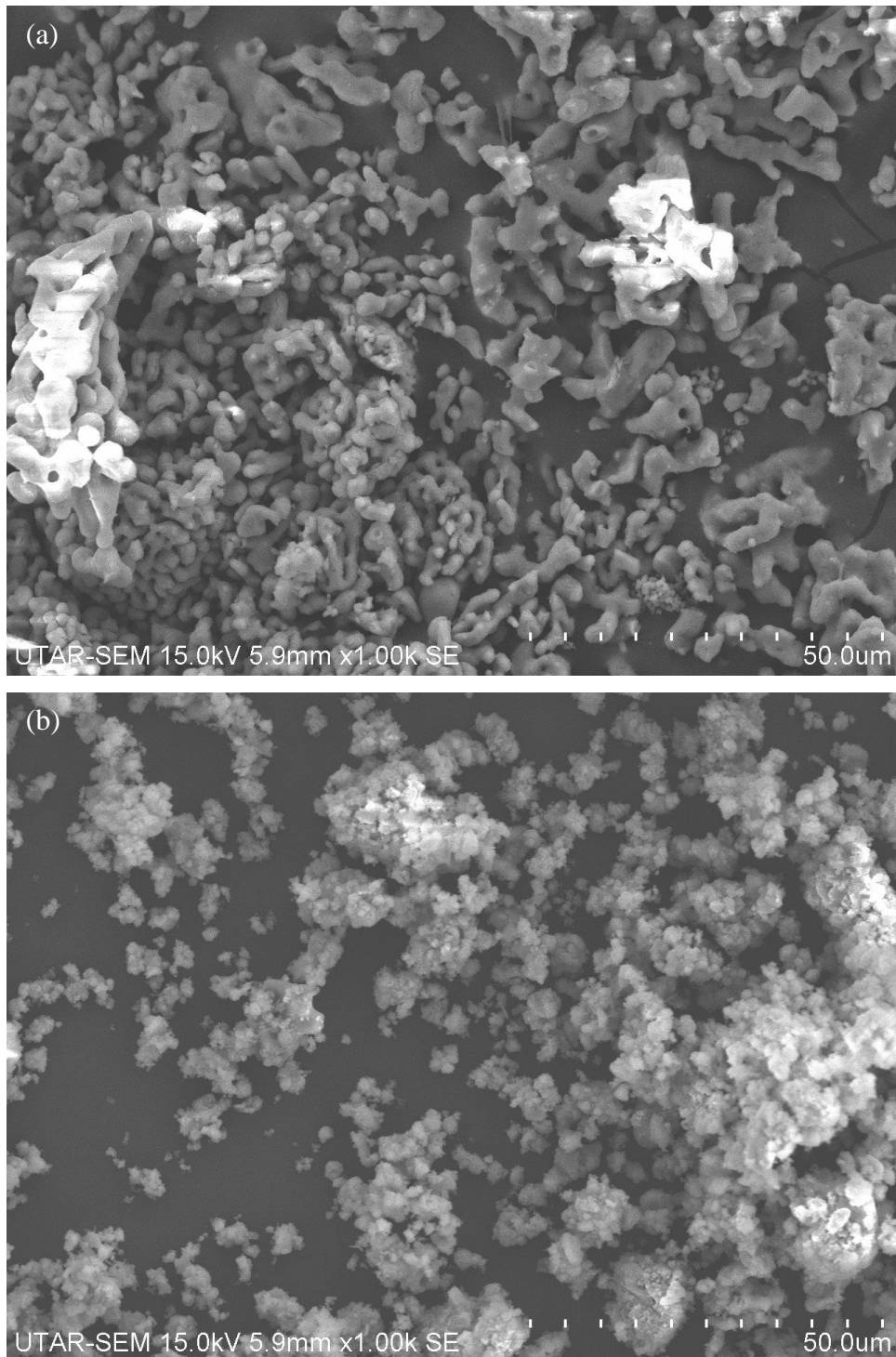
Figure K-1: SEM Micrographs of (a) Undoped CaO and (b) Treated CaO at 1000x Magnification.
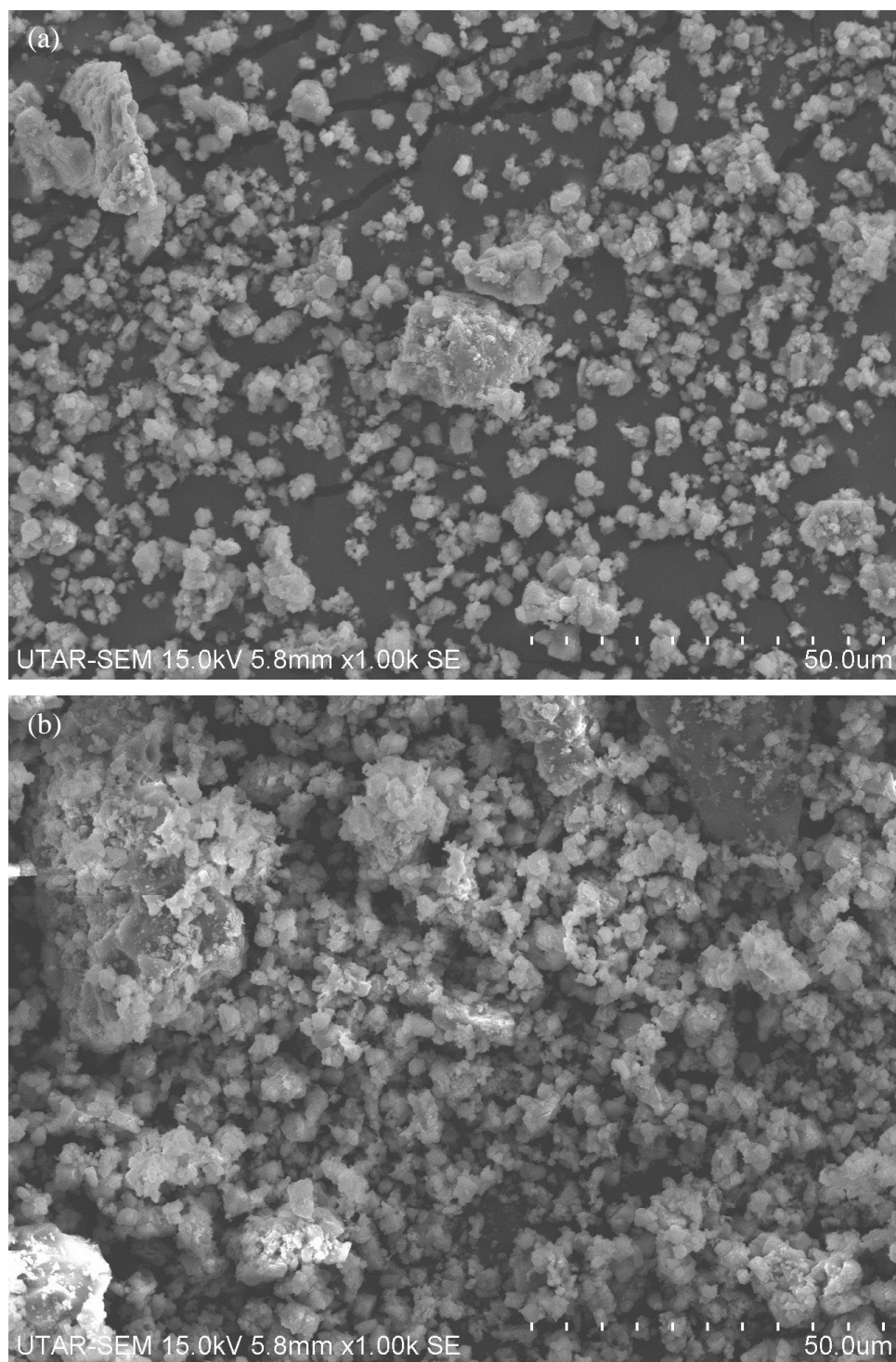
Figure K-2: SEM Micrographs of (a) 1-Ni/CaO-600 and (b) 1-Ni/CaO-700 at 1000x Magnification.
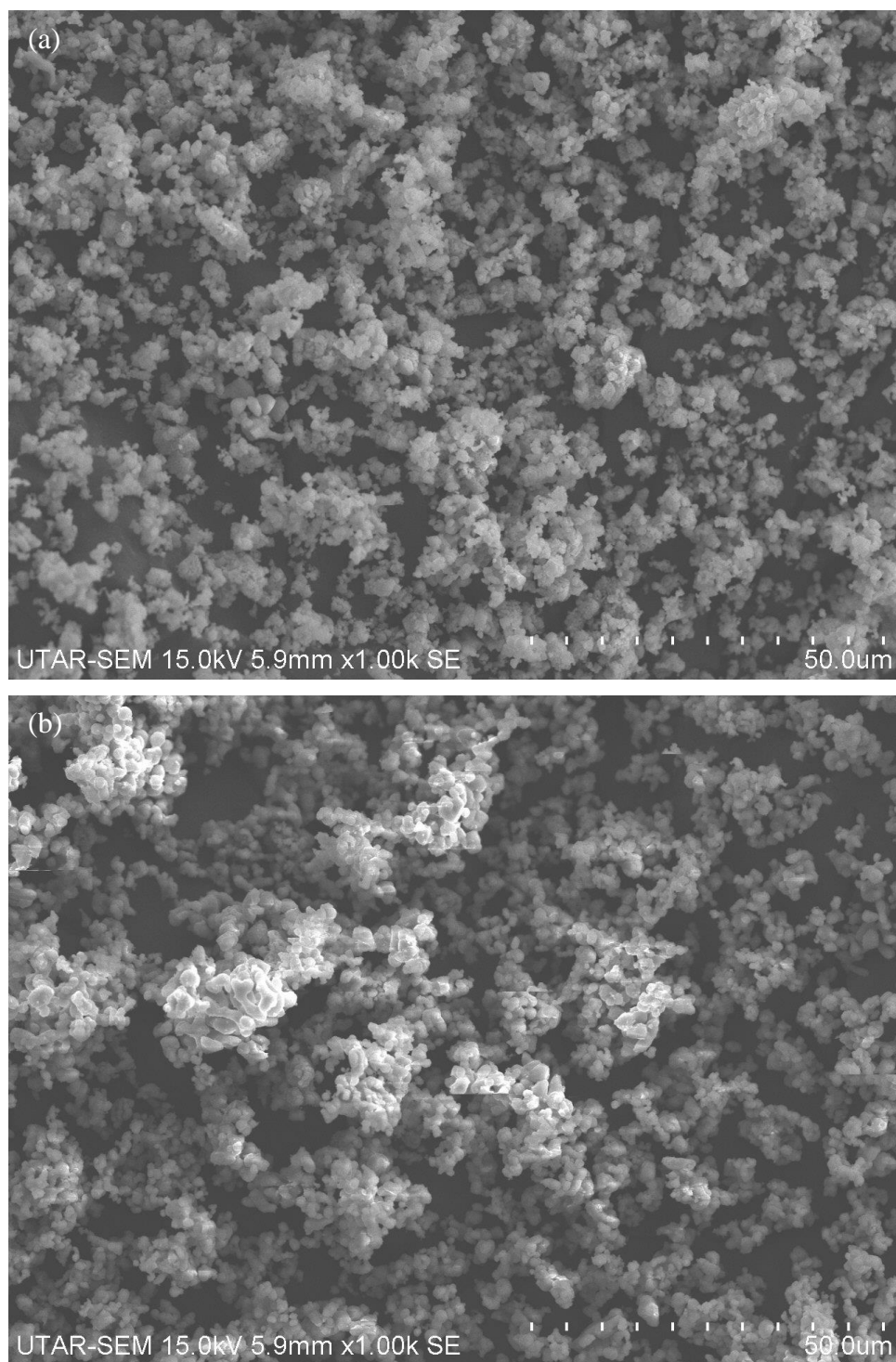
Figure K-3: SEM Micrographs of (a) 1-Ni/CaO-800 and (b) 1-Ni/CaO-900 at 1000x Magnification.

UTAR-SEM 15.0kV 5.9mm x1.00k SE   50.0um

UTAR-SEM 15.0kV 5.8mm x1.00k SE   50.0um
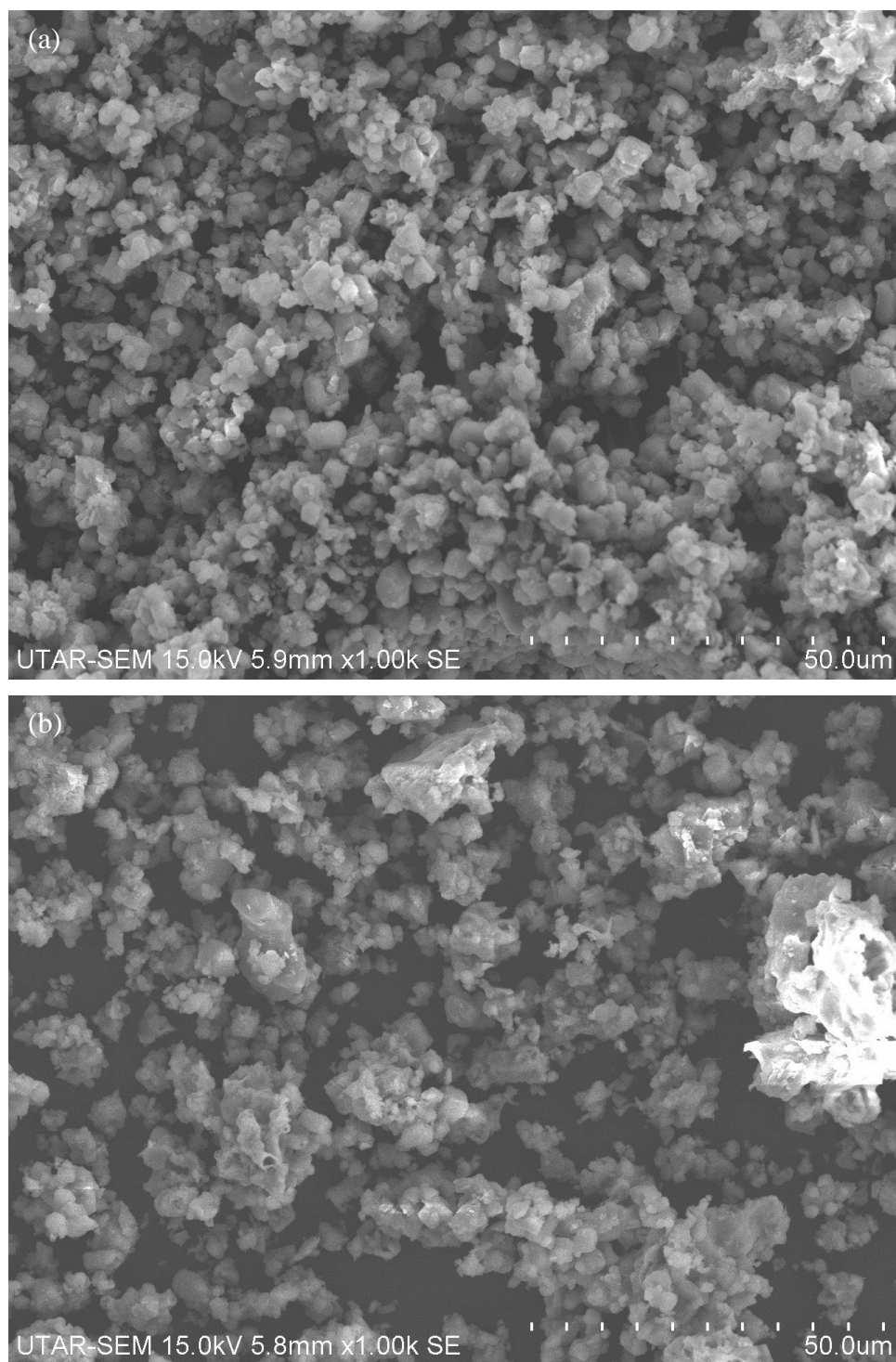
Figure K-4: SEM Micrographs of (a) 2-Ni/CaO-600 and (b) 3-Ni/CaO-600 at 1000x Magnification.

UTAR-SEM 15.0kV 5.8mm x1.00k SE   50.0um

UTAR-SEM 15.0kV 5.7mm x1.00k SE   50.0um
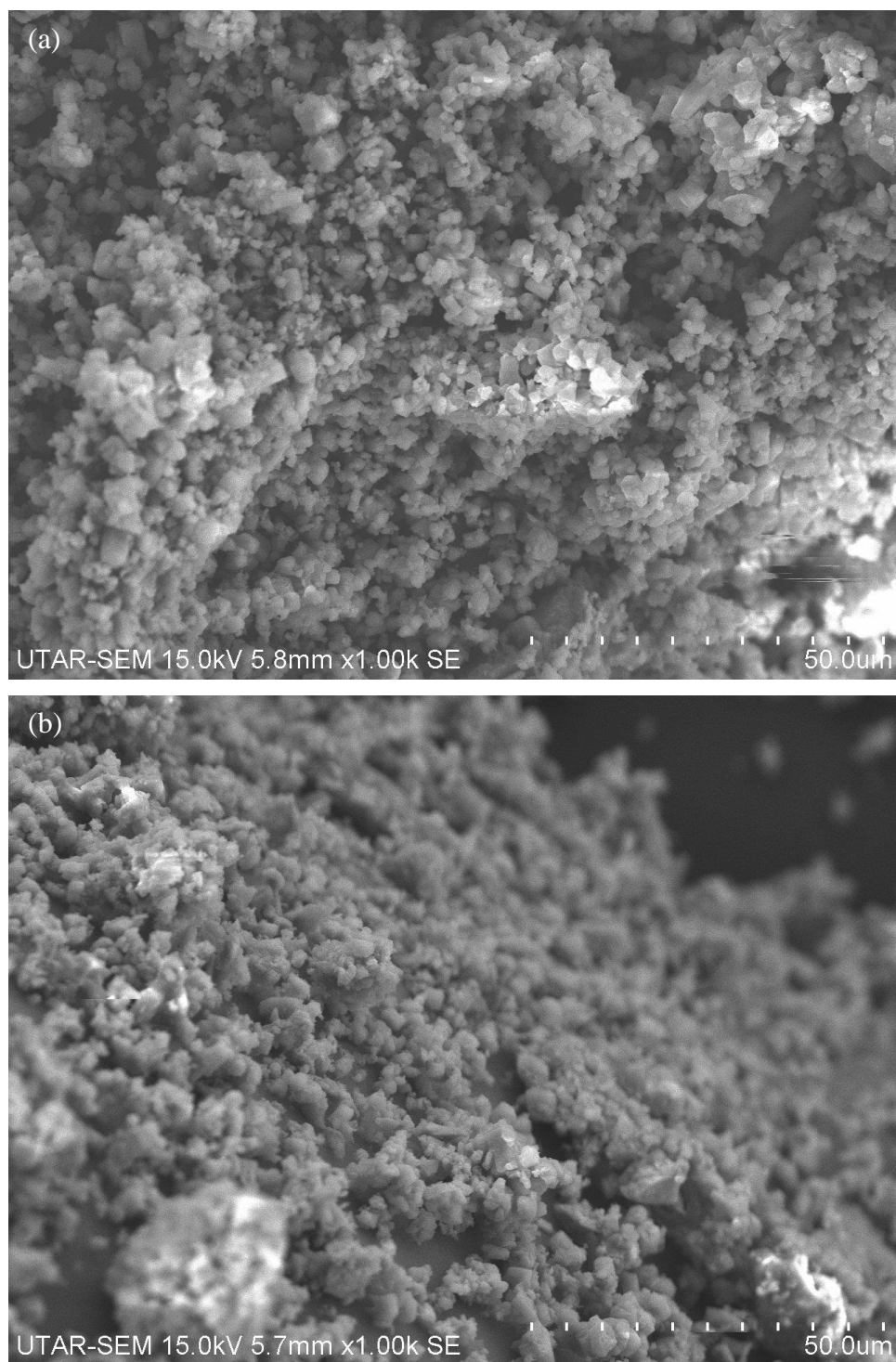
Figure K-5: SEM Micrographs of (a) 4-Ni/CaO-600 and (b) 5-Ni/CaO-600 at 1000x Magnification.

APPENDIX L: EDX Analysis Report

Element	Wt%	At%
CaK	60.64	37.61
OK	36.96	57.42
CK	02.40	04.97
Matrix	Correction	ZAF

Element	Wt%	At%
CaK	59.30	36.47
OK	39.07	60.20
CK	01.62	03.33
Matrix	Correction	ZAF

Element	Wt%	At%
CaK	60.41	37.54
OK	38.01	59.17
CK	01.58	03.28
Matrix	Correction	ZAF
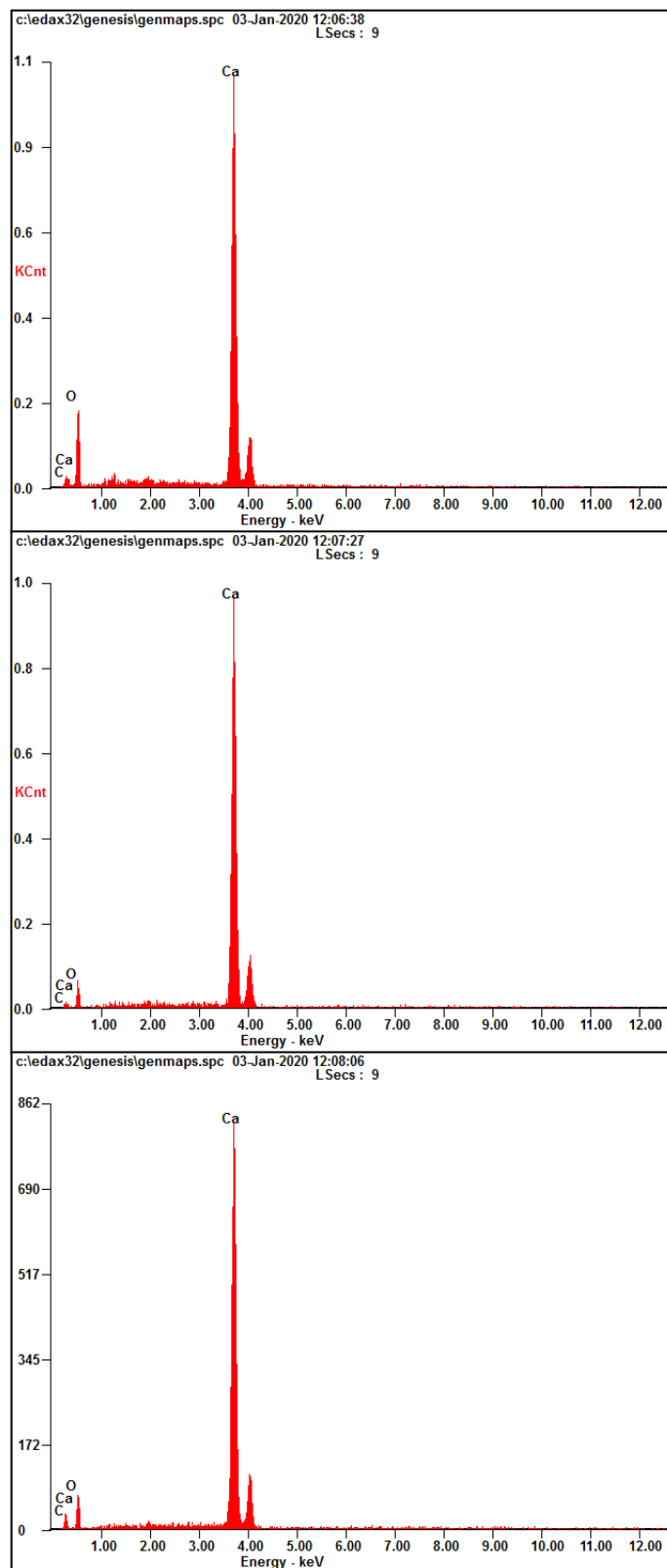
Figure L-1: Element Report and EDX Spectrum at Different Locations of Undoped CaO.

Element	Wt%	At%
CaK	67.78	44.71
OK	28.49	47.08
CK	03.73	08.21
Matrix	Correction	ZAF
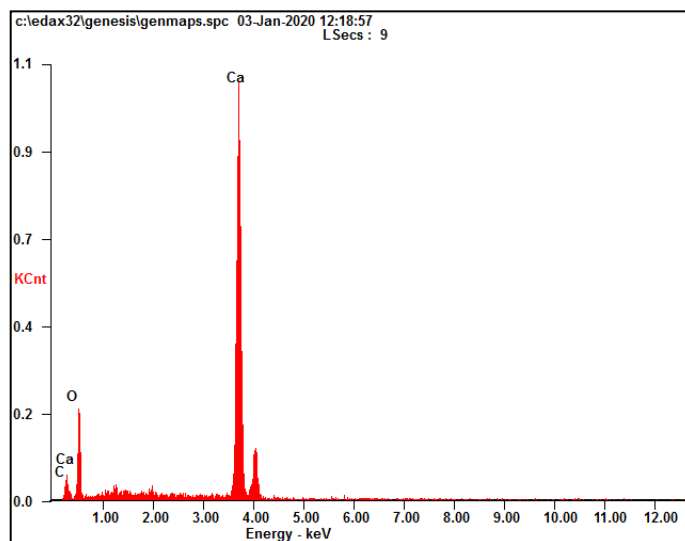
Element	Wt%	At%
CaK	66.19	42.94
OK	29.88	48.57
CK	03.92	08.50
Matrix	Correction	ZAF
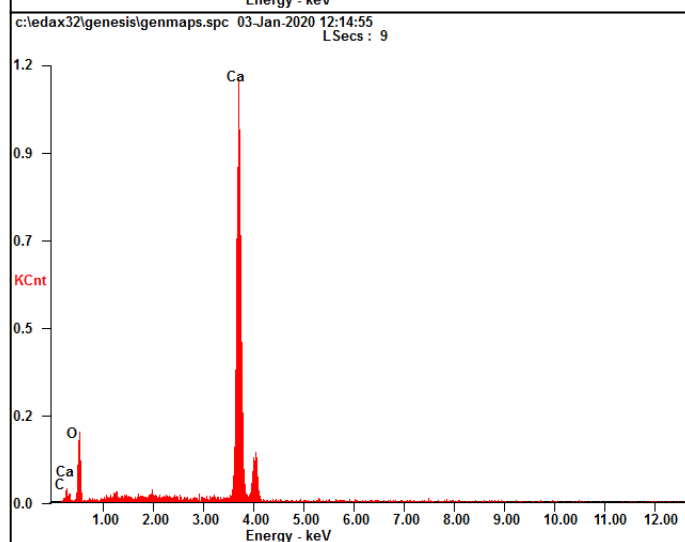
Element	Wt%	At%
CaK	65.78	42.78
OK	31.54	51.40
CK	02.68	05.82
Matrix	Correction	ZAF
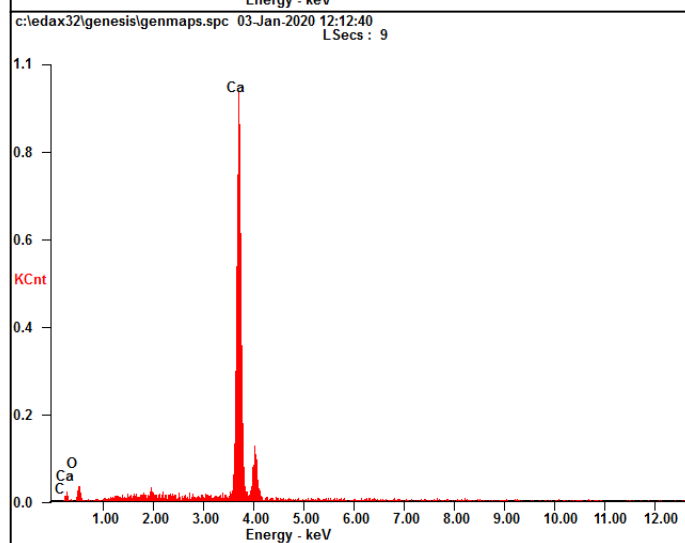
Figure L-2: Element Report and EDX Spectrum at Different Locations of Treated CaO.

Element	Wt%	At%
CaK	54.01	31.29
OK	38.89	56.44
CK	06.15	11.90
NiK	00.94	00.37
Matrix	Correction	ZAF

Element	Wt%	At%
CaK	49.70	28.40
OK	43.08	61.68
CK	04.68	08.93
NiK	02.54	00.99
Matrix	Correction	ZAF

Element	Wt%	At%
CaK	55.07	31.70
OK	35.00	50.48
CK	09.11	17.50
NiK	00.82	00.32
Matrix	Correction	ZAF
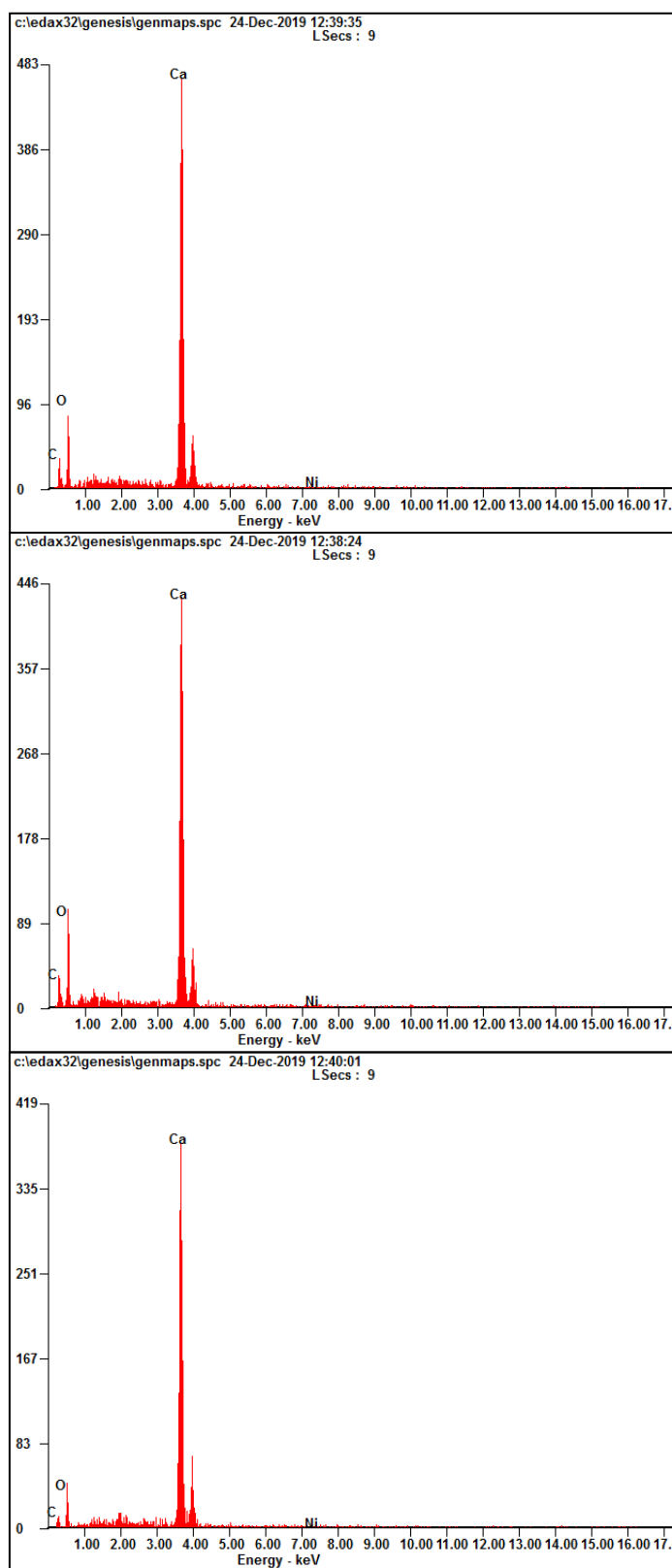
Figure L-3: Element Report and EDX Spectrum at Different Locations of 1-Ni/CaO-600.

Element	Wt%	At%
CaK	64.27	41.58
OK	31.61	51.24
CK	03.12	06.73
NiK	01.00	00.44
Matrix	Correction	ZAF
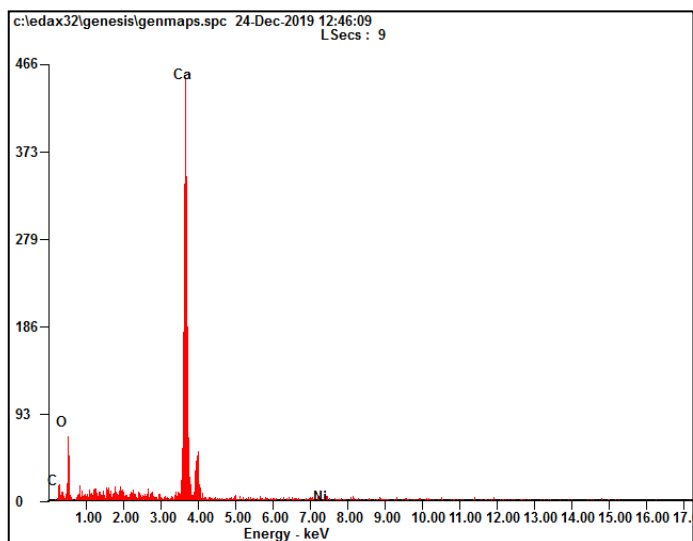
Element	Wt%	At%
CaK	60.67	37.63
OK	34.22	53.17
CK	04.28	08.85
NiK	00.83	00.35
Matrix	Correction	ZAF
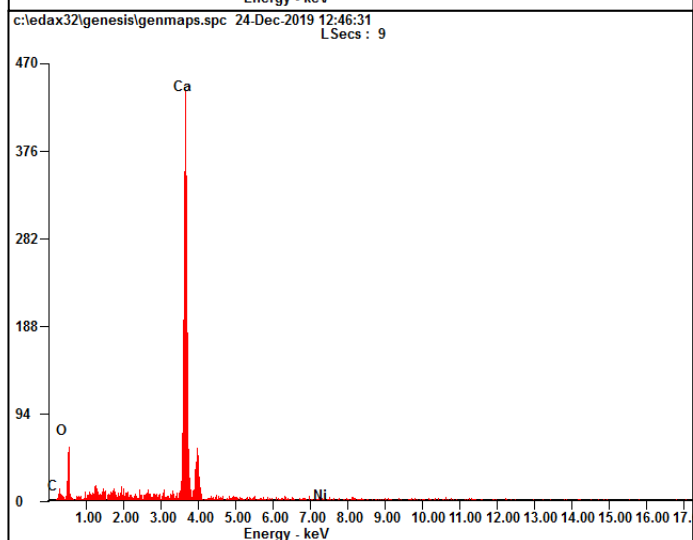
Element	Wt%	At%
CaK	68.30	46.50
OK	26.49	45.18
CK	03.26	07.42
NiK	01.94	00.90
Matrix	Correction	ZAF
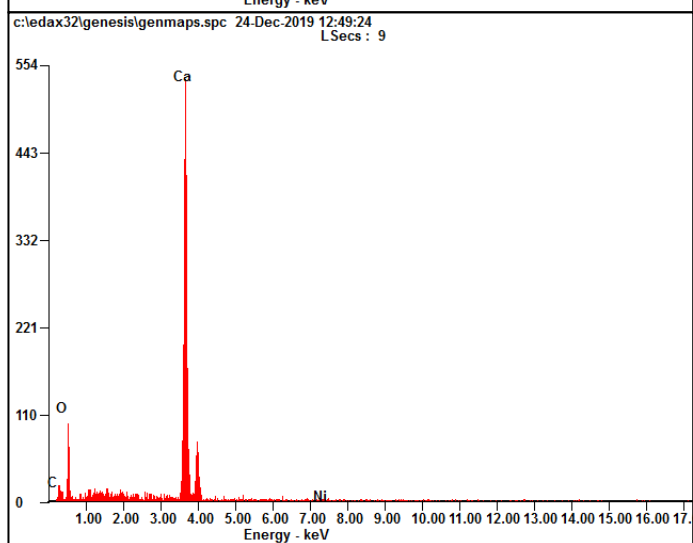
Figure L-4: Element Report and EDX Spectrum at Different Locations of 1-Ni/CaO-700.

Element	Wt%	At%
CaK	49.87	27.37
OK	39.16	53.84
CK	10.08	18.47
NiK	00.89	00.33
Matrix	Correction	ZAF
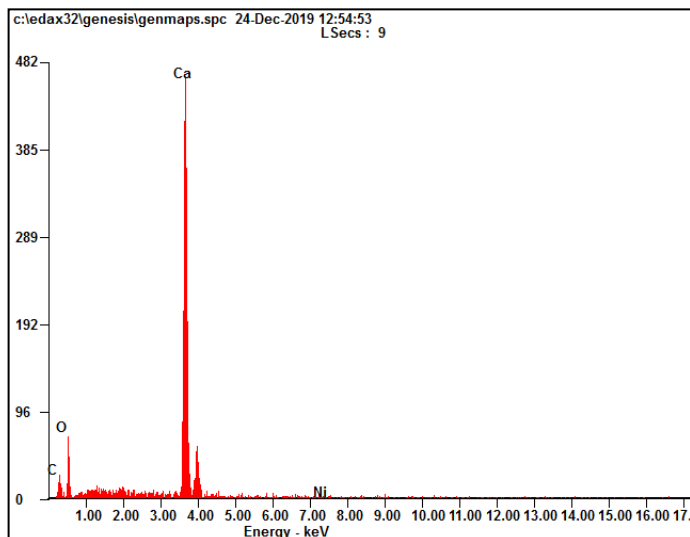
Element	Wt%	At%
CaK	50.44	28.57
OK	45.18	64.10
CK	03.75	07.09
NiK	00.63	00.24
Matrix	Correction	ZAF
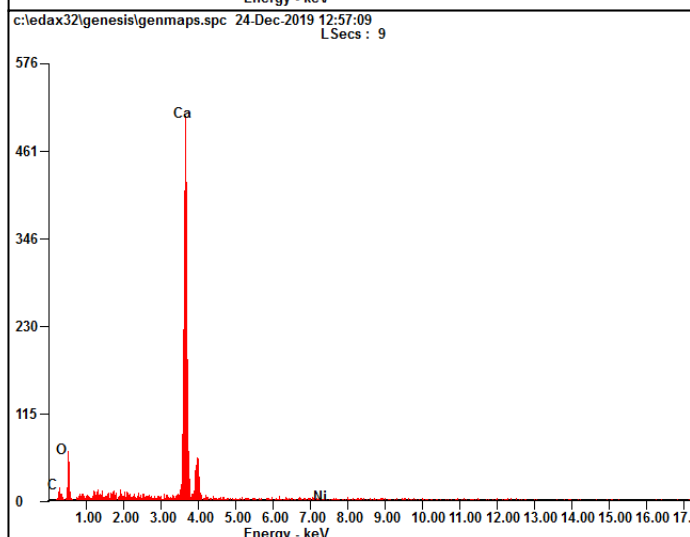
Element	Wt%	At%
CaK	63.61	40.43
OK	31.25	49.76
CK	04.49	09.53
NiK	00.65	00.28
Matrix	Correction	ZAF
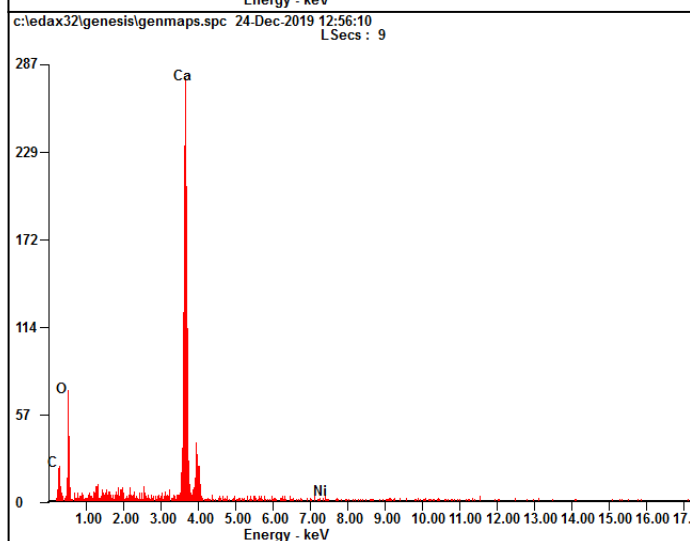
Figure L-5: Element Report and EDX Spectrum at Different Locations of 1-Ni/CaO-800.

Element	Wt%	At%
CaK	52.40	29.78
OK	39.48	56.22
CK	07.20	13.65
NiK	00.92	00.36
Matrix	Correction	ZAF
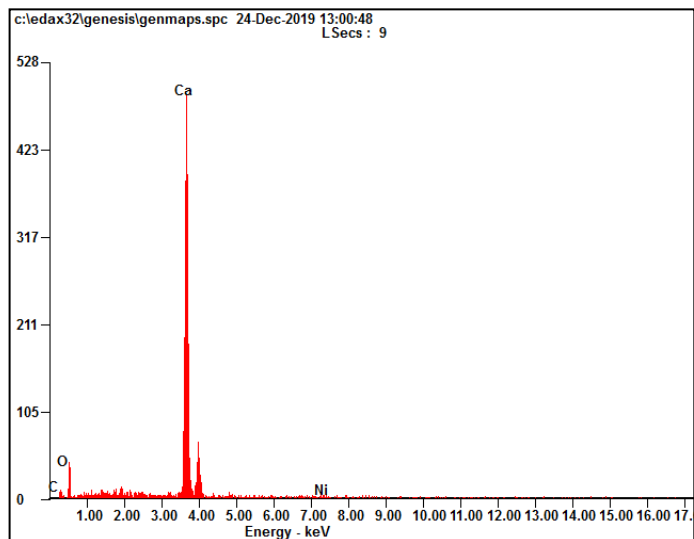
Element	Wt%	At%
CaK	63.70	40.98
OK	32.18	51.87
CK	03.12	06.70
NiK	01.00	00.44
Matrix	Correction	ZAF
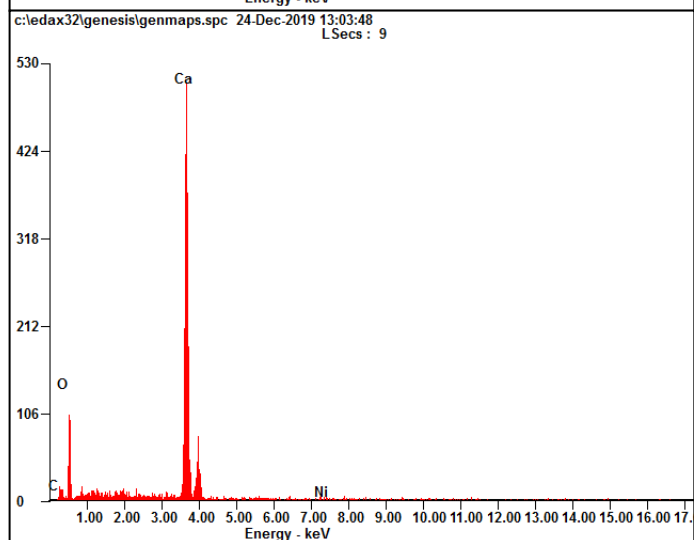
Element	Wt%	At%
CaK	61.67	39.32
OK	34.48	55.07
CK	02.33	04.95
NiK	01.53	00.66
Matrix	Correction	ZAF
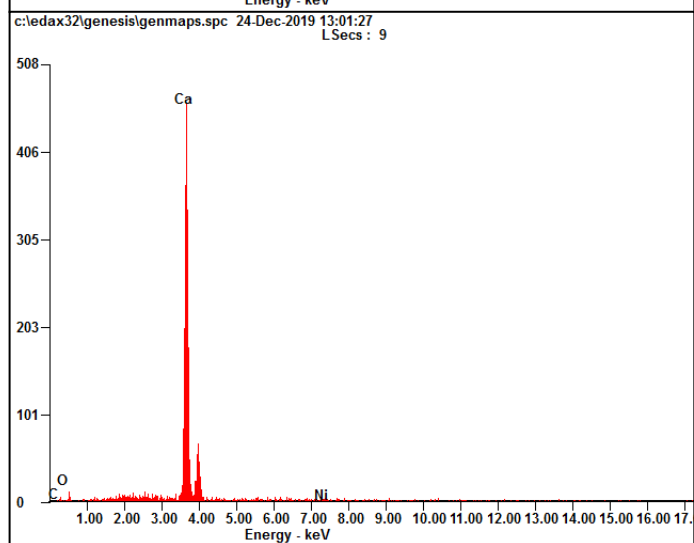
Figure L-6: Element Report and EDX Spectrum at Different Locations of 1-Ni/CaO-900.

Element	Wt%	At%
CaK	66.24	44.18
OK	28.63	47.84
CK	03.18	07.09
NiK	01.95	00.89
Matrix	Correction	ZAF
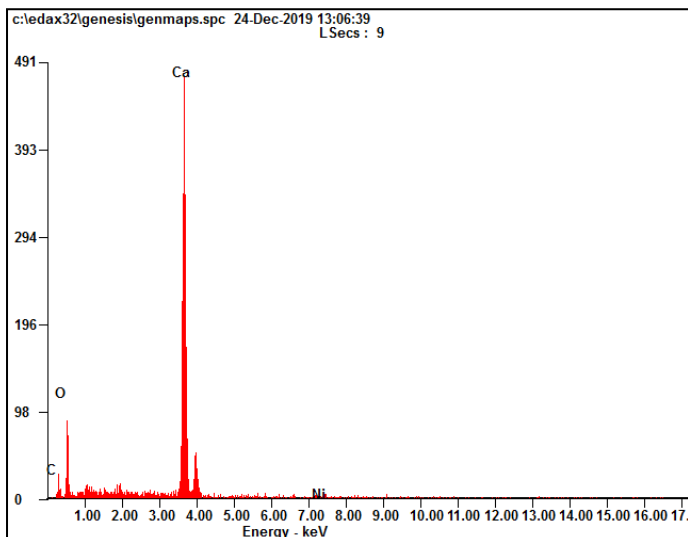
Element	Wt%	At%
CaK	63.00	40.43
OK	31.21	50.18
CK	04.02	08.61
NiK	01.77	00.78
Matrix	Correction	ZAF
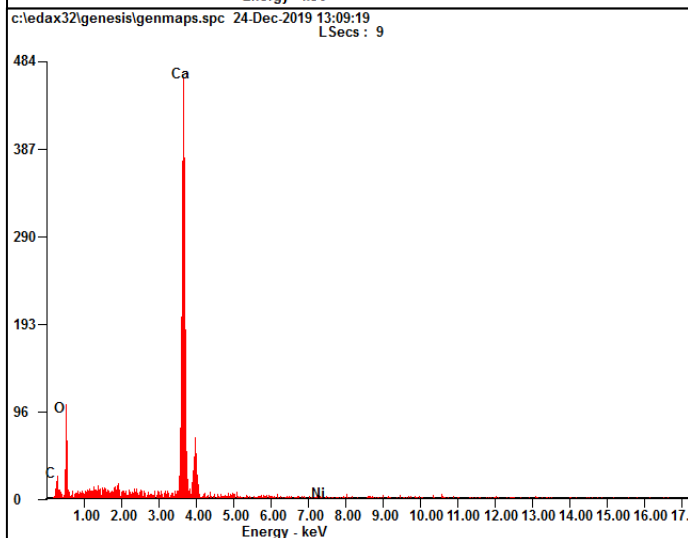
Element	Wt%	At%
CaK	65.44	43.09
OK	30.15	49.74
CK	02.97	06.52
NiK	01.44	00.65
Matrix	Correction	ZAF
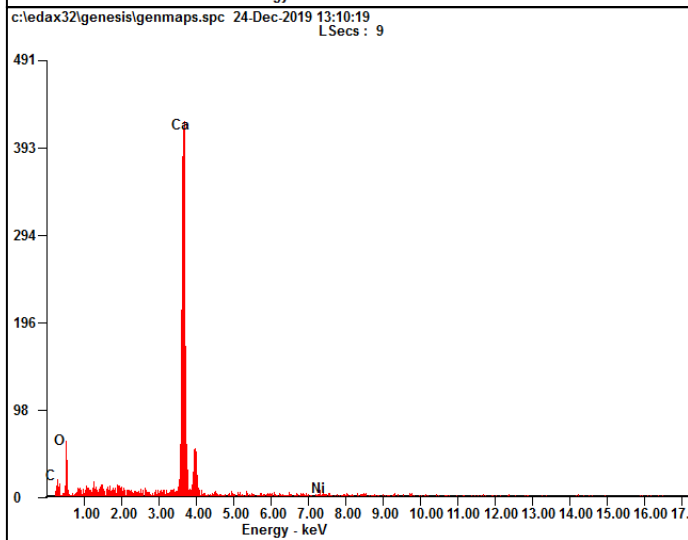
Figure L-7: Element Report and EDX Spectrum at Different Locations of 2-Ni/CaO-600.

Element	Wt%	At%
CaK	74.72	56.02
OK	20.14	37.82
CK	01.77	04.43
NiK	03.37	01.72
Matrix	Correction	ZAF
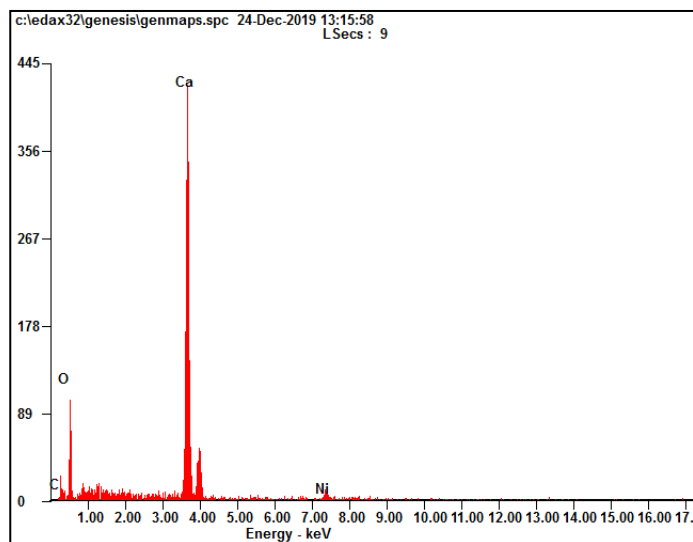
Element	Wt%	At%
CaK	53.78	32.59
OK	38.04	57.75
CK	03.90	07.88
NiK	04.29	01.77
Matrix	Correction	ZAF
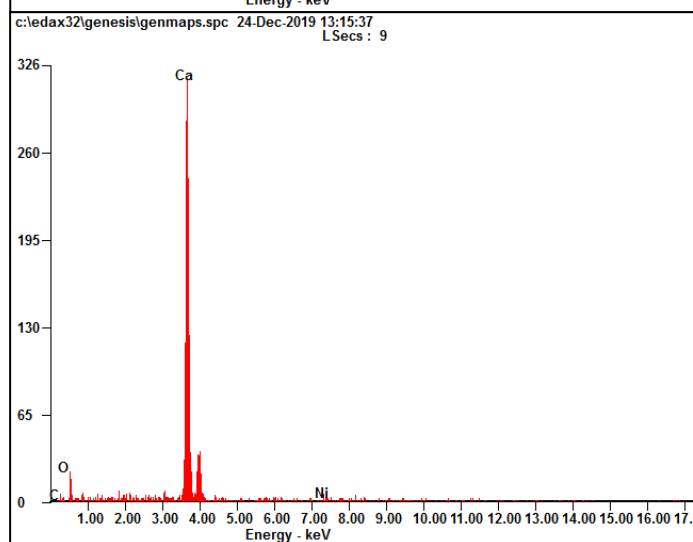
Element	Wt%	At%
CaK	66.05	44.05
OK	29.46	49.22
CK	02.64	05.88
NiK	01.85	00.84
Matrix	Correction	ZAF
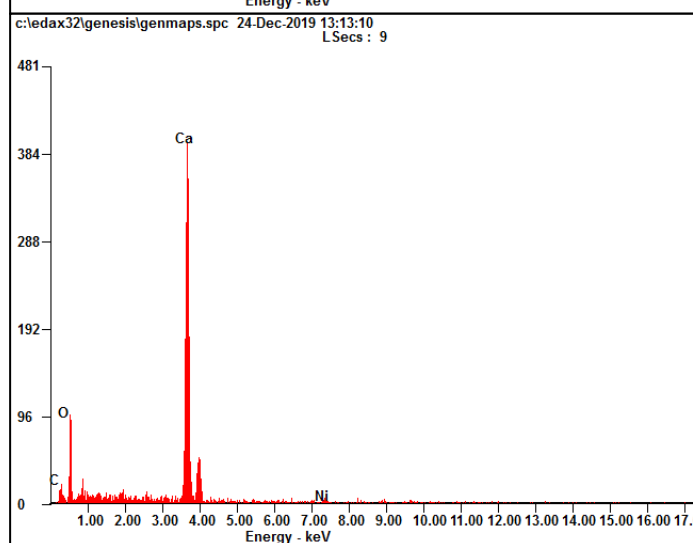
Figure L-8: Element Report and EDX Spectrum at Different Locations of 3-Ni/CaO-600.

Element	Wt%	At%
CaK	48.96	28.17
OK	42.18	60.81
CK	04.93	09.47
NiK	03.93	01.54
Matrix	Correction	ZAF
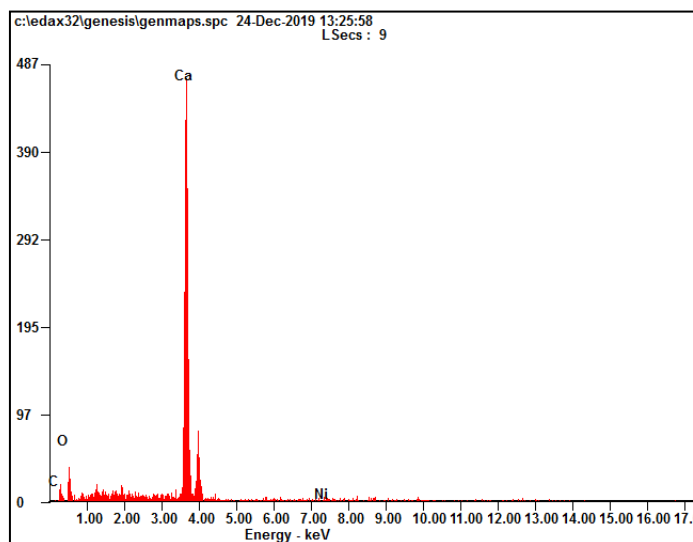
Element	Wt%	At%
CaK	63.87	42.31
OK	29.53	49.01
CK	03.24	07.17
NiK	03.35	01.52
Matrix	Correction	ZAF
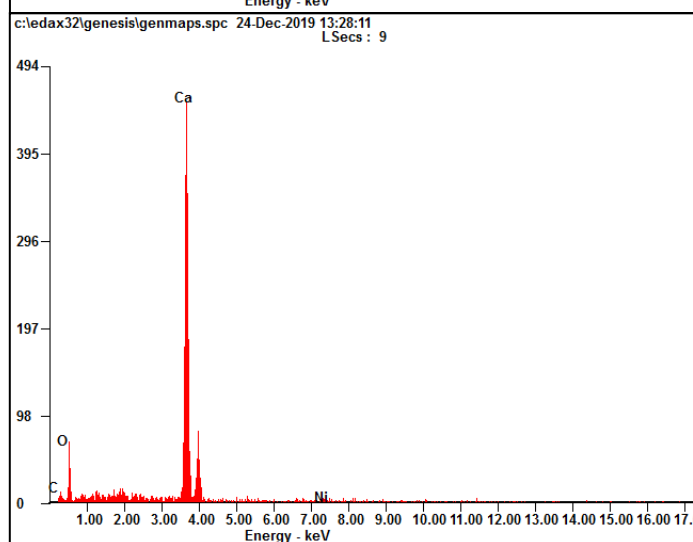
Element	Wt%	At%
CaK	59.85	38.53
OK	31.87	51.40
CK	03.76	08.08
NiK	04.52	01.98
Matrix	Correction	ZAF
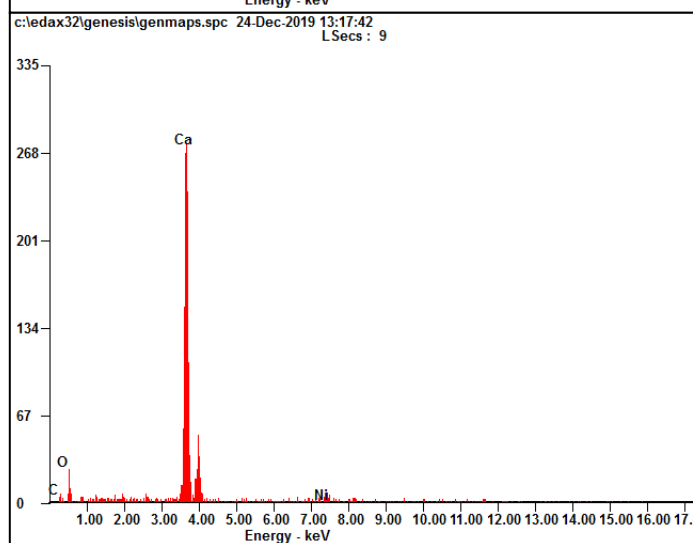
Figure L-9: Element Report and EDX Spectrum at Different Locations of 4-Ni/CaO-600.

Element	Wt%	At%
CaK	54.31	32.52
OK	32.32	48.47
CK	08.52	17.03
NiK	04.84	01.98
Matrix	Correction	ZAF

Element	Wt%	At%
CaK	50.48	30.42
OK	40.19	60.68
CK	03.17	06.37
NiK	06.16	02.53
Matrix	Correction	ZAF

Element	Wt%	At%
CaK	61.00	38.81
OK	30.74	49.00
CK	05.09	10.82
NiK	03.17	01.38
Matrix	Correction	ZAF
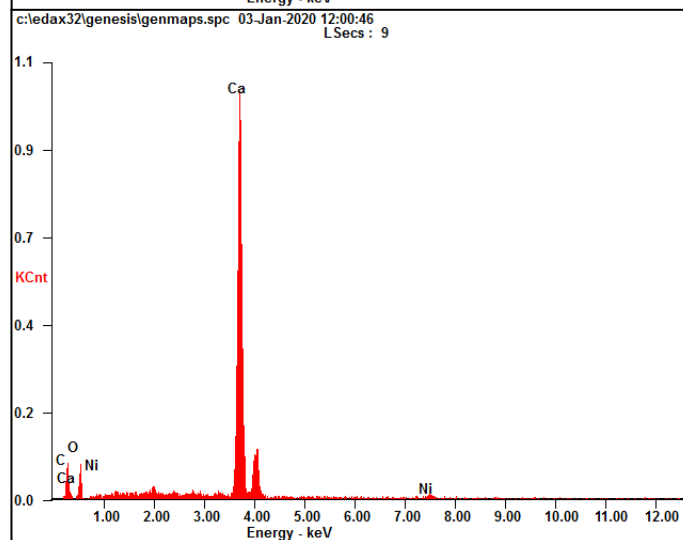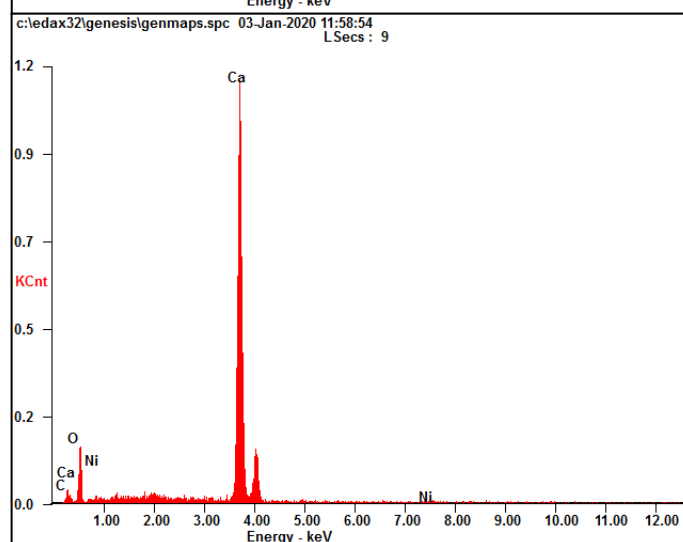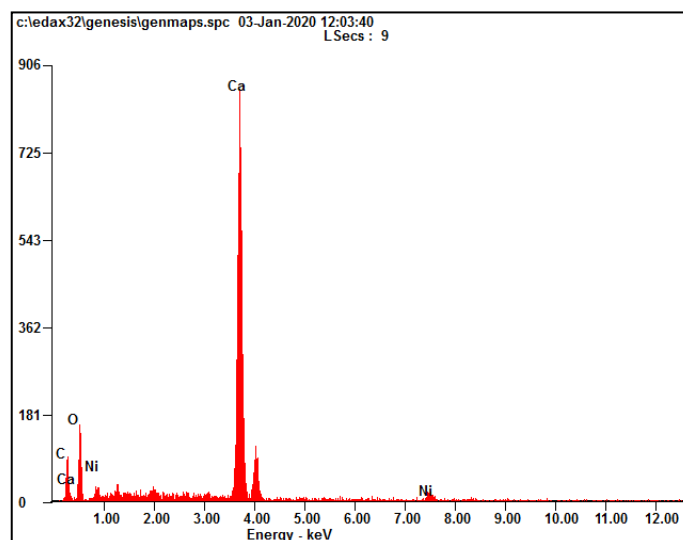
Figure L-10: Element Report and EDX Spectrum at Different Locations of 5-Ni/CaO-600.

APPENDIX M: CO_2-TPD Analysis Report

Standard Data Report

Results

Amount gas adsorbed: 1599.53140 µmol/g

Peaks

#	Start [min]	Stop [min]	Maximum [min]	T [°C]	Integral [mVs]	[µmol/g]	[%]
1	22.9667	43.2500	35.7333	730	72438.14	1599.53140	100.00

Chromatogram Report
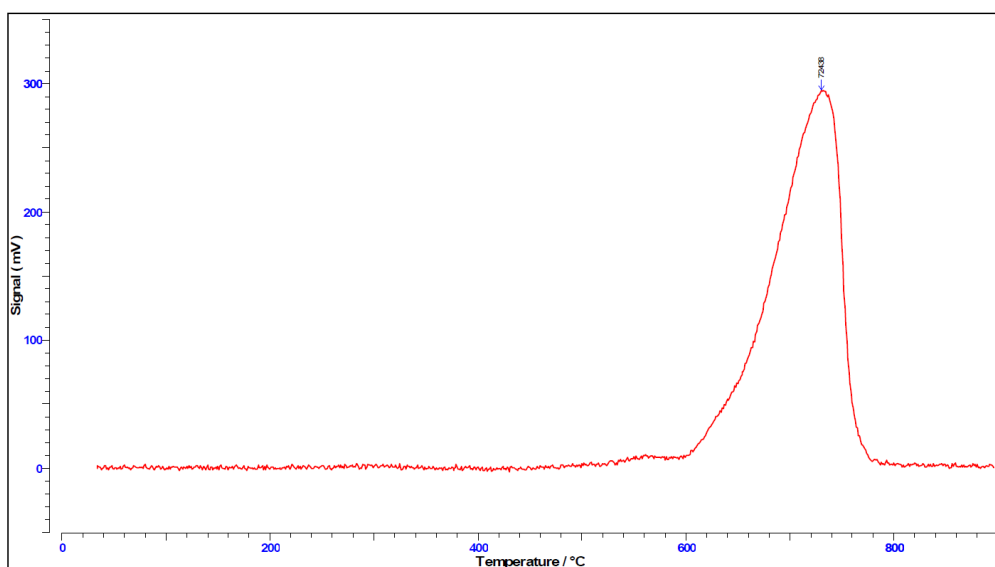
Figure M-1: Peak Report and TPD Chromatogram of Undoped CaO.

Standard Data Report

Results

Amount gas adsorbed: 2134.92701 µmol/g

Peaks

#	Start [min]	Stop [min]	Maximum [min]	T [°C]	Integral [mVs]	[µmol/g]	[%]
1	31.2000	38.8333	36.8333	754	107721.71	2134.92700	100.00

Chromatogram Report
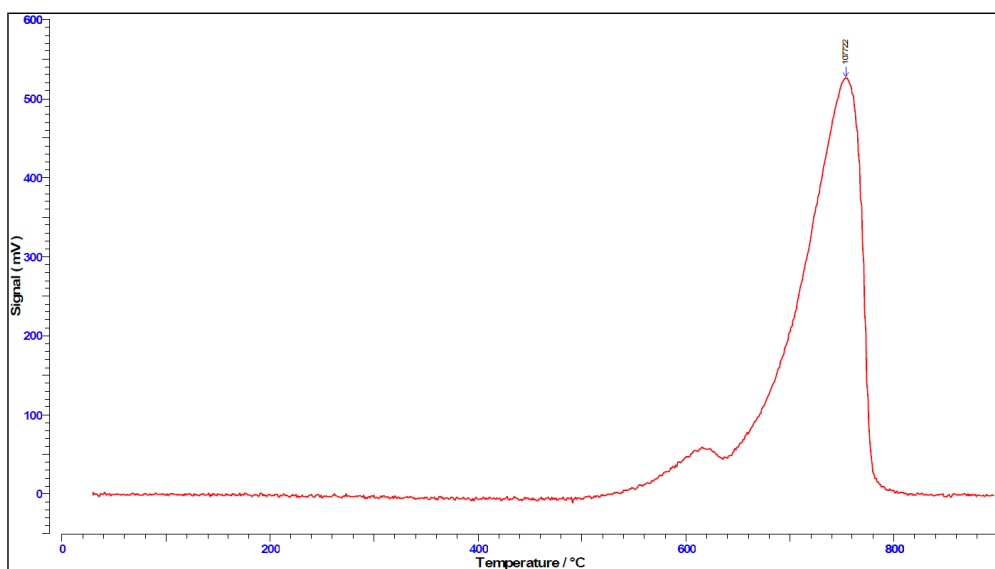
Figure M-2: Peak Report and TPD Chromatogram of Treated CaO.

Standard Data Report

Results

Amount gas adsorbed: 2561.33291 μmol/g

Peaks

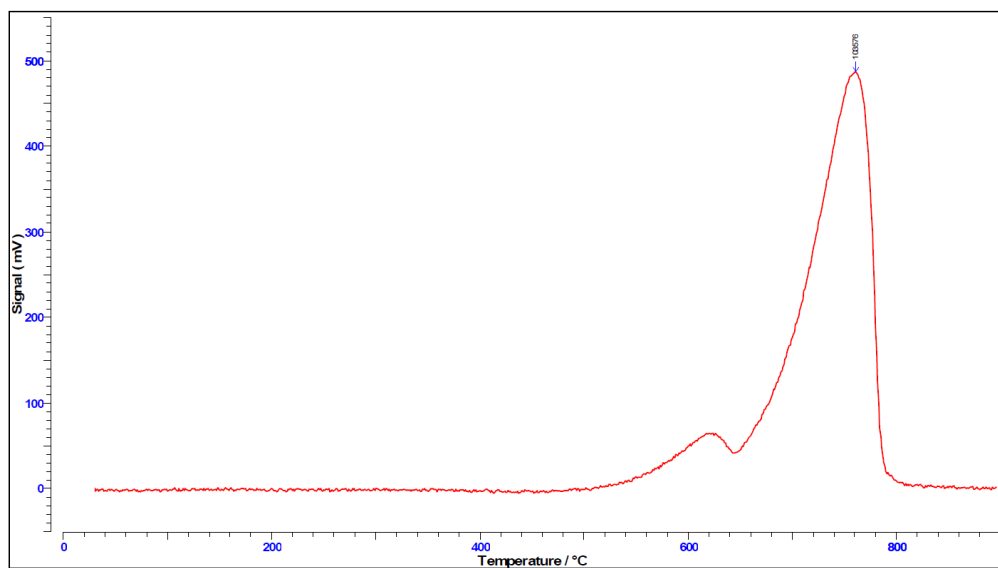| #	Start [min]	Stop [min]	Maximum [min]	T [°C]	Integral [mVs]	[μmol/g]	[%]
1	32.3500	39.9833	37.8000	774	135063.07	2561.33290	100.00

Chromatogram Report
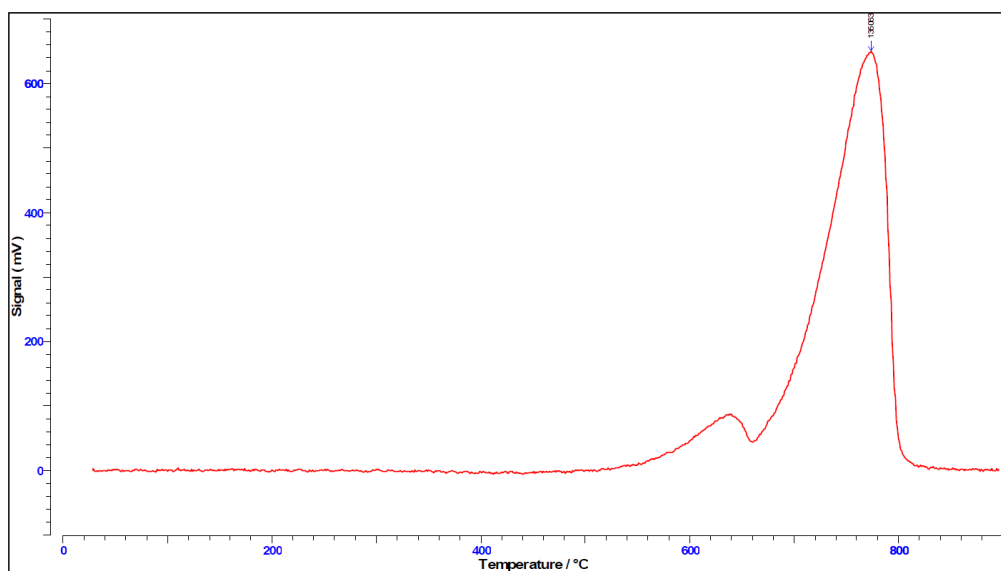
Figure M-3: Peak Report and TPD Chromatogram of 1-Ni/CaO-600.

Standard Data Report

Results

Amount gas adsorbed: 2539.86270 µmol/g

Peaks

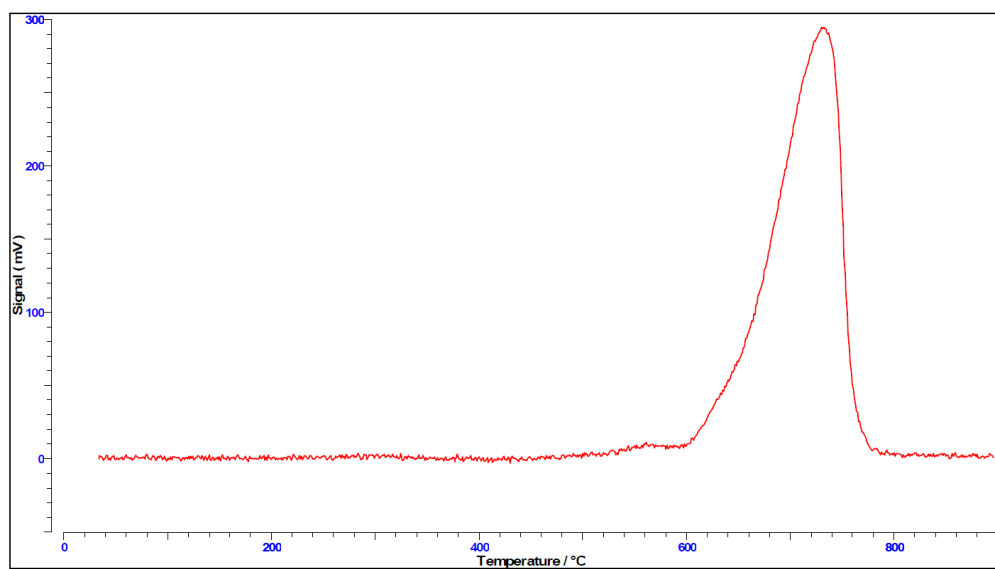| #	Start [min]	Stop [min]	Maximum [min]	T [°C]	Integral [mVs]	[µmol/g]	[%]
1	30.4000	39.7667	37.2167	760	125002.18	2539.86270	100.00

Chromatogram Report
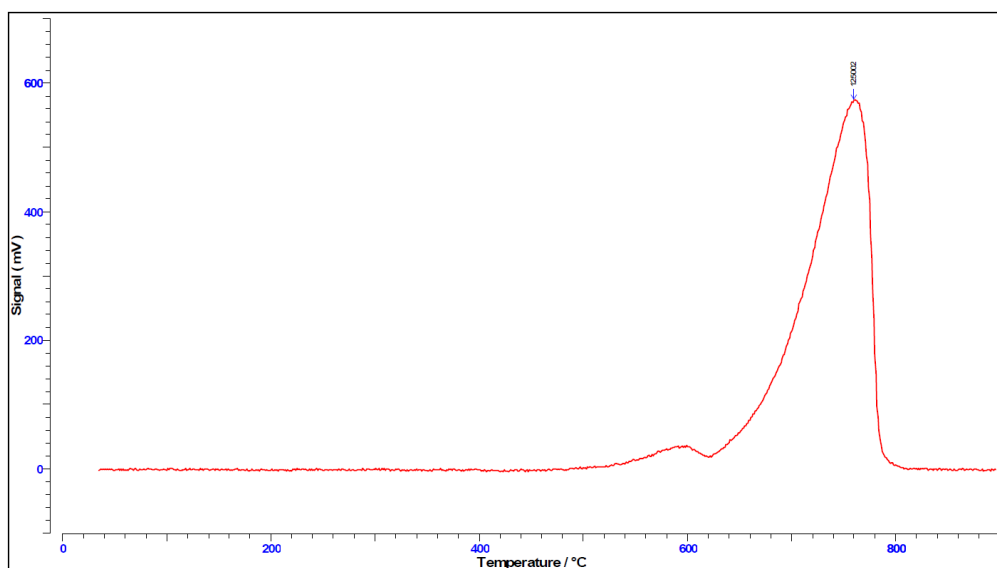
Figure M-4: Peak Report and TPD Chromatogram of 1-Ni/CaO-700.

Standard Data Report

Results

Amount gas adsorbed: 2297.58614 μmol/g

Peaks

#	Start [min]	Stop [min]	Maximum [min]	T [°C]	Integral [mVs]	[μmol/g]	[%]
1	31.5833	39.4667	37.1167	761	103575.89	2297.58610	100.00

Chromatogram Report

Figure M-5: Peak Report and TPD Chromatogram of 1-Ni/CaO-800.

Standard Data Report

Results

Amount gas adsorbed: 1787.52703 μmol/g

Peaks

#	Start [min]	Stop [min]	Maximum [min]	T [°C]	Integral [mVs]	[μmol/g]	[%]
1	29.2667	39.8333	36.3333	743	80951.91	1787.52700	100.00

Chromatogram Report

Figure M-6: Peak Report and TPD Chromatogram of 1-Ni/CaO-900.

Standard Data Report

Results

Amount gas adsorbed: 2725.44643 μmol/g

Peaks

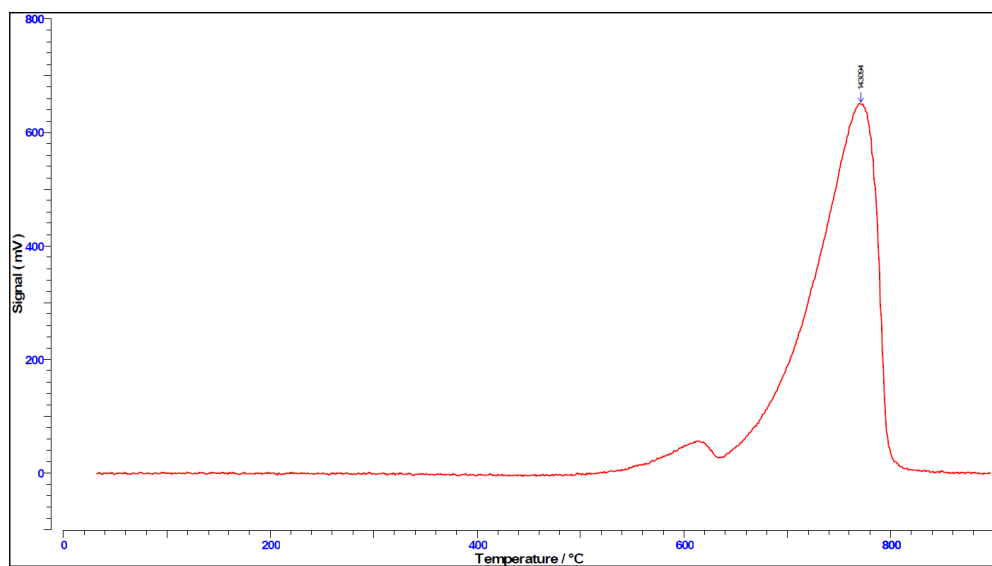| #	Start [min]	Stop [min]	Maximum [min]	T [°C]	Integral [mVs]	[μmol/g]	[%]
1	30.1333	39.3000	36.9833	756	116664.41	2725.44640	100.00

Chromatogram Report
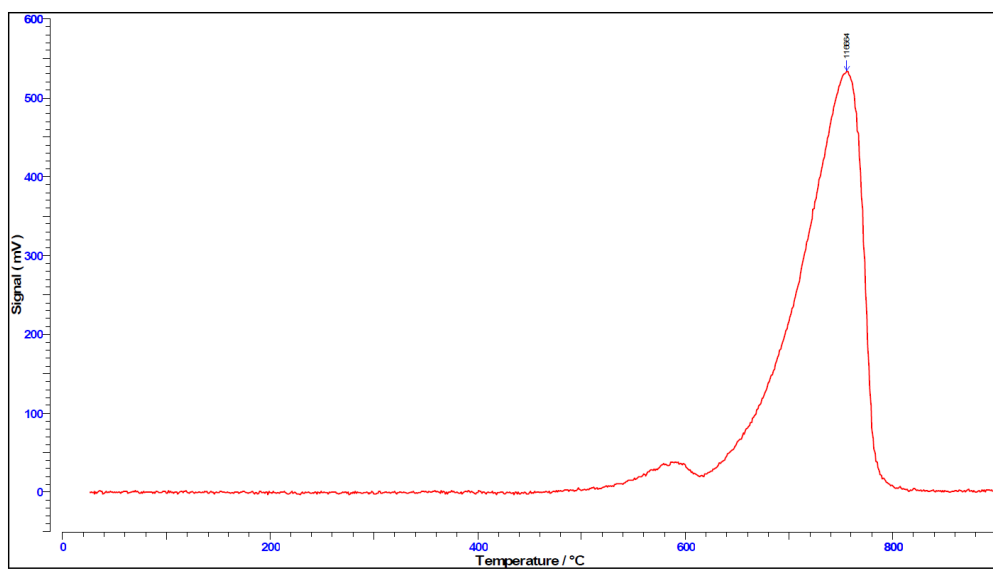
Figure M-7: Peak Report and TPD Chromatogram of 2-Ni/CaO-600.

Standard Data Report

Results

Amount gas adsorbed: 2957.16087 μmol/g

Peaks

#	Start [min]	Stop [min]	Maximum [min]	T [°C]	Integral [mVs]	[μmol/g]	[%]
1	31.0667	40.5333	37.6167	771	143093.93	2957.16090	100.00

Chromatogram Report

Figure M-8: Peak Report and TPD Chromatogram of 3-Ni/CaO-600.

Standard Data Report

Results

Amount gas adsorbed: 2458.54746 µmol/g

Peaks

#	Start [min]	Stop [min]	Maximum [min]	T [°C]	Integral [mVs]	[µmol/g]	[%]
1	31.6667	39.8000	37.2167	760	117949.74	2458.54750	100.00

Chromatogram Report
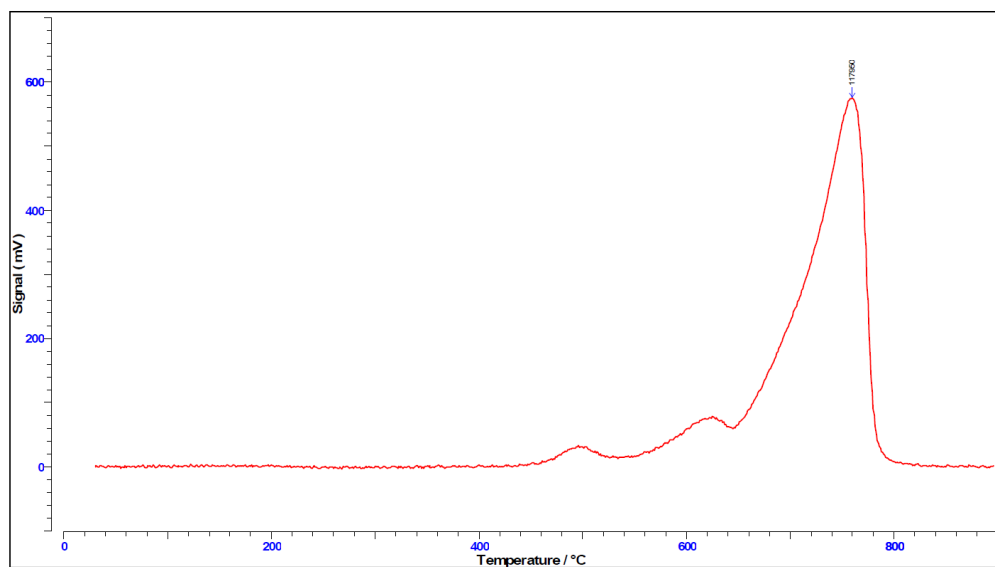
Figure M-9: Peak Report and TPD Chromatogram of 4-Ni/CaO-600.

Standard Data Report

Results

Amount gas adsorbed: 1524.13100 μmol/g

Peaks

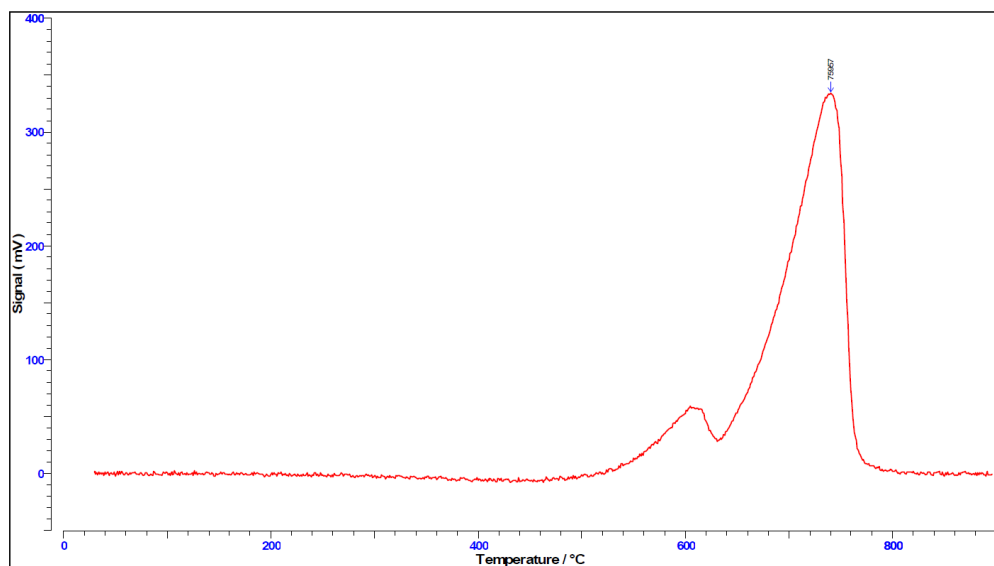| #	Start [min]	Stop [min]	Maximum [min]	T [°C]	Integral [mVs]	[μmol/g]	[%]
1	19.5833	43.0833	36.1167	740	75957.34	1524.13100	100.00

Chromatogram Report

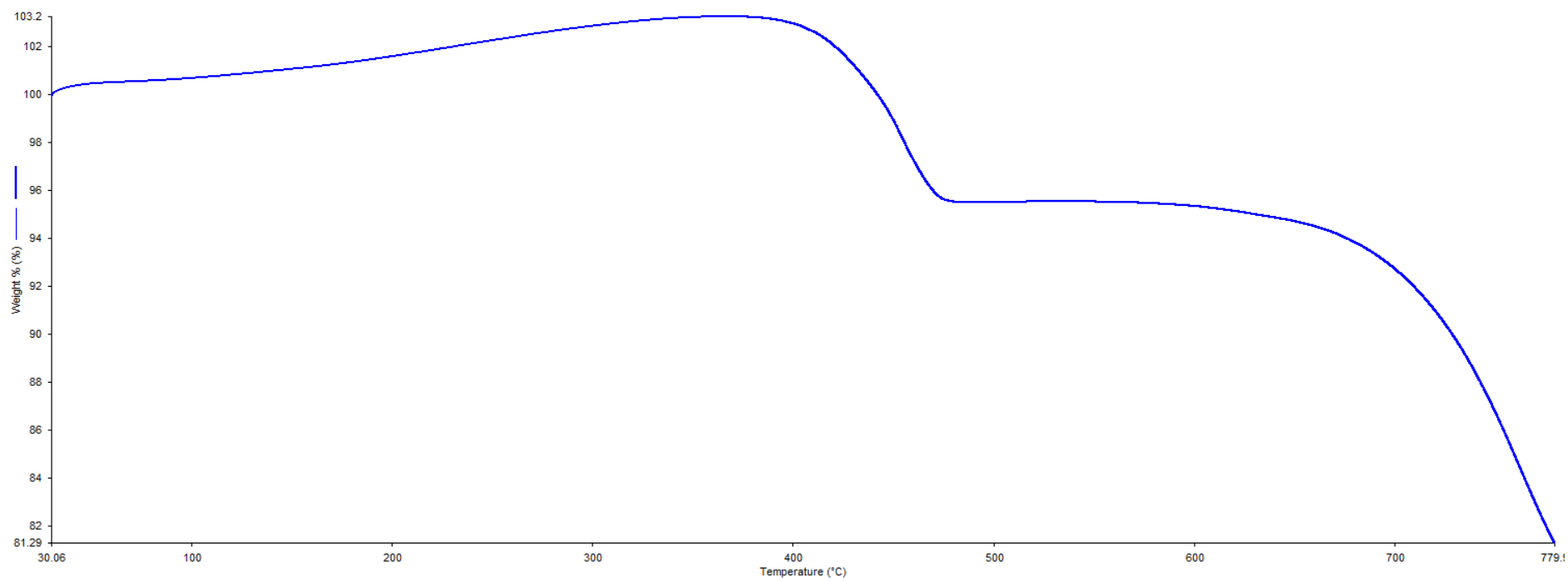Figure M-10: Peak Report and TPD Chromatogram of 5-Ni/CaO-600.

APPENDIX N: TGA Report

Figure N-1: TGA Thermogram of 1-Ni/CaO-600.